frontiers | Research Topics

Novel mechanisms involved in urinary bladder control: advances in neural, humoral and local factors underlying function and disease, volume III

Edited by
Monica Akemi Sato, Patrik Aronsson and Russ Chess-Williams

Published in
Frontiers in Physiology

ISSN 1664-8714
ISBN 978-2-8325-6228-4
DOI 10.3389/978-2-8325-6228-4

About Frontiers

Frontiers is more than just an open access publisher of scholarly articles: it is a pioneering approach to the world of academia, radically improving the way scholarly research is managed. The grand vision of Frontiers is a world where all people have an equal opportunity to seek, share and generate knowledge. Frontiers provides immediate and permanent online open access to all its publications, but this alone is not enough to realize our grand goals.

Frontiers journal series

The Frontiers journal series is a multi-tier and interdisciplinary set of open-access, online journals, promising a paradigm shift from the current review, selection and dissemination processes in academic publishing. All Frontiers journals are driven by researchers for researchers; therefore, they constitute a service to the scholarly community. At the same time, the *Frontiers journal series* operates on a revolutionary invention, the tiered publishing system, initially addressing specific communities of scholars, and gradually climbing up to broader public understanding, thus serving the interests of the lay society, too.

Dedication to quality

Each Frontiers article is a landmark of the highest quality, thanks to genuinely collaborative interactions between authors and review editors, who include some of the world's best academicians. Research must be certified by peers before entering a stream of knowledge that may eventually reach the public - and shape society; therefore, Frontiers only applies the most rigorous and unbiased reviews. Frontiers revolutionizes research publishing by freely delivering the most outstanding research, evaluated with no bias from both the academic and social point of view. By applying the most advanced information technologies, Frontiers is catapulting scholarly publishing into a new generation.

What are Frontiers Research Topics?

Frontiers Research Topics are very popular trademarks of the *Frontiers journals series*: they are collections of at least ten articles, all centered on a particular subject. With their unique mix of varied contributions from Original Research to Review Articles, Frontiers Research Topics unify the most influential researchers, the latest key findings and historical advances in a hot research area.

Find out more on how to host your own Frontiers Research Topic or contribute to one as an author by contacting the Frontiers editorial office: frontiersin.org/about/contact

Novel mechanisms involved in urinary bladder control: advances in neural, humoral and local factors underlying function and disease, volume III

Topic editors

Monica Akemi Sato — Faculdade de Medicina do ABC, Brazil

Patrik Aronsson — University of Gothenburg, Sweden

Russ Chess-Williams — Bond University, Australia

Citation

Sato, M. A., Aronsson, P., Chess-Williams, R., eds. (2025). *Novel mechanisms involved in urinary bladder control: advances in neural, humoral and local factors underlying function and disease, volume III*. Lausanne: Frontiers Media SA.

doi: 10.3389/978-2-8325-6228-4

Table of contents

frontiers | Frontiers in Physiology

TYPE Editorial
PUBLISHED 27 February 2025
DOI 10.3389/fphys.2025.1576452

OPEN ACCESS

EDITED AND REVIEWED BY
Geoffrey A. Head,
Baker Heart and Diabetes Institute, Australia

*CORRESPONDENCE
Monica A. Sato,
monica.akemi.sato@gmail.com

RECEIVED 14 February 2025
ACCEPTED 21 February 2025
PUBLISHED 27 February 2025

CITATION
Sato MA, Chess-Williams R and Aronsson P (2025) Editorial: Novel mechanisms involved in urinary bladder control: advances in neural, humoral and local factors underlying function and disease, volume III.
Front. Physiol. 16:1576452.
doi: 10.3389/fphys.2025.1576452

Editorial: Novel mechanisms involved in urinary bladder control: advances in neural, humoral and local factors underlying function and disease, volume III

Monica A. Sato[1]*, Russ Chess-Williams[2] and Patrik Aronsson[3]

[1]Department of Morphology and Physiology, Faculdade de Medicina do ABC, Centro Universitario FMABC, Santo Andre, Brazil, [2]Faculty of Health Sciences & Medicine, Bond University, Gold Coast, QLD, Australia, [3]Department of Pharmacology, Institute of Neuroscience and Physiology, University of Gothenburg, Sahlgrenska Academy, Gothenburg, Sweden

KEYWORDS

urinary bladder, overactive bladder, medial preoptic area, ectonucleotidases, tibial nerves, sickle cell disease (SCD), pituitary adenylate cyclase-activating polypeptide (PACAP), nitric oxide

Editorial on the Research Topic
Novel mechanisms involved in urinary bladder control: advances in neural, humoral and local factors underlying function and disease, volume III

This Research Topic brings several novelties about physiological and pathological aspects focusing on the urinary bladder. In the third volume about this subject that follows the earlier volumes (Sato et al., 2020; Sato et al., 2022), the different authors show with multiple angles, from the molecular to the systemic level, a variety of features displayed by the urinary bladder, allowing the reader to unravel the physiology of this fascinating organ.

Regulation of the urinary bladder is classically known for being dependent on both central and peripheral mechanisms. Although it has been deemed that the neural mechanisms involved in urinary bladder control are well stablished (De Groat et al., 2015), in recent years, novel central areas and their neurotransmissions have revealed that much more needs to be uncovered regarding these central mechanisms. Daiuto et al. have shown that the medial preoptic area (mPOA) is involved in urinary bladder regulation through a phasic mechanism in female Wistar rats. In this brain area, it is the angiotensinergic transmission by activation of AT-1 receptors, but not the GABAergic neurotransmission, that mediates the intravesical pressure control.

Peripherally, the urinary bladder is innervated by the autonomic nervous system. Burnstock (2014) has shown that adenosine 5′-triphosphate (ATP) is released as a co-transmitter with acetylcholine from parasympathetic nerves and also is likely a co-transmitter with norepinephrine/noradrenaline from the sympathetic innervation of the bladder. The release of ATP by efferent neurons can modulate smooth muscle tone (Vial and Evans, 2000). In contrast, urothelial ATP can act on suburothelial interstitial

cells/myofibroblasts (Wu et al., 2004; Cheng et al., 2011), in autocrine and paracrine ways to stimulate urothelial cells (Ferguson et al., 2015; Chess-Williams et al., 2019), and sensory nerves (Cockayne et al., 2000; Kaan et al., 2010). The activation of purinergic receptors on sensory nerves is thought to convey the sensation of bladder fullness and onset of the micturition reflex (Cockayne et al., 2000; Kaan et al., 2010). However, released ATP is easily hydrolyzed by membrane-bound and soluble forms of ectonucleotidases to ADP, AMP, and adenosine (ADO) (Yu, 2015; Aresta Branco et al., 2022; Gutierrez Cruz et al., 2022). Particularly, ADP and ADO are biologically active metabolites that can modulate detrusor function, in which ADP actions result in detrusor muscle contraction (Yu et al., 2014), whereas ADO causes smooth muscle relaxation (Hao et al., 2019). Branco et al. have used RNAscope™, an RNA *in situ* hybridization technology, to demonstrate the distribution and measure the levels of ectonucleotidases gene expression in large high-resolution images of murine bladder sections. They suggested that layer-specific differences of ectonucleotidases gene expression found in their study could be relevant for regulation of purine availability and subsequent functions in the bladder wall.

Interestingly, animal studies have shown that the afferent tibial nerve may be also responsible for bladder modulation (Kovacevic and Yoo, 2015). Evidence suggests that unmyelinated C-fibers, but not Aδ or Aβ-fibers, were recruited during tibial nerve stimulation in a continuous-fill rat model (Paquette and Yoo, 2019). Zhou et al. investigated if the stimulation of C-fibers in tibial nerves can induce bladder inhibition by optogenetic transdermal illumination by cystometric evaluation. They demonstrated that prolonged bladder inhibition is mediated by the stimulation of C-fibers in the tibial nerves, with no frequency-dependent characteristics, and suggested that 473-nm blue light has limited penetration efficacy, but it is enough to modulate bladder functions through transdermal illumination on the superficial peripheral nervous system.

Pathological conditions affecting the urinary bladder and the understanding of mechanisms underlying these disorders have been also focused in this Research Topic. Sickle cell disease (SCD), an autosomal recessive genetic disorder that causes abnormal hemoglobin S (HbS) production due to a single amino acid substitution in the β-globin chain, can be evoked by genetic mutation. This triggers the polymerization of HbS under hypoxic or dehydrated conditions, forming sickle-shaped erythrocytes (Kato et al., 2018). Such altered cells exhibit increased stiffness and a reduced lifespan, leading to intravascular and extravascular hemolysis, which are critical features of SCD and yielding several clinical manifestations (Kato et al., 2018). A relevant molecular consequence of intravascular hemolysis is the reduction of nitric oxide (NO) bioavailability due to direct NO-hemoglobin interactions and increased reactive oxygen species (ROS) production, which act as NO scavengers (Reiter et al., 2002; Vona et al., 2021). This reduction in NO availability is associated with severe SCD complications, including the overactive bladder (OAB) (Kato et al., 2017). Rebecchi e Silveira et al. have investigated the effects of intravascular hemolysis on the micturition process and the contractile mechanisms of the detrusor smooth muscle (DSM) in a mouse model with phenylhydrazine (PHZ)-induced hemolysis. In addition, the role of intravascular hemolysis in the dysfunction of nitric oxide (NO) signaling and oxidative stress in the bladder was evaluated. They demonstrated that intravascular hemolysis promotes voiding dysfunction that correlated with alterations in the NO signaling pathway in the bladder. In addition, increases in oxidative stress were evoked by intravascular hemolysis. They suggested that intravascular hemolysis elicited an OAB phenotype similar to those observed in patients and mice with SCD.

Another pathological aspect has been shown by Oliveira et al. in this Research Topic. As hyperglycemia in diabetic individuals causes accumulation of the highly reactive dicarbonyl compound methylglyoxal (MGO), which modulates TRPA1 activity, and long-term oral intake of MGO causes mouse bladder dysfunction, they investigated the TRPA1 expression in the bladder and the effects of 1 h-intravesical infusion of the selective TRPA1 blocker on cystometric alterations induced by MGO. Their findings demonstrated that TRPA1 activation is implicated in mouse overactive bladder induced by MGO, and suggested that TRPA1 blockers could be useful for the treatment of diabetic bladder dysfunction in individuals with high MGO levels.

Tay and Grundy bring a review about the different animal models of interstitial cystitis/bladder pain syndrome (IC/BPS), and the mechanisms underlying these models. They highlight that many of the animal models mimic the major symptoms of IC/BPS. The refining of these models to induce chronic symptomatology can resemble the IC/BPS phenotype, nevertheless, it is noteworthy that no single model can fully replicate all aspects of the human disease. Thus, likely different models still will be necessary for preclinical drug development, depending on the unique etiology of IC/BPS under investigation.

Ke et al. have demonstrated the role of Pituitary Adenylate Cyclase-Activating Polypeptide (PACAP) and its receptor PAC1 in IC/BPS and the potential involvement in inflammation and sensory dysfunction. Using different approaches such as transcriptomic analysis, immunohistochemistry, and bladder function assays, Ke et al. assessed the possible correlations between PACAP/PAC1 activation, bladder inflammation, and sensory dysfunction. In addition, the modulation of the PACAP/PAC1 pathway was evaluated in rats to determine its effects on bladder inflammation and function. The findings suggested that the PACAP/PAC1 pathway is involved in the inflammatory and sensory changes observed in IC/BPS, opening perspectives for the development of new targeted treatments.

Another study by Aronsson et al. used a method to produce NO in an aqueous solution and validated its capacity to induce functional responses in isolated rat bladders, as well as comparing the NO responses to the commonly used NO donor sodium nitroprusside (SNP). The authors also evaluated the impact of ongoing inflammation on the involvement of soluble guanylate cyclase (sGC) dependent signaling in NO relaxation. They found that aqueous NO solution induces relaxation of the rat detrusor muscle by activating sGC in both control and inflamed bladder strips in an experimental cystitis induced by a single injection of cyclophosphamide. However, inflammation possibly leads to decreased sGC expression in the detrusor muscle. The authors emphasize the usefulness of the aqueous NO solution as a valuable pharmacological tool for studies of the lower urinary tract.

In conclusion, this Research Topic covers an array of studies addressing physiological and pathological aspects of the urinary bladder. We believe that the enriching lessons of the valuable

approaches shown here will raise novel issues as well as open new avenues for further studies that may ultimately lead to novel therapies for patients with bladder dysfunctions.

Author contributions

MS: Writing–original draft, Writing–review and editing. RC-W: Writing–review and editing. PA: Writing–review and editing.

Funding

The author(s) declare that no financial support was received for the research, authorship, and/or publication of this article.

Acknowledgments

We would like to thank all contributing authors for their time and effort. We also thank the kind Frontiers in Physiology editorial team for all their support.

Conflict of interest

The authors declare that the research was conducted in the absence of any commercial or financial relationships that could be construed as a potential conflict of interest.

Generative AI statement

The author(s) declare that no Generative AI was used in the creation of this manuscript.

Publisher's note

References

Aresta Branco, M. S. L., Gutierrez Cruz, A., Dayton, J., Perrino, B. A., and Mutafova-Yambolieva, V. N. (2022). Mechanosensitive hydrolysis of ATP and ADP in lamina propria of the murine bladder by membrane-bound and soluble nucleotidases. *Front. Physiol.* 13, 918100. doi:10.3389/fphys.2022.918100

Burnstock, G. (2014). Purinergic signalling in the urinary tract in health and disease. *Purinergic Signal* 10, 103–155. doi:10.1007/s11302-013-9395-y

Cheng, S., Scigalla, F. P., Speroni di Fenizio, P., Zhang, Z. G., Stolzenburg, J.-U., and Neuhaus, J. (2011). ATP enhances spontaneous calcium activity in cultured suburothelial myofibroblasts of the human bladder. *PLoS One* 6, e25769. doi:10.1371/journal.pone.0025769

Chess-Williams, R., Sellers, D. J., Brierley, S. M., Grundy, D., and Grundy, L. (2019). Purinergic receptor mediated calcium signalling in urothelial cells. *Sci. Rep.* 9, 16101. doi:10.1038/S41598-019-52531-9

Cockayne, D. A., Hamilton, S. G., Zhu, Q. M., Dunn, P. M., Zhong, Y., Novakovic, S., et al. (2000). Urinary bladder hyporeflexia and reduced pain-related behaviour in P2X3-deficient mice. *Nat* 407, 1011–1015. doi:10.1038/35039519

Daiuto, S. A., de Carvalho, R. P., do Vale, B., Dsouki, N. A., Giannocco, G., Cafarchio, E. M., et al. (2023). Angiotensinergic and GABAergic transmission in the medial preoptic area: role in urinary bladder and cardiovascular control in female rats. *Front. Physiol.* 14, 1224505. doi:10.3389/fphys.2023.1224505

De Groat, W. C., Griffiths, D., and Yoshimura, N. (2015). Neural control of the lower urinary tract. *Compr. Physiol.*5 (1), 327–396. doi:10.1002/cphy.c130056

Ferguson, A. C., Sutton, B. W., Boone, T. B., Ford, A. P., and Munoz, A. (2015). Inhibition of urothelial P2X3 receptors prevents desensitization of purinergic detrusor contractions in the rat bladder. *BJU Int.* 116, 293–301. doi:10.1111/BJU.13003

Gutierrez Cruz, A., Aresta Branco, M. S. L., Perrino, B. A., Sanders, K. M., and Mutafova-Yambolieva, V. N. (2022). Urinary ATP levels are controlled by nucleotidases released from the urothelium in a regulated manner. *Metabolites* 13, 30. doi:10.3390/metabo13010030

Hao, Y., Wang, L., Chen, H., Hill, W. G., Robson, S. C., Zeidel, M. L., et al. (2019). Targetable purinergic receptors P2Y12 and A2b antagonistically regulate bladder function. *JCI Insight* 4, e122112. doi:10.1172/jci.insight.122112

Kaan, T. K. Y., Yip, P. K., Grist, J., Cefalu, J. S., Nunn, P. A., Ford, A. P. D. W., et al. (2010). Endogenous purinergic control of bladder activity via presynaptic P2X 3 and P2X 2/3 receptors in the spinal cord. *J. Neurosci.* 30, 4503–4507. doi:10.1523/JNEUROSCI.6132-09.2010

Kato, G. J., Piel, F. B., Reid, C. D., Gaston, M. H., Ohene-Frempong, K., Krishnamurti, L., et al. (2018). Sickle cell disease. *Nat. Rev. Dis. Prim.* 4, 18010. doi:10.1038/nrdp.2018.10

Kato, G. J., Steinberg, M. H., and Gladwin, M. T. (2017). Intravascular hemolysis and the pathophysiology of sickle cell disease. *J. Clin. Investig.* 127, 750–760. doi:10.1172/JCI89741

Kovacevic, M., and Yoo, P. B. (2015). Reflex neuromodulation of bladder function elicited by posterior tibial nerve stimulation in anesthetized rats. *Am. J. Physiol. Ren. Physiol.* 308 (4), F320–F329. doi:10.1152/ajprenal.00212.2014

Paquette, J. P., and Yoo, P. B. (2019). Recruitment of unmyelinated C-fibers mediates the bladder-inhibitory effects of tibial nerve stimulation in a continuous-fill anesthetized rat model. *Am. J. Physiol. Ren. Physiol.* 317 (1), F163–F171. doi:10.1152/ajprenal.00502.2018

Reiter, C. D., Wang, X., Tanus-Santos, J. E., Hogg, N., Cannon, R. O., Schechter, A. N., et al. (2002). Cell-free hemoglobin limits nitric oxide bioavailability in sickle-cell disease. *Nat. Med.* 8, 1383–1389. doi:10.1038/nm1202-799

Sato, M. A., De Luca, L. A., Jr., Chess-Williams, R., and Aronsson, P. (2022). Editorial: novel mechanisms involved in urinary bladder control: Advances in neural, humoral and local factors underlying function and disease, volume II. *Front. Physiol.* 13, 1056316. doi:10.3389/fphys.2022.1056316

Sato, M. A., De Luca, L. A., Jr, Aronsson, P., and Chess-Williams, R. (2020). Editorial: novel mechanisms involved in urinary bladder control: Advances in neural, humoral and local factors underlying function and disease. *Front. Physiol.* 11, 606265. doi:10.3389/fphys.2020.606265

Vial, C., and Evans, R. J. (2000). P2X receptor expression in mouse urinary bladder and the requirement of P2X 1 receptors for functional P2X receptor responses in the mouse urinary bladder smooth muscle. *Br. J. Pharmacol.* 131, 1489–1495. doi:10.1038/sj.bjp.0703720

Vona, R., Sposi, N. M., Mattia, L., Gambardella, L., Straface, E., and Pietraforte, D. (2021). Sickle cell disease: role of oxidative stress and antioxidant therapy. *Antioxidants* 10, 296. doi:10.3390/antiox10020296

Wu, C., Sui, G. P., and Fry, C. H. (2004). Purinergic regulation of Guinea pig suburothelial myofibroblasts. *J. Physiol.* 559, 231–243. doi:10.1113/jphysiol.2004.067934

Yu, W. (2015). Polarized ATP distribution in urothelial mucosal and serosal space is differentially regulated by stretch and ectonucleotidases. *Am. J. Physiol. Physiol.* 309, F864–F872. doi:10.1152/ajprenal.00175.2015

Yu, W., Sun, X., Robson, S. C., and Hill, W. G. (2014). ADP-induced bladder contractility is mediated by P2Y 12 receptor and temporally regulated by ectonucleotidases and adenosine signaling. *FASEB J.* 28, 5288–5298. doi:10.1096/fj.14-255885

frontiers | Frontiers in Physiology

TYPE Original Research
PUBLISHED 29 June 2023
DOI 10.3389/fphys.2023.1224088

OPEN ACCESS

EDITED BY
Monica Akemi Sato,
Faculdade de Medicina do ABC, Brazil

REVIEWED BY
Roberto Almeida,
Faculdade de Medicina do ABC, Brazil
Jun-Ho La,
University of Texas Medical Branch at Galveston, United States

*CORRESPONDENCE
Limin Liao,
lmliao@263.net

RECEIVED 17 May 2023
ACCEPTED 19 June 2023
PUBLISHED 29 June 2023

CITATION
Zhou Z, Wang X, Li X and Liao L (2023), Transdermal tibial nerve optogenetic stimulation targeting C-fibers.
Front. Physiol. 14:1224088.
doi: 10.3389/fphys.2023.1224088

Transdermal tibial nerve optogenetic stimulation targeting C-fibers

Zhonghan Zhou[1,2,3,5,6], Xuesheng Wang[2,3,4,5,6], Xunhua Li[2,3,4,5,6] and Limin Liao[1,2,3,4,5,6]*

[1]Shandong University, Jinan, Shandong, China, [2]Department of Urology, China Rehabilitation Research Center, Beijing, China, [3]University of Health and Rehabilitation Sciences, Qingdao, Shandong, China, [4]School of Rehabilitation, Capital Medical University, Beijing, China, [5]China Rehabilitation Science Institute, Beijing, China, [6]Beijing Key Laboratory of Neural Injury and Rehabilitation, Beijing, China

Purpose: To explore whether stimulation of C-fibers in tibial nerves can induce bladder inhibition by optogenetic transdermal illumination.

Methods: Ten rats were injected with AAV2/6-hSyn-ChR2(H134R)-EYFP into the tibial nerves. Transurethral cystometry was performed 4 weeks after the virus injection. Illumination (473-nm blue light at 100 mW) was performed with the fiber positioned above the right hind paw near the ankle. The light transmission efficiency was examined with a laser power meter. The effects on cystometry were compared before and after illumination with the bladder infused with normal saline and acetic acid, respectively.

Result: Upon transdermal delivery of 473-nm light at a peak power of 100 mW, the irradiance value of 0.653 mW/mm2 at the target region was detected, which is sufficient to activate opsins. The photothermal effect of 473-nm light is unremarkable. Acute inhibitory responses were not observed during stimulation regarding any of the bladder parameters; whereas, after laser illumination for 30 min, a statistically significant increase in bladder capacity with the bladder infused with normal saline (from 0.53 ± 0.04 mL to 0.72 ± 0.05 mL, $p < 0.001$) and acetic acid (from 0.25 ± 0.02 mL to 0.37 ± 0.04 mL, $p < 0.001$) was detected. A similar inhibitory response was observed with pulsed illumination at both 10Hz and 50Hz. However, illumination did not significantly influence base pressure, threshold pressure, or peak pressure.

Conclusion: In this preliminary study, it can be inferred that the prolonged bladder inhibition is mediated by the stimulation of C-fibers in the tibial nerves, with no frequency-dependent characteristics. Although the 473-nm blue light has limited penetration efficacy, it is sufficient to modulate bladder functions through transdermal illumination on the superficial peripheral nervous system.

KEYWORDS

optogenetics, tibial nerve, transdermal stimulation, bladder, rats

1 Introduction

Tibial nerve stimulation (TNS), approved by the Food and Drug Administration (FDA) in 2005, is a well-established third-line therapy for overactive bladder (OAB) (Gupta et al., 2015). The precise mechanism is still unclear; however, accumulating evidence suggests that bladder inhibitory reflexes play an important role (Yecies et al., 2018; Paquette and Yoo,

2019). Evidence from animal studies indicates that the small myelinated Aδ in the afferent tibial nerve may be responsible for bladder modulation; recruiting C-fibers does not enhance the bladder-inhibitory effects further (Sato et al., 1980; Kovacevic and Yoo, 2015). This conclusion is supported by the fact that a low stimulation amplitude (4–10T_{mot}) was sufficient for inhibiting OAB, the range of which was consistent with the Aβ-fiber activation threshold. However, recently a study revealed that unmyelinated C-fibers, not Aδ or Aβ, were recruited during TNS in a continuous-fill rat model. The authors argued that repeated bladder filling and emptying reinforces excitatory neural circuitry and propensity to void; the activation of C-fibers under the continuous-fill bladder condition (at 100T_{mot}) is required for eliciting inhibitory responses (Paquette and Yoo, 2019). There are also studies suggesting that stimulating C fibers may lead to bladder excitation (McPherson, 1966; Kovacevic and Yoo, 2015). These inconsistent results indicate that the role of C fibers in the tibial nerve remains unclear.

Optogenetics is an emerging technology that enables the activation or inhibition of specific cells with light (Zhou and Liao, 2021). The expression of the light-sensitive protein, opsin, is genetically encoded, providing a way to target the neurons of interest. Channelrhodopsin 2 (ChR2) is the most commonly employed unselective depolarizing opsin. Exposure to blue light with a wavelength of 473 nm can induce a structural conformational inversion of 11-cis-retinal to all-trans-retinal, resulting in the opening of channels, the influx of positive ions, depolarization of the membrane, and activation of neurons. Optogenetics has revolutionized our ability to influence neural activity with high precision. Previous studies reported that AAV2/6 was largely specific to unmyelinated nociceptive neurons (Iyer et al., 2014). In this study, we selectively expressed ChR2 in C-fibers, and investigated whether stimulation of C-fibers in tibial nerves can induce bladder inhibition, bladder activation, or neither. Moreover, instead of traditional optogenetics that requires an invasive light-delivery device to be surgically implanted in the body (Zhou and Liao, 2021), we utilized transdermal illumination as a non-invasive approach to target superficial nerves, and subsequently discussed the potential of this method as an alternative or supplementary approach to traditional neural electrical stimulation.

2 Materials and methods

2.1 Experimental animals

Ten female Sprague-Dawley rats (180–220 g [g]) were used in this experiment. Animals were housed under standard conditions with food and water *ad libitum*. All procedures were performed in accordance with protocols approved by the Capital Medical University Laboratory Animal Welfare and Ethical Review Board (permit number, AEEI-2022-102).

2.2 Virus injection

The AAV2/6-hSyn-ChR2(H134R)-EYFP and AAV2/6-hSyn-EYFP were purchased from OBIO Technology Co. (China), which is reported to target nociceptive neurons (Iyer et al., 2014). During surgery, rats underwent anesthesia with 2% pentobarbital (30 mg/kg) by intraperitoneal injection. Breathing was monitored, and body temperature was maintained with a heating plate throughout the experiment. The tibial nerve was accessed through the medial side of the right hind leg near the ankle. The nerve was removed from the underlying fascia under a microscope. A 30-gauge Hamilton syringe (10 μL) was inserted under the epineurium of the nerve, and a total of 5×10^{10} vector genomes were injected. Fast Green (1%; 1 μL) was added to visualize the injected solution. After the injection, the incision was closed with sutures, and the rats were treated with ampicillin sodium for 3 days.

2.3 Cystometry

Transurethral cystometry under urethane anesthesia (1.2 g/kg, intraperitoneal) was performed 4 weeks after virus injection, as described previously (Kashyap et al., 2018). A polyethylene catheter (PE-50) was inserted transurethrally into the bladder, and the catheter was connected by a three-way stopcock to a micro-infusion pump (Stoelting, IL) and pressure transducer (MP150; Biopac, CA). The bladder was filled with normal saline (NS) at a rate of 0.08 mL/min. The bladder capacity (BC) was defined as the volume of infusion that triggered the first micturition waves and corresponding urine leakage. Bladders were emptied by gently pressing on the abdomen. The average of at least 3 BCs was measured after the stabilization of the cystometry. An OAB model was induced by infusion of 0.25% acetic acid (AA). A significant decrease in BC indicated successful disease induction.

2.4 Blue light illumination

A blue light was generated from a 473-nm laser with a 100-μm optical fiber (1–100 mW, RWD Life Science Co., Shenzhen, China). Illumination (100 mW, constant/10Hz/50Hz) was performed with the fiber positioned 1 cm above the right hind paw near the ankle, with the fur shaved. Acute bladder responses (during the illumination) and prolonged bladder responses (after illumination for 30 min) were both explored. An LP10 laser power meter (Sanwa Electric Instrument Co., Tokyo, Japan) was used to assess light transmission efficiency. An SDR473 radiometer (Shenzhen Speedre Technology Co., Guangzhou, China) was used to assess the light intensity. A thermocouple sensor (K-type) connected to a digital thermometer (DM6801A) was used to detect temperature changes under illumination. The tip of the thermocouple sensor was inserted into the target tibial nerve region or placed at the skin surface for local temperature detection.

2.5 Immunofluorescence assessment

The rats were sacrificed after cystometry, and the tibial nerves and L6-S1 dorsal root ganglions (DRGs) were obtained immediately. Tissues were fixed with 4% PFA and then embedded with OCT compound. Tissues were washed in OBS and incubated with blocking solution. Primary antibodies (1:100 Anti-Peripherin, ab246502) were diluted in blocking solution and incubated in sections. Slides were washed 3 times and incubated with secondary antibodies (1:200 Goat anti-rabbit IgG Alexa Fluor 488). Samples were imaged using a DMI8 microscope (Leica).

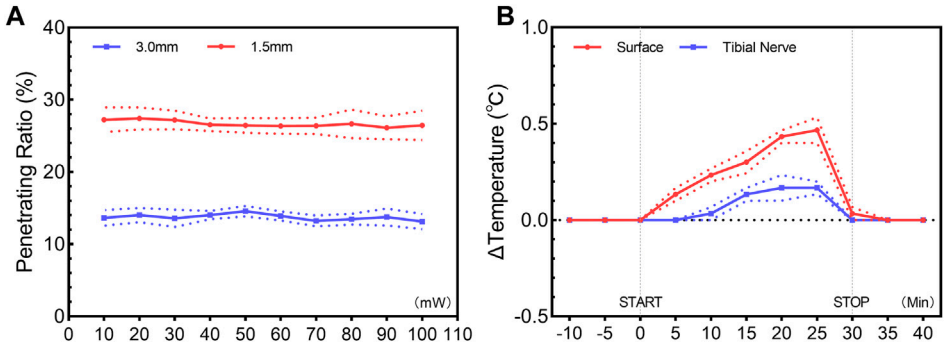

FIGURE 1
Penetration ratio **(A)** and photothermal effect **(B)** of transdermal illumination. **(A)** Penetration ratio of 473-nm constant illumination through skin and subcutaneous tissue, showing a ratio of 26.7% ± 0.2% and 13.7% ± 0.2% at a depth of 1.5 mm and 3.0 mm, with little dependence on the incident intensity. **(B)** Temporal change of temperature for skin surface and target tibial nerve region, showing the unremarkable photothermal effect of a 473-nm constant illumination. Data are presented as mean ± SEM (n = 3 for all experiments).

2.6 Statistics

Statistical analysis was performed using R (version 4.2.0; The R Foundation, Vienna, Austria). Results are expressed as means ± SEM. A paired *t*-test was used to compare the cystometry parameters before and after transdermal illumination. A value of $p < 0.05$ was considered statistically significant for all comparisons.

3 Results

3.1 Penetrating ratio and photothermal effect of a 473-nm light

Previous studies have revealed the relatively limited penetration depth of visible light in biological tissues (Ash et al., 2017). Our results revealed a penetrating ratio of 26.7% ± 0.2% at a depth of 1.5 mm and 13.7% ± 0.2% at a depth of 3.0 mm, showing little dependence on the incident intensity (Figure 1A). Upon transdermal delivery of 473-nm light at a peak power of 100 mW, the irradiance value of 0.653 mW/mm^2 at the target region was detected. Although the tissue penetration of the 473-nm light was limited, for the superficial tibial nerve at the hind leg near the ankle, the light is sufficient to activate ChR2 for cation influx (Chen et al., 2018). The photothermal effect of a 473-nm light was unremarkable. After illumination of 30 min, only a slight temperature increase at the skin surface (0.47°C ± 0.09°C) and the target region (0.16°C ± 0.04°C) were detected (Figure 1B). Based on these results, we confirmed it is possible to manipulate the tibial nerve through transdermal illumination.

3.2 Acute bladder responses under illumination

Expression of ChR2-EYFP in C-fibers was confirmed by the immunohistology of the tibial nerves and DRGs 4 weeks after transfection (Figure 2). We tested whether transdermal tibial nerve optogenetic stimulation targeting C-fibers influences bladder activity. Acute inhibitory responses were not observed during infusion with NS regarding any of the bladder parameters (Figure 3A). The irritation of AA successfully induced the OAB model, with the BC from 0.61 ± 0.05 mL to 0.35 ± 0.05 mL ($p = 0.042$). Similarly, in the OAB rats, no acute bladder responses were detected during illumination (Figure 3B).

3.3 Prolonged bladder responses after illumination for 30 min

After illumination for 30 min in the physiological bladder, a statistically significant increase of BC (0.72 ± 0.05 mL) compared with baseline (0.53 ± 0.04 mL, $p < 0.001$; Figure 3C) was detected. The results showed in pathologic bladder a statistically significant increase of BC after illumination of the tibial nerve for 30 min (0.37 ± 0.04 mL) compared with baseline (0.25 ± 0.02 mL, $p < 0.001$, Figure 3D). Illumination did not significantly influence base pressure, threshold pressure, or peak pressure in both physiologic and pathologic conditions. We furtherly explored whether the inhibitory response was associated with illumination frequency. Continuous stimulation, pulsed 10Hz stimulation, and 50Hz stimulation all elicited an inhibitory response in BC, with no significant differences among different stimulation protocols (Figure 3E).

4 Discussion

4.1 The functional role of C-fibers in tibial nerves

The functional role of different fiber types is still not clear. Previous studies revealed that the Aδ-fibers were activated under the required stimulation intensity for TNS(4–10 T_{mot}), while C-fibers were activated in a much higher range (100–200 T_{mot}) (Sato et al., 1980; Kovacevic and Yoo, 2015). Based on these results, it is inferred that the inhibitory responses were mediated by Aδ fibers rather than C-fiber afferents. However, a recent study revealed that TNS leads to bladder-inhibitory effects only at stimulation amplitudes that

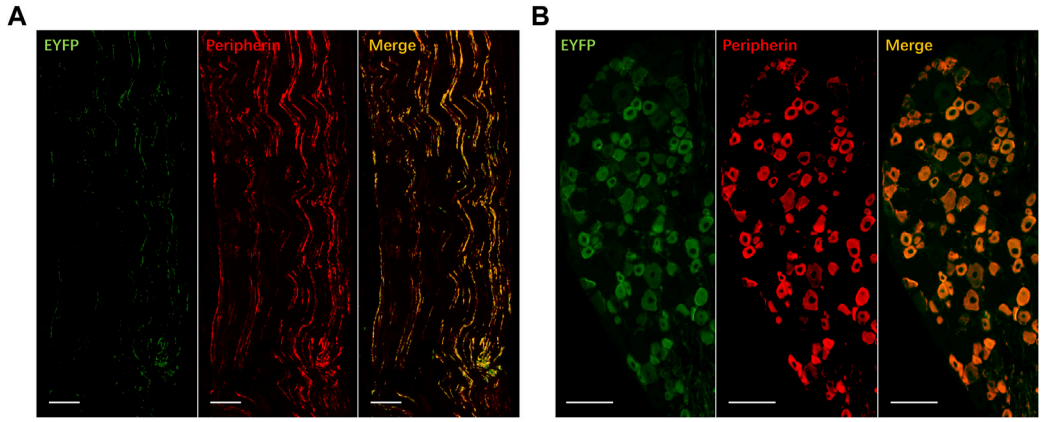

FIGURE 2
Expression of EYFP for ChR2 transfection in tibial nerve **(A)** and dorsal root ganglion **(B)**. ChR2-EYFP: green; Peripherin: red, marker for C-fibers; Co-expressed: yellow. Bar: 100 μm.

electrically recruited unmyelinated C-fibers (Paquette and Yoo, 2019). Similarly, Wallace et al. found that stimulation of C-fibers can relieve bladder pain. What's more intriguing is that Mapherson et al. reported bladder excitation evoked by applying ice to the hind paws in cats, which was attributed to C-fibers activated by low-temperature input (McPherson, 1966; Kovacevic and Yoo, 2015). Based on these results, it is still unknown whether stimulating C fibers are inactive, inhibitory, or excitatory in nature. In previous studies, the activation of different fiber types was achieved by choosing the electrical stimulation intensity. However, electrical stimulation lacks selectivity in nature. Optogenetics provides a powerful tool to target C-fibers in a high spatial precision manner. Previous studies have revealed that AAV2/6 has a preference for transducing unmyelinated fibers (Yu et al., 2013; Kudo et al., 2021). Our immunofluorescence result also suggests that most ChR2 expression is detected on peripherin-positive fibers and neurons, and the "off-target effect" of AAV2/6 transfection is relatively low. In this preliminary study, we found that illumination of C-fibers can both induce prolonged bladder inhibitory responses when the bladder was infused with NS and AA, respectively.

4.2 Absence of acute inhibitory responses

Previous experimental studies have shown that TNS can elicit acute inhibitory effects in rats (Su et al., 2012a; Su et al., 2015)and cats (Tai et al., 2011a; Tai et al., 2011b), with the mechanism still largely unknown. In contrast, our results did not show any significant acute responses in all bladder parameters. The acute inhibitory effect observed during electrical stimulation appears to differ from prolonged bladder inhibition in our study (Paquette and Yoo, 2019). The former acts like an "on-and-off" switch and can take only a few seconds or minutes to observe the influence on the bladder, whereas the latter indicates a different mechanism of neuromodulation. The illumination directly leads to the depolarization of the membrane and activation of C-fibers, while the exact mechanisms of the responses remain unclear. Previous studies revealed that intense stimulation of C-fibers may exert efferent effects, secreting neuropeptide, including substance P, calcitonin gene-related peptide, neurokinin, et al., and recruiting other fibers in the periphery (Lao and Marvizon, 2005; Adelson et al., 2009; Edvinsson et al., 2019). Further investigation is needed to explore whether the prolonged stimulation of C-fibers in the tibial nerve also affects bladder function through this mechanism. Prolonged inhibition may resemble the long-term depression of the central micturition reflex, which requires more time to develop (Jiang and Lindstrom, 1998; Su et al., 2012b). The signals may be transmitted to the spinal cord and then to higher regions in the central nervous system. Research has shown that electrical stimulation of peripheral nerves can lead to an increase in endogenous opioid peptide levels within the central nervous system (Yaksh and Elde, 1981; Wang et al., 2005). Of specific note, the level of stimulation required to produce this opioid peptide release is one that activates small nociceptive fibers. It can be inferred that the prolonged bladder inhibition may be mediated by the stimulation of C-fibers in the tibial nerves, but the recruitment and activation of other nerve fibers as well as the upstream targets remain unclear. More research is required to elucidate this potential peripheral and central mechanism in the future.

4.3 Consideration of stimulation frequency

The bladder reflex elicited by electrical stimulation of tibial nerves exhibits frequency-dependent characteristics, where an inhibitory response can be obtained at low frequencies (5 Hz–30 Hz in rats and cats) and an excitatory response can be evoked at high frequencies (50 Hz) (Kovacevic and Yoo, 2015). We found that both 10 Hz and 50 Hz illumination resulted in an inhibitory effect similar to constant illumination. The excitatory response was not observed at high frequencies. It appears that

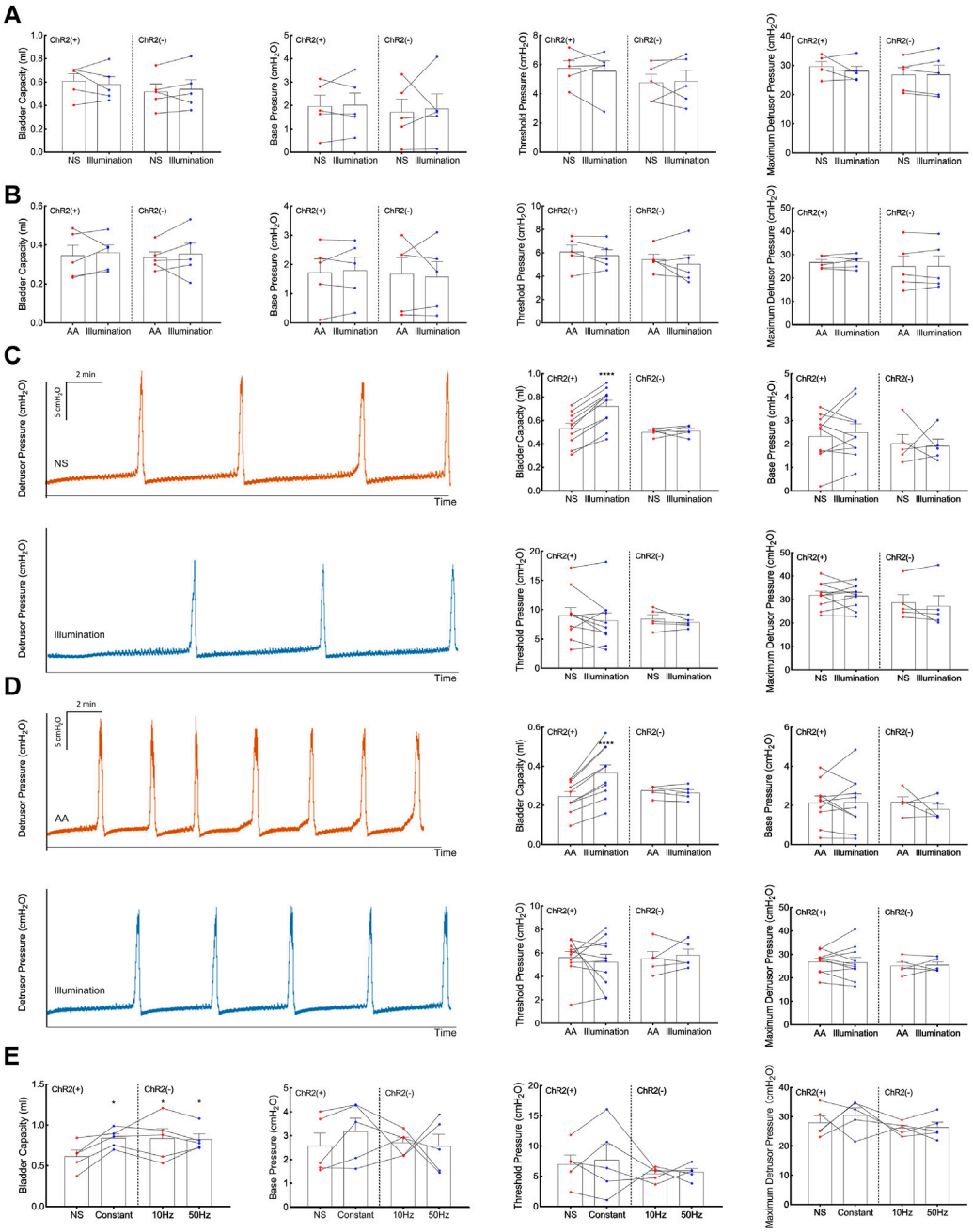

FIGURE 3
Acute and prolonged bladder responses to 473-nm illumination. **(A)** Acute bladder responses during illumination on the physiologic (normal saline-infused) bladder. **(B)** Acute bladder responses during illumination on the pathologic (acetic acid-infused) bladder. **(C)** Prolonged bladder responses after constant illumination for 30 min on the physiologic (normal saline-infused) bladder. **(D)** Prolonged bladder responses after constant illumination for 30 min on the pathologic (acetic acid-infused) bladder. **(E)** Prolonged bladder responses under different illumination protocols (Constant, pulsed 10Hz, pulsed 50Hz, 30 min). Data are presented as mean ± SEM. *: $p < 0.05$; ****: $p < 0.0001$.

evoking excitatory response by TNS depends on multiple factors, and the underlying mechanism remains unknown. In this optogenetic experiment, we directly manipulate C-fibers, which excluded the possible impact of frequency and intensity on the selective activation of nerve fibers. The bladder responses elicited by the excitation of C-fibers did not exhibit frequency-dependent characteristics, indicating that there may be other mechanisms underlying bladder excitation at specific electrical frequencies.

4.4 Concerns of further clinical application

Optogenetics has become a powerful cell type-specific tool that enables light-mediated activation or inhibition of neural functions (Zhou and Liao, 2021). Optogenetic modulation is a potential alternative to electrical modulation. There is still a long way to go before it can be applied clinically. Traditionally, optogenetic manipulation requires surgical device implantation

of tethered fiber optics or microscale light-emitting diodes, which is invasive and limited the feasibility of clinical applications. Transdermal illumination provides a noninvasive way to achieve optogenetic control of superficial peripheral afferents or muscles. It's known that blue light with a wavelength of 473 nm has limited penetration. Our research confirmed the acceptable penetrating ratio of 473-nm blue light, which is sufficient to activate ChR2 for tibial nerve stimulation in rats. Although we confirmed the feasibility of transdermal illumination using a 473-nm blue light, there are still concerns about the limited penetration depth, especially when considering application in human beings. Many attempts have been made to improve the optogenetic activation of deep tissues. Maimon et al. (2017) revealed that higher virus concentrations can deliver more transgene copies to the neuron genome; therefore, increased density of ChR2 channels can lead to a lower required fluence rate for activation. The absorption and scattering coefficients of red light are significantly lower than those of blue light. Chrimson (Urmann et al., 2017) and ReaChR (Lin et al., 2013) were two red-shifted channelrhodopsin with a wavelength peak of 600–700 nm. These two opsin variations enable the activation of deeper tissues and can reduce the required illumination power. Near-infrared light (NIR), with a wavelength of 650–1350 nm, achieves a maximal penetration depth. Chen et al. (2018) developed transcranial NIR optogenetic stimulation of deep-brain tissues via lanthanide-doped upconversion nanoparticles (UCNPs), which can convert NIR photons into visible photons. The emission of UCNPs can be restricted to a specific wavelength using selective lanthanide-ion doping. The Yb^{3+}-Tm^{3+} couple emits blue light compatible with activation of ChR2, while the Yb^{3+}-Er^{3+} couple leads to green light for activation of halorhodopsin (NpHR) or archaerhodopsin (Arch). Hong (2020) developed an ultrasound-mediated deep-tissue light source for optogenetics. They made zinc sulfide nanoparticles doped with silver and cobalt, which can trap electrons and store energy until triggered by focused ultrasound and emitting blue light. Compared with direct light illumination, focused ultrasound enables a penetration depth of roughly 5 cm. These approaches provide a possible solution for noninvasive neuromodulation of the bladder, including the targets of the sacral nerve, pudendal nerve, or direct bladder smooth muscle cells (Park et al., 2017).

There are still challenges and limitations to be solved before further application of transdermal illumination of the peripheral nerves. First, the expression of ChR2 usually decreases after several weeks or months. New stable viruses should be developed to achieve persistent expression. Second, the thickness of skin and subcutaneous fat as well as the angle of the incident beam affects opsin activation. Improvement of the light-delivery device would decrease exposure variation. Third, exploring a more noninvasive and effective transducing route rather than intranerve injection is essential for translation into clinical practice. Recently, attempts have been made to introduce optogenetics as a therapeutic approach in humans, including the PIONEER study (NCT03326336) (Sahel et al., 2021). We believe such investigations can reveal the prospect of future therapeutic strategies.

5 Conclusion

In this preliminary study, we optogenetically stimulated C-fibers in the tibial nerves. It can be inferred that the prolonged bladder inhibition is mediated by the stimulation of C-fibers in the tibial nerves, with no frequency-dependent characteristics. Although a 473-nm blue light has limited penetration efficacy, it is sufficient to modulate bladder functions through transdermal illumination on the superficial peripheral nervous system. More effects need to be paid to this approach before we see the dawn of clinical translation for optogenetics.

Data availability statement

The raw data supporting the conclusion of this article will be made available by the authors, without undue reservation.

Ethics statement

The animal study was reviewed and approved by the Capital Medical University Laboratory Animal Welfare and Ethical Review Board (permit number, AEEI-2022-102).

Author contributions

LL conceptualization; funding acquisition and project administration; writing-review and editing. ZZ experiment; writing-original draft. XW assistance in performing the experiment. XL assistance in performing the experiment. All authors contributed to the article and approved the submitted version.

Funding

This study was funded by the Natural Science Foundation of Beijing, China (Grant no. 7222234), the fundamental research funds for central public welfare research institutes (Grant no. 2023CZ-1), the National Natural Science Foundation of China (Grant no. 82170792), and the Research Projects of China Rehabilitation Research Center (Grant no. 2021zx-10).

Conflict of interest

The authors declare that the research was conducted in the absence of any commercial or financial relationships that could be construed as a potential conflict of interest.

Publisher's note

References

Adelson, D., Lao, L., Zhang, G., Kim, W., and Marvizon, J. C. (2009). Substance P release and neurokinin 1 receptor activation in the rat spinal cord increase with the firing frequency of C-fibers. *Neuroscience* 161 (2), 538–553. doi:10.1016/j.neuroscience.2009.03.058

Ash, C., Dubec, M., Donne, K., and Bashford, T. (2017). Effect of wavelength and beam width on penetration in light-tissue interaction using computational methods. *Lasers Med. Sci.* 32 (8), 1909–1918. doi:10.1007/s10103-017-2317-4

Chen, S., Weitemier, A. Z., Zeng, X., He, L., Wang, X., Tao, Y., et al. (2018). Near-infrared deep brain stimulation via upconversion nanoparticle-mediated optogenetics. *Science* 359 (6376), 679–684. doi:10.1126/science.aaq1144

Edvinsson, J. C. A., Warfvinge, K., Krause, D. N., Blixt, F. W., Sheykhzade, M., Edvinsson, L., et al. (2019). C-fibers may modulate adjacent Aδ-fibers through axon-axon CGRP signaling at nodes of Ranvier in the trigeminal system. *J. Headache Pain* 20 (1), 105. doi:10.1186/s10194-019-1055-3

Gupta, P., Ehlert, M. J., Sirls, L. T., and Peters, K. M. (2015). Percutaneous tibial nerve stimulation and sacral neuromodulation: An update. *Curr. Urol. Rep.* 16 (2), 4. doi:10.1007/s11934-014-0479-1

Hong, G. (2020). Seeing the sound. *Science* 369 (6504), 638. doi:10.1126/science.abd3636

Iyer, S. M., Montgomery, K. L., Towne, C., Lee, S. Y., Ramakrishnan, C., Deisseroth, K., et al. (2014). Virally mediated optogenetic excitation and inhibition of pain in freely moving nontransgenic mice. *Nat. Biotechnol.* 32 (3), 274–278. doi:10.1038/nbt.2834

Jiang, C. H., and Lindstrom, S. (1998). Prolonged increase in micturition threshold volume by anogenital afferent stimulation in the rat. *Br. J. Urol.* 82 (3), 398–403. doi:10.1046/j.1464-410x.1998.00682.x

Kashyap, M. P., Pore, S. K., de Groat, W. C., Chermansky, C. J., Yoshimura, N., and Tyagi, P. (2018). BDNF overexpression in the bladder induces neuronal changes to mediate bladder overactivity. *Am. J. Physiol. Ren. Physiol.* 315 (1), F45–F56. doi:10.1152/ajprenal.00386.2017

Kovacevic, M., and Yoo, P. B. (2015). Reflex neuromodulation of bladder function elicited by posterior tibial nerve stimulation in anesthetized rats. *Am. J. Physiol. Ren. Physiol.* 308 (4), F320–F329. doi:10.1152/ajprenal.00212.2014

Kudo, M., Wupuer, S., Fujiwara, M., Saito, Y., Kubota, S., Inoue, K. I., et al. (2021). Specific gene expression in unmyelinated dorsal root ganglion neurons in nonhuman primates by intra-nerve injection of AAV 6 vector. *Mol. Ther. Methods Clin. Dev.* 23, 11–22. doi:10.1016/j.omtm.2021.07.009

Lao, L., and Marvizon, J. C. (2005). GABA(A) receptor facilitation of neurokinin release from primary afferent terminals in the rat spinal cord. *Neuroscience* 130 (4), 1013–1027. doi:10.1016/j.neuroscience.2004.10.019

Lin, J. Y., Knutsen, P. M., Muller, A., Kleinfeld, D., and Tsien, R. Y. (2013). ReaChR: A red-shifted variant of channelrhodopsin enables deep transcranial optogenetic excitation. *Nat. Neurosci.* 16 (10), 1499–1508. doi:10.1038/nn.3502

Maimon, B. E., Zorzos, A. N., Bendell, R., Harding, A., Fahmi, M., Srinivasan, S., et al. (2017). Transdermal optogenetic peripheral nerve stimulation. *J. Neural Eng.* 14 (3), 034002. doi:10.1088/1741-2552/aa5e20

McPherson, A. (1966). The effects of somatic stimuli on the bladder in the cat. *J. Physiol.* 185 (1), 185–196. doi:10.1113/jphysiol.1966.sp007980

Paquette, J. P., and Yoo, P. B. (2019). Recruitment of unmyelinated C-fibers mediates the bladder-inhibitory effects of tibial nerve stimulation in a continuous-fill anesthetized rat model. *Am. J. Physiol. Ren. Physiol.* 317 (1), F163–F171. doi:10.1152/ajprenal.00502.2018

Park, J. H., Hong, J. K., Jang, J. Y., An, J., Lee, K. S., Kang, T. M., et al. (2017). Optogenetic modulation of urinary bladder contraction for lower urinary tract dysfunction. *Sci. Rep.* 7, 40872. doi:10.1038/srep40872

Sahel, J. A., Boulanger-Scemama, E., Pagot, C., Arleo, A., Galluppi, F., Martel, J. N., et al. (2021). Partial recovery of visual function in a blind patient after optogenetic therapy. *Nat. Med.* 27 (7), 1223–1229. doi:10.1038/s41591-021-01351-4

Sato, A., Sato, Y., and Schmidt, R. F. (1980). Reflex bladder activity induced by electrical stimulation of hind limb somatic afferents in the cat. *J. Auton. Nerv. Syst.* 1 (3), 229–241. doi:10.1016/0165-1838(80)90019-3

Su, X., Nickles, A., and Nelson, D. E. (2012a). Comparison of neural targets for neuromodulation of bladder micturition reflex in the rat. *Am. J. Physiol. Ren. Physiol.* 303 (8), F1196–F1206. doi:10.1152/ajprenal.00343.2012

Su, X., Nickles, A., and Nelson, D. E. (2015). Differentiation and interaction of tibial versus spinal nerve stimulation for micturition control in the rat. *Neurourol. Urodyn.* 34 (1), 92–97. doi:10.1002/nau.22506

Su, X., Nickles, A., and Nelson, D. E. (2012b). Neuromodulation in a rat model of the bladder micturition reflex. *Am. J. Physiol. Ren. Physiol.* 302 (4), F477–F486. doi:10.1152/ajprenal.00515.2011

Tai, C., Chen, M., Shen, B., Wang, J., Roppolo, J. R., and de Groat, W. C. (2011b). Irritation induced bladder overactivity is suppressed by tibial nerve stimulation in cats. *J. Urol.* 186 (1), 326–330. doi:10.1016/j.juro.2011.04.023

Tai, C., Shen, B., Chen, M., Wang, J., Roppolo, J. R., and de Groat, W. C. (2011a). Prolonged poststimulation inhibition of bladder activity induced by tibial nerve stimulation in cats. *Am. J. Physiol. Ren. Physiol.* 300 (2), F385–F392. doi:10.1152/ajprenal.00526.2010

Urmann, D., Lorenz, C., Linker, S. M., Braun, M., Wachtveitl, J., and Bamann, C. (2017). Photochemical properties of the red-shifted channelrhodopsin chrimson. *Photochem Photobiol.* 93 (3), 782–795. doi:10.1111/php.12741

Wang, Y., Zhang, Y., Wang, W., Cao, Y., and Han, J. S. (2005). Effects of synchronous or asynchronous electroacupuncture stimulation with low versus high frequency on spinal opioid release and tail flick nociception. *Exp. Neurol.* 192 (1), 156–162. doi:10.1016/j.expneurol.2004.11.003

Yaksh, T. L., and Elde, R. P. (1981). Factors governing release of methionine enkephalin-like immunoreactivity from mesencephalon and spinal cord of the cat *in vivo*. *J. Neurophysiol.* 46 (5), 1056–1075. doi:10.1152/jn.1981.46.5.1056

Yecies, T., Li, S., Zhang, Y., Cai, H., Shen, B., Wang, J., et al. (2018). Spinal interneuronal mechanisms underlying pudendal and tibial neuromodulation of bladder function in cats. *Exp. Neurol.* 308, 100–110. doi:10.1016/j.expneurol.2018.06.015

Yu, H., Fischer, G., Ferhatovic, L., Fan, F., Light, A. R., Weihrauch, D., et al. (2013). Intraganglionic AAV6 results in efficient and long-term gene transfer to peripheral sensory nervous system in adult rats. *PLoS One* 8 (4), e61266. doi:10.1371/journal.pone.0061266

Zhou, Z., and Liao, L. (2021). Optogenetic neuromodulation of the urinary bladder. *Neuromodulation* 24 (7), 1229–1236. doi:10.1111/ner.13516

frontiers | Frontiers in Physiology

TYPE Original Research
PUBLISHED 04 September 2023
DOI 10.3389/fphys.2023.1249560

OPEN ACCESS

EDITED BY
Brian James Morris,
The University of Sydney, Australia

REVIEWED BY
Peter Sandner,
Bayer, Germany
Aura Kullmann,
NeuroOne Medical Technology Corporation, United States

*CORRESPONDENCE
Patrik Aronsson,
patrik.aronsson@pharm.gu.se

RECEIVED 28 June 2023
ACCEPTED 22 August 2023
PUBLISHED 04 September 2023

CITATION
Aronsson P, Stenqvist J, Ferizovic E, Danielsson E, Jensen A, Simonsen U and Winder M (2023), Soluble guanylate cyclase mediates the relaxation of healthy and inflamed bladder smooth muscle by aqueous nitric oxide.
Front. Physiol. 14:1249560.
doi: 10.3389/fphys.2023.1249560

Soluble guanylate cyclase mediates the relaxation of healthy and inflamed bladder smooth muscle by aqueous nitric oxide

Patrik Aronsson [1]*, Johanna Stenqvist[1], Ena Ferizovic[1], Emelie Danielsson[1], Anna Jensen[1], Ulf Simonsen[2] and Michael Winder[1]

[1]Department of Pharmacology, Institute of Neuroscience and Physiology, The Sahlgrenska Academy, University of Gothenburg, Gothenburg, Sweden, [2]Department of Biomedicine, Faculty of Health, University of Aarhus, Aarhus, Denmark

Introduction: Due to its chemical properties, functional responses to nitric oxide (NO) are often difficult to examine. In the present study, we established a method to produce NO in an aqueous solution and validated its capacity to evoke functional responses in isolated rat bladders. Furthermore, we compared the NO responses to the commonly used NO donor sodium nitroprusside (SNP). We also investigated the impact of ongoing inflammation on the involvement of soluble guanylate cyclase (sGC) dependent signaling in NO relaxation.

Methods: A setup to produce an aqueous NO solution was established, allowing the production of an aqueous solution containing a calculated NO concentration of 2 mM. Sixty male Sprague-Dawley rats received either no treatment (controls) or cyclophosphamide (CYP; 100 mg*kg^{-1} i.p., 60 h prior to the experiment) to induce experimental cystitis. Bladder strip preparations were mounted in organ baths and studied at basal tension or pre-contracted with methacholine (3 μM). Aqueous NO solution (40–400 μL; 2 mM corresponding to 4–40 μM) or SNP (1–1,000 μM) was added cumulatively in increasing concentrations. Relaxation to aqueous NO was also studied in the presence of the sGC inhibitor ODQ (0.25–25 μM). The expression of sGC was investigated by immunohistochemical analysis.

Results: The NO solution caused functional relaxations in both controls and inflamed bladder preparations. NO-induced relaxations were significantly greater in inflamed bladder strips at basal tension, whereas no differences were seen in methacholine pre-contracted strips. In the presence of the sGC inhibitor ODQ in a high concentration, the NO-evoked relaxations were abolished in both control and inflamed preparations. At a lower concentration of ODQ, only NO relaxations in inflamed preparations were attenuated. Immunohistochemical analysis showed that sGC was expressed in the detrusor and mucosa, with a significantly lower expression in the inflamed detrusor.

Conclusion: In the present study, we found that aqueous NO solution induces relaxation of the rat detrusor by activating soluble guanylate cyclase in both control and inflamed bladder strips. Induction of inflammation conceivably leads to decreased sGC expression in the detrusor, which may explain the different susceptibility towards inhibition of sGC in inflamed versus control tissue. The use

10.3389/fphys.2023.1249560

of an aqueous NO solution should be further considered as a valuable complement to the pharmacological tools currently used.

KEYWORDS

nitric oxide, bladder, cystitis, relaxation, sGC (soluble guanylate cyclase), NO donor, sodium nitroprusside (SNP), animal study

Introduction

Over the past quarter century, the functional role of nitric oxide (NO) in the lower urinary tract has been outlined. Early on, NO was established as one of the non-adrenergic, non-cholinergic (NANC) signaling molecules released by the urothelium (Winder et al., 2014). A number of studies imply that NO exerts a relaxatory functional effect on the detrusor and modulates afferent signaling (Ozawa et al., 1999; Fujiwara et al., 2000; Andersson et al., 2008; Caremel et al., 2010). However, some studies have indicated that in certain conditions, NO can cause detrusor contractions (Liu and Lin-Shiau, 1997; Moon, 2002; Gillespie and Drake, 2004; Yanai et al., 2008). Apart from via activation of TRPV1 receptors, NO production can also be evoked by stimulation of autonomic receptors. Studies have shown that activation of β-adrenoceptors leads to NO release, mainly from the urothelium (Birder et al., 1998; Winder et al., 2017). During cystitis, urothelial NO production can also be evoked by activation of muscarinic receptors (Andersson et al., 2008; Andersson et al., 2012). The notion of altered nitrergic signaling in inflammation can today be considered an established feature that has been extensively demonstrated in a number of studies (Ozawa et al., 1999; Kang et al., 2004; Andersson et al., 2011; Sancho et al., 2014; Patel et al., 2020).

Despite the considerable number of studies that have been conducted to outline the functional roles of NO in the lower urinary tract, there are still missing pieces to the puzzle, for instance, an accurate description of which intracellular pathways that are involved in nitrergic signaling. Nevertheless, the involvement of the NO-sGC-cGMP pathway (Figure 1) has repeatedly been demonstrated in basic and clinical studies on various lower urinary tract pathologies (Logadottir et al., 2004; Kedia et al., 2008; Cho et al., 2017; Monica and Antunes, 2018; Zabbarova et al., 2021; Aydogdu et al., 2022). The effects of NO on detrusor contractility have been extensively examined using a wide range of experimental designs. These include *in vivo* (often cystometry), *ex vivo* (organ bath), and *in vitro* (cell cultures) methods (Andersson et al., 2008; Kajioka et al., 2008; Bustamante et al., 2010). Further, studies have utilized different approaches to investigate functional effects of NO. Commonly, either NO donors, such as sodium nitroprusside, nitric oxide synthase inhibitors like L-NNA and L-NAME, or PDE5-inhibitors, such as sildenafil, have been used (Gillespie and Drake, 2004; Andersson et al., 2012; Chakrabarty et al., 2019). Previous studies have in common the non-usage of NO *per se* as an agonist. The main reason for this is the rapid turnover of NO, with an approximate half-life of a few seconds in a normal oxygenated aqueous solution (Moncada et al., 1991). However, in the late 1990s, a method to produce NO in an oxygen-free aqueous solution was established by Simonsen and colleagues at Aarhus University (Feelisch and Kelm, 1991; Simonsen et al., 1999). In brief, pure argon followed by nitric oxide gas is led through

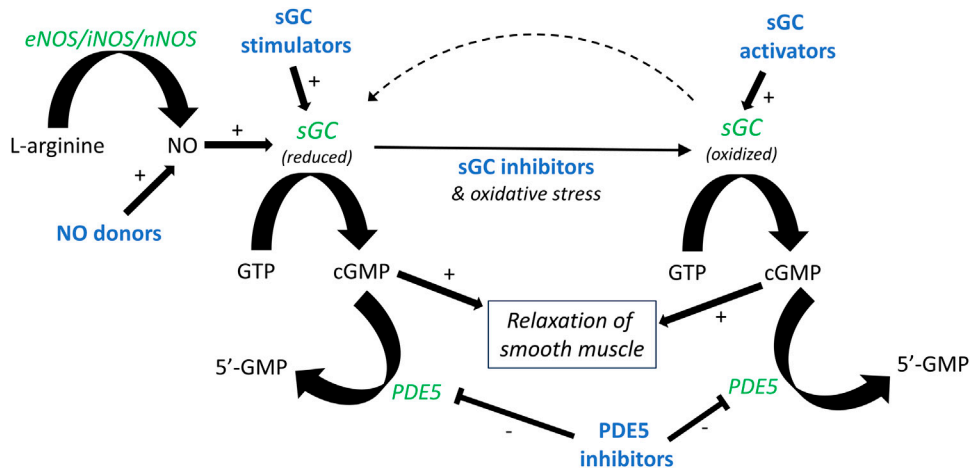

FIGURE 1
Outline of the NO-sGC-cGMP pathway. The formation of nitric oxide (NO) from L-arginine and molecular oxygen is catalyzed by nitric oxide synthase (NOS). NO binds to soluble guanylate cyclase (sGC), forming cyclic GMP (cGMP) and, in turn, leading to smooth muscle relaxation. Production of cGMP can similarly be induced by NO donors and sGC stimulators. Oxidative stress, for instance during inflammation, leads to oxidation of sGC. A similar effect is achieved by sGC inhibitors such as ODQ. Oxidized sGC cannot be activated by NO, but can instead be activated by sGC activators. Pharmacologically active drugs are illustrated in bold blue, and enzymes in green italics.

pyrogallol and/or sodium hydroxide, removing any traces of oxygen and higher nitrogen oxides, before reaching vials filled with Milli-Q water. Subsequently, NO is dissolved in an aqueous solution capped by inert argon gas. This yields a deoxygenized solution of pure NO in water, thus eliminating the risk of oxidation and breakdown of the substance, which opens the possibility for studies using NO as a classical agonist.

The current study had three interdependent aims. First, to validate the production and use of NO in aqueous solution for studies on bladder functional properties. Second, to study if the relaxations to NO were altered in a state of inflammation. Third, to test the hypothesis that NO in aqueous solution induces bladder relaxation via activation of soluble guanylate cyclase. For these purposes, rats were pre-treated with either saline, serving as control, or cyclophosphamide (CYP; 100 $mg^{*}kg^{-1}$ i.p.), to induce experimental cystitis. NO in aqueous solution was produced according to a previously published protocol (Simonsen et al., 1999). Bladder functional responses to NO in an aqueous solution were examined in a tissue bath setup and compared to those induced by the commonly used NO donor sodium nitroprusside (SNP) in the presence and absence of the soluble guanylate cyclase inhibitor 1H-[1,2,4]oxadiazolo[4,3-a]quinoxalin-1-one (ODQ). Further, the expression of soluble guanylate cyclase was examined by immunohistochemistry.

Methods and materials

The current study was approved by the local ethics committee at the University of Gothenburg, Sweden (ethical permit 1794/18). A total of 60 male Sprague-Dawley rats (235–440 g) purchased from Charles River (Calco, Italy) were used. Male rats were chosen to allow for comparison to previous studies and to avoid any influence of oestrous cycle on the data. Careful notice was taken to follow all rules and regulations stipulated by the ethical permit, and the number of observations was chosen to obtain sufficient power while minimizing the number of animals included in the study. All experimental procedures had full adherence to the ARRIVE 2.0 guidelines.

Experimental design and tissue preparation

The rats were housed under standard conditions with access to food and water *ad libitum*. Animals belonging to the control group received no treatment, whereas experimental cystitis was induced through a single injection of cyclophosphamide (CYP, 100 mg/kg i.p.) 60 h prior to the experimental procedures, ensuring peak inflammation at the time of sacrifice (Giglio et al., 2005), when anaesthesia and euthanasia were induced by an overdose of pentobarbitone (>60 mg/kg i.p.; APL, Stockholm, Sweden). The pelvic cavity was opened, and the urinary bladder was excised and placed in Krebs solution (composition: see section "Tissue bath experiments"). To ensure euthanization, a subsequent excision of the heart was performed.

Full-thickness bladder strips (2 mm × 6 mm) were cut from above the trigone and proximal to the ureters according to a standard procedure (Aronsson et al., 2010) and mounted in organ baths (see below). 1-2 strips were taken from each rat bladder.

Production of aqueous nitric oxide

An aqueous NO solution with a calculated concentration of 2 mM, based on NO solubility, and a shelf-life of up to 1 week was prepared (Simonsen et al., 1999). As schematically shown in Figure 2, a system with five 20 mL glass vials with septum closure was set up in a fume hood; the first containing pyrogallol (10 mM), the next NaOH (10 mM), then an empty vial, and finally two vials filled with Milli-Q water. To minimize oxidization, all solutions were prepared directly in the glass vials, and the pyrogallol vial was covered with aluminum foil due to its photosensitive nature. The vials were connected in sequence with Teflon tubes with flowing argon gas, pushing out oxygen from the solutions. After all vials had been connected, the argon flow was kept for 1 h and then switched to pure NO gas, entering the NaOH vial, without interruption for an additional 20 min. The final vial had a Teflon tube leading into the open air, functioning as a "chimney" for the supplied gas. The same procedure was conducted in a pilot experiment, except for the final gassing with NO, serving as negative control (vehicle) for validation purposes.

Tissue bath experiments

The full-thickness bladder strip preparations were mounted between two steel rods, one adjustable and one fixed, connected to an isometric force transducer (TSD125C, Biopac Systems Inc., Goleta, United States) and immersed into organ baths (20 mL) filled with Krebs solution [NaCl, 118 mM; KCl, 4.6 mM; KH_2PO_4, 1.15 mM; $MgSO_4$ (anhydrous), 1.15 mM; $NaHCO_3$, 25 mM; $CaCl_2$, 1.25 mM; and glucose, 5.5 mM] gassed with 95% O_2 and 5% CO_2 at 37°C. The bladder strip preparations were stretched to 10 mN and let to equilibrate, resulting in a stable tension of about 5–7 mN after 45 min. The resulting tension was the starting point for measurements of responses to subsequent drug administration at basal tension.

The viability of the preparations was assessed by an administration of methacholine (3×10^{-5} M), after which the tissue was washed twice and left to equilibrate for 20 min. Pre-contraction of the tissue was achieved, where applicable, by administration of methacholine (3×10^{-6} M). In a few pilot experiments, high potassium Krebs solution (50 mM; sodium exchanged for potassium) was instead used to achieve pre-contraction. However, the results were identical to those when using methacholine (data not shown).

All administrations were given at a volume of 100 µL using a micropipette, except for the NO solution (or corresponding vehicle in a few control experiments), which was administered with a gas-tight Hamilton syringe in close proximity to the tissue. The NO solution was produced in a set concentration (2 mM) and administered in volumes of 40, 100, 200, and 400 µL, resulting in the desired final concentrations (4×10^{-6}, 10^{-5}, 2×10^{-5}, and 4×10^{-5} M).

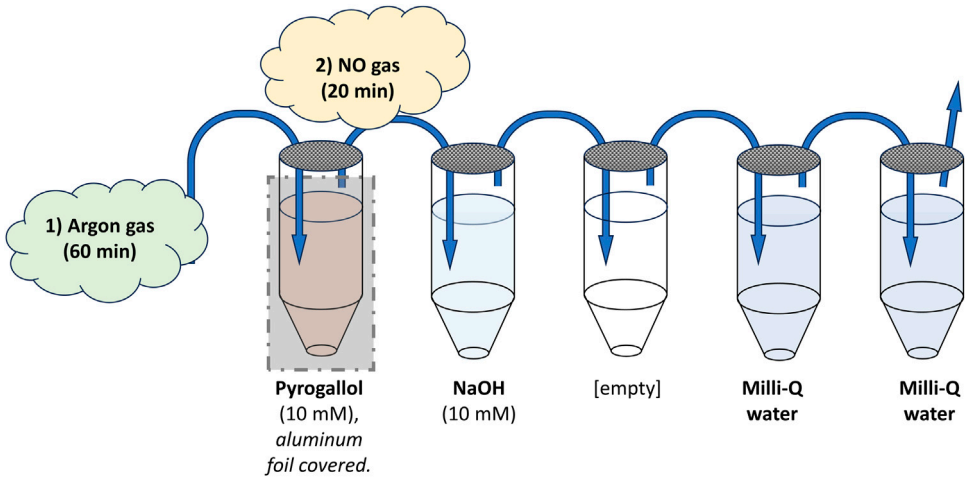

FIGURE 2
Schematic illustration of the setup for producing the aqueous NO solution. Five 20 mL glass vials with septum closure were set up in a fume hood. The first was filled with 18.5 mL of pyrogallol (10 mM) to remove any traces of oxygen from the argon gas led through it. The next contained 18.5 mL of NaOH (10 mM) to remove higher nitrogen species from any gas flowing through it. Thereafter, an empty vial was placed to ensure no spillover into the final vials containing pure Milli-Q water. All vials were connected with Teflon tubing (blue arrows), entering each vial into the liquid and exiting above. The final vial had a Teflon tube leading into the open air, functioning as a "chimney" for the supplied gas. To minimize oxidization, all solutions were prepared directly in the glass vials, and the pyrogallol vial was covered with aluminum foil due to its photosensitive nature. Argon gas, pushing out oxygen from the solutions and vials, was first led through the system for 60 min. Then the gas was switched, without interruption, to pure NO gas, entering through the NaOH vial, for an additional 20 min. The end result was two vials of Milli-Q water saturated with pure NO.

The soluble guanylyl cyclase inhibitor 1H-[1,2,4]oxadiazolo[4,3-a]quinoxalin-1-one (ODQ; 2.5×10^{-7}–2.5×10^{-5} M) was, where applicable, let to equilibrate for 20 min before the addition of any agonist, i.e., NO solution or NO donor (SNP). Before adding NO or NO donor, the tissues were pre-contracted with methacholine (3×10^{-6} M). The concentrations of ODQ were chosen based on previous studies in the literature and observations from pilot studies (Artim et al., 2009).

All concentrations stated are the resulting concentrations in the organ baths, and subsequent administrations were done cumulatively. All substances were diluted in Milli-Q water.

The following substances were used: pentobarbitone (APL, Stockholm, Sweden), argon gas (Linde Gas AB, Enköping, Sweden), NO gas (Linde Gas AB, Enköping, Sweden), pyrogallol, sodium hydroxide (NaOH), sodium chloride (NaCl), potassium chloride (KCl), potassium dihydrogen phosphate (KH_2PO_4), magnesium sulphate ($MgSO_4$), sodium bicarbonate ($NaHCO_3$), calcium chloride ($CaCl_2$), glucose ($C_6H_{12}O_6$), cyclophosphamide, sodium-nitroprusside (SNP), 1H-[1,2,4]oxadiazolo[4,3-a]quinoxalin-1-one (ODQ; Biotechne, Minneapolis, United States) and methacholine. All substances were purchased from Sigma-Aldrich (St Louis, United States) unless otherwise stated.

Immunofluorescence

Expression of soluble guanylate cyclase (sGC) was examined by fluorescent immunohistochemistry. Immediately following an organ bath experiment, the tissues were fixed in paraformaldehyde (4% in 0.1 M phosphate buffered saline). Thereafter, the tissues were embedded in paraffin and sectioned into 10 µm thin tissue sections (two sections per glass; Histolab, Gothenburg, Sweden). The immunofluorescent staining procedure was then commenced by deparaffinizing the paraffin-embedded tissues in xylene, followed by rehydration in 99.5%, 95%, 70%, and 50% ethanol. To remove autofluorescence, copper(II) sulfate ($CuSO_4$, 1 mM; pH = 5) was added to each section for 10 min. Thereafter, heat-induced epitope retrieval was achieved by heating the sections to 70°C in sodium citrate buffer (pH 5.0; Sigma-Aldrich) in a microwave oven for 30 min. Upon reaching room temperature, a blocking solution (5% goat serum, Vector Laboratories, Burlingame, United States and 0.25% Triton X-100, Thermo Fisher Scientific, Rockford, IL, United States, in PBS) was added for 1 h. Next, the primary rabbit polyclonal anti-sGC beta 2 antibody was added to one section on each glass (50 µL; ab53084, Abcam, Cambridge, United Kingdom; 1:100 in 1% goat serum and 0.25% Triton X-100, in PBS), while the other section was kept as a negative control (50 µL; 1% goat serum and 0.25% Triton X-100, in PBS; no antibody). The sections were thereafter incubated overnight at 4°C. The following day, a secondary antibody (ab6719, Abcam, Cambridge, United Kingdom; 1:500 in 1% goat serum and 0.25% Triton, in PBS) was added to the sections and let to incubate for 1 h at room temperature. The sections were thereafter dehydrated in 50%, 70%, 90%, and 99.5% ethanol, respectively. Finally, the sections were mounted under a cover glass with ProLong Gold antifade reagent with DAPI (Thermo Fischer Scientific, Eugene, United States).

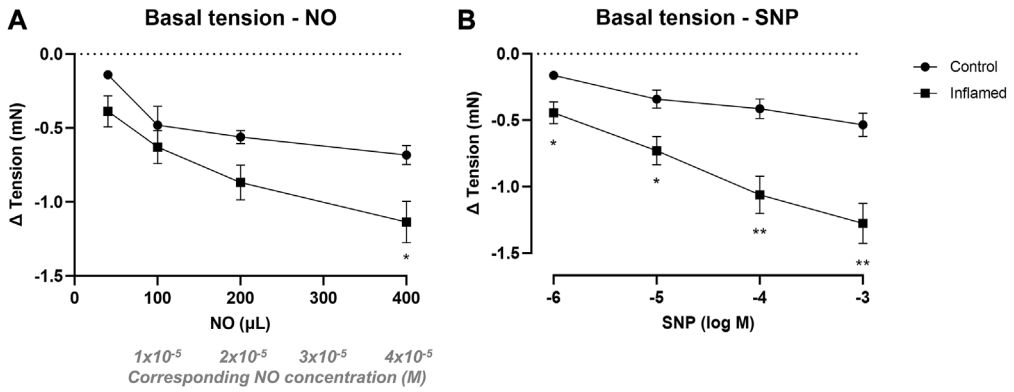

FIGURE 3
Nitrergic relaxation of basal tension in bladder preparations. Functional relaxatory responses at mechanically attained basal tension to increasing volumes of **(A)** aqueous NO solution or concentrations of **(B)** the NO donor SNP in full-thickness urinary bladder strip preparations from healthy controls (●) or rats with cyclophosphamide-induced cystitis (▪). * and ** denotes $p < 0.05$ and $p < 0.01$, respectively. $n = 8$ in each group. Vertical bars indicate the SEM.

Data analysis and statistics

Statistical calculations were performed using GraphPad Prism version 9.5.0 (GraphPad Software Inc., San Diego, United States). Two-way ANOVA followed by Šidák`s correction for multiple comparisons was used for statistical comparisons of tissue bath data, i.e., of concentration-response curves. Statistical significance was regarded for p-values < 0.05. Data are presented as mean ± SEM.

Protein expression was analyzed semi-quantitatively by grading the expression of sGC in each tissue on a scale from 0 to 3 where 0 = no protein expression, 1 = weak protein expression, 2 = moderate protein expression and 3 = strong protein expression. The grading was performed by three blinded evaluators (MW, ED, JS) on images taken with a DS-Fi camera mounted in a Nikon 90i fluorescence microscope (Nikon Corporation, Tokyo, Japan). All images were taken after digital subtraction of background staining measured in corresponding negative controls (i.e., in which the primary antbody was excluded), using the NIS Element Imaging Software v. 4.40 (Nikon Corporation). Each evaluator graded each tissue. Subsequently, a consensus grade was determined for each tissue. Thereafter, the tissues were decoded and a non-parametric statistical calculation was carried out by running a Mann-Whitney rank test.

Results

Relaxation of bladder basal tension

NO in aqueous solution (40–400 µL; 2 mM corresponding to 4×10^{-6}, 1×10^{-5}, 2×10^{-5}, and 4×10^{-5} M) induced concentration-dependent relaxation in both healthy and inflamed detrusor strips (Figure 3A). The relaxations were significantly greater in inflamed tissues when adding the largest volume of NO (i.e., at 400 µL; −0.68 ± 0.06 mN and −1.14 ± 0.14 mN in healthy and inflamed detrusor strips, respectively; $p = 0.039$; Figure 3A). Similarly, SNP (10^{-6}–10^{-3} M) induced concentration-dependent relaxation of basal tension in both healthy and inflamed detrusor strips (Figure 3B). The relaxations were significantly greater in inflamed tissues at all SNP concentrations (1–1,000 µM; $p < 0.05$; Figure 3B). The addition of vehicle (pilot experiments), i.e., Milli-Q water prepared in the same way as the NO-solution but in the absence of NO, did not produce any functional responses in neither healthy nor inflamed tissues (data not shown).

Relaxation of pre-contracted bladder tissue

In preparations contracted with methacholine (3×10^{-6} M), NO in aqueous solution (40–400 µL; 2 mM) induced concentration-dependent relaxations in detrusor strips from both healthy and inflamed bladders (from −0.64 ± 0.25 to −1.41 ± 0.27 and from −0.57 ± 0.12 to −1.98 ± 0.42 mN in healthy and inflamed tissues, respectively; Figure 4A). SNP (10^{-6}–10^{-3} M) induced similar concentration-dependent relaxations in pre-contracted detrusor strips from both healthy and inflamed bladders (from −0.30 ± 0.13 to −1.14 ± 0.25 and from −0.30 ± 0.07 to −1.38 ± 0.22 mN in healthy and inflamed tissues, respectively; Figure 4B). There were no significant differences in the relaxations to neither NO nor SNP in healthy vs. inflamed detrusor strips (Figures 4A, B).

Inhibition of bladder relaxation via soluble guanylate cyclase

Relaxations to NO in aqueous solution were completely abolished in both healthy and inflamed tissues in the presence of a high concentration (2.5×10^{-5} M) of the soluble guanylate cyclase inhibitor ODQ ($p < 0.01$ at all concentrations; Figures 5A, B). In the presence of a low concentration (2.5×10^{-6} M) of ODQ, the relaxations to NO remained intact in healthy

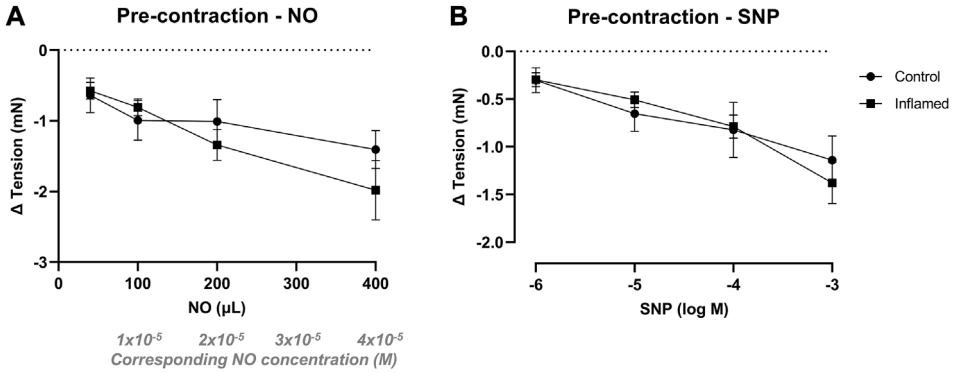

FIGURE 4
Nitrergic relaxation of pre-contracted bladder preparations. Functional relaxatory responses to increasing volumes of **(A)** aqueous NO solution or concentrations of **(B)** the NO donor SNP in methacholine pre-contracted full-thickness urinary bladder strip preparations from healthy controls (●) or rats with cyclophosphamide-induced cystitis (▪). *n* = 8 in each group. Vertical bars indicate the SEM.

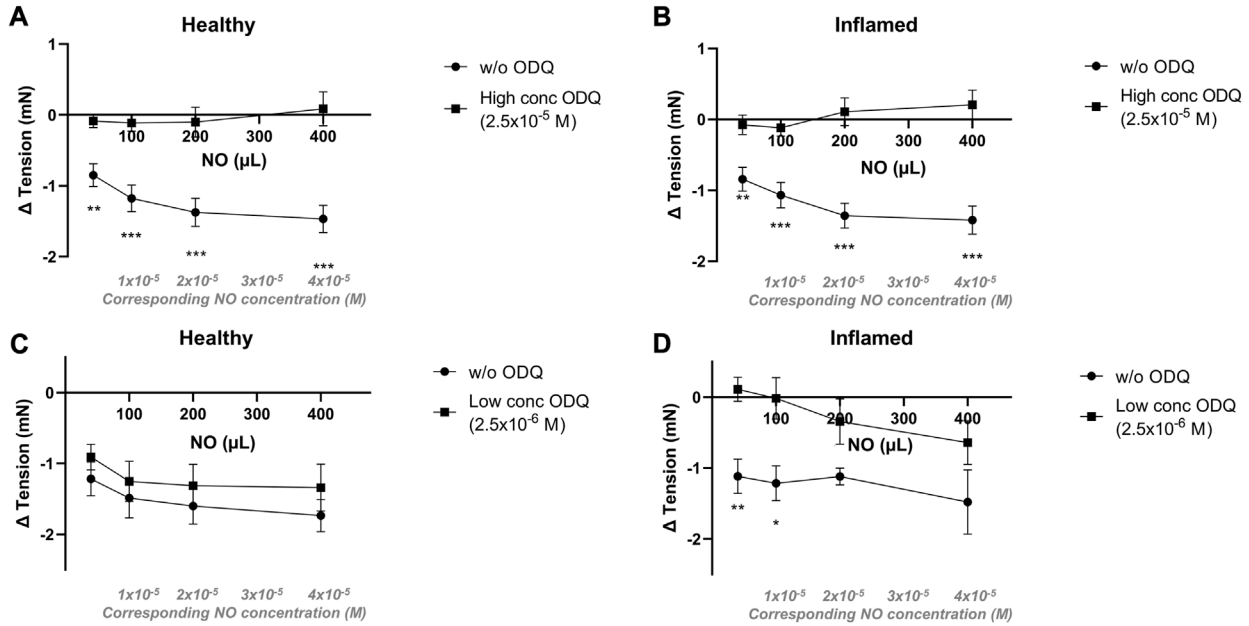

FIGURE 5
Effects of the sGC inhibitor ODQ on nitrergic relaxatory responses in pre-contracted bladder preparations. Nitrergic relaxations to increasing volumes of aqueous NO solution in the absence (●) or presence (▪) of ODQ in full-thickness urinary bladder strip preparations from healthy controls **(A,C)** or rats with cyclophosphamide-induced cystitis **(B,D)**. In the upper panels **(A,B)**, the ODQ concentrations used were high (2.5×10^{-5} M), and in the lower panels **(C,D)**, the concentrations were low (2.5×10^{-6} M) in the lower. *, **, and *** denotes $p < 0.05$, $p < 0.01$, and $p < 0.001$, respectively. *n* = 11 in each group. Vertical bars indicate the SEM.

tissues ($p > 0.05$ at all concentrations; Figure 5C). However, in inflamed bladder strip preparations, a low concentration of ODQ significantly attenuated the relaxations to lower but not higher concentrations of NO ($p = 0.0023$ and 0.021 at 40 and 100 µL of a 2 mM aqueous solution, corresponding to NO concentrations of 4×10^{-6} and 1×10^{-5} M, respectively; Figure 5D). No blocking of the relaxations to NO was observed in the presence of an additionally lower concentration of ODQ (i.e., 2.5×10^{-7} M; data not shown).

Expression of soluble guanylate cyclase

The immunohistochemical analysis showed soluble guanylate cyclase (sGC) expression in both the detrusor and mucosa in all tissues (Figure 6). The semi-quantitative analysis revealed a significantly lower expression of sGC in the inflamed detrusor than in healthy tissues ($p = 0.023$; Figure 6A). No significant differences in sGC expression were observed in the mucosa (Figure 6B).

10.3389/fphys.2023.1249560

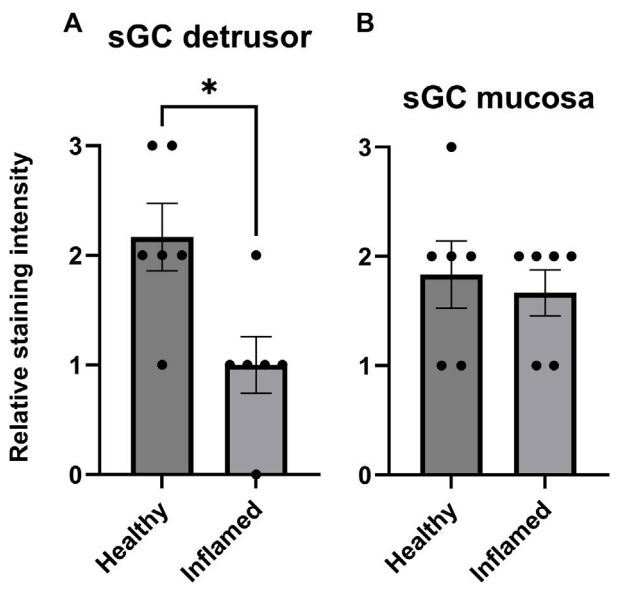

FIGURE 6
Expression of sGC in the rat detrusor and urothelium. Comparison of fluorescent sGC expression in healthy and inflamed **(A)** detrusor and **(B)** urothelium. Expression was graded on a relative scale from 0–3 where 0 denoted no expression and 3 denoted maximum fluorescent intensity. n = 6 in each group; each individual grade is indicated by a black point in the figure. *$p < 0.05$.

Discussion

The current study demonstrates the usefulness of NO in aqueous solution when studying contractile smooth muscle responses in a tissue bath setup. No differences between functional responses to NO in aqueous solution and those of SNP could be seen. Thus, the NO solution and SNP can be used interchangeably. However, NO in aqueous solution has advantageous properties compared to SNP. Most importantly, the amount of freely available NO is known and can exert its effect immediately upon addition to the tissue bath. When adding SNP, the amount of freely available NO is unknown and dependent on the cleavage rate of the parent drug. This pharmacokinetic component is avoided when using NO in an aqueous solution, thus mimicking the physiological situation more closely. This does not limit the use of SNP as a pharmacological substance. Ideally, both aqueous NO and NO donors can be used in parallel in experimental setups. It would also be essential to examine NO in aqueous solution for use *in vivo*, e.g., for instillation in the bladder, which should be addressed in future studies.

When measuring nitrergic responses at basal tension, the relaxations to aqueous NO and, in particular, SNP were greater in inflamed tissues as compared to healthy tissues. This indicates that the inflamed tissue is more sensitive to nitrergic relaxation when in a resting, uncontracted state than normal tissue. When considering that induction of inflammation reduces the expression of sGC in the detrusor, as well as potentially increases oxidation of sGC, this is a surprising finding. In contrast, the relaxations to both NO in aqueous solution and SNP were similar in methacholine pre-contracted healthy and inflamed tissues. This finding is also quite surprising, considering that several previous studies have shown that significant changes regarding nitrergic signaling arise upon induction of inflammation (Andersson et al., 2008; de Oliveira et al., 2016). Apparently, muscarinic receptor-mediated contraction still allows NO to exert its relaxatory effects, but manages to mask the differences between bladder preparations from normal rats and rats with cystitis. The mechanism behind this is presently left unexplained but may emanate from the higher tensions involved or a variety of receptor subtypes being activated by the agonist. This is interesting and should be investigated further, but nonetheless, the current data indicate that responses to NO, and its effects on sGC, remain the same also in the inflamed bladder.

It has long been known that NO induces smooth muscle relaxation by stimulating the formation of cyclic GMP (cGMP) (Kukovetz et al., 1987). It does so by binding to the heme moiety in sGC. However, NO can only bind to heme in its reduced state. ODQ blocks sGC by oxidizing the heme group (Zhao et al., 2000), thus disrupting the ability of NO to bind. In the current study, a higher concentration of ODQ led to the total abolishment of NO-induced relaxations in both healthy and inflamed tissues. In the presence of a lower concentration of ODQ (2.5×10^{-7} M), the inhibition of NO-induced relaxation was absent. Thus, the inhibitory effect of ODQ was concentration-dependent and specific, demonstrating that NO-induced detrusor relaxation occurs via the activation of sGC and the subsequent formation of cGMP. This is in line with previous findings in other disease models (Bau et al., 2010; Fullhase et al., 2015). It should be noted that inflammation is a common cause of oxidative stress, which can lead to oxidation of the heme moiety in sGC. However, the current data clearly show that despite bladder inflammation, NO can still induce smooth muscle relaxation via sGC. Thus, the present findings indicate that induction of bladder inflammation with CYP does not induce substantial oxidative stress, at least not above the threshold, allowing sGC to remain functional. However, the amounts of NO used in the current study to induce detrusor relaxation may be greater than what is produced *in vivo*. Considering that several previous studies have demonstrated that impairment of the NO-sGC-cGMP pathway is strongly associated with lower urinary tract symptoms, and that restoring this pathway ameliorates symptoms (Monica and Antunes, 2018; Aydogdu et al., 2022), the current data should be interpreted with this in mind. It should also be noted that levels of cGMP were not measured in the current study.

The immunofluorescent analysis showed that sGC is expressed throughout the bladder wall, albeit with a relatively low level of expression in the submucosa. Mucosal, i.e., mainly urothelial, expression was similar when comparing healthy and inflamed tissues. However, upon induction of inflammation, the expression of sGC was attenuated in the detrusor. This aligns with previous studies in various lower urinary tract disease models showing decreased sGC expression upon induction of bladder dysfunction (Fullhase et al., 2015; de Oliveira et al.,

2016). The currently used primary antibody cannot distinguish between reduced and oxidized sGC. However, the immunostainings indicated a lower level of expression of sGC in the inflamed detrusor. When considering the blocking ability of ODQ in healthy as compared to inflamed tissues, the data could be interpreted as ODQ in a lower concentration (2.5×10^{-6} M; Figures 5C, D) being able to block NO-induced relaxation in inflamed tissues but not in healthy as a result of a lower amount of sGC, or a fraction of sGC already being oxidized, in the inflamed detrusor. The immunofluorescent analysis thus supports the findings in the tissue baths regarding relaxations to NO in the presence of ODQ.

Even though the present study validated the method of producing and employing NO in aqueous solution, a few experimental challenges are worth noting. First, the administration of the NO solution must be performed in close proximity to the preparation in the organ bath to avoid rapid breakdown. While this could theoretically be an issue, the current results demonstrate concentration-dependent effects, indicating a proper diffusion of the substance. Second, since the aqueous NO solution is produced in a set concentration, the volume administered will increase with the intended concentration. This was found not to present any problem experimentally since administration of the vehicle in the relevant volumes did not alter the tension of the preparations.

Future studies should be designed to examine the intracellular pathways in play upon activation of sGC, including the resulting amounts of cGMP. Various time points during cystitis development should be investigated to further unravel bladder alterations due to inflammation. This would increase the understanding of nitrergic signaling in the urinary bladder. It would also be beneficial to specifically examine activation of sGC in its oxidized form, for example, by utilizing sGC activators. If simultaneously examining responses to NO, it may be possible to quantify the functional proportion of sGC, i.e., the amount of reduced vs. oxidized sGC, in different disease states.

Conclusion

In the present study, we found that aqueous NO solution induces relaxation of the rat detrusor by activating soluble guanylate cyclase in both control and inflamed bladder strips. Induction of inflammation conceivably leads to decreased sGC expression in the detrusor, which may explain the different susceptibility towards inhibition of sGC in inflamed versus control tissue. Further, the current findings verify the usefulness of utilizing NO in aqueous solution for studies of the lower urinary tract, indicating this to be a good complement to currently used pharmacological tools.

Data availability statement

The raw data supporting the conclusion of this article will be made available by the authors, without undue reservation.

Ethics statement

The animal study was approved by the local ethics committee at the University of Gothenburg, Sweden (ethical permit 1794/18). The study was conducted in accordance with the local legislation and institutional requirements.

Author contributions

PA and MW: Conceived and designed the study, performed data analysis and wrote the manuscript. JS, EF, ED, and AJ: Collected and analyzed data. US: Performed data analysis and contributed to writing the manuscript. All authors contributed to the article and approved the submitted version.

Funding

The study was supported by generous grants from the Colliander Foundation, the Royal Swedish Society, and the Wilhelm and Martina Lundgren's Foundation.

Acknowledgments

The authors would like to thank Jenny Steen for her valuable technical assistance.

Conflict of interest

The authors declare that the research was conducted in the absence of any commercial or financial relationships that could be construed as a potential conflict of interest.

Publisher's note

References

Andersson, M., Aronsson, P., Doufish, D., Lampert, A., and Tobin, G. (2012). Muscarinic receptor subtypes involved in urothelium-derived relaxatory effects in the inflamed rat urinary bladder. *Auton. Neurosci.* 170, 5–11. doi:10.1016/j.autneu.2012.06.004

Andersson, M., Aronsson, P., Giglio, D., Wilhelmson, A., Jeřábek, P., and Tobin, G. (2011). Pharmacological modulation of the micturition pattern in normal and cyclophosphamide pre-treated conscious rats. *Auton. Neurosci.* 159, 77–83. doi:10.1016/j.autneu.2010.08.008

Andersson, M. C., Tobin, G., and Giglio, D. (2008). Cholinergic nitric oxide release from the urinary bladder mucosa in cyclophosphamide-induced cystitis of the anaesthetized rat. *Br. J. Pharmacol.* 153, 1438–1444. doi:10.1038/bjp.2008.6

Aronsson, P., Andersson, M., Ericsson, T., and Giglio, D. (2010). Assessment and characterization of purinergic contractions and relaxations in the rat urinary bladder. *Basic Clin. Pharmacol. Toxicol.* 107, 603–613. doi:10.1111/j.1742-7843.2010.00554.x

Artim, D. E., Kullmann, F. A., Daugherty, S. L., Wu, H. Y., and de Groat, W. C. (2009). Activation of the nitric oxide-cGMP pathway reduces phasic contractions in neonatal rat bladder strips via protein kinase G. *Am. J. Physiol. Ren. Physiol.* 297, F333–F340. doi:10.1152/ajprenal.00207.2009

Aydogdu, O., Perez, F., Aronsson, P., Uyar Gocun, P., Carlsson, T., Sandner, P., et al. (2022). Treatment with the soluble guanylate cyclase activator BAY 60-2770 normalizes bladder function in an *in vivo* rat model of chronic prostatitis. *Eur. J. Pharmacol.* 927, 175052. doi:10.1016/j.ejphar.2022.175052

Bau, F. R., Mónica, F. Z. T., Priviero, F. B. M., Baldissera, L., de Nucci, G., and Antunes, E. (2010). Evaluation of the relaxant effect of the nitric oxide-independent soluble guanylyl cyclase stimulator BAY 41-2272 in isolated detrusor smooth muscle. *Eur. J. Pharmacol.* 637, 171–177. doi:10.1016/j.ejphar.2010.04.008

Birder, L. A., Apodaca, G., De Groat, W. C., and Kanai, A. J. (1998). Adrenergic- and capsaicin-evoked nitric oxide release from urothelium and afferent nerves in urinary bladder. *Am. J. Physiol.* 275, F226–F229. doi:10.1152/ajprenal.1998.275.2.F226

Bustamante, S., Orensanz, L. M., Recio, P., Carballido, J., García-Sacristán, A., Prieto, D., et al. (2010). Functional evidence of nitrergic neurotransmission in the human urinary bladder neck. *Neurosci. Lett.* 477, 91–94. doi:10.1016/j.neulet.2010.04.040

Caremel, R., Oger-Roussel, S., Behr-Roussel, D., Grise, P., and Giuliano, F. A. (2010). Nitric oxide/cyclic guanosine monophosphate signalling mediates an inhibitory action on sensory pathways of the micturition reflex in the rat. *Eur. Urol.* 58, 616–625. doi:10.1016/j.eururo.2010.07.026

Chakrabarty, B., Ito, H., Ximenes, M., Nishikawa, N., Vahabi, B., Kanai, A. J., et al. (2019). Influence of sildenafil on the purinergic components of nerve-mediated and urothelial ATP release from the bladder of normal and spinal cord injured mice. *Br. J. Pharmacol.* 176, 2227–2237. doi:10.1111/bph.14669

Cho, K. J., Koh, J. S., Choi, J., and Kim, J. C. (2017). Changes in adenosine triphosphate and nitric oxide in the urothelium of patients with benign prostatic hyperplasia and detrusor underactivity. *J. Urol.* 198, 1392–1396. doi:10.1016/j.juro.2017.06.080

de Oliveira, M. G., Calmasini, F. B., Alexandre, E. C., De Nucci, G., Mónica, F. Z., and Antunes, E. (2016). Activation of soluble guanylyl cyclase by BAY 58-2667 improves bladder function in cyclophosphamide-induced cystitis in mice. *Am. J. Physiol. Ren. Physiol.* 311, F85–F93. doi:10.1152/ajprenal.00041.2016

Feelisch, M., and Kelm, M. (1991). Biotransformation of organic nitrates to nitric oxide by vascular smooth muscle and endothelial cells. *Biochem. Biophys. Res. Commun.* 180, 286–293. doi:10.1016/s0006-291x(05)81290-2

Fujiwara, M., Andersson, K., and Persson, K. (2000). Nitric oxide-induced cGMP accumulation in the mouse bladder is not related to smooth muscle relaxation. *Eur. J. Pharmacol.* 401, 241–250. doi:10.1016/s0014-2999(00)00457-x

Fullhase, C., Hennenberg, M., Sandner, P., Strittmatter, F., Niedworok, C., Bauer, R. M., et al. (2015). Reduction of obstruction related bladder overactivity by the guanylyl cyclase modulators BAY 41-2272 and BAY 60-2770 alone or in combination with a phosphodiesterase type 5 inhibitor. *Neurourol. Urodyn.* 34, 787–793. doi:10.1002/nau.22665

Giglio, D., Ryberg, A. T., To, K., Delbro, D. S., and Tobin, G. (2005). Altered muscarinic receptor subtype expression and functional responses in cyclophosphamide induced cystitis in rats. *Auton. Neurosci.* 122, 9–20. doi:10.1016/j.autneu.2005.07.005

Gillespie, J. I., and Drake, M. J. (2004). The actions of sodium nitroprusside and the phosphodiesterase inhibitor dipyridamole on phasic activity in the isolated Guinea-pig bladder. *BJU Int.* 93, 851–858. doi:10.1111/j.1464-410X.2003.04727.x

Kajioka, S., Nakayama, S., Seki, N., Naito, S., and Brading, A. F. (2008). Oscillatory membrane currents paradoxically induced via NO-activated pathways in detrusor cells. *Cell. Calcium* 44, 202–209. doi:10.1016/j.ceca.2007.11.008

Kang, W. S., Tamarkin, F. J., Wheeler, M. A., and Weiss, R. M. (2004). Rapid up-regulation of endothelial nitric-oxide synthase in a mouse model of *Escherichia coli* lipopolysaccharide-induced bladder inflammation. *J. Pharmacol. Exp. Ther.* 310, 452–458. doi:10.1124/jpet.104.066506

Kedia, G. T., Uckert, S., Jonas, U., Kuczyk, M. A., and Burchardt, M. (2008). The nitric oxide pathway in the human prostate: clinical implications in men with lower urinary tract symptoms. *World J. Urol.* 26, 603–609. doi:10.1007/s00345-008-0303-y

Kukovetz, W. R., Holzmann, S., and Romanin, C. (1987). Mechanism of vasodilation by nitrates: role of cyclic GMP. *Cardiology* 74 (Suppl. 1), 12–19. doi:10.1159/000174258

Liu, S. H., and Lin-Shiau, S. Y. (1997). Enhancement by nitric oxide of neurogenic contraction in the mouse urinary bladder. *Naunyn Schmiedeb. Arch. Pharmacol.* 356, 850–852. doi:10.1007/pl00005127

Logadottir, Y. R., Ehren, I., Fall, M., Wiklund, N. P., Peeker, R., and Hanno, P. M. (2004). Intravesical nitric oxide production discriminates between classic and nonulcer interstitial cystitis. *J. Urol.* 171, 1148–1150. doi:10.1097/01.ju.0000110501.96416.40)

Moncada, S., Palmer, R. M., and Higgs, E. A. (1991). Nitric oxide: physiology, pathophysiology, and pharmacology. *Pharmacol. Rev.* 43, 109–142.

Monica, F. Z., and Antunes, E. (2018). Stimulators and activators of soluble guanylate cyclase for urogenital disorders. *Nat. Rev. Urol.* 15, 42–54. doi:10.1038/nrurol.2017.181

Moon, A. (2002). Influence of nitric oxide signalling pathways on pre-contracted human detrusor smooth muscle *in vitro*. *BJU Int.* 89, 942–949. doi:10.1046/j.1464-410x.2002.02795.x

Ozawa, H., Chancellor, M. B., Jung, S. Y., Yokoyama, T., Fraser, M. O., Yu, Y., et al. (1999). Effect of intravesical nitric oxide therapy on cyclophosphamide-induced cystitis. *J. Urol.* 162, 2211–2216. doi:10.1016/s0022-5347(05)68161-x

Patel, B., Perez, F., Aronsson, P., Alothmani, R., Carlsson, T., and Winder, M. (2020). Combination drug therapy against OAB normalizes micturition parameters and increases the release of nitric oxide during chemically induced cystitis. *Pharmacol. Res. Perspect.* 8, e00564. doi:10.1002/prp2.564

Sancho, M., Ferrero, J. J., Triguero, D., Torres, M., and Garcia-Pascual, A. (2014). Altered neuronal and endothelial nitric oxide synthase expression in the bladder and urethra of cyclophosphamide-treated rats. *Nitric Oxide* 39C, 8–19. doi:10.1016/j.niox.2014.04.002

Simonsen, U., Wadsworth, R. M., Buus, N. H., and Mulvany, M. J. (1999). *In vitro* simultaneous measurements of relaxation and nitric oxide concentration in rat superior mesenteric artery. *J. Physiol.* 516 (Pt 1), 271–282. doi:10.1111/j.1469-7793.1999.271aa.x

Winder, M., Tobin, G., Zupancic, D., and Romih, R. (2014). Signalling molecules in the urothelium. *Biomed. Res. Int.* 2014, 297295. doi:10.1155/2014/297295

Winder, M., Vesela, R., Aronsson, P., Patel, B., and Carlsson, T. (2017). *Autonomic receptor-mediated regulation of production and release of nitric oxide in normal and malignant human urothelial cells*. Basic Clin Pharmacol Toxicol.

Yanai, Y., Hashitani, H., Hayase, M., Sasaki, S., Suzuki, H., and Kohri, K. (2008). *Role of nitric oxide/cyclic GMP pathway in regulating spontaneous excitations in detrusor smooth muscle of the Guinea-pig bladder*. *Neurourol. Urodyn.* 27, 446–453. doi:10.1002/nau.20517

Zabbarova, I. V., Ikeda, Y., Kozlowski, M. G., Tyagi, P., Birder, L. A., Chakrabarty, B., et al. (2021). Benign prostatic hyperplasia/obstruction ameliorated using a soluble guanylate cyclase activator. *J. Pathol.* 256, 442–454. doi:10.1002/path.5859

Zhao, Y., Brandish, P. E., Di Valentin, M., DiValentin, M., Schelvis, J. P., Babcock, G. T., et al. (2000). Inhibition of soluble guanylate cyclase by ODQ. *Biochemistry* 39, 10848–10854. doi:10.1021/bi9929296

frontiers | Frontiers in Physiology

TYPE Review
PUBLISHED 04 September 2023
DOI 10.3389/fphys.2023.1232017

OPEN ACCESS

EDITED BY
Russ Chess-Williams,
Bond University, Australia

REVIEWED BY
Jonathan M. Beckel,
University of Pittsburgh, United States
Warren G. Hill,
Beth Israel Deaconess Medical Center and Harvard Medical School,
United States

*CORRESPONDENCE
Luke Grundy,
luke.grundy@flinders.edu.au
Cindy Tay,
tay0112@flinders.edu.au

RECEIVED 31 May 2023
ACCEPTED 01 August 2023
PUBLISHED 04 September 2023

CITATION
Tay C and Grundy L (2023), Animal models of interstitial cystitis/bladder pain syndrome.
Front. Physiol. 14:1232017.
doi: 10.3389/fphys.2023.1232017

Animal models of interstitial cystitis/bladder pain syndrome

Cindy Tay* and Luke Grundy*

Neurourology Research Group, College of Medicine and Public Health, Flinders Health and Medical Research Institute, Flinders University, Adelaide, SA, Australia

Interstitial Cystitis/Bladder Pain Syndrome (IC/BPS) is a chronic disorder characterized by pelvic and/or bladder pain, along with lower urinary tract symptoms that have a significant impact on an individual's quality of life. The diverse range of symptoms and underlying causes in IC/BPS patients pose a significant challenge for effective disease management and the development of new and effective treatments. To facilitate the development of innovative therapies for IC/BPS, numerous preclinical animal models have been developed, each focusing on distinct pathophysiological components such as localized urothelial permeability or inflammation, psychological stress, autoimmunity, and central sensitization. However, since the precise etiopathophysiology of IC/BPS remains undefined, these animal models have primarily aimed to replicate the key clinical symptoms of bladder hypersensitivity and pain to enhance the translatability of potential therapeutics. Several animal models have now been characterized to mimic the major symptoms of IC/BPS, and significant progress has been made in refining these models to induce chronic symptomatology that more closely resembles the IC/BPS phenotype. Nevertheless, it's important to note that no single model can fully replicate all aspects of the human disease. When selecting an appropriate model for preclinical therapeutic evaluation, consideration must be given to the specific pathology believed to underlie the development of IC/BPS symptoms in a particular patient group, as well as the type and severity of the model, its duration, and the proposed intervention's mechanism of action. Therefore, it is likely that different models will continue to be necessary for preclinical drug development, depending on the unique etiology of IC/BPS being investigated.

KEYWORDS

interstitial cystitis, bladder pain syndrome, IC/BPS, animal models, clinical translation

1 Introduction

Interstitial Cystitis/Bladder Pain Syndrome (IC/BPS) is a chronic disorder characterised by pelvic and/or bladder pain that is commonly reported with urinary urgency (Berry et al., 2011; Grundy et al., 2018a). However, significant heterogeneity exists in both the clinical symptoms and pathophysiological presentation of IC/BPS patients, presenting a major challenge to diagnosis, effective disease management, and the development of efficacious treatments. Consequently, IC/BPS is associated with a significant ongoing health burden, and a corresponding social and economic cost of greater than $20 Billion per annum in the United States (Pierce and Christianson, 2015).

To advance the understanding of IC/BPS and the development of novel therapeutics, numerous animal models have been developed that recapitulate the most common pathophysiological features of IC/BPS, including urothelial permeability, bladder inflammation, bladder/pelvic pain, and urinary frequency. However, clinical translation

of preclinical research into novel and efficacious pharmacological treatments has been limited and there are still no effective long-term treatments for the debilitating symptoms of IC/BPS (Garzon et al., 2020a).

This review summarises current IC/BPS diagnosis and treatment options, the mechanisms thought to underlie IC/BPS pathophysiology, and the animal models available to investigate the pathophysiology and symptoms of IC/BPS. We discuss these models in the context of clinical relevance and offer insights into how these models can be used in future studies to increase our understanding of IC/BPS pathophysiology and advance the development of efficacious therapeutic strategies.

2 Epidemiology and clinical significance

IC/BPS affects approximately 4% of the population in western countries with a five times higher incidence in women than men (Jones and Nyberg, 1997; Berry et al., 2011; Pierce and Christianson, 2015). Patients with IC/BPS exhibit bladder-centric symptoms including urinary urgency and bladder pain at physiological bladder volumes (Kim et al., 2009; Grundy et al., 2019). The chronic nature of IC/BPS symptoms drastically diminishes quality of life, relentlessly impacting all aspects of personal and professional life, with ~84% of IC/BPS patients finding employment or keeping a job difficult (Koziol et al., 1993; Tubaro, 2004; Dmochowski and Newman, 2007; Nickel et al., 2010; Berry et al., 2011; Bosch and Bosch, 2014; Vasudevan and Moldwin, 2017; Nunez-Badinez et al., 2021). As a result, psychosocial comorbidities are common in IC/BPS patients, with higher reported incidences of anxiety and depression that lead to a chronic decline in patient's mental and physical health (Tubaro, 2004; Clemens et al., 2008; Chung et al., 2014; Nunez-Badinez et al., 2021; Ueda et al., 2021). Despite this burden, and decades of research, effective long-term treatments for IC/BPS are lacking (Garzon et al., 2020a). As a result, IC/BPS patients in the United States alone carry an economic burden of ~$20–40 billion per annum (Pierce and Christianson, 2015). Therefore, there is an urgent need to develop effective treatments that improve the quality of life for IC/BPS patients.

3 Classification of IC/BPS

The American Urological Association defines IC/BPS as 'An unpleasant sensation (pain, pressure, discomfort) perceived to be related to the urinary bladder, associated with lower urinary tract symptoms of more than 6 weeks duration, in the absence of infection or other identifiable causes' (Hanno et al., 2011a).

Although IC/BPS patients present with common symptoms, including bladder pain and lower urinary tract symptoms, it is a heterogeneous clinical syndrome. Distinct subgroups or phenotypes exist that are categorised by highly divergent pathophysiology or responses to treatment. 5%–57% of IC/BPS patients have Hunner lesions (Whitmore et al., 2019; Akiyama et al., 2020), reddish mucosal lesions accompanied by abnormal capillary structures that are associated with more severe bladder inflammation and urothelial denudation (Peeker and Fall 2002; Logadottir et al., 2014; Jhang and Kuo, 2016a; Kim et al., 2017; Akiyama et al., 2018). Non-Hunner lesion IC/BPS patients exhibit less bladder inflammation (Peters et al., 2011; Warren, 2014; Whitmore et al., 2019), but commonly report more widespread symptoms and painful comorbidities including irritable bowel syndrome, fibromyalgia, and migraines indicative of a systemic syndrome (Jhang and Kuo, 2016a). Whilst the etiopathophysiology of IC/BPS is still unknown, it is increasingly likely that IC/BPS with Hunner lesions and IC/BPS without Hunner lesions have distinct pathophysiological origins (Fall et al., 2014; Maeda et al., 2015; Whitmore et al., 2019).

4 Diagnosis

Diagnosis for IC/BPS relies predominantly on the presence of chronic pelvic pain, which can include suprapubic pain, pressure or discomfort related to bladder filling and pain throughout the pelvis, in the absence of other definable disease (Hanno et al., 2011a; Hanno et al., 2015). As such, clinical diagnosis requires a comprehensive analysis of patient personal and medical history to rule out alternative sources of bladder pain and dysfunction such as medication, chemo- or radiotherapy induced cystitis, or neurological disorders associated with bladder dysfunction including spinal cord injury, stroke, Parkinson's disease, and multiple sclerosis. Patients will also commonly undergo an abdominal and pelvic examination to exclude vaginitis and urethritis in addition to urinalysis and urine culture to exclude urinary tract infections, sexually transmitted infections, as well as malignancy of the bladder, uterus, vagina and ovaries (Hanno et al., 2015). Performing cystoscopy and urodynamic testing is not required for diagnosis, but can be performed to confirm the presence of Hunner lesions if the patient fits the relevant risk factors (Hanno et al., 2015). Cystoscopy is a necessary procedure in diagnosing IC/BPS based on East Asian guidelines (Ueda et al., 2021).

5 Mechanisms underlying IC/BPS

Bladder sensations arise following the activation of peripheral sensory afferent nerves embedded within the bladder wall, and the transmission of sensory signals into the central nervous system and brain where they can be processed and perceived (Fowler et al., 2008). Hypersensitivity of bladder-innervating afferents, such that exaggerated sensory signals are generated from the bladder during normal function, is considered a crucial component in the pathogenesis of IC/BPS symptoms (de Groat and Yoshimura, 2009; Grundy et al., 2018a). A variety of factors have been proposed to contribute to bladder afferent hypersensitivity in IC/BPS, including increased urothelial permeability, inflammation, and dysregulation of spinal and/or cortical networks (Figure 1) (de Groat et al., 2015; Grundy et al., 2018a). Despite the pathophysiology underlying afferent sensitisation being currently undefined, it is generally agreed that disruption of mucosal homeostasis, characterised by an increase in urothelial permeability and inflammation, is a major contributing factor to neuronal hypersensitivity and the painful symptoms of IC/BPS (Parsons, 2007; de Groat et al.,

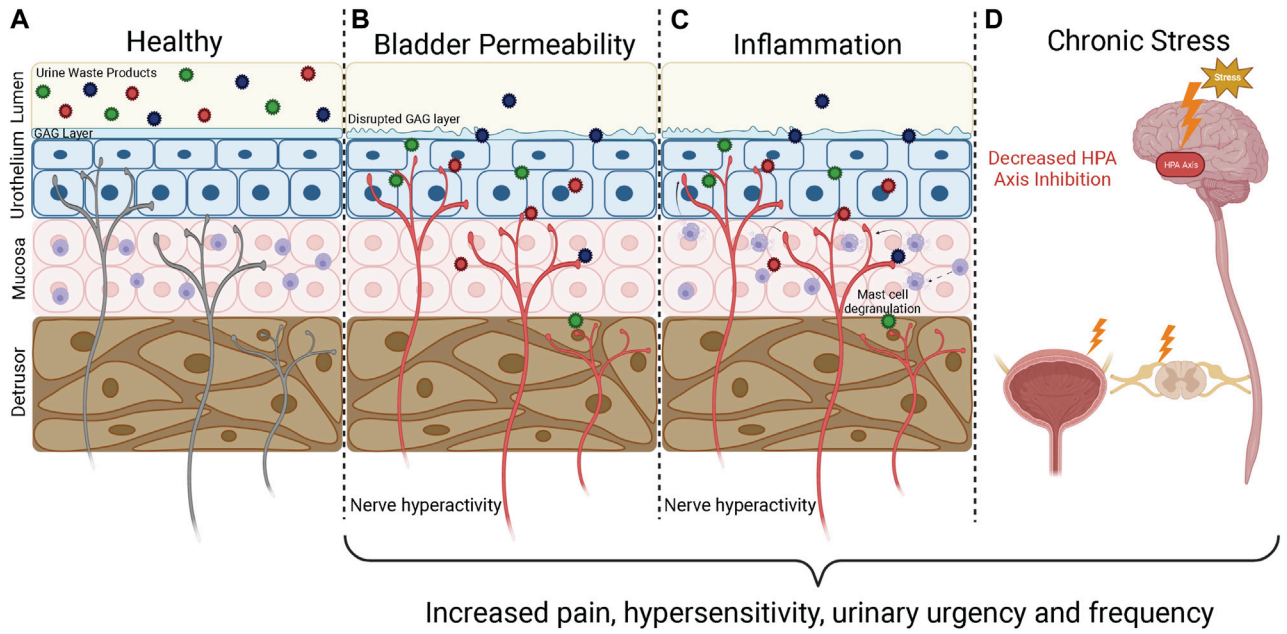

FIGURE 1
Underlying mechanisms of IC/BPS pathophysiology. The bladder wall is innervated by a dense network of afferent nerves that detect bladder stretch during bladder filling and danger signals generated during inflammation and barrier breakdown. If these sensory nerves become sensitised, they respond to physiological stimuli with greater intensity, leading to the generation of bladder hypersensitivity symptoms characteristic of IC/BPS including urinary urgency and pain. **(A)** In a healthy bladder the urothelium is impermeable, providing a barrier that prevents the toxic waste products contained within urine from accessing the bladder wall to activate the underlying sensory nerves. **(B)** An increase in bladder permeability due to breakdown of the urothelial barrier allows urine waste products to access the bladder interstitium. The influx of waste products causes further damage to the urothelium, increasing bladder permeability and allowing urine to reach deeper layers of the bladder to activate and sensitise bladder sensory nerve endings. **(C)** Persistent bladder permeability, bacterial infections, and autoimmunity trigger an inflammatory response within the bladder wall characterised by immune cell infiltration, mast cell degranulation, and the release of pro-inflammatory mediators including histamine and cytokines that can sensitise and activate nearby afferent nerve endings. Inflammation also enhances bladder permeability, allowing toxic waste products to enter the bladder and perpetuate the inflammatory state. **(D)** The HPA axis is responsible for regulating the stress response and provides input to the limbic system and prefrontal cortex to modulate sensory perception. Chronic HPA axis activation caused by severe stress leads to dysregulation of the HPA axis. HPA axis dysregulation can impact pain perception directly by modulating central nervous systems inputs and can lead to downstream effects on the spinal cord and hypersensitivity of bladder afferent nerves. GAG, Glycosaminoglycan; HPA, Hypothalamic Pituitary Adrenal. Figure was created using Biorender.com.

2015; Pierce and Christianson, 2015; Grundy et al., 2018a; Grundy et al., 2019; Karamali et al., 2019) (Figure 1). As such, unravelling the specific pathophysiological mechanisms involved in the development of neuronal hypersensitivity is likely to be critical to the development of novel therapeutics that effectively treat IC/BPS symptoms.

5.1 Increased bladder permeability

Urine contains a variety of toxic waste metabolites that are prevented from accessing the underlying bladder interstitium and sensory nerve endings by the usually impermeable urothelium. The urothelial barrier is maintained by tight junctions between apical urothelial cells, hydrophobic uroplakin plaques, and a considerable glycosaminoglycan (GAG) mucus layer of glycoproteins and proteoglycans that acts as a protective barrier between urine and urothelial cells (Jafari and Rohn, 2022; Klingler, 2016; Wyndaele et al., 2019). Several clinical studies have revealed that IC/BPS patients have a diminished or damaged urothelium (Elbadawi and Light, 1996; Tomaszewski et al., 2001; Keay et al., 2014; Hurst et al., 2015), providing toxic irritants and urea greater access to the cell membranes of urothelial cells (Figure 1). IC/BPS patients also have reduced expression of tight junction proteins, including E-cadherin and zonula-occludens-1 compared with healthy controls (Liu et al., 2012a; Jhang and Kuo, 2016a). A decrease in tight junction proteins allows urinary solutes to diffuse through the urothelium into the lamina propria to activate afferent nerve endings and precipitate urological symptoms consistent with IC/BPS (Davis et al., 2014). The urothelium can also be damaged further when in contact with high concentrations of cationic urinary components (Parsons et al., 2000; Parsons et al., 2014), allowing increasing amounts of urine to leak through to the deeper layers, exacerbating afferent hypersensitivity.

Whilst an increase in urothelial permeability clearly exaggerates bladder pain symptoms in IC/BPS, it is not yet known if urothelial permeability is a crucial component in the pathogenesis of bladder hypersensitivity in IC/PBS or a consequence of inflammation that acts to entrench a chronic disease state.

5.2 Inflammation

Inflammatory mediator sensitisation of afferent nerves is a pivotal component of the healing process, providing awareness of an injury to alter behaviour and promote tissue regeneration.

However, if inflammation becomes uncontrolled this can be detrimental to tissue repair (Eming et al., 2007; Leoni et al., 2015; Landén et al., 2016), and can trigger long term changes in sensory afferent networks to induce a persistent hypersensitive state.

Only a minority of IC/BPS patients exhibit significant bladder inflammation and the development of Hunner's lesions (Leiby et al., 2007; Whitmore et al., 2019). However, some degree of inflammation is common in the bladders of IC/BPS patients without Hunner lesions, with higher levels of pro-inflammatory mediators, including cytokines, chemokines, histamine, and nerve growth factor compared to healthy control bladders. IC/BPS bladders have also been shown to overexpress pro-inflammatory genes, exhibit mild oedema and tissue granulation, and have elevated numbers of immune cells, including mast cell, macrophages, eosinophils as well as T and B cell markers compared to healthy control bladders (Grundy et al., 2018a; Jhang and Kuo, 2016b; Peters et al., 1999; Liu and Kuo, 2012; Furuta et al., 2018; Liu et al., 2012a; Jacobs et al., 2010; el-Mansoury et al., 1994; Kastrup et al., 1983; Abernethy et al., 2017a; Hauser et al., 2008a; Sant et al., 2007; Grover et al., 2011; Hauser et al., 2008b; Abernethy et al., 2017a). Preclinical studies have confirmed that pro-inflammatory mediators can directly sensitise afferent nerve endings within the bladder wall (de Groat and Yoshimura, 2009; Hughes et al., 2013; Davidson et al., 2014; Grundy et al., 2020a; Grundy et al., 2021), providing a crucial link between inflammation and exaggerated sensation. Furthermore, it is well known that an inflammatory environment disrupts mucosal homeostasis and is detrimental to epithelial regeneration and repair during wound healing (Raziyeva et al., 2021). As such, localised inflammation within the bladder mucosa has the potential to increase bladder permeability, combining to establish a positive feedback cycle that further promotes an inflammatory state and chronic sensitisation of peripheral afferent endings within the bladder wall (Figure 1) (Sant et al., 2007; Grover et al., 2011; Grundy et al., 2018a). Whilst numerous inflammatory factors are elevated in the bladders of IC/BPS patients, whether these factors are a consequence of IC/BPS pathophysiology or contribute to the pathogenesis of IC/BPS in an otherwise healthy bladder has yet to be determined.

5.3 Chronic stress

Bladder sensory signals converge in the periaqueductal gray (PAG) of the midbrain with inputs from the limbic system (amygdala, hypothalamus, thalamus, cingulate gyrus), insula, and prefrontal cortex (Fowler et al., 2008). The hypothalamic pituitary adrenal (HPA) axis mediates the major adaptive component of the stress response and is a significant modulator of both the limbic system and sensory perception. Furthermore, bladder muscle function is under autonomic regulation, with stress imparting direct effects on bladder function. Modulation of the emotional affective state and homeostasis of the HPA axis can thus have overwhelming effects on bladder sensation and function and has been proposed as a key underlying mechanism in the development, persistence, and exacerbation of IC/BPS symptoms. In healthy patients, stress modulation of bladder sensation and function is commonly observed as urinary urgency during acutely stressful situations. However, in addition to the acute impacts of stress on the bladder, strong correlations exist between chronic stress and anxiety in the symptomology of IC/BPS as well as other visceral pain disorders such as irritable bowel syndrome (Pierce and Christianson, 2015; Moloney et al., 2016). Furthermore, acute and chronic stress can exacerbate urgency and the severity of pain in established IC/BPS patients (Koziol et al., 1993; Lutgendorf et al., 2000; Rothrock et al., 2001; Pierce and Christianson, 2015). With this in mind, chronic stress has been identified as a key risk factor in developing IC/BPS in otherwise healthy patients (Birder, 2019), and a number of studies have reported higher incidences of early life stress in IC/BPS patients than healthy controls (Fuentes and Christianson, 2018a). The precise mechanisms regulating stress induced IC/BPS are unclear, however, evidence is accumulating that the functional impacts of stress on bladder function and the perception of painful stimuli are likely mediated by long-term perturbations of the HPA axis and the sympathetic-adrenal medulla pathway (Figure 1) (de Groat et al., 2015; Fuentes and Christianson, 2018b; Bendrick et al., 2022). The downstream effectors of these pathways, including CRF, cortisol, and noradrenaline are well known regulators of urinary function and thought to be crucial in regulating centrally mediated changes that induce IC/BPS symptoms (Ulrich-Lai and Herman, 2009; Pierce and Christianson, 2015). Furthermore, clinical studies have revealed that chronic psychological stress induces heightened inflammatory responses in peripheral tissues, including elevated levels of circulating proinflammatory cytokines, and mastocytosis in the bladder (Charrua et al., 2015). Crucially, stress alleviation has been shown to be effective in reducing the severity of IC/BPS symptoms in some patients (Bosch and Bosch, 2014; Webster and Brennan, 1998; Carrico et al.).

6 Current available treatment for IC/BPS

Treatments for IC/BPS are delivered in a personalised and progressive manner in order of their invasiveness, potential to induce harmful side effects, and evidence for clinical success. We have summarised the clinical targets for each type of treatment (Table 1).

6.1 Non-pharmacological treatments

Non-pharmacological treatments including diet and behavioural adaptations are initially offered to all patients to reduce symptom severity. Urine with an acidic pH is thought to exacerbate bladder irritation and can thus be harmful for IC/BPS patients with a diminished urothelium by increasing inflammation (Ueda et al., 2014; Ueda et al., 2021). Dietary modifications that exclude or limit certain foods such as citrus, coffee and alcohol can decrease urine pH to reduce bladder irritation (Koziol et al., 1993; Lai et al., 2019; Garzon et al., 2020b).

Behavioural adaptations incorporate a variety of modifications, including control of fluid intake, bladder training, and stress management. Bladder training is used to control urgency by

TABLE 1 The first-fourth line treatments available for IC/BPS.

Treatment type	Name of treatment	Target
Non-pharmacological Garzon et al. (2020a); Koziol et al. (1993); Lai et al. (2019); Hanno et al. (2015); Ueda et al. (2021); Ogawa et al. (2015); Davis et al. (2014)	Diet Modification Bladder Training	• Control voiding frequency • Reduce bladder pain
Oral Medications Ogawa et al. (2015); Garzon et al. (2020a); van Ophoven et al. (2019); Taneja, (2021); Grigoryan et al. (2022)	Pentosan Polysulphate (PPS)	• Reduce urothelial permeability • Relieve bladder pain • Reduce urinary urgency • Reduce frequency of micturition
Intravesical Instillations Garzon et al. (2020a); Birder et al. (1997); Yoshimura et al. (2021); Tomoe, (2015); Grundy et al. (2018a); Parsons et al. (2015); Welk and Teichman, (2008); Parsons, (2005); Henry et al. (2015); Parsons et al. (2012); Henry et al. (2001); Nickel et al. (2009); Digesu et al. (2020)	Dimethylsulfoxide (DMSO)	• Smooth muscle relaxation • Blocks nerve activity • Provides anti-inflammatory effects • Relieve bladder pain and urinary frequency
	Lidocaine	• Blocks sensory nerve fibres in the bladder • Relieves bladder pain, urgency and nocturia
	Heparin	• Reproduce the activity of native bladder mucosa • Reduces transepithelial migration of solutes such as potassium that could depolarise sensory nerves to stimulate bladder pain, urgency and nocturia
Procedures Hanno et al. (2011a); McCahy and Styles, (1995); Glemain et al. (2002); Yamada et al. (2003); Ueda et al. (2021); Garzon et al. (2020a); Peters et al. (2007); Clemens et al. (2022a); Padilla-Fernandez et al. (2022); Hernández-Hernández et al. (2020)	Hydrodistension	• Increases bladder capacity to relieve urinary symptoms • Relives urinary urgency and frequency • Relieves bladder pain
	Neuromodulation	• Modulates neural pathways responsible for controlling bladder voiding • Relieves urinary urgency and frequency

incrementally and progressively increasing voiding intervals over 1–3 months (Davis et al., 2014; Hanno et al., 2015; Ogawa et al., 2015; Garzon et al., 2020b; Ueda et al., 2021). Bladder training is commonly employed for other urological disorders including overactive bladder syndrome and may be more useful in IC/BPS patients with mild/moderate symptoms (Chaiken et al., 1993; Foster et al., 2010). Patients are also encouraged to implement stress management practices, including increased exercise, as well as non-physical breathing/relaxation techniques, and psychotherapy if deemed necessary.

6.2 Oral medications

Pentosan polysulphate (PPS) is the only FDA approved treatment for IC/BPS (Garzon et al., 2020b; Ueda et al., 2021). PPS is a heparin-like agent that is intended to mimic glycosaminoglycans (GAG) within the bladder to restore urothelial impermeability (Ogawa et al., 2015; Garzon et al., 2020b). Meta-analyses of clinical trials using PPS have shown efficacy compared to placebo in providing moderate relief of bladder pain, urinary urgency, and frequency of micturition without significant side effects in specific subsets of patients (van Ophoven et al., 2019; Taneja, 2021; Grigoryan et al., 2022). However, long term use of PPS presents a risk of macular damage, vision-related injuries, gastrointestinal symptoms, and alopecia.

No new pharmacotherapies specifically designed for treating IC/BPS have been successfully developed, however, clinical data is now accumulating that repurposing immunosuppressive agents, such as Cyclosporine A (CyA) (Sairanen et al., 2004; Forrest et al., 2012; Ehrén et al., 2013; Crescenze et al., 2017), and Certolizumab Pegol (Bosch, 2018) may be efficacious in treating IC/BPS symptoms in patients refractory to approved oral and intravesical treatments. In particular CyA has been shown to have greater efficacy in patients with Hunner lesions, and the AUA now recommends oral CyA as fifth-line therapy for patients with Hunner lesions refractory to current treatments (Clemens et al., 2022a). Larger, longer, and multicenter randomized controlled trials are still required to further investigate certolizumab pegol as a treatment for IC/BPS. Whilst it is common for early-stage drug development not to translate into the clinic, there has been a significant and obvious lack of new oral medications for the treatment of IC/BPS. As a consequence, a variety of pre-existing medications have been trialled and are commonly prescribed in the hope of managing symptoms, including tricyclic antidepressants (amitriptyline), histamine receptor inhibitors (cimetidine and hydroxyzine) for which there is some evidence of efficacy (Henry Lai and Moldwin, 2017; Garzon et al., 2020b; Colemeadow et al., 2020).

6.3 Intravesical instillations

For those patients who do not respond to non-pharmacological or oral medications, intravesical instillations may be recommended.

Dimethylsulfoxide (DMSO) via temporary urethral catheter is an FDA-approved treatment for IC/BPS (Garzon et al., 2020b; Ueda et al., 2021), however, the optimal dwell time, length of induction therapy or length of maintenance therapy is unknown. DMSO induces smooth muscle relaxation, blocks sensory nerve activity, and is anti-inflammatory, and has been used effectively to relieve pain and urinary frequency in IC/BPS patients (Birder et al., 1997; Garzon et al., 2020b). DMSO is especially beneficial for IC/BPS with Hunner lesions (Tomoe, 2015; Yoshimura et al., 2021), however, a large proportion of patients relapse within 2 months of treatment.

Lidocaine/heparin: Lidocaine is a local anaesthetic that blocks voltage gated sodium channels present on the peripheral ends of bladder-innervating sensory nerves (Grundy et al., 2018c). Alkalinisation of lidocaine with sodium bicarbonate increase absorption via the urothelium and increases absorption into the neuronal cytoplasm to enhance the therapeutic effect. The inclusion of heparin within the infusion formulation, a naturally occurring glycosaminoglycan, is considered to provide additional benefits to the treatment of IC/BPS by restoring urothelial impermeability (Parsons et al., 1994). Clinical trials of intravesical instillation of lidocaine/heparin show efficacy in relieving IC/BPS symptoms (Henry et al., 2001; Parsons, 2005; Welk and Teichman, 2008; Nickel et al., 2009; Parsons et al., 2012; Henry et al., 2015; Parsons et al., 2015; Digesu et al., 2020), however, an optimal formulation of combined lidocaine and heparin has not been agreed upon, and its widespread use is limited by the requirement for urethral catheterisation.

6.4 Procedures

If behavioural, oral pharmacology, and intravesical instillations are unsuccessful at controlling symptoms, patients may be recommended for more invasive procedures including bladder hydrodistension or neuromodulation.

Hydrodistension of the bladder under high pressure (60–80 cm H_2O) for a short duration (less than 10 min) can offer relief from urinary symptoms in 30%–55% of patients. However, symptom improvement decreases over time, requiring repeated procedures after only a few months (Hanno et al., 2011a; Garzon et al., 2020b; Ueda et al., 2021).

Neuromodulation has not been FDA-approved as a treatment for IC/BPS but has recently been clinically approved for select patients who have success in a nerve stimulation trial (Clemens et al., 2022b). Neuromodulation can lead to control over urinary symptoms through the emission of electrical stimulation that targets nerve activity due to bladder filling (International Neuromodulation Society, 2013; Padilla-Fernandez et al., 2022). There are two main neuromodulation techniques that are currently being explored to treat IC/BPS; sacral nerve stimulation and pudendal nerve stimulation (Clemens et al., 2022b; Padilla-Fernandez et al., 2022).

Sacral nerve stimulation involves the implantation of a generator under the skin and in the upper buttock area. A small electrode is also placed near the sacral nerve, which will receive electrical impulses from the neurotransmitter, that controls voiding function in the lower spine (Hernández-Hernández et al., 2020; International Neuromodulation Society, 2021a). Pudendal nerve stimulation is seen as an alternative method to sacral nerve stimulation. Similarly, the generator is placed in the upper buttock area, but the electrode is implanted near the pudendal nerve (Peters et al., 2007). The impulses from the generator will stimulate the pudendal nerve and control the pelvic floor muscle during bladder filling (International Neuromodulation Society, 2021b).

Both sacral and pudendal nerve stimulation has been shown to improve urinary symptoms, including bladder capacity, urinary frequency, voided volume, nocturia and pain (Peters et al., 2007; Clemens et al., 2022b; Padilla-Fernandez et al., 2022). However, only a small number of patients have been studied and there is a lack of evidence to suggest that neuromodulation is effective for long periods of time. The AUA guidelines state that sacral/pudendal neuromodulation may be effective in carefully selected patients and emphasise that the procedure can improve frequency/urgency symptoms but is less effective for pelvic pain (Clemens et al., 2022b).

6.5 Issues with available treatments

Despite the availability of multiple treatment options for IC/BPS, no currently available treatment has been shown to permanently reverse disease symptoms, and many patients remain refractory to treatment. As a result, patients continue to suffer with symptoms indefinitely, with available treatments generally only providing temporary relief of chronic pain or are sufficient in a sub-population of patients. At the time of writing, there are 30 clinical trials recruiting or active for interstitial cystitis (ClinicalTrials.gov, 2023), however, the only pharmacological tool being tested is the opioid antagonist Naltrexone (NorthShore University, 2022; Stanford, 2023).

Developing novel and efficacious treatments for IC/BPS is extremely challenging. The diversity of symptoms means that patients may need to take multiple medications or engage in additional interventions that target distinct symptomology. Furthermore, the lack of a defined pathophysiology means that the origin of IC/BPS symptoms may be highly distinct between patients. These clinical challenges are also replicated preclinically, with the diversity of disease and symptoms translating into a difficulty in establishing animal models that can faithfully recapitulate the full spectrum of IC/BPS pathophysiology and symptoms.

7 Animal models of IC/BPS

A key step in identifying novel therapeutic targets for a disease is being able to accurately mirror the human condition in an animal model, which allows determination of the pathological mechanisms that drive symptoms and the subsequent testing of novel therapeutics for symptom alleviation. Unfortunately, because myriad pathophysiological mechanisms have been proposed to mediate the development of bladder dysfunction and bladder hypersensitivity in IC/BPS, this has made the establishment of

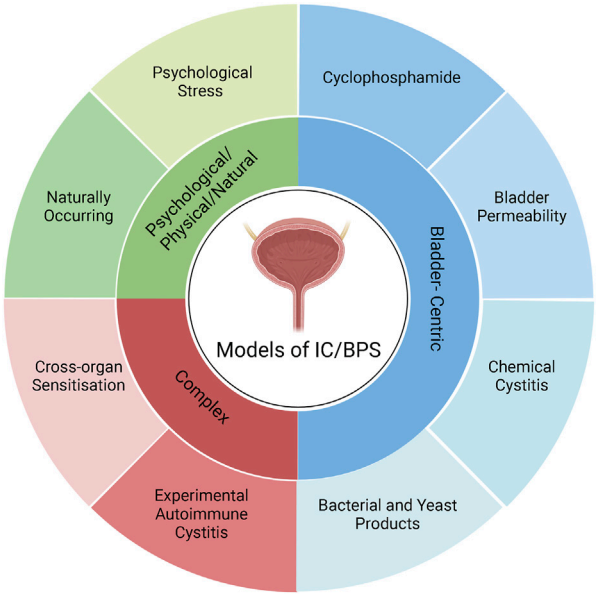

FIGURE 2
Classification of IC/BPS animal models. IC/BPS animal models can be broadly categorised into three different types: Bladder-centric models, models with complex mechanisms, and psychological and physical stressors/natural disease models. Bladder centric models induce an IC/BPS phenotype by direct insult to the bladder that recapitulates the inflammatory or bladder permeability pathophysiology of IC/BPS. Bladder centric models can be further stratified by the type of insult and/or the stimuli used and are the most utilised animal models of IC/BPS. Psychological/Physical/Natural models either have a naturally occurring IC/BPS phenotype such as feline interstitial cystitis or cause IC/BPS like symptoms via psychological stress that models the contribution of stress to the development of IC/BPS. Complex models of IC/BPS employ indirect interventions to generate an IC/BPS phenotype including cross-organ sensitisation from the colon and experimental autoimmune cystitis which have both been implicated in the pathophysiology of IC/BPS. Figure was created using Biorender.com.

accurate animal models and the development of efficacious therapies for these disorders extremely challenging.

A variety of animal models have been developed to recapitulate the complex pathophysiology of IC/BPS (Figure 2). However, as the pathophysiology of IC/BPS is yet to be fully defined, and consists of numerous subclassifications, animal models have focussed primarily on establishing the defining symptoms of bladder hypersensitivity and pain utilising a variety of different methods (Figure 3). The following sections summarise the diverse range of currently utilised animal models and review the ability of these models to resemble distinct aspects of IC/BPS as well as their strengths and limitations (Table 2). The advantages, disadvantages and clinical relevance of each model has been summarised in Table 3.

7.1 Urothelial permeability models

Despite the wealth of clinical evidence supporting a role for increased urothelial permeability in the pathophysiology of IC/BPS, there are relatively few animal models that exclusively target this pathophysiology.

In vivo bladder instillation of protamine sulphate is the most common method for specifically inducing urothelial permeability (Figure 3) (Lavelle et al., 2002; Shin et al., 2011; Hurst et al., 2015). Protamine sulphate promotes an increase in urothelial permeability by inactivating the sulphated polysaccharides of the GAG layer, increasing transcellular permeability of the urothelium and thus increasing absorption of urine solutes (Lasič et al., 2015). At low doses (1–10 mg/ml) protamine sulphate induces only mild urothelial damage, including urothelial sloughing and an increase in transcellular permeability that returns to normal over a period of 7 days (Lavelle et al., 2002; Meerveld et al., 2015). At higher doses (50 mg/ml), however, bladders have been shown to develop urothelial ulceration and infiltration of neutrophils into the mucosa (Soler et al., 2008). Whilst this goes beyond an isolated urothelial permeability model, it provides insight into IC/BPS pathophysiology by confirming that a significant increase in bladder permeability is able to induce bladder inflammation (Figure 4) (Soler et al., 2008). The impact of protamine sulphate on bladder function has not been reported, and the two studies that have assessed bladder sensory output have described contrasting results. A single low dose of protamine sulphate (1 mg/ml) was found to induce bladder afferent hypersensitivity *ex vivo* at 1 day post infusion (Grundy et al., 2020b). Afferent hypersensitivity was characterised by an increase in peak firing and decreased activation thresholds to bladder distension that returned to baseline by day 7 post infusion (Grundy et al., 2020b). In contrast, Stemler et al. reported protamine sulphate treated mice (10 mg/ml) had significantly blunted visceromotor responses (VMR) to bladder distension at noxious bladder distension pressures (Stemler et al., 2013), indicative of reduced peripheral sensory drive from the bladder into the spinal cord. A recent study utilising a cocktail mixture of chondroitinase ABC and heparanase III to deglycosylate the proteoglycans of the GAG layer as an alternate method of

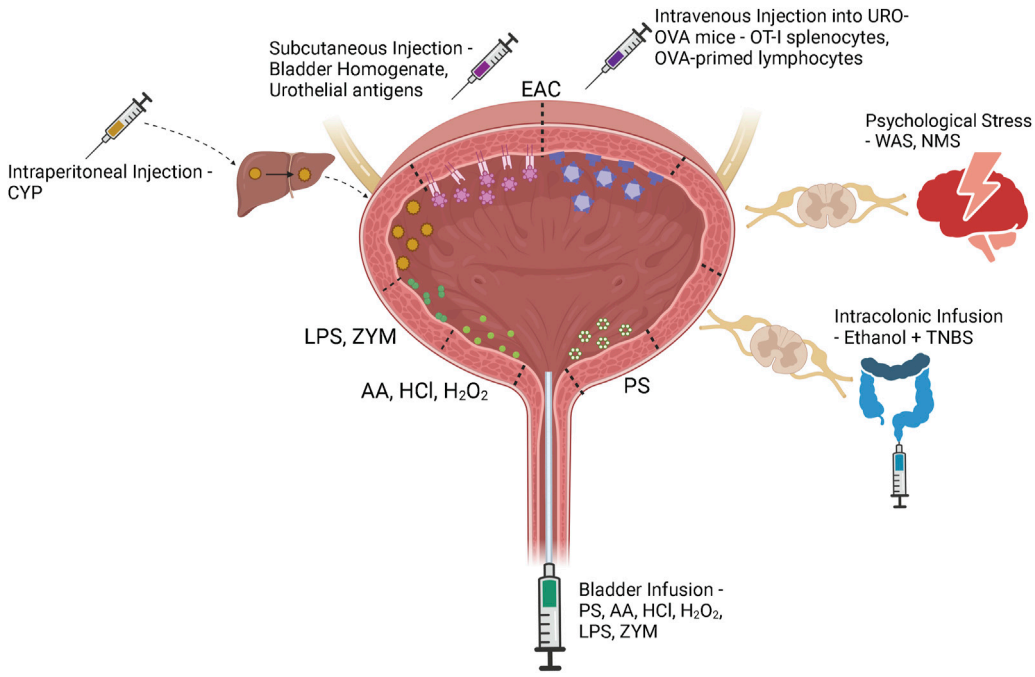

FIGURE 3
IC/BPS model induction methods. Bladder centric models including bladder permeability, chemical cystitis and bacterial and yeast models are induced by direct intravesical instillation of protamine sulfate (PS), acetic acid (AA), hydrochloric acid (HCl), hydrogen peroxide (H_2O_2), lipopolysaccharide (LPS), or zymosan (ZYM) via a bladder catheter. Although cyclophosphamide (CYP) is injected intraperitoneally into the animal, it is metabolised to acrolein in the liver and excreted in the urine to induce bladder damage and inflammation. Experimental autoimmune cystitis (EAC) models can be generated by subcutaneous injection of bladder homogenate or urothelial antigens that trigger autoimmunity through interactions with the membrane expressed MHC Class II molecules. The transgenic EAC model utilises urothelium-ovalbumin (URO-OVA) mice that express an OVA 'self' antigen on the membrane of urothelial cells. When OT-I splenocytes or OVA-primed lymphocytes are intravenously injected into URO-OVA mice they interact with the OVA antigen and trigger an autoimmune response. Psychological stress models including water avoidance stress (WAS) and neonatal maternal separation (NMS) induce bladder hypersensitivity via chronic stress induced dysregulation of the hypothalamic-pituitary-adrenal axis. Continued exposure to a stressful environment can deteriorate the animal's stress response, affecting downstream bladder activity. Cross-organ sensitisation models are induced via intracolonic infusion of ethanol and TNBS. Colonic inflammation sensitises colonic afferents which induces bladder afferent hypersensitivity through viscero-visceral crosstalk between overlapping sensory networks. Figure was created using Biorender.com.

urothelial barrier disruption (Offiah et al., 2017) induces acute increases in c-fos immunoreactivity in the spinal cord, significant decreases in abdominal mechanical withdrawal threshold to von-Frey hair (VFH) probing, and a significant increase in micturition reflex excitability. However, increased pelvic sensitivity and voiding parameters returned to control levels by day 7 post treatment (Offiah et al., 2017), which corresponds with urothelial barrier recovery in low-dose protamine sulphate treated bladders.

7.2 Inflammatory models of IC/BPS

Most animal models of IC/BPS attempt to create an inflammatory phenotype. This has been achieved by irritating the bladder urothelium with chemicals, chemotherapeutics, bacterial products and fungal ligands, and via induced urothelial autoimmunity. Importantly, these inflammatory models are not used because they are thought to be part of the underlying pathophysiology of IC/BPS in humans, although this may be true in some specific cases of cystitis, but because they induce bladder inflammation which leads to bladder hypersensitivity and recapitulates the key symptoms of IC/BPS patients, including increased urinary frequency and pelvic pain.

7.2.1 Irritant models of inflammation

7.2.1.1 Cyclophosphamide

Cyclophosphamide (CYP) is the most frequently used agent to induce cystitis in rodents. CYP is a chemotherapeutic for B cell malignant diseases and some solid tumours (Lee et al., 2014). A common and debilitating side effect of CYP treatment in humans is the development of chronic bladder inflammation and haemorrhagic cystitis, mimicking the most severe phenotypes of IC/BPS. CYP is metabolised to acrolein in the liver, a highly reactive aldehyde which is then renally excreted into the bladder (Figure 3) (Lee et al., 2014). While it accumulates in the bladder, acrolein interacts with the umbrella cells of the luminal urothelium, inducing an inflammatory response (Figure 4) (Lee et al., 2014). Both acute and chronic CYP dosing regimens have been used to generate cystitis in rodents, inducing urothelial permeability and a hypersensitive state characterised by altered voiding parameters and pelvic hypersensitivity (Hu et al., 2003; Chopra et al., 2005; Juszczak et al., 2010; Boudes et al., 2011; Auge et al., 2013; DeBerry et al., 2014; DeBerry et al., 2015; Auge et al., 2020; Chen et al., 2020; Yang et al., 2021; Yoshimura et al., 2021).

TABLE 2 Summary of key characteristics of IC/BPS animal models.

Model	Species	Technique	Acute/Chronic dosing	Bladder damage	Inflammation	Permeability	Nociception	Voiding frequency
Protamine Sulphate Instillation Lavelle et al. (2002); Meerveld et al. (2015); Soler et al. (2008); Offiah et al. (2017); Grundy et al. (2020a); Stemler et al. (2013); Soler et al. (2008); Lasič et al. (2015); Hurst et al. (2015); Shin et al. (2011)	Female Mice and Rats	Bladder Instillation	Acute (single dose)	• Low doses—mild urothelial damage • Higher doses—develop urothelial ulceration and infiltration of neutrophils into the mucosa (dependent on the presence of urine)	• High doses: Infiltration of neutrophils into mucosa at higher doses	• Low dosage: Increase in transcellular permeability that returns to normal over 3–7 days	• Increased bladder afferent peak firing and decreased activation thresholds to bladder distension that returned to baseline by 7 days post infusion • Significantly blunted VMR to bladder distension at noxious bladder distension pressures that returned to control levels by 7 days post treatment	• Increased number of contractions and total contraction time and decreased micturition threshold that returned to baseline after 7 days
Cyclophosphamide Auge et al. (2013); Juszczak et al. (2010); Boucher et al. (2000); Smaldone et al. (2009); Chen et al. (2020); Okinami et al. (2014); Malley and Vizzard, (2002); Hu et al. (2003); Chopra et al. (2005); Coelho et al. (2015); Yoshimura and de Groat, (1999); Mills et al. (2020); Yang et al., (2021); Dang et al. (2008); Boudes et al. (2011), Boudes et al. (2013); DeBerry et al. (2014); Sugino et al. (2015); DeBerry et al. (2015); Gao et al. (2015); Auge et al. (2020); Yoshimura et al. (2021)	Male and Female Mice and Rats	IP injection	Acute (single 150–200 mg/kg dose) results taken within 1 day	• Thick bladder wall • Mucosal erosion on the luminal surface of the urothelium • Severe oedema • Redness • Ulceration • Haemorrhage	• Infiltration of inflammatory cells	• Increased urothelial permeability to water and urea	• Decreased nociceptive threshold in response to innocuous stimulation with von-Frey hairs	• Increased non voiding contractions • Decreased ICI
			Chronic (40–100mg//kg every 2–3 days for 7 or 10 days)	• Extensive mucosal erosion • Ulceration • Oedema • Petechial haemorrhages • Irregular ectasia vessels	• Increased number of inflammatory cells • Upregulation of inflammatory cytokines	• Bladder permeability experiments have not been performed in this model	• Exaggerated EMG responses to noxious bladder distension • Increased pERK immunoreactivity in the LS dorsal horn following bladder distension	• Increased voiding frequency • Decreased voided volume • Reduced ICI
Chemical Cystitis Hauser et al. (2009); Song et al. (2017); Dogishi et al. (2017); Sahiner et al. (2018); Danacioglu et al. (2021); Kirimoto et al. (2007); Song et al. (2015); Çayan et al. (2003); Fraser et al. (2003)	Female Mice	Bladder Instillation	Acetic acid Acute	• Urothelial thinning and cellular loss or erosion after 14 days	• No reported changes in inflammatory response	• Bladder permeability experiments have not been performed in this model	• Nociception experiments have not been performed on this model	• Reduced ICI compared to controls that persisted for up to 7 days

(Continued on following page)

10.3389/fphys.2023.1232017

TABLE 2 (*Continued*) Summary of key characteristics of IC/BPS animal models.

Model	Species	Technique	Acute/Chronic dosing	Bladder damage	Inflammation	Permeability	Nociception	Voiding frequency
			Hydrochloric Acid (HCl) Acute	• Urothelial thinning and cellular loss or erosion after 14 days • Lesions in the epithelium and lamina propria • Oedema • Thickening of the transitional epithelium • Fibroblast swelling	• Infiltration of chronic inflammatory cells (eosinophils, mast cells)	• Bladder permeability experiments have not been performed in this model	• Nociception experiments have not been performed on this model	• Irregular voiding frequency • Decreased inter-contraction interval for up to 7 days • Decreased voided volume • Smaller bladder capacity
			Hydrogen Peroxide (H_2O_2) Acute	• Haemorrhage, oedema and urothelium denudation observed after 1, 7 and 14 days • Vascularisation of the lamina propria observed after 7 and 14 days • Eventual hyperplasia by 7 and 14 days due to thickening of urothelium	• Large number of neutrophils and mast cells from 1 to 14 days • Severe neutrophilic and mononuclear infiltration after 7 days • Small number of infiltrated eosinophils and lymphocytes on 7 and 14 days	• Bladder permeability experiments have not been performed in this model	• Nociception experiments have not been performed on this model	• Significantly more frequent micturition events • Decreased voided volume after 1 day • Significantly lower ICI
Zymosan Randich et al., (2006b), Randich et al., (2006a); DeBerry et al., (2007); Clodfelder-Miller et al., (2022); Ramsay et al., DeBerry et al., (2010); Randich et al., (2009); Ness et al., (2021); Liu et al., (2021)	Female—Rats (neonates for chronic), mice and guinea pigs	Bladder Instillation	Acute (Single dose of zymosan + protamine sulfate (guinea pigs))	• Increased mucosal thickness	• Increased white blood cells within bladder wall observed 1 day after induction	• Enhanced bladder permeability 1 day post infusion	• Enhanced VMR to UBD 1 day post infusion • Bladder hypersensitivity of mucosal afferents to mucosal stroking and high threshold muscular afferents to bladder stretch	• Increased voiding frequency • Decreased voided volume
			Chronic (Repetitive zymosan instillation in neonatal rats)	• No histological abnormalities/ damage between zymosan and controls	• Inflammatory response has not been comprehensively characterised. • Overall reports suggest it is amongst the mildest of bladder-centric models	• Increased neurogenic plasma extravasation in the bladder as adults	• Bladder hypersensitivity to infusion of ice-cold saline • Enhanced VMR to bladder distension	• Significantly more micturition events • Decreased micturition volumes

(Continued on following page)

10.3389/fphys.2023.1232017

TABLE 2 (*Continued*) Summary of key characteristics of IC/BPS animal models.

Model	Species	Technique	Acute/Chronic dosing	Bladder damage	Inflammation	Permeability	Nociception	Voiding frequency
								• Decreased micturition volume thresholds • Increased micturition frequency as adults
Bacterial Products—Lipopolysaccharide (LPS)	Female—rats and mice	Bladder Instillation + protamine sulfate	Acute (Single LPS instillation)	• Oedema and haemorrhage • Vacuolisation of urothelial cells	• Infiltration of mononuclear and polymorphonuclear leukocytes and neutrophils 1 day post LPS • Mast cell infiltration up to 5 days after infusion • Increased expression of pro-inflammatory cytokines	• Bladder permeability experiments have not been performed in this model	• Nociception experiments have not been performed in this model	• Altered bladder voiding behaviour • Increased intra-bladder pressure in response to bladder filling and shorter ICI at 1–3 days after LPS instillation • Higher micturition frequency • Lower maximum pressure
Jerde et al. (2000), Lv et al. (2012), Ryu et al. (2019), Yoshizumi et al. (2021), Li et al. (2017), Sinanoglu et al. (2014), Saban et al. (2002), Tambaro et al. (2014), Song et al. (2017), Raetz and Whitfield (2002), Bjorling et al. (2011)			Chronic (Multiple LPS instillations across several weeks)	• Severely compromised urothelium leading to bladder remodelling • Increased urothelial cells • Abnormally thick re-epithelialisation and tissue fibrosis	• Severe inflammatory cell infiltration of macrophages, lymphocytes and mast cells • Enhanced urinary cytokine concentrations	• Bladder permeability experiments have not been performed in this model	• Increased bladder hypersensitivity after 7, 14 and 21 days • Significantly decreased withdrawal thresholds in the abdomen and hind paw	• Shorter voiding intervals (7 days) • Increased non voiding contractions • Decreased bladder capacity and significantly decreased peak and threshold pressures
Feline Interstitial Cystitis Mohamaden et al. (2019); Jones et al. (2021); Kruger et al. (1991), Kruger et al. (2009); Defauw et al. (2010); Lulich et al. (2010); Lavelle et al. (2000); Roppolo et al. (2005); Birder and Andersson, (2013)	Felines	Naturally occurring	Chronic	• Thinning and denudation of the urothelium • Urothelial spongiosis—loss of cell-cell adhesion • Tight junctions come apart	• Infiltration of lymphocytes and inflammatory cells in the bladder interstitium • Increased mast cells • Significantly higher serum concentrations urinary cytokines	• Significantly reduced transepithelial resistance of the urothelium • Water and urea permeability significantly increased • Lower expression of E-cadherin tight junction protein	• Bladder Aδ afferents from FIC cats are hypersensitive to bladder distension	• Voiding experiments have not been performed in this model

(Continued on following page)

10.3389/fphys.2023.1232017

TABLE 2 (*Continued*) Summary of key characteristics of IC/BPS animal models.

Model	Species	Technique	Acute/Chronic dosing	Bladder damage	Inflammation	Permeability	Nociception	Voiding frequency
Experimental Autoimmune Cystitis Jin et al. (2017); Lin et al. (2008); Liu et al. (2019); Singh et al. (2013); Izgi et al. (2013); Altuntas et al. (2012); Bicer et al. (2015); Liu et al. (2007); Akiyama et al. (2021); Cui et al. (2019); Kim et al. (2011); Kullmann et al. (2018); Wang et al. (2016)	Female Mice	Urinary bladder Homogenate (Subcutaneous injection of bladder homogenates)	Chronic	• Submucosal oedema • Urothelial detachment from the lamina propria • Thickening of the lamina propria 28 days from first immunisation	• Increased levels of cytokines, chemokines, mast cells, neutrophils and infiltration of $CD4^+$ lymphocytes 14 days from second immunisation	• Bladder permeability experiments have not been performed for this model	• Hyperalgesia to von Frey hair probing of the pelvic area and decreased pelvic pain threshold 14 days after second immunisation	• Shorter voiding intervals • Decreased voided volume • Increased number of urine spots
		Uroplakin (Subcutaneous injection of recombinant mouse uroplakin proteins)	Chronic	• Bladder remodelling	• Increased gene expression of inflammatory cytokines • Extensive perivascular leukocyte • Higher expression of the mast cell chemoattractant/activator CCL2 • Increased numbers of activated, resting and total mast cells in the bladder detrusor at 10, 20 and 40 days after immunisation	• Bladder permeability experiments have not been performed for this model	• Greater sensitivity to von Frey probing of the suprapubic region from 5 to 40 days after immunisation	• Altered bladder function developed 35 days after immunisation • Increased urinary frequency • Decreased mean urine outputs per void
		Transgenic URO-OVA Models (Intravenous injection of activated OVA-specific T-cells into URO-OVA mice)	Chronic	• Interstitial oedema • Increased vascularity • Epithelial hyperplasia lasts for 7–28 days after adoptive transfer	• Mononuclear cellular infiltration—T ($CD3^+$) and B ($CD19^+$) lymphocytes • Mucosal hyperemia • Increased mRNA expression of mast cell and sensory neuron-derived inflammatory factors • 2-fold increase in mast cells within the lamina propria and the detrusor	• Bladder permeability experiments have not been performed for this model	• Significantly increased pelvic nociceptive responses to von Frey hairs • Significantly decreased sensory thresholds to pelvic nociception • Increased VMR to bladder distension	• Altered voiding behaviours developed 7–28 days after cystitis induction • Decreased maximum volume voided per micturition • Significant increase in the frequency of urination

(Continued on following page)

10.3389/fphys.2023.1232017

TABLE 2 (*Continued*) Summary of key characteristics of IC/BPS animal models.

Model	Species	Technique	Acute/Chronic dosing	Bladder damage	Inflammation	Permeability	Nociception	Voiding frequency
Psychological Stress Models Pierce et al. (2018), Pierce et al. (2016); West et al. (2021); Matos et al. (2017); Lee et al. (2015); Gao et al. (2018); Wang et al. (2017); Robbins et al. (2007); Dias et al. (2019)	Male and Female Rats and Mice	Water Avoidance Stress Models (Rats placed on a platform in the middle of a tank filled with water—performed 1h a day over 10 days)	Chronic	• Loss of superficial umbrella cells • Altered urothelial surface	• Increased inflammatory cells infiltration in the mucosa • Higher number of mast cells	• Bladder permeability experiments have not been performed for this model	• Significantly increased frequency of responses to von-Frey hairs at 5 days • Reached a plateau after 8 days • VMR evoked at lower bladder pressure and for a longer duration	• Significant increase in urinary frequency • Decrease in the average void size • Increase in the number of small voids by 3 days of WAS exposure
		Neonatal Maternal Separation (Separation of litters of pups from the dam for up to 21 days from postnatal D1)	Chronic	• Bladder damage has not been studied for this model	• Lower mRNA levels of CRF_1 and GR and higher BDNF in the hippocampus • Low CRF and GR levels indicate decreased inhibition on the HPA axis • Decreases animal resilience to stress over time • Significantly higher percentage of degranulate mast cells in the bladder	• Bladder permeability experiments have not been performed for this model	• Greater VMR response to UBD after 56 days	• Increased voiding frequency • Smaller void spots
Cross-organ Sensitisation Models Antoniou et al. (2016); Hughes et al. (2009); Vannucchi and Evangelista, (2018); Grundy and Brierley, (2018); Grundy et al. (2018a); Meerveld et al. (2015); Towner et al. (2015); Lei and Malykhina, (2012); Xia et al. (2012); Fitzgerald et al. (2013); Ustinova et al. (2007); Liang et al. (2007); Lamb et al. (2006); Ustinova et al. (2006)	Male and Female Rats and Mice	Intracolonic co-administration of ethanol and TNBS	Chronic	• No changes in bladder histology	• No marked bladder inflammation	• Urothelial permeability increases during the active phase of colonic inflammation from 1 to 7 days post TNBS	• Bladder sensory nerves exhibit hypersensitivity to UBD during the active inflammatory phase of TNBS colitis and 28 days post colitis • Enhanced bladder VMR to UBD	• Reduced bladder capacity, voided volumes, ICI and changes in bladder voiding patterns persist up to 90 days post TNBS

10.3389/fphys.2023.1232017

TABLE 3 Advantages, disadvantages and clinical relevance of each IC/BPS model.

Model	Advantage	Disadvantage	Clinical relevance
Bladder Permeability Models with Protamine Sulphate	• Results in bladder permeability • Bladder damage dependent on the presence of urine supports concept well established leaky urothelium to bladder inflammation pathomechanism	• Can only be performed in female rodents due to catheterisation • Shows limited inflammation • No reported changes in bladder function • Inconsistent reports of alterations of bladder sensation or sensory signalling • Also supports pathophysiology that inflammation is necessary to maintain urothelial permeability generating a feedback loop	• Recapitulates only limited aspects of the IC/BPS phenotype
Cyclophosphamide (CYP)	• Can be easily done in both male and female animals • Model is well established and supported by a large amount of literature • Animals develop increased voiding frequency and bladder hypersensitivity which are key hallmarks of IC/BPS • Animals also develop bladder damage and infiltration which mostly mirror clinical observations from IC/BPS patients	• Results in a relatively transient effect on the bladder and does not recapitulate the chronic and progressive nature of IC/BPS • Results in a relatively transient effect on the bladder and does not recapitulate the chronic and progressive nature of IC/BPS	• This best models IC/BPS without Hunner lesions. • Clinically relevant to patients who develop post-chemotherapy induced cystitis
Chemical Cystitis—using Acetic Acid (AA), Hydrogen chloride (HCl) and Hydrogen Peroxide (H_2O_2)	• Effects are bladder-centric and there are no confounding impacts on the body • Has a long lasting effect and develop into chronic changes in bladder function • Model results in altered voiding behaviours	• Can only be performed in female rodents • Results in severe bladder inflammation that exceeds IC/BPS without Hunner lesions • No reports on whether animals develop bladder hypersensitivity	• Extremely severe bladder damage that seems to be more characteristic of IC/BPS with Hunner lesions
Zymosan	• Dual insult version of this model recapitulates IC/BPS patients with previous bladder infection well • After second inflammatory insult, adult mice develop greater bladder hypersensitivity and altered voiding behaviour	• Can only be performed in female rodents due to catheterisation • No reports of developed bladder damage in chronic models	• Chronic model of IC/BPS without Hunner lesions • Clinically relevant to IC/BPS patients who have previously had an early life bladder infection
Bacterial Products (Lipopolysaccharide)	• Developed chronic model that results in urothelial denudation, tissue fibrosis and infiltration of inflammatory cells and cytokines • Animals also developed altered voiding behaviours and bladder hypersensitivity	• Can only be performed in female rodents due to catheterisation • Results in severe bladder damage	• The chronic model results in a severely compromised urothelium that eventually results in bladder remodelling and tissue fibrosis as well as mast cell infiltration which are characteristics of IC/BPS without Hunner lesions
Naturally Occurring—Feline Interstitial Cystitis	• Model does not require external intervention • Development of histological features—urothelial denudation, submucosal oedema, chronic inflammatory cell infiltrates and muscularis fibrosis • Bladder afferents from FIC cats become hypersensitive to bladder distension	• Natural occurring in felines where the aetiology is unknown • Model is not widely available—difficult to find reasonable numbers of cats for experimental purposes • Ethical considerations with studying cats for more in depth bladder activity—organising and consulting with a veterinarian and a higher cost of maintenance	• While there are many shared phenotypes between FIC and IC/BPS without Hunner lesions, the underlying cause for either disease is still unknown, therefore unclear whether FIC is a reliable model of IC/BPS
Urinary bladder homogenate	• Can be performed in C57BL/6J mice which are widely used and also express IA^B MHB class II molecules that are identical to human beings • Animals developed bladder damage, inflammation, increased urinary frequency and bladder hyperalgesia	• Induces non-specific immune response as bladder homogenate is not a tissue-specific protein for immunisation	• Model closely represents IC/BPS with Hunner lesions which has been hypothesised to have an autoimmune nature

(Continued on following page)

TABLE 3 (*Continued*) Advantages, disadvantages and clinical relevance of each IC/BPS model.

Model	Advantage	Disadvantage	Clinical relevance
Uroplakin	• Models exhibit extensive bladder damage and inflammation • Developed increased urinary frequency • UPK3A 65–84 mice showed bladder hypersensitivity	• Not performed in C57BL/6J mice—less accessible • UPK3A 65–84 is a specific peptide to induce autoimmunity in BALB/c mice	• Model closely represents IC/BPS with Hunner lesions which has been hypothesised to have an autoimmune nature
Transgenic URO-OVA	• Animals developed bladder inflammation • Some bladder damage but not urothelial denudation • Had increased urinary frequency • Exhibited bladder hypersensitivity	• OVA is not an endogenous antigen of bladder • Have been used only in female mice so far	• Model closely represents IC/BPS with Hunner lesions which has been hypothesised to have an autoimmune nature
Water Avoidance Stress	• Animals develop altered voiding behaviour and bladder hypersensitivity • Loss of superficial umbrella cells leading to an altered urothelial surface • Signs of increased inflammatory cells infiltration in the mucosa	• Gut and bladder interact in health and disease and therefore delineating the direct from indirect effects of WAS on bladder function are difficult • Majority of effects on bladder function have only been characterised at relatively short intervals	• Model represents patients with chronic stress and anxiety who develop IC/BPS without Hunners lesions
Neonatal Maternal Separation (NMS) Models	• Can be performed in both male and female animals • Does not cause significant inflammation in the bladder • Induces long lasting sensory hypersensitivity • Induces long lasting bladder hyperactivity • Induces mild bladder permeability • NMS has been shown to have effects on brain structures affecting HPA axis signalling	• No disadvantages found	• Models the high proportion of IC/BPS without Hunner lesions patients that also have comorbid anxiety and or history of psychological trauma
Cross-organ sensitisation	• Does not cause significant inflammation in the bladder • Induces long lasting sensory hypersensitivity • Induces long lasting bladder hyperactivity • Induces short-lasting bladder permeability • Can be performed in both male and female animals • Relatively simple to establish (inexpensive)	• No reports of bladder inflammation	• Models the high proportion of IC/BPS patients that also have chronic abdominal pain, IBS

7.2.1.1.1 Acute CYP treatment. Acute CYP treatment in rodents consists of a single high (150–200 mg/kg) dose injected intraperitoneally which leads to severe inflammation and dramatic alterations to bladder tissue morphology, bladder overactivity, and acute pelvic pain within 24 h (Boucher et al., 2000; Malley and Vizzard, 2002; Hu et al., 2003; Chopra et al., 2005; Smaldone et al., 2009; Juszczak et al., 2010; Auge et al., 2013; Okinami et al., 2014; Coelho et al., 2015; Chen et al., 2020). Bladder damage and inflammation following acute CYP treatment is characterised by a thickening of the bladder wall, mucosal erosion on the luminal surface of the urothelium, severe oedema, redness, ulceration of the urothelium and haemorrhage. This severe tissue damage is associated with infiltration of inflammatory cells (Yoshimura and de Groat, 1999; Boucher et al., 2000; Malley and Vizzard, 2002; Hu et al., 2003; Chopra et al., 2005; Smaldone et al., 2009; Juszczak et al., 2010; Auge et al., 2013; Chen et al., 2020), and elevated inflammatory cytokines, including IL-α, IL-1β, IL-2, IL-4, IL-5, IL-6, IL-10, IL-18, TNF-α/β, as well as the chemokine MCP-1 in the bladder wall (Malley and Vizzard, 2002; Smaldone et al., 2009; Auge et al., 2013; Jhang and Kuo, 2016a; Chen et al., 2020). Acute-CYP treatment in rats also significantly reduces transepithelial resistance and increases urothelial permeability to water and urea (Chopra et al., 2005).

Acute CYP treatment induces marked bladder hyperreflexia, characterised by an increase in non-voiding contractions and micturition frequency, and a decrease in the intercontraction

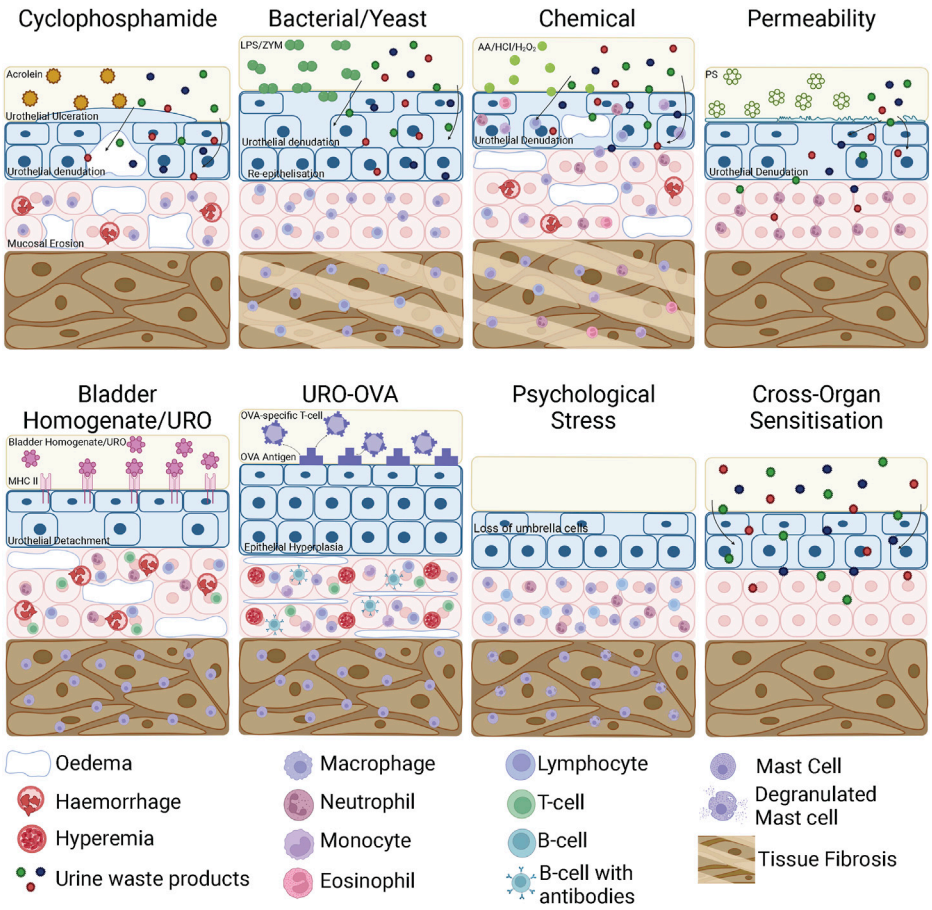

FIGURE 4
Bladder inflammation and damage in bladder cystitis animal models. In a CYP model, acrolein in the urine interacts with the urothelium to initiate an inflammatory response characterised by urothelial denudation and increased permeability, ulceration, interstitial oedema, mucosal erosion, haemorrhage and mast cell infiltration. LPS and ZYM bind to receptors on the surface of the urothelium, initiating an inflammatory response that results in urothelial denudation and bladder permeability. In chronic models, the urothelium thickens due to re-epithelisation and the detrusor layer undergoes tissue fibrosis. Chemical cystitis models induced by AA/HCl/H_2O_2 directly damage urothelial cells leading to urothelial denudation and severe inflammation characterised by mast cell, lymphocyte, monocyte, neutrophil and eosinophil infiltration as well as oedema and haemorrhage. In chronic stages of chemical cystitis models, the detrusor undergoes tissue fibrosis. Bladder permeability models such as protamine sulfate disrupt the GAG layer, increasing urothelial permeability and inducing mild inflammation that allows toxic waste products contained within the urine to access the bladder wall. In EAC models using bladder homogenates or urothelial products, the bladder homogenates/urothelial products interact with the membrane bound MHC Class II molecule and triggers an autoimmune reaction. This consists of urothelial detachment from the mucosa, mucosal oedema, haemorrhage and the recruitment of mast cells to the detrusor and neutrophils, lymphocytes and T-cells to the mucosa. In transgenic EAC models, OVA specific T-cells are recognised by the OVA 'self' antigen expressed on the urothelium of URO-OVA mice. This triggers an autoimmune response including epithelial hyperplasia, mucosal oedema, hyperaemia, infiltrating mononuclear cells and the recruitment of mast cells to the mucosa and detrusor. In psychological stress models, there is a loss of superficial umbrella cells in the urothelium, increased inflammatory cell infiltration into the mucosa and mast cell degranulation. Cross-organ sensitisation models increase bladder permeability but do not induce inflammation. CYP, Cyclophosphamide; EAC, Experimental Autoimmune Cystitis; AA, Acetic Acid; HCl, Hydrochloric acid; H_2O_2, Hydrogen Peroxide; PS, Protamine Sulphate; LPS, lipopolysaccharide; ZYM, zymosan; TNBS, trinitrobenzene sulfonic acid; WAS, Water Avoidance Stress; NMS, Neonatal Maternal Separation; URO-OVA, urothelium-ovalbumin. Figure was created using Biorender.com.

interval and maximum voided volume for up to 36 h post CYP administration (Hu et al., 2003; Chopra et al., 2005; Juszczak et al., 2010; Okinami et al., 2014; Chen et al., 2020). Acute CYP treatment also results in a decreased nociceptive threshold in response to innocuous mechanical stimulation of the peritoneum with von Frey hairs *in vivo* in the 4 hours post CYP, and increased bladder afferent responses to distension *ex vivo* 24 h after CYP (Auge et al., 2013; Mills et al., 2020).

7.2.1.1.2 Chronic cyclophosphamide treatment. Chronic dosing regimens involve repetitive doses of CYP at lower concentrations (40–100 mg/kg), given every 2–3 days for 7 or 10 days (Yoshimura and de Groat, 1999; Malley and Vizzard, 2002; Hu et al., 2003; Chopra et al., 2005; Dang et al., 2008; Juszczak et al., 2010; Boudes et al., 2011; Boudes et al., 2013; DeBerry et al., 2014; DeBerry et al., 2015; Gao et al., 2015; Sugino et al., 2015; Auge et al., 2020; Yang et al., 2021; Yoshimura et al., 2021), and have an added advantage of more closely mimicking a cyclophosphamide chemotherapy dosing schedule.

Like acute high-dose CYP, chronic CYP treatment in rats induces severe bladder inflammation including extensive mucosal erosion, ulcerations, oedema, occasional petechial haemorrhages and irregular ectasia vessels (Figure 4) (Malley and Vizzard,

2002; Hu et al., 2003; Juszczak et al., 2010; DeBerry et al., 2014; Gao et al., 2015; Sugino et al., 2015; Yoshimura et al., 2021). Inflammation is characterised by an increase in the number of inflammatory cells, including mast cells infiltrating the bladder mucosa (Malley and Vizzard, 2002; Juszczak et al., 2010; Yang et al., 2021; Yoshimura et al., 2021), and significant upregulation of inflammatory cytokines including IL-1β, IL-2, IL-6, IL-10 and TNF-α.

Chronic CYP treated rodents show increased sensory innervation within the bladder wall, hypersensitivity of bladder sensory nerves, and allodynia and hyperalgesia to VFH probing of the abdomen (Boudes et al., 2011; Auge et al., 2020). Chronic CYP-treated mice also develop an exaggerated VMR to noxious bladder distension (DeBerry et al., 2014) and increased pERK immunoreactivity in the lumbosacral dorsal horn following bladder distension (DeBerry et al., 2014), indicating there is an increased peripheral drive into the spinal cord due to exaggerated peripheral sensory signalling. These changes in bladder sensation and sensory signalling are also associated with significant alterations in cystometric parameters characteristic of an inflammatory phenotype (Yoshimura and de Groat, 1999; Dang et al., 2008; Boudes et al., 2013), including increased voiding frequency, decreased voided volume, reduced intercontraction intervals and increases in mean basal pressure compared to control animals (Dang et al., 2008; Juszczak et al., 2010; Yang et al., 2021; Yoshimura et al., 2021). Changes in bladder function and sensitivity evoked by chronic CYP treatment have been shown to persist long after treatment but most studies see the effects of treatment return to baseline by 7–10 days post treatment, highlighting the relative transience of even chronic CYP models. Whilst this is longer than the 1–3-day window of hypersensitivity that is induced by acute CYP dosing, it does not recapitulate the chronic and reportedly progressive nature of IC/BPS. CYP is also known to have global impacts on health, including body condition, weight loss, gastrointestinal dysfunction, and stress amongst others, yet the impacts of these extra-bladder effects are rarely considered when interpreting data from CYP animal models.

7.2.1.2 Chemical cystitis

Rodent models of acute and chronic cystitis have also been induced by intravesical instillation of a variety of chemicals including hydrochloric acid (HCl), hydrogen peroxide (H_2O_2) and acetic acid (AA) (Figure 3).

Induction of chemical cystitis in animals using AA, HCl or H_2O_2 leads to severe bladder damage and inflammation (Figure 4). During the early stages of cystitis induction (1–3 days after chemical instillation), the bladder shows denudation of urothelial umbrella cells and an increase in urothelial permeability (Hauser et al., 2009). There is also the appearance of haemorrhage and oedema, and the infiltration of inflammatory cells throughout the bladder including neutrophils, monocytes, lymphocytes and natural killer cells (Dogishi et al., 2017; Song et al., 2017; Sahiner et al., 2018). In the later stages of cystitis progression, 7–14 days after chemical instillation, bladder damage becomes more severe with large fibrotic patches, vascular congestion and submucosal oedema as well as infiltration of chronic inflammatory cells including eosinophils and mast cells (Kirimoto et al., 2007; Dogishi et al., 2017; Danacioglu et al., 2021). By day 14, due to epithelial denudation, the bladder has significantly increased tissue fibrosis which leads to thickening of the bladder wall and hyperplasia (Song et al., 2015; Dogishi et al., 2017).

Intravesical AA in rats causes immediate bladder dysfunction, with reduced intercontraction intervals and bladder compliance 20–30 min after infusion that can persist for up to 2 weeks (Fraser et al., 2003). H_2O_2 instillation also leads to significantly more frequent micturition events and decreased voided volume after 24 h (Dogishi et al., 2017). Significantly shorter mean intercontraction intervals and the development of irregular non-voiding bladder contractions are also seen after bladder instillation of HCl or AA in rats (Çayan et al., 2003; Kirimoto et al., 2007; Song et al., 2015; Dogishi et al., 2017; Song et al., 2017). These effects are maintained 7–14 days after chemical instillation of HCl, AA or H_2O_2, highlighting the development of a persistent disease phenotype. Despite these well characterised changes in bladder function, reports of altered bladder sensation and or sensory signalling are lacking from preclinical studies.

7.2.2 Bacterial and yeast products

Bacterial and fungal infections of the urinary tract are natural causes of bladder inflammation. To model this natural inflammation, a variety of studies have instilled biological inflammogens into the bladder, including Lipopolysaccharide (LPS), a bacterial product found in the outer membrane of gram-negative bacteria, and Zymosan, a ligand found on the surface of fungi, like yeast (Figure 3). In contrast to chemical irritants which rely on extensive tissue damage to induce inflammation, natural inflammogens produce a receptor-mediated reactive cellular process to induce inflammation. Zymosan binds to Toll-like receptor 2 (TLR2) and dectin 1 (Underhill et al., 1999; Sato et al., 2006), whilst LPS is detected by a diverse repertoire of proteins, including Toll-like receptors (TLRs), integrins, G-protein coupled receptors (GPCRs), and proteases (Kagan, 2017).

7.2.2.1 Bacterial products

Lipopolysaccharide (LPS) has been commonly used to induce cystitis via direct infusion into the bladder for up to 45 min (Jerde et al., 2000; Lv et al., 2012; Sinanoglu et al., 2014; Li et al., 2017; Ryu et al., 2019; Yoshizumi et al., 2021). Protamine sulphate is often instilled into the bladder prior to LPS to weaken the GAG layer and allow LPS to interact directly with the urothelium (Lv et al., 2012; Sinanoglu et al., 2014; Li et al., 2017; Ryu et al., 2019). Modifications to the concentration, dwell time, and frequency of LPS instillations has allowed the development of both acute and chronic cystitis models.

Instillation of LPS in rodents induces bladder inflammation and bladder damage that persists up to 5 days after a single instillation. This includes severe disruption of bladder submucosal structures, vacuolisation of urothelial cells, infiltration of mononuclear and polymorphonuclear leukocytes and neutrophils and increased expression of pro-inflammatory cytokines IL-1α, IL-1β, IFN and TNF-α 24 h after a single LPS instillation (Jerde et al., 2000; Saban et al., 2002; Lv et al., 2012; Sinanoglu et al., 2014; Tambaro et al., 2014; Li et al., 2017). Bladder damage and inflammation is correlated with altered bladder voiding behaviour, increased intra-bladder

pressure in response to bladder filling and shorter intercontraction intervals at 1–3 days post LPS instillation (Tambaro et al., 2014; Song et al., 2017). A single combined treatment of protamine sulphate and LPS leads to a significantly higher micturition frequency, as well as a significantly lower maximum storage pressure compared to that of controls 5 days after instillation in rats (Li et al., 2017).

To develop a more chronic cystitis phenotype LPS is instilled into bladders more than once, either daily for 4–14 days, twice weekly for 5 weeks, or once weekly for 4 weeks (Saban et al., 2007; Ryu et al., 2019; Chen et al., 2021; Yoshizumi et al., 2021). Chronic treatments result in a severely compromised urothelium that eventually leads to bladder remodelling caused by abnormally thick re-epithelialisation and tissue fibrosis (Figure 4) (Ryu et al., 2019; Chen et al., 2021; Yoshizumi et al., 2021). Inflammatory cells including macrophages, lymphocytes and mast cells infiltrate the bladder mucosa and enhanced cytokine concentrations are found in the urine (Saban et al., 2007; Ryu et al., 2019; Chen et al., 2021; Yoshizumi et al., 2021). At least 7 days after the final LPS instillations rodents exhibit bladder dysfunction characterised by shorter voiding intervals, increased non voiding contractions, decreased bladder capacity and significantly decreased peak and void threshold pressures compared to control animals (Song et al., 2017; Ryu et al., 2019; Chen et al., 2021; Yoshizumi et al., 2021). Additionally, chronic LPS-treated rats have increased pelvic hypersensitivity after 7, 14 and 21 days, with withdrawal thresholds to von-Frey hair probing of the abdomen and hind paw significantly decreased compared to controls (Yoshizumi et al., 2021) suggestive of altered bladder sensory signalling and pain processing.

7.2.2.2 Zymosan

Various concentrations and dosing schedules of intrabladder zymosan infusion have been utilised to develop animal models of IC/BPS. The first reported use of zymosan as a model of cystitis employed a single intrabladder infusion of zymosan in rats. Rats developed an enhanced VMR to bladder distension and Evans blue extravasation in the bladder 24 h post infusion indicative of enhanced bladder permeability and bladder hypersensitivity to distension (Randich et al., 2006a; Randich et al., 2006b; DeBerry et al., 2007). Zymosan has also been shown to exaggerate the VMR to bladder distension in mice 24 h post infusion (Clodfelder-Miller et al., 2022). Combining zymosan with protamine sulphate (10 mg/ml) pre-treatment has recently been described in adult guinea pigs and was shown to induce inflammation and mucosal thickening 24 h post-infusion, sensitise bladder afferents to mechanical stimuli, and enhance the VMR to high pressure bladder distensions and increase voiding frequency (Ramsay et al., 2023).

Separate studies have investigated the long-term impact of zymosan induced cystitis utilising neonate rats. Epidemiological data indicates that inflammation in early life has correlative if not causative relevance to the pathophysiology of IC/BPS (Sharma et al., 2023). As such, this model was designed to recapitulate the real-world experience of early in life bladder inflammation and its potential to induce chronic changes in bladder sensation and function. Daily intrabladder instillation of zymosan in neonatal (p-14-18) rats resulted in bladder hypersensitivity in response to the infusion of ice-cold saline, increased sensitivity to intravesical potassium infusion and enhanced the VMR to bladder distension (Randich et al., 2006a; Randich et al., 2009; DeBerry et al., 2010; Ness et al., 2021). Neonatal zymosan also increased neurogenic plasma extravasation in the bladder and urinary frequency as adults, indicating the development of chronic changes in urothelial permeability and bladder sensitivity (Randich et al., 2006a; Randich et al., 2009; DeBerry et al., 2010; Ness et al., 2021). Intriguingly, no obvious histological abnormalities/damage are reported between neonatal zymosan, and control treated rats, suggesting changes in bladder function and sensitivity might be 'locked in' even following the resolution of zymosan induced inflammation in neonates (DeBerry et al., 2010). In mice, following the same neonatal zymosan treatment paradigm, neonatal bladder inflammation increases voiding frequency, and decreases intercontraction interval during cystometry. Neonatal bladder inflammation in mice did not evoke enhanced VMR to bladder distension suggesting species and/or mouse strains may be a defining feature in zymosan induced chronic hypersensitivity (Clodfelder-Miller et al., 2022).

Further exploration of the zymosan cystitis model has employed dual insults in both mice and rats, with neonatal multi-day zymosan being followed by a single zymosan infusion in adults. In general, the effect of this dual insult on cystitis induction is greater when compared directly to a single neonatal or adult insult, with animals exhibiting greater changes in bladder function and hypersensitivity. Rats and mice were reported to have decreased maximum micturition pressure and micturition weight as well as a significantly greater VMR to bladder distension (Randich et al., 2006a; Ness et al., 2021; Clodfelder-Miller et al., 2022), enhanced detrusor EMG responses to rapid increases in bladder pressure and enhanced abdominal withdrawal reflex scores 2–3 days after the final treatment as adults (Liu et al., 2021).

7.3 Autoimmune cystitis models

Experimental autoimmune cystitis (EAC) models have been developed based on the hypothesis that IC/BPS is caused by out-of-control bladder autoimmunity (Akiyama et al., 2020). Several methods of stimulating autoimmunity within the bladder wall have been explored.

7.3.1 Urinary bladder homogenate

Subcutaneous injection of bladder homogenates into mice can induce EAC by making the bladder a target for autoimmunity (Figure 3). Briefly, bladders from female mice are homogenised and then lyophilised before being used to immunise recipient mice (Lin et al., 2008; Jin et al., 2017).

Urinary bladder homogenates have been used to induce EAC in both SWXJ and C57BL/6J mice strains (Lin et al., 2008; Jin et al., 2017; Liu et al., 2019). SWXJ strains are genetically more susceptible to the development of several autoimmune diseases initiated by Th1-type responses (Lin et al., 2008). However, immunising mice with bladder homogenates leads to the induction of EAC in both strains, but dual immunisation of bladder homogenates made 2 weeks apart was required to induce EAC in C57BL/6J mice. EAC was

characterised by mast cell, neutrophil, and lymphocyte infiltration and significantly elevated levels of cytokines and chemokines within the bladder wall (Lin et al., 2008; Singh et al., 2013; Lin et al., 2008; Jin et al., 2017; Liu et al., 2019). Bladders developed submucosal oedema, urothelial detachment from the lamina propria, and mucosal thickening (Figure 4) (Lin et al., 2008).

Both SWXJ and C57BL/6 mice receiving subcutaneous injection of bladder homogenates develop bladder dysfunction in the form of shorter voiding intervals, decreased voided volume, and increased number of urine spots that were of a smaller size indicative of urinary frequency (Lin et al., 2008; Jin et al., 2017; Liu et al., 2019). Mice also developed hyperalgesia to von-Frey hair probing of the pelvic area and a decreased pelvic pain threshold 2 weeks after the second immunisation (Jin et al., 2017; Liu et al., 2019). To date, no assessment of bladder sensory nerve signalling or evoked pain responses such as VMR have been performed using this EAC model.

7.3.2 Uroplakin models

Uroplakins (UP-Ia, UP-Ib, UP-II and UP-III) are a family of transmembrane proteins that are exclusively expressed in the bladder urothelium (Altuntas et al., 2012). Uroplakin EAC models are induced by subcutaneous injection of recombinant mouse uroplakin proteins that induce a urothelial-mediated cystitis (Figure 3).

Uroplakin EAC induced in SWXJ and BALB/c mice using rmUPK2 and UPK3A 65-84 respectively leads to extensive perivascular leukocyte (predominantly $CD3^+$ T cells) infiltration (Altuntas et al., 2012; Izgi et al., 2013) and significantly elevated expression of genes encoding inflammatory cytokines TNF-α, IL-17A, IFN-γ, and IL-1β within the bladder (Altuntas et al., 2012; Izgi et al., 2013). A separate study also found significantly higher expression of the mast cell chemoattractant/activator CCL2 in the bladders of EAC mice; a contributing factor to the increased numbers of activated, resting and total mast cells in the bladder detrusor at up to 40 days after EAC induction (Bicer et al., 2015). Uroplakin EAC mice developed altered bladder function indicative of cystitis 5 weeks after immunisation, including increased urinary frequency and significantly decreased voided volume (Altuntas et al., 2012; Izgi et al., 2013). UPK3A 65-84 mice also showed greater sensitivity to von-Frey probing of the suprapubic region from day 5 after immunisation (Izgi et al., 2013; Bicer et al., 2015) that persisted for at least 40 days (Bicer et al., 2015). EAC induced in the rmUPK2 model did not demonstrate enhanced pelvic pain to noxious von-Frey forces (Altuntas et al., 2012). As different mouse strains as well as different recombinant mouse uroplakin proteins were used in these studies, it is not clear which is the fundamentally crucial variable. No assessments of bladder sensory nerve signalling or evoked pain responses such as VMR have been performed using this EAC model.

7.3.3 Transgenic URO-OVA models

The most studied transgenic EAC mouse model is the URO-OVA model which requires the expression of the membrane form of model antigen ovalbumin (OVA) as a self-antigen on the bladder urothelium (Liu et al., 2007). This is achieved via the adoptive transfer of activated OVA-specific T-cells. These can either be OVA-specific $CD8^+$ T cells from OT-I mice that express the transgenic $CD8^+$ T-cell receptor specific for the $OVA_{257-264}$ epitope peptide, or adoptive transfer of OVA-primed splenocytes after immunisation in C57BL/6 mice (Liu et al., 2007; Akiyama et al., 2021). These activated OVA-specific cells are then intravenously injected via the orbital sinus of URO-OVA mice to induce bladder cystitis (Figure 3) (Liu et al., 2007; Akiyama et al., 2021).

URO-OVA mice develop bladder inflammation from 7 days after adoptive T-cell transfer. Mice immunised with either OT-I or OVA-primed splenocytes developed interstitial oedema, increased vascularity, mononuclear cellular infiltration (predominantly T ($CD3^+$) and B ($CD19^+$) lymphocytes), mucosal hyperemia and epithelial hyperplasia (Figure 4) (Liu et al., 2007; Kim et al., 2011; Wang et al., 2016; Akiyama et al., 2021). However, no clear urothelial denudation was observed in the inflamed bladders (Akiyama et al., 2021). Increased mRNA expression of mast cell and sensory neuron-derived inflammatory factors MCP-1, IL-6, IFN-γ, TNF-α, NGF, pre-SP and substance P (Liu et al., 2007; Kim et al., 2011; Wang et al., 2016; Kullmann et al., 2018; Cui et al., 2019; Akiyama et al., 2021) as well as a two-fold increase in mast cells within the lamina propria and the detrusor of the bladder have been reported (Liu et al., 2007; Wang et al., 2016).

URO-OVA cystitis mice exhibit altered voiding behaviours characteristic of IC/BPS, including a decrease in maximum volume voided per micturition and an overall increase in the frequency of urination compared to control mice (Wang et al., 2016; Cui et al., 2019; Akiyama et al., 2021). URO-OVA cystitis mice also exhibited significantly decreased sensory thresholds to pelvic nociception (Cui et al., 2019; Akiyama et al., 2021) and an exaggerated VMR to bladder distension indicative of a pain phenotype (Cui et al., 2019). As with the previous models of autoimmune cystitis, no assessments of bladder sensory signalling have been performed in this EAC model.

7.4 Naturally occurring inflammatory models

Feline interstitial cystitis (FIC) is a naturally occurring idiopathic condition of domestic cats that exhibits physiological changes similar to those associated with IC/BPS without Hunner lesions (Birder et al., 2003; Kullmann et al., 2018; Mohamaden et al., 2019; Jones et al., 2021). FIC is broadly described as the presence of chronic, waxing and waning clinical signs of irritative voiding (pollakiuria, stranguria and dysuria) with an absence of neoplasia or bacteriuria, with or without the presence of uroliths or urethral plugs (Kruger et al., 1991; Kruger et al., 2009; Defauw et al., 2010; Lulich et al., 2010; Mohamaden et al., 2019; Jones et al., 2021). FIC exhibits similar histological features to IC/BPS without Hunner lesions including urothelial denudation or ulceration, submucosal oedema, chronic inflammatory cell infiltrates and muscularis fibrosis (Jones et al., 2021).

FIC cats have shown denudation and thinning of the urothelium (Lavelle et al., 2000), and urothelial spongiosis suggestive of a loss of cell-cell adhesion. Tight junctions were also found to have come apart leading to the disruption of the epithelial layer (Lavelle et al., 2000) and expression of E-cadherin tight junction protein was also significantly downregulated in FIC bladders compared with those of controls (Kullmann et al., 2018; Mohamaden et al., 2019). As a result, transepithelial

resistance (TER) of the urothelium was significantly reduced, while water and urea permeability were significantly increased (Lavelle et al., 2000). Bladder oedema, haemorrhage, congestion of blood vessels, and infiltration of inflammatory cells in the bladder interstitium is also common in FIC (Kullmann et al., 2018; Mohamaden et al., 2019). FIC cats have been shown to have significantly higher serum concentrations of IL-1β, IL-6 and TNF-α compared to control cats (Mohamaden et al., 2019). Urine levels for IL-1β and IL-6, but not TNF-α were significantly higher than controls (Mohamaden et al., 2019), and a significant increase in mast cell number is observed in both the urothelium and lamina propria of FIC cats (Kullmann et al., 2018; Mohamaden et al., 2019).

Bladder Aδ afferents from FIC cats are hypersensitive to bladder distension (Roppolo et al., 2005), and urothelial cells from the bladders of FIC cats also demonstrate altered ATP release during cell swelling (Birder et al., 2003), which may contribute to additional activation or sensitisation of sensory afferent nerves (Birder and Andersson, 2013).

7.5 Psychological stress models

Chronic stress has been identified as a key factor in the development of IC/BPS, and early life stress has been shown to significantly increase the chances of developing chronic pelvic pain in later life (Fuentes and Christianson, 2018b). A large proportion of IC/BPS patients have experienced early-life adverse or traumatic events (Kullmann et al., 2018). Rodent psychological stress models are designed to recapitulate these human stressors via the induction of one or more stressful events that vary in their induction method and intensity. The most widely employed stress models to generate an IC/BPS phenotype are Water Avoidance Stress (WAS) or Neonatal Maternal-Separation (NMS).

7.5.1 Water avoidance stress (WAS) models

WAS models are generated by exploiting the behavioural instincts of rats and mice, but is most commonly performed in rats (Chess-Williams et al., 2021; Gao and Rodríguez, 2022). A stressful environment is generated by placing rodents on a platform in the middle of a tank filled with water. Rodents will naturally avoid going into the water and, as there is no alternative way to escape, this raises systemic stress levels and leads to the development of anxiety (Figure 3). To establish a chronic stress phenotype, WAS is usually performed for 1 h a day over a period of 10 days (Robbins et al., 2007; Matos et al., 2017; Wang et al., 2017; Dias et al., 2019).

Wistar-Kyoto (WK) rats are commonly used for psychological stress models, as they are genetically predisposed to elevated levels of anxiety (Robbins et al., 2007). Compared to Sprague-Dawley (SD) rats, which are generally considered to be a low/moderate-anxiety strain, WK rats exhibit both neurochemical and behavioural differences in response to stress (Robbins et al., 2007). This includes a greater sensitivity to adverse events leading to an amplified HPA axis response and an attenuated brain noradrenergic system response (Robbins et al., 2007). WK, but not SD rats develop a significantly exaggerated VMR to urinary bladder distension following 10 consecutive days of WAS (Robbins et al., 2007).

WAS in WK rats results in a significant increase in urinary frequency, which includes a decrease in the average void size and an increase in the number of small voids as early as day 3 of the chronic WAS exposure protocol (West et al., 2021). Frequency of responses to von-Frey probing of the pelvic suprapubic area significantly increased during WAS from day 5 onwards to plateau on day 8 of treatment (Lee et al., 2015; Matos et al., 2017). WAS rats also develop altered bladder function, with cystometry revealing the voiding phase of micturition occurs at a significantly decreased pressure threshold (Wang et al., 2017; Gao et al., 2018). The VMR to urinary bladder distension is also evoked at a lower bladder pressure and for a longer duration in WAS rats compared to controls, representing a longer sensory/pain response to bladder stimuli (Wang et al., 2017; Gao et al., 2018). No assessments of bladder sensory signaling have been reported following WAS and so it is unclear if alterations in bladder sensitivity and function are due to changes in central processing circuits, sensitisation of peripheral sensory nerves, or both. Interestingly, the changes in bladder sensation and function observed during and following WAS also evoke changes in bladder physiology that show similarity to changes observed in humans (Chess-Williams et al., 2021), including loss of superficial umbrella cells leading to an altered urothelial surface, inflammatory cell infiltration into the mucosa, and mastocytosis (Figure 4) (Matos et al., 2017). WAS has also been frequently used as an animal model of irritable bowel syndrome (Moloney et al., 2016), a disorder characterised by chronic abdominal pain which commonly occurs with IC/BPS.

7.5.2 Neonatal maternal separation (NMS) models

NMS models are generated by separating litters of pups from the dam for up to 3 weeks from postnatal day one, depriving the pups of innate needs and natural connection with their mother that imitates early-life trauma in humans (Figure 3). NMS induces chronic changes in bladder sensitivity and function in adult mice including increased voiding frequency with smaller void spots as compared to naïve mice (Pierce et al., 2018), and a significantly greater VMR in response to UBD at 8 weeks of age (Pierce et al., 2018).

The psychological nature of this model is shown in the effects NMS has on brain function. Mice exposed to NMS show significantly lower mRNA levels of corticotropin-releasing factor (CRF_1) and glucocorticoid (GR), and higher brain-derived neurotrophic factor (BDNF) in the hippocampus (Pierce et al., 2018). As CRF is the main activator of HPA axis signalling, lower CRF and GR levels indicate decreased inhibition on the HPA axis (Pierce et al., 2018), which would explain the chronic changes in corticosterone response (Kalinichev et al., 2002; Nishi et al., 2014). This is hypothesised to have a cumulative effect, decreasing animal resilience to stress over the lifetime. As with WAS, a translation of psychological insult to physiological changes in the bladder occurs, with NMS mice having a significantly higher percentage of degranulated mast cells in the bladder (Figure 4) (Pierce et al., 2018).

To model the human experience more closely, whereby early life stress is commonly followed by numerous additional stressors, a psychological stress model has recently been generated that combines NMS followed by WAS at 8+ weeks of age (Pierce

et al., 2016). Combining NMS and WAS impacted bladder function, as measured by a significant increase in the number of voids and a higher total urine output in mice 1d-post WAS that returned to baseline at 8d-post WAS (Pierce et al., 2016). Implementation of these combined models also led to an altered VMR to urinary bladder distension (Pierce et al., 2016). At 1d post-WAS, NMS mice exhibited a transient decrease in VMR during bladder distension which was later significantly increased at 8d post-WAS (Pierce et al., 2016) suggesting combined stressors may induce more longer lasting changes in bladder sensitivity than WAS alone.

7.6 Cross-organ sensitisation models

Considerable clinical evidence links diseases of the colon, such as irritable bowel syndrome (IBS) and inflammatory bowel disease (IBD), with IC/BPS (Grundy and Brierley, 2018). 20%–30% of both men and women with IC/BPS report IBS as among their most common comorbidity (Alagiri et al.; Clemens et al., 2006) and IC/BPS patients are 100 times more likely to have concurrent IBD than healthy controls (Alagiri et al.). More recently, it has been shown that having IBS increases the risk of developing IC/BPS (Chang et al., 2021), however, the underlying mechanisms responsible for the development of comorbid visceral pain syndromes have yet to be fully elucidated. Cross-sensitisation of the peripheral and central sensory pathways that co-innervate pelvic organs such as the bladder and colon has been proposed as a major contributing factor (Grundy and Brierley, 2018).

Animal models have been generated to recapitulate cross-organ sensitisation between the colon and bladder by inducing long term hypersensitivity of the sensory pathways that innervate the colon. By far the most well characterised of these methods is following intracolonic co-administration of ethanol and trinitrobenzene sulfonic acid (TNBS) (Figure 3). Ethanol is required to disrupt the intestinal barrier and enable the interaction of TNBS within the colon wall to elicit an immune response (Antoniou et al., 2016). The severity of colitis in these models is directly related to the doses of ethanol and TNBS, and shows significant variability between species (rat vs. mouse) as well as genotype (Antoniou et al., 2016). In general, the first week following a single TNBS/ethanol enema is characterised by severe colonic inflammation (Hughes et al., 2009; Vannucchi and Evangelista, 2018). By 7 days post-TNBS administration, colonic inflammation has begun to spontaneously resolve, with a corresponding increase in the integrity of the colonic wall (Hughes et al., 2009). By 28 days post-TNBS, there are no observable histological changes in the colon compared with healthy control mice, yet hypersensitivity of peripheral sensory pathways persists (Hughes et al., 2009). Whilst TNBS colitis has not been observed to induce marked inflammation in the bladder (Grundy et al., 2018d; Grundy and Brierley, 2018), studies in rats have demonstrated that urothelial permeability increases during the active phase of TNBS-induced colonic inflammation (0–7 days) in the absence of overt histological damage to the bladder (Figure 4) (Meerveld et al., 2015; Towner et al., 2015).

Mice and rats in the acute phase of TNBS colitis develop bladder hypersensitivity characterised by changes in micturition parameters and exaggerated bladder afferent sensitivity in the absence of overt changes in bladder histology (Lei and Malykhina, 2012; Xia et al.). Despite the resolution of colonic inflammation, reduced bladder capacity, voided volumes, and intermicturition intervals and changes in bladder voiding patterns indicative of bladder overactivity persist in both rats and mice up to 90 days post-TNBS (Lamb et al., 2006; Liang et al., 2007; Ustinova et al., 2007; Fitzgerald et al., 2013; Grundy et al., 2018d). TNBS colitis has also been shown to enhance the VMR to urinary bladder distension (Lamb et al., 2006) and induce hypersensitivity of bladder-innervating sensory nerves to bladder distension both during the active and post-inflammatory phase of TNBS colitis (Ustinova et al., 2006; Ustinova et al., 2007; Grundy et al., 2018d). Together, these studies show that experimental colitis can induce chronic changes in the sensory networks that regulate bladder sensory signalling and provide important information on the mechanisms that might underlie the development of IC/BPS in patients that have comorbid visceral pain disorders such as IBS.

8 Discussion

Animal models of human disease have two primary aims: to unravel the pathophysiological mechanisms that drive the development and maintenance of the disease, and the testing of therapeutics for clinical translation. Developing a single animal model of IC/BPS to achieve these aims has been a major challenge, as there is significant heterogeneity in the pathological presentation of IC/BPS patient cohorts. As such, effective clinical translation may very well depend on the degree of progress made towards determining the mechanisms underlying the development of IC/BPS in patient cohorts. As these knowledge gains have an unknown timeline, researchers have in the interim developed a large variety of animal models that focus on specific aspects of known IC/BPS pathophysiology. Validation of these models for relevance to IC/BPS and therapeutic translation has primarily focused on recapitulating the major clinical symptoms seen in IC/BPS patients.

8.1 Recapitulating IC/BPS symptoms

Chronic pelvic or bladder pain are the defining and most debilitating symptoms of IC/BPS. IC/BPS patients display hypersensitivity to bladder distension that translates into increased pain during bladder filling and the development of lower urinary tract symptoms including increased urinary urgency and frequency (Hanno et al., 2011a; Hanno et al., 2011b; Lai et al., 2015). Patients will also demonstrate mechanical hypersensitivity to noxious stimulation in the suprapubic area during sensory testing that reflects the development of referred hyperalgesia from the bladder (Lai et al., 2014; Warren, 2014). As such, it is essential that any animal model intended to be used in the preclinical evaluation of therapeutics for IC/BPS patients develops bladder and/or pelvic pain. Furthermore, as patients with IC/BPS have painful symptoms that persist indefinitely, and often develop additional comorbidities over time (Driscoll and Teichman, 2001), animal models of IC/BPS should ideally see the development of a

pelvic/bladder pain phenotype that endures or even increases in intensity over time.

8.2 Pain and hypersensitivity

Significant progress has been made in developing animal models of IC/BPS that exhibit pelvic/bladder pain, including the development and validation of techniques to accurately assess evoked bladder pain and hypersensitivity. These include the VMR to measure abdominal contractions as a surrogate for bladder pain during bladder distension, von-Frey hair probing of the suprapubic region to assess referred hyperalgesia, and sensory nerve recordings during bladder distension to directly record sensory nerve output in response to bladder distension or stretch. Combinations of these techniques have been used extensively to characterise the development of an IC/BPS phenotype in the models presented in this review. The use of different techniques to assess bladder hypersensitivity and pain both across and within animal models reflects the diversity of experimental techniques available to individual research groups. However, as most models have now been validated by multiple research groups, a reliable assessment of each model has started to emerge (Table 2). Bladder permeability, cyclophosphamide, zymosan, lipopolysaccharide, autoimmune cystitis, feline interstitial cystitis, psychological stress, and cross-organ sensitisation models all report the development of evoked bladder hypersensitivity and/or pain reflective of an IC/BPS phenotype. The variability in the degree of bladder pain/hypersensitivity across these models is dependent on both the intensity of the sensitising stimulus as well as the method of induction. In bladder centric models, increased bladder pain/hypersensitivity is typically correlated with a greater severity of inflammation/permeability, with models that combine to simultaneously impact permeability and inflammation shown to impart greater effects on peripheral afferent sensitisation and pain signaling.

Psychological stress and cross-organ sensitisation models can induce both bladder pain and hypersensitivity in the absence of significant bladder inflammation. However, the intensity of the stimulus, including the duration or timing of psychological stress, or magnitude of the colonic insult, remains a crucial factor in determining whether animals develop measurable bladder pain/hypersensitivity. Furthermore, for psychological stress models, utilising specific rodent species and strains that are predisposed to anxiety are crucial for the successful development of bladder pain/hypersensitivity.

The evidence generated from these models supports comprehensive clinical data showing that the aetiology of IC/BPS can be highly diverse, with multiple mechanisms capable of contributing to the development of bladder centric symptoms. The ability to accurately recapitulate the major clinical features of IC/BPS in animal models also supports their continued use in unravelling the mechanisms responsible for the development and maintenance of IC/BPS symptoms. However, as described in detail for each model, the relative transience of bladder pain/hypersensitivity in many of these models remains a limiting factor in their utilisation for exploring novel therapeutics for IC/BPS. Furthermore, whilst these studies comprehensively characterise evoked pain in animal models of IC/BPS, experimental assessment of non-evoked pain, such as grimace scales, burrowing, and automated behavioural analysis that have been employed in a variety of other pain models is not commonly reported (Deuis et al., 2017). As IC/BPS patients report both evoked pain relating to bladder filling as well as non-evoked pain, incorporating experimental techniques that assess non-evoked pain into future research designs may be useful in fully characterising the clinical translatability of IC/BPS animal models. Non-evoked pain assessments are primarily observation based and therefore have the advantage that they can be easily incorporated into an experimental design without the need for additional animal cohorts or specialised equipment.

8.3 Chronicity

Although many animal models accurately recapitulate the evoked bladder pain and hypersensitivity phenotype of IC/BPS, animal models that develop a chronic pain phenotype are scarce. In the most explored bladder-centric permeability and inflammatory models, pain and/or hypersensitivity effects are commonly reported only in the day/s, or first week after ceasing treatment. Whether this is due to not exploring more chronic time points or reflects a resolution of hypersensitivity and pain is not always clear, but it is of paramount importance, as IC/BPS is by definition a chronic disorder. As a result, the last decade has seen a discernible drive to refine preclinical models of IC/BPS to induce a more chronic pain state. This has been achieved by modulating the strength, timing, and duration of the model induction, such as with multiple lower doses of cyclophosphamide administered over a longer period, several LPS administrations over a longer time course, neonatal insult, or chronic exposure to stressful stimuli during a specific developmental phase. These refinements will likely prove crucial in developing the next-generation of treatments for IC/BPS, as they provide greater opportunities to interrogate the mechanisms underlying long term changes in bladder sensation.

Further development of IC/BPS animal models has revealed neonatal maternal stress, neonatal zymosan, and colon-bladder cross-sensitisation models exhibit bladder hypersensitivity and pain long after the resolution of the initial sensitising stimulus and in the absence of overt bladder damage. This is crucial, as it reveals that chronic changes in bladder sensory pathways can occur to embed a hypersensitive state long after an initiating stimulus. Many IC/BPS patients present without obvious bladder pathophysiology at the time of diagnosis, but have a history of chronic psychological stress, urinary tract infections, or comorbidities including IBS. As such, the development of animal models that see a chronic pelvic/bladder pain phenotype in the absence or following resolution of inflammation represents a crucial step towards accurate pre-clinical modelling of these IC/BPS patient subsets.

A logical next step in the development of chronic IC/BPS models is to expand the dual insult models established using intrabladder zymosan to include heterogenous elements of distinct animal models. This may include combining an early in life event, such as neonatal inflammation to mirror childhood UTI, followed by chronic stress in adulthood or visa-versa.

8.4 Translational potential

The ability to accurately recapitulate the major symptoms of IC/BPS in animal models is a crucial step towards the development of novel therapeutics for IC/BPS. However, the variety of animal models available that develop an IC/BPS like phenotype, and the stark differences in induction methods, raises important questions as to which model is most suited for the pre-clinical evaluation of therapeutics for future clinical translation. Consideration must be given to the pathophysiological origin, the type/severity of model, and the time after model induction that assessments are made.

A balance must be sought between how closely an animal model of IC/BPS shares pathophysiological traits with IC/BPS patients, and model presentation. For example, chemical models such as acetic/hydrochloric acid and hydrogen peroxide induce a well characterised cystitis phenotype. However, chemical cystitis methods appear limited in their translational potential by an artificial method of induction that lacks an obvious link to the pathophysiology of IC/BPS. In contrast, models of urothelial permeability induce an acute IC/BPS phenotype that closely mirrors the presentation of many IC/BPS patients with a diminished urothelial barrier. However, as is well documented, in the absence of inflammation, the urothelial barrier is rapidly restored, and bladder hypersensitivity normalises, undermining its relevance to studying the chronic nature of IC/BPS. Current studies indicate zymosan and LPS models may represent a good choice for investigating an inflammatory IC/BPS phenotype. Both LPS and zymosan induce an IC/BPS like phenotype characterised by bladder inflammation and bladder pain. However, in contrast to chemical cystitis, inflammation is induced via the recruitment of natural inflammatory pathways associated with receptor activation rather than direct tissue damage. By more closely mirroring the natural inflammatory pathways reported to be activated in the bladders of IC/BPS patients, these models appear to have greater translational potential for investigating therapies that target bladder inflammation and/or inflammation induced hypersensitivity. Experimental autoimmune cystitis (EAC) mice also develop IC/BPS like symptoms, but whilst the inflammation is initiated by a cellular mediated mechanism, the severity is beyond the pathophysiology characterised for most IC/BPS patients. However, as some evidence supports an autoimmunological inflammatory process as an underlying contributor to pathophysiology in IC/BPS with Hunner lesions (Akiyama et al., 2020), EAC models may represent the best choice for investigating novel therapies for this severe IC/BPS phentypes.

The translational potential of an animal model also requires consideration of the mechanism of action of any proposed intervention in relation to the pathology that is thought to underlie the development of IC/BPS symptoms in a specific patient cohort. For instance, bladder hypersensitivity and pain in psychological stress models is caused by chronic dysregulation of the HPA axis. As such, preclinical evaluation of therapies that have peripheral sites of action, such as direct bladder infusions or anti-inflammatory agents are unlikely to be as efficacious as those that are tailored to central stress mechanisms such as psychotherapy, exercise, or bladder training. Similarly, targeting the HPA axis to treat IC/BPS symptoms that develop due to localised bladder inflammation and the sensitisation of bladder-innervating sensory nerves is unlikely to be as effective as directly targeting the bladder or peripheral sensory pathways. Exploring therapies in animal models of cross-organ sensitisation or early in life intervention will likely need a different approach entirely, as the pathophysiology of these disorders is embedded within the chronic remodelling of peripheral and central sensory circuits that establishes a chronically sensitised state. Considering these factors in the design of clinical trials for IC/BPS to aid patient stratification would also have major implications for interpreting success/failure of a particular intervention.

9 Conclusion

Significant progress continues to be made in the development of animal models of IC/BPS that more closely mimic the human condition. At present it appears unlikely that animal models will ever be able to perfectly model IC/BPS, owing to both symptom and pathophysiological heterogeneity amongst patients. However, as described in this review, multiple animal models of IC/BPS are now able to accurately reflect the major symptoms of IC/BPS including bladder hypersensitivity and pain. Whilst pre-clinical models need to be refined further to unravel the pathological mechanisms underlying the development of IC/BPS, being able to assess impacts of interventions on the primary symptoms of IC/BPS should hopefully pave the way for the development of novel therapeutics. However, with a large variety of distinct animal models available, care must be taken to select the appropriate model to ensure potential pre-clinical translation is maximised. Therefore, it is likely that different models will continue to be required for pre-clinical drug development based on the unique IC/BPS aetiology under investigation.

Author contributions

CT and LG performed literature searches, wrote, and edited the manuscript, tables and figures. All authors contributed to the article and approved the submitted version.

Conflict of interest

The authors declare that the research was conducted in the absence of any commercial or financial relationships that could be construed as a potential conflict of interest.

Publisher's note

References

Abernethy, M. G., Rosenfeld, A., White, J. R., Mueller, M. G., Lewicky-Gaupp, C., and Kenton, K. (2017a). Urinary microbiome and cytokine levels in women with interstitial cystitis. *Obstet. Gynecol.* 129 (3), 500–506. doi:10.1097/AOG.0000000000001892

Akiyama, Y., Luo, Y., Hanno, P. M., Maeda, D., and Homma, Y. (2020). Interstitial cystitis/bladder pain syndrome: The evolving landscape, animal models and future perspectives. *Int. J. Urol.* 27 (6), 491–503. doi:10.1111/iju.14229

Akiyama, Y., Maeda, D., Morikawa, T., Niimi, A., Nomiya, A., Yamada, Y., et al. (2018). Digital quantitative analysis of mast cell infiltration in interstitial cystitis. *Neurourol. Urodyn.* 37 (2), 650–657. doi:10.1002/nau.23365

Akiyama, Y., Yao, J. R., Kreder, K. J., O'Donnell, M. A., Lutgendorf, S. K., Lyu, D., et al. (2021). Autoimmunity to urothelial antigen causes bladder inflammation, pelvic pain, and voiding dysfunction: A novel animal model for hunner-type interstitial cystitis. *Am. J. Physiol. Ren. Physiol.* 320 (2), F174–F182. doi:10.1152/ajprenal.00290.2020

Alagiri, M., Chottiner, S., Ratner, V., Slade, D., and Hanno, P. M. (1997). Interstitial cystitis: Unexplained associations with other chronic disease and pain syndromes. *Urology* 49 (5A Suppl. l), 52–57. doi:10.1016/s0090-4295(99)80332-x

Altuntas, C. Z., Daneshgari, F., Sakalar, C., Goksoy, E., Gulen, M. F., Kavran, M., et al. (2012). Autoimmunity to uroplakin II causes cystitis in mice: A novel model of interstitial cystitis. *Eur. Urol.* 61 (1), 193–200. doi:10.1016/j.eururo.2011.06.028

Antoniou, E., Margonis, G. A., Angelou, A., Pikouli, A., Argiri, P., Karavokyros, I., et al. (2016). The TNBS-induced colitis animal model: An overview. *Ann. Med. Surg. (Lond)* 11, 9–15. doi:10.1016/j.amsu.2016.07.019

Auge, C., Chene, G., Dubourdeau, M., Desoubzdanne, D., Corman, B., Palea, S., et al. (2013). Relevance of the cyclophosphamide-induced cystitis model for pharmacological studies targeting inflammation and pain of the bladder. *Eur. J. Pharmacol.* 707 (1-3), 32–40. doi:10.1016/j.ejphar.2013.03.008

Auge, C., Gamé, X., Vergnolle, N., Lluel, P., and Chabot, S. (2020). Characterization and validation of a chronic model of cyclophosphamide-induced interstitial cystitis/bladder pain syndrome in rats. *Front. Pharmacol.* 11, 1305. doi:10.3389/fphar.2020.01305

Bendrick, T. R., Sitenga, G. L., Booth, C., Sacco, M. P., Erie, C., Anderson, D. J., et al. (2022). The implications of mental health and trauma in interstitial cystitis. *Health Psychol. Res.* 10 (4), 40321. doi:10.52965/001c.40321

Berry, S. H., Elliott, M. N., Suttorp, M., Bogart, L. M., Stoto, M. A., Eggers, P., et al. (2011). Prevalence of symptoms of bladder pain syndrome/interstitial cystitis among adult females in the United States. *J. urology* 186 (2), 540–544. doi:10.1016/j.juro.2011.03.132

Bicer, F., Altuntas, C. Z., Izgi, K., Ozer, A., Kavran, M., Tuohy, V. K., et al. (2015). Chronic pelvic allodynia is mediated by CCL2 through mast cells in an experimental autoimmune cystitis model. *Am. J. Physiol. Ren. Physiol.* 308 (2), F103–F113. doi:10.1152/ajprenal.00202.2014

Birder, L. A., Barrick, S. R., Roppolo, J. R., Kanai, A. J., de Groat, W. C., Kiss, S., et al. (2003). Feline interstitial cystitis results in mechanical hypersensitivity and altered ATP release from bladder urothelium. *Am. J. Physiol. Ren. Physiol.* 285 (3), F423–F429. doi:10.1152/ajprenal.00056.2003

Birder, L. A., Kanai, A. J., and de Groat, W. C. (1997). Dmso: Effect on bladder afferent neurons and nitric oxide release. *J. Urol.* 158 (5), 1989–1995. doi:10.1016/s0022-5347(01)64199-5

Birder, L., and Andersson, K.-E. (2013). Urothelial signaling. *Physiol. Rev.* 93 (2), 653–680. doi:10.1152/physrev.00030.2012

Birder, L. A. (2019). Pathophysiology of interstitial cystitis. *Int. J. Urol.* 26 (Suppl. 1), 12–15. doi:10.1111/iju.13985

Bosch, P. C. (2018). A randomized, double-blind, placebo-controlled trial of certolizumab pegol in women with refractory interstitial cystitis/bladder pain syndrome. *Eur. Urol.* 74 (5), 623–630. doi:10.1016/j.eururo.2018.07.026

Bosch, P. C., and Bosch, D. C. (2014). Treating interstitial cystitis/bladder pain syndrome as a chronic disease. *Rev. Urol.* 16 (2), 83–87. doi:10.3909/riu0603

Boucher, M., Meen, M., Codron, J. P., Coudore, F., Kemeny, J. L., and Eschalier, A. (2000). Cyclophosphamide-induced cystitis in freely-moving conscious rats: Behavioral approach to a new model of visceral pain. *J. Urol.* 164 (1), 203–208. doi:10.1097/00005392-200007000-00061

Boudes, M., Uvin, P., Kerselaers, S., Vennekens, R., Voets, T., and De Ridder, D. (2011). Functional characterization of a chronic cyclophosphamide-induced overactive bladder model in mice. *Neurourol. Urodyn.* 30 (8), 1659–1665. doi:10.1002/nau.21180

Boudes, M., Uvin, P., Pinto, S., Freichel, M., Birnbaumer, L., Voets, T., et al. (2013). Crucial role of TRPC1 and TRPC4 in cystitis-induced neuronal sprouting and bladder overactivity. *PLoS One* 8 (7), e69550. doi:10.1371/journal.pone.0069550

Carrico, D. J., Peters, K. M., and Diokno, A. C. (2008). Guided imagery for women with interstitial cystitis: Results of a prospective, randomized controlled pilot study. *J. Altern. Complement. Med.* 14 (1), 53–60. doi:10.1089/acm.2007.7070

Çayan, S., Coşkun, B., Bozlu, M., Acar, D., Akbay, E., and Ulusoy, E. (2003). Botulinum toxin type A may improve bladder function in a rat chemical cystitis model. *Urological Res.* 30 (6), 399–404. doi:10.1007/s00240-002-0291-0

Chaiken, D. C., Blaivas, J. G., and Blaivas, S. T. (1993). Behavioral therapy for the treatment of refractory interstitial cystitis. *J. Urol.* 149 (6), 1445–1448. doi:10.1016/s0022-5347(17)36411-x

Chang, K. M., Lee, M. H., Lin, H. H., Wu, S. L., and Wu, H. C. (2021). Does irritable bowel syndrome increase the risk of interstitial cystitis/bladder pain syndrome? A cohort study of long term follow-up. *Int. Urogynecol J.* 32 (5), 1307–1312. doi:10.1007/s00192-021-04711-3

Charrua, A., Pinto, R., Birder, L. A., and Cruz, F. (2015). Sympathetic nervous system and chronic bladder pain: A new tune for an old song. *Transl. Androl. Urol.* 4 (5), 534–542. doi:10.3978/j.issn.2223-4683.2015.09.06

Chen, C. H., Liao, C. H., Chen, K. C., Wang, K. L., Tseng, X. W., Tsai, W. K., et al. (2021). B6 mouse strain: The best fit for LPS-induced interstitial cystitis model. *Int. J. Mol. Sci.* 22 (21), 12053. doi:10.3390/ijms222112053

Chen, Y. H., Man, K. M., Chen, W. C., Liu, P. L., Tsai, K. S., Tsai, M. Y., et al. (2020). Platelet-rich plasma ameliorates cyclophosphamide-induced acute interstitial cystitis/painful bladder syndrome in a rat model. *Diagn. (Basel)* 10 (6), 381. doi:10.3390/diagnostics10060381

Chess-Williams, R., McDermott, C., Sellers, D. J., West, E. G., and Mills, K. A. (2021). Chronic psychological stress and lower urinary tract symptoms. *LUTS Low. Urin. Tract. Symptoms* 13 (4), 414–424. doi:10.1111/luts.12395

Chopra, B., Barrick, S. R., Meyers, S., Beckel, J. M., Zeidel, M. L., Ford, A. P. D. W., et al. (2005). Expression and function of bradykinin B1 and B2 receptors in normal and inflamed rat urinary bladder urothelium. *J. Physiol.* 562 (Pt 3), 859–871. doi:10.1113/jphysiol.2004.071159

Chung, K.-H., Liu, S. P., Lin, H. C., and Chung, S. D. (2014). Bladder pain syndrome/interstitial cystitis is associated with anxiety disorder. *Neurourol. Urodynamics* 33 (1), 101–105. doi:10.1002/nau.22382

Clemens, J. Q., Brown, S. O., and Calhoun, E. A. (2008). Mental health diagnoses in patients with interstitial cystitis/painful bladder syndrome and chronic prostatitis/chronic pelvic pain syndrome: A case/control study. *J. Urol.* 180 (4), 1378–1382. doi:10.1016/j.juro.2008.06.032

Clemens, J. Q., Brown, S. O., Kozloff, L., and Calhoun, E. A. (2006). Predictors of symptom severity in patients with chronic prostatitis and interstitial cystitis. *J. Urol.* 175 (3 Pt 1), 963–966. ; discussion 967. doi:10.1016/S0022-5347(05)00351-4

Clemens, J. Q., Erickson, D. R., and Lai, H. H. (2022b). Diagnosis and treatment of interstitial cystitis/bladder pain syndrome. Reply. Diagnosis Treat. Interstitial Cystitis/Bladder Pain Syndrome. Reply. *J Urol* 208 (6), 1178–1179. doi:10.1097/JU.0000000000002974

Clemens, J. Q., Erickson, D. R., Varela, N. P., and Lai, H. H. (2022a). Diagnosis and treatment of interstitial cystitis/bladder pain syndrome. *J. Urology* 208 (1), 34–42. doi:10.1097/JU.0000000000002756

ClinicalTrials.gov (2023). *Recruiting, Active, not recruiting studies for Interstitial Cystitis*. Bethesda, MD: National Library of Medicine (US). Available at: https://clinicaltrials.gov/search?cond=Interstitial%20Cystitis&aggFilters=status:rec%20act (Accessed April 6, 2023).

Clodfelder-Miller, B., Ness, T. J., and DeBerry, J. J. (2022). Neonatal bladder inflammation results in adult female mouse phenotype with increased frequency and nociceptive responses to bladder filling. *Front. Syst. Neurosci.* 16, 858220. doi:10.3389/fnsys.2022.858220

Coelho, A., Wolf-Johnston, A. S., Shinde, S., Cruz, C. D., Cruz, F., Avelino, A., et al. (2015). Urinary bladder inflammation induces changes in urothelial nerve growth factor and TRPV1 channels. *Br. J. Pharmacol.* 172 (7), 1691–1699. doi:10.1111/bph.12958

Colemeadow, J., Sahai, A., and Malde, S. (2020). Clinical management of bladder pain syndrome/interstitial cystitis: A review on current recommendations and emerging treatment options. *Res. Rep. Urol.* 12, 331–343. doi:10.2147/RRU.S238746

Crescenze, I. M., Tucky, B., Li, J., Moore, C., and Shoskes, D. A. (2017). Efficacy, side effects, and monitoring of oral cyclosporine in interstitial cystitis-bladder pain syndrome. *Urology* 107, 49–54. doi:10.1016/j.urology.2017.05.016

Cui, X., Jing, X., Lutgendorf, S. K., Bradley, C. S., Schrepf, A., Erickson, B. A., et al. (2019). Cystitis-induced bladder pain is toll-like receptor 4 dependent in a transgenic autoimmune cystitis murine model: A MAPP research network animal study. *Am. J. Physiol. Ren. Physiol.* 317 (1), F90-F98–F98. doi:10.1152/ajprenal.00017.2019

Danacioglu, Y. O., Erol, B., Ozkanli, S., Yildirim, A., Atis, R. G., Silay, M. S., et al. (2021). Comparison of intravesical hyaluronic acid, chondroitin sulfate, and combination of hyaluronic acid-chondroitin sulfate therapies in animal model of interstitial cystitis. *Int. Neurourol. J.* 25 (1), 42–50. doi:10.5213/inj.1938176.088

Dang, K., Lamb, K., Cohen, M., Bielefeldt, K., and Gebhart, G. F. (2008). Cyclophosphamide-induced bladder inflammation sensitizes and enhances P2X receptor function in rat bladder sensory neurons. *J. Neurophysiol.* 99 (1), 49–59. doi:10.1152/jn.00211.2007

Davidson, S., Copits, B. A., Zhang, J., Page, G., Ghetti, A., and Gereau, R. W. (2014). Human sensory neurons: Membrane properties and sensitization by inflammatory mediators. *Pain* 155 (9), 1861–1870. doi:10.1016/j.pain.2014.06.017

Davis, N. F., Brady, C. M., and Creagh, T. (2014). Interstitial cystitis/painful bladder syndrome: Epidemiology, pathophysiology and evidence-based treatment options. *Eur. J. Obstet. Gynecol. Reprod. Biol.* 175, 30–37. doi:10.1016/j.ejogrb.2013.12.041

de Groat, W. C., Griffiths, D., and Yoshimura, N. (2015). Neural control of the lower urinary tract. *Compr. Physiol.* 5 (1), 327–396. doi:10.1002/cphy.c130056

de Groat, W. C., and Yoshimura, N. (2009). Afferent nerve regulation of bladder function in health and disease. *Handb. Exp. Pharmacol.* (194), 91–138. doi:10.1007/978-3-540-79090-7_4

DeBerry, J. J., Saloman, J. L., Dragoo, B. K., Albers, K. M., and Davis, B. M. (2015). Artemin immunotherapy is effective in preventing and reversing cystitis-induced bladder hyperalgesia via TRPA1 regulation. *J. Pain* 16 (7), 628–636. doi:10.1016/j.jpain.2015.03.014

DeBerry, J. J., Schwartz, E. S., and Davis, B. M. (2014). TRPA1 mediates bladder hyperalgesia in a mouse model of cystitis. *Pain* 155 (7), 1280–1287. doi:10.1016/j.pain.2014.03.023

DeBerry, J., Ness, T. J., Robbins, M. T., and Randich, A. (2007). Inflammation-induced enhancement of the visceromotor reflex to urinary bladder distention: Modulation by endogenous opioids and the effects of early-in-life experience with bladder inflammation. *J. Pain* 8 (12), 914–923. doi:10.1016/j.jpain.2007.06.011

DeBerry, J., Randich, A., Shaffer, A. D., Robbins, M. T., and Ness, T. J. (2010). Neonatal bladder inflammation produces functional changes and alters neuropeptide content in bladders of adult female rats. *J. Pain* 11 (3), 247–255. doi:10.1016/j.jpain.2009.07.010

Defauw, P., et al. (2010). *Evaluation of possible risk factors for feline idiopathic cystitis. Proceedings of the*, 53. Birmingham: BSAVA Annual Congress, 478–479.

Deuis, J. R., Dvorakova, L. S., and Vetter, I. (2017). Methods used to evaluate pain behaviors in rodents. *Front. Mol. Neurosci.* 10, 284. doi:10.3389/fnmol.2017.00284

Dias, B., Serrão, P., Cruz, F., and Charrua, A. (2019). Effect of water avoidance stress on serum and urinary NGF levels in rats: Diagnostic and therapeutic implications for BPS/IC patients. *Sci. Rep.* 9 (1), 14113. doi:10.1038/s41598-019-50576-4

Digesu, G. A., Tailor, V., Bhide, A. A., and Khullar, V. (2020). The role of bladder instillation in the treatment of bladder pain syndrome: Is intravesical treatment an effective option for patients with bladder pain as well as LUTS? *Int. Urogynecol J.* 31 (7), 1387–1392. doi:10.1007/s00192-020-04303-7

Dmochowski, R. R., and Newman, D. K. (2007). Impact of overactive bladder on women in the United States: Results of a national survey. *Curr. Med. Res. Opin.* 23 (1), 65–76. doi:10.1185/030079907X159533

Dogishi, K., Okamoto, K., Majima, T., Konishi-Shiotsu, S., Homan, T., Kodera, M., et al. (2017). A rat long-lasting cystitis model induced by intravesical injection of hydrogen peroxide. *Physiol. Rep.* 5 (4), e13127. doi:10.14814/phy2.13127

Driscoll, A., and Teichman, J. M. H. (2001). HOW do patients with interstitial cystitis present? *J. Urology* 166 (6), 2118–2120. doi:10.1097/00005392-200112000-00023

Ehrén, I., Hallén Grufman, K., Vrba, M., Sundelin, R., and Lafolie, P. (2013). Nitric oxide as a marker for evaluation of treatment effect of cyclosporine A in patients with bladder pain syndrome/interstitial cystitis type 3C. *Scand. J. Urology* 47 (6), 503–508. doi:10.3109/21681805.2013.788552

el-Mansoury, M., Boucher, W., Sant, G. R., and Theoharides, T. C. (1994). Increased urine histamine and methylhistamine in interstitial cystitis. *J. Urol.* 152 (2 Pt 1), 350–353. doi:10.1016/s0022-5347(17)32737-4

Elbadawi, A. E., and Light, J. K. (1996). Distinctive ultrastructural pathology of nonulcerative interstitial cystitis: New observations and their potential significance in pathogenesis. *Urol. Int.* 56 (3), 137–162. doi:10.1159/000282832

Eming, S. A., Krieg, T., and Davidson, J. M. (2007). Inflammation in wound repair: Molecular and cellular mechanisms. *J. Investigative Dermatology* 127 (3), 514–525. doi:10.1038/sj.jid.5700701

Fall, M., Logadottir, Y., and Peeker, R. (2014). Interstitial cystitis is bladder pain syndrome with Hunner's lesion. *Int. J. Urol.* 21 (Suppl. 1), 79–82. doi:10.1111/iju.12325

Fitzgerald, J. J., Ustinova, E., Koronowski, K. B., de Groat, W. C., and Pezzone, M. A. (2013). Evidence for the role of mast cells in colon-bladder cross organ sensitization. *Auton. Neurosci.* 173 (1-2), 6–13. doi:10.1016/j.autneu.2012.09.002

Forrest, J. B., Payne, C. K., and Erickson, D. R. (2012). Cyclosporine A for refractory interstitial cystitis/bladder pain syndrome: Experience of 3 tertiary centers. *J. Urology* 188 (4), 1186–1191. doi:10.1016/j.juro.2012.06.023

Foster, H. E., Jr., Hanno, P. M., Nickel, J. C., Payne, C. K., Mayer, R. D., Burks, D. A., et al. (2010). Effect of amitriptyline on symptoms in treatment naïve patients with interstitial cystitis/painful bladder syndrome. *J. Urol.* 183 (5), 1853–1858. doi:10.1016/j.juro.2009.12.106

Fowler, C. J., Griffiths, D., and de Groat, W. C. (2008). The neural control of micturition. *Nat. Rev. Neurosci.* 9 (6), 453–466. doi:10.1038/nrn2401

Fraser, M. O., Chuang, Y. C., Tyagi, P., Yokoyama, T., Yoshimura, N., Huang, L., et al. (2003). Intravesical liposome administration--a novel treatment for hyperactive bladder in the rat. *Urology* 61 (3), 656–663. doi:10.1016/s0090-4295(02)02281-1

Fuentes, I. M., and Christianson, J. A. (2018a). The influence of early life experience on visceral pain. *Front. Syst. Neurosci.* 12, 2. doi:10.3389/fnsys.2018.00002

Fuentes, I. M., and Christianson, J. A. (2018b). The influence of early life experience on visceral pain. *Front. Syst. Neurosci.* 12, 2. doi:10.3389/fnsys.2018.00002

Furuta, A., Yamamoto, T., Suzuki, Y., Gotoh, M., Egawa, S., and Yoshimura, N. (2018). Comparison of inflammatory urine markers in patients with interstitial cystitis and overactive bladder. *Int. Urogynecol J.* 29 (7), 961–966. doi:10.1007/s00192-017-3547-5

Gao, X. F., Feng, J. F., Wang, W., Xiang, Z. H., Liu, X. J., Zhu, C., et al. (2015). Pirt reduces bladder overactivity by inhibiting purinergic receptor P2X3. *Nat. Commun.* 6, 7650. doi:10.1038/ncomms8650

Gao, Y., and Rodríguez, L. V. (2022). The effect of chronic psychological stress on lower urinary tract function: An animal model perspective. *Front. Physiol.* 13, 818993. doi:10.3389/fphys.2022.818993

Gao, Y., Zhang, R., Chang, H. H., and Rodríguez, L. V. (2018). The role of C-fibers in the development of chronic psychological stress induced enhanced bladder sensations and nociceptive responses: A multidisciplinary approach to the study of urologic chronic pelvic pain syndrome (mapp) research network study. *Neurourol. Urodyn.* 37 (2), 673–680. doi:10.1002/nau.23374

Garzon, S., Laganà, A. S., Casarin, J., Raffaelli, R., Cromi, A., Sturla, D., et al. (2020b). An update on treatment options for interstitial cystitis. *Prz. Menopauzalny* 19 (1), 35–43. doi:10.5114/pm.2020.95334

Garzon, S., Laganà, A. S., Casarin, J., Raffaelli, R., Cromi, A., Sturla, D., et al. (2020a). An update on treatment options for interstitial cystitis. *Przeglad menopauzalny = Menopause Rev.* 19 (1), 35–43. doi:10.5114/pm.2020.95334

Grigoryan, B., Kasyan, G., Pivazyan, L., and Pushkar, D. (2022). Pentosan polysulfate in patients with bladder pain syndrome/interstitial cystitis with hunner's lesions or glomerulations: Systematic review and meta-analysis. *Ther. Adv. Urol.* 14, 17562872221102809. doi:10.1177/17562872221102809

Grover, S., Srivastava, A., Lee, R., Tewari, A. K., and Te, A. E. (2011). Role of inflammation in bladder function and interstitial cystitis. *Ther. Adv. Urology* 3 (1), 19–33. doi:10.1177/1756287211398255

Grundy, L., and Brierley, S. M. (2018). Cross-organ sensitization between the colon and bladder: To pee or not to pee? *Am. J. Physiology-Gastrointestinal Liver Physiology* 314 (3), G301-G308–G308. doi:10.1152/ajpgi.00272.2017

Grundy, L., Caldwell, A., and Brierley, S. M. (2018a). Mechanisms underlying overactive bladder and interstitial cystitis/painful bladder syndrome. *Front. Neurosci.* 12, 931. doi:10.3389/fnins.2018.00931

Grundy, L., Caldwell, A., Garcia Caraballo, S., Erickson, A., Schober, G., Castro, J., et al. (2020a). Histamine induces peripheral and central hypersensitivity to bladder distension via the histamine H(1) receptor and TRPV1. *Am. J. Physiol. Ren. Physiol.* 318 (2), F298-F314–f314. doi:10.1152/ajprenal.00435.2019

Grundy, L., Caldwell, A., Garcia-Caraballo, S., Grundy, D., Spencer, N. J., Dong, X., et al. (2021). Activation of MrgprA3 and MrgprC11 on bladder-innervating afferents induces peripheral and central hypersensitivity to bladder distension. *J. Neurosci.* 41 (17), 3900–3916. doi:10.1523/JNEUROSCI.0033-21.2021

Grundy, L., Caldwell, A., Lumsden, A., Mohammadi, E., Hannig, G., Greenwood Van-Meervald, B., et al. (2020b). Experimentally induced bladder permeability evokes bladder afferent hypersensitivity in the absence of inflammation. *Front. Neurosci.* 14, 590871. doi:10.3389/fnins.2020.590871

Grundy, L., Erickson, A., and Brierley, S. M. (2019). Visceral pain. *Annu. Rev. Physiol.* 81, 261–284. doi:10.1146/annurev-physiol-020518-114525

Grundy, L., Erickson, A., Caldwell, A., Garcia-Caraballo, S., Rychkov, G., Harrington, A., et al. (2018c). Tetrodotoxin-sensitive voltage-gated sodium channels regulate bladder afferent responses to distension. *Pain* 159 (12), 2573–2584. doi:10.1097/j.pain.0000000000001368

Grundy, L., Harrington, A. M., Castro, J., Garcia-Caraballo, S., Deiteren, A., Maddern, J., et al. (2018d). Chronic linaclotide treatment reduces colitis-induced neuroplasticity and reverses persistent bladder dysfunction. *JCI Insight* 3 (19), e121841. doi:10.1172/jci.insight.121841

Hanno, P. M., Burks, D. A., Clemens, J. Q., Dmochowski, R. R., Erickson, D., Fitzgerald, M. P., et al. (2011a). AUA guideline for the diagnosis and treatment of interstitial cystitis/bladder pain syndrome. *J. Urol.* 185 (6), 2162–2170. doi:10.1016/j.juro.2011.03.064

Hanno, P. M., Burks, D. A., Clemens, J. Q., Dmochowski, R. R., Erickson, D., Fitzgerald, M. P., et al. (2011b). AUA guideline for the diagnosis and treatment of interstitial cystitis/bladder pain syndrome. *J. Urology* 185 (6), 2162–2170. doi:10.1016/j.juro.2011.03.064

Hanno, P. M., Erickson, D., Moldwin, R., and Faraday, M. M.American Urological Association (2015). Diagnosis and treatment of interstitial cystitis/bladder pain syndrome: AUA guideline amendment. *J. Urol.* 193 (5), 1545–1553. doi:10.1016/j.juro.2015.01.086

Hauser, P. J., Buethe, D. A., Califano, J., Sofinowski, T. M., Culkin, D. J., and Hurst, R. E. (2009). Restoring barrier function to acid damaged bladder by intravesical chondroitin sulfate. *J. Urology* 182 (5), 2477–2482. doi:10.1016/j.juro.2009.07.013

Hauser, P. J., Dozmorov, M. G., Bane, B. L., Slobodov, G., Culkin, D. J., and Hurst, R. E. (2008a). Abnormal expression of differentiation related proteins and proteoglycan core proteins in the urothelium of patients with interstitial cystitis. *J. Urol.* 179 (2), 764–769. doi:10.1016/j.juro.2007.09.022

Hauser, P. J., Dozmorov, M. G., Bane, B. L., Slobodov, G., Culkin, D. J., and Hurst, R. E. (2008b). Abnormal expression of differentiation related proteins and proteoglycan core proteins in the urothelium of patients with interstitial cystitis. *J. Urology* 179 (2), 764–769. doi:10.1016/j.juro.2007.09.022

Henry Lai, H. (2017). "Management of interstitial cystitis/bladder pain syndrome with tricyclic antidepressants," in *Urological and gynaecological chronic pelvic pain: Current therapies*. Editor R. M. Moldwin (Cham: Springer International Publishing), 107–117.

Henry, R. A., Morales, A., and Cahill, C. M. (2015). Beyond a simple anesthetic effect: Lidocaine in the diagnosis and treatment of interstitial cystitis/bladder pain syndrome. *Urology* 85 (5), 1025–1033. doi:10.1016/j.urology.2015.01.021

Henry, R., Patterson, L., Avery, N., Tanzola, R., Tod, D., Hunter, D., et al. (2001). Absorption of alkalized intravesical lidocaine in normal and inflamed bladders: A simple method for improving bladder anesthesia. *J. Urol.* 165 (6 Pt 1), 1900–1903. doi:10.1097/00005392-200106000-00014

Hernández-Hernández, D., Padilla-Fernández, B., Navarro-Galmés, M. Á., Hess-Medler, S., Castro-Romera, M. M., and Castro-Díaz, D. M. (2020). Sacral neuromodulation in the management of bladder pain syndrome/interstitial cystitis. *Curr. Bladder Dysfunct. Rep.* 15 (2), 83–92. doi:10.1007/s11884-020-00579-z

Hu, V. Y., Malley, S., Dattilio, A., Folsom, J. B., Zvara, P., and Vizzard, M. A. (2003). COX-2 and prostanoid expression in micturition pathways after cyclophosphamide-induced cystitis in the rat. *Am. J. Physiol. Regul. Integr. Comp. Physiol.* 284 (2), R574–R585. doi:10.1152/ajpregu.00465.2002

Hughes, P. A., Brierley, S. M., Martin, C. M., Brookes, S. J. H., Linden, D. R., and Blackshaw, L. A. (2009). Post-inflammatory colonic afferent sensitisation: Different subtypes, different pathways and different time courses. *Gut* 58 (10), 1333–1341. doi:10.1136/gut.2008.170811

Hughes, P. A., Harrington, A. M., Castro, J., Liebregts, T., Adam, B., Grasby, D. J., et al. (2013). Sensory neuro-immune interactions differ between irritable bowel syndrome subtypes. *Gut* 62 (10), 1456–1465. doi:10.1136/gutjnl-2011-301856

Hurst, R. E., Greenwood-Van Meerveld, B., Wisniewski, A. B., VanGordon, S., Lin, H., Kropp, B. P., et al. (2015). Increased bladder permeability in interstitial cystitis/painful bladder syndrome. *Transl. Androl. Urol.* 4 (5), 563–571. doi:10.3978/j.issn.2223-4683.2015.10.03

International Neuromodulation Society (2013). Neuromodulation, or neuromodulatory effect. Available at: https://www.neuromodulation.com/neuromodulation-defined.

International Neuromodulation Society (2021b). Pudendal nerve stimulation. Available at: https://www.neuromodulation.com/pudendal-nerve.

International Neuromodulation Society (2021a). *Sacral nerve stimulation*. Available at: https://www.neuromodulation.com/sacral-nerve.

Izgi, K., Altuntas, C. Z., Bicer, F., Ozer, A., Sakalar, C., Li, X., et al. (2013). Uroplakin peptide-specific autoimmunity initiates interstitial cystitis/painful bladder syndrome in mice. *PLoS One* 8 (8), e72067. doi:10.1371/journal.pone.0072067

Jacobs, B. L., Smaldone, M. C., Tyagi, V., Philips, B. J., Jackman, S. V., Leng, W. W., et al. (2010). Increased nerve growth factor in neurogenic overactive bladder and interstitial cystitis patients. *Can. J. Urol.* 17 (1), 4989–4994.

Jafari, N. V., and Rohn, J. L. (2022). The urothelium: A multi-faceted barrier against a harsh environment. *Mucosal Immunol.* 15 (6), 1127–1142. doi:10.1038/s41385-022-00565-0

Jerde, T. J., Bjorling, D. E., Steinberg, H., Warner, T., and Saban, R. (2000). Determination of mouse bladder inflammatory response to *E. coli* lipopolysaccharide. *Urol. Res.* 28 (4), 269–273. doi:10.1007/s002400000114

Jhang, J.-F., and Kuo, H.-C. (2016b). Pathomechanism of interstitial cystitis/bladder pain syndrome and mapping the heterogeneity of disease. *Int. Neurourol. J.* 20 (Suppl. 2), S95–S104. doi:10.5213/inj.1632712.356

Jhang, J. F., and Kuo, H. C. (2016a). Pathomechanism of interstitial cystitis/bladder pain syndrome and mapping the heterogeneity of disease. *Int. Neurourol. J.* 20 (Suppl. 2), S95–S104. doi:10.5213/inj.1632712.356

Jin, X. W., Liu, B. K., Zhang, X., Zhao, Z. H., and Shao, Y. (2017). Establishment of a novel autoimmune experimental model of bladder pain syndrome/interstitial cystitis in C57bl/6 mice. *Inflammation* 40 (3), 861–870. doi:10.1007/s10753-017-0531-7

Jones, C. A., and Nyberg, L. (1997). Epidemiology of interstitial cystitis. *Urology* 49 (5), 2–9. doi:10.1016/s0090-4295(99)80327-6

Jones, E., Palmieri, C., Thompson, M., Jackson, K., and Allavena, R. (2021). Feline idiopathic cystitis: Pathogenesis, histopathology and comparative potential. *J. Comp. Pathol.* 185, 18–29. doi:10.1016/j.jcpa.2021.03.006

Juszczak, K., Gil, K., Wyczolkowski, M., and Thor, P. J. (2010). Functional, histological structure and mastocytes alterations in rat urinary bladders following acute and [corrected] chronic cyclophosphamide treatment. *J. Physiol. Pharmacol.* 61 (4), 477–482.

Kagan, J. C. (2017). Lipopolysaccharide detection across the kingdoms of life. *Trends Immunol.* 38 (10), 696–704. doi:10.1016/j.it.2017.05.001

Kalinichev, M., Easterling, K. W., Plotsky, P. M., and Holtzman, S. G. (2002). Long-lasting changes in stress-induced corticosterone response and anxiety-like behaviors as a consequence of neonatal maternal separation in Long–Evans rats. *Pharmacol. Biochem. Behav.* 73 (1), 131–140. doi:10.1016/s0091-3057(02)00781-5

Karamali, M., Shafabakhsh, R., Ghanbari, Z., Eftekhar, T., and Asemi, Z. (2019). Molecular pathogenesis of interstitial cystitis/bladder pain syndrome based on gene expression. *J. Cell. Physiol.* 234 (8), 12301–12308. doi:10.1002/jcp.28009

Kastrup, J., Hald, T., Larsen, S., and Nielsen, V. G. (1983). Histamine content and mast cell count of detrusor muscle in patients with interstitial cystitis and other types of chronic cystitis. *Br. J. Urol.* 55 (5), 495–500. doi:10.1111/j.1464-410x.1983.tb03356.x

Keay, S. K., Birder, L. A., and Chai, T. C. (2014). Evidence for bladder urothelial pathophysiology in functional bladder disorders. *Biomed. Res. Int.* 2014, 865463. doi:10.1155/2014/865463

Kim, A., Han, J. Y., Ryu, C. M., Yu, H. Y., Lee, S., Kim, Y., et al. (2017). Histopathological characteristics of interstitial cystitis/bladder pain syndrome without Hunner lesion. *Histopathology* 71 (3), 415–424. doi:10.1111/his.13235

Kim, R., Liu, W., Chen, X., Kreder, K. J., and Luo, Y. (2011). Intravesical dimethyl sulfoxide inhibits acute and chronic bladder inflammation in transgenic experimental autoimmune cystitis models. *J. Biomed. Biotechnol.* 2011, 937061. doi:10.1155/2011/937061

Kim, S. H., Kim, T. B., and Oh, S. J. (2009). Urodynamic findings of the painful bladder syndrome/interstitial cystitis: A comparison with idiopathic overactive bladder. *J. Urol.* 181 (6), 2550–2554. doi:10.1016/j.juro.2009.01.106

Kirimoto, T., Nakano, K., Irimura, K., Hayashi, Y., Matsuura, N., Kiniwa, M., et al. (2007). Beneficial effects of suplatast tosilate (IPD-1151T) in a rat cystitis model induced by intravesical hydrochloric acid. *BJU Int.* 100 (4), 935–939. doi:10.1111/j.1464-410X.2007.07044.x

Klingler, C. H. (2016). Glycosaminoglycans: How much do we know about their role in the bladder? *Urologia* 83 (Suppl. 1), 11–14. doi:10.5301/uro.5000184

Koziol, J. A., Clark, D. C., Gittes, R. F., and Tan, E. M. (1993). The natural history of interstitial cystitis: A survey of 374 patients. *J. Urol.* 149 (3), 465–469. doi:10.1016/s0022-5347(17)36120-7

Kruger, J. M., Osborne, C. A., Goyal, S. M., Wickstrom, S. L., Johnston, G. R., Fletcher, T. F., et al. (1991). Clinical evaluation of cats with lower urinary tract disease. *J. Am. Vet. Med. Assoc.* 199 (2), 211–216.

Kruger, J. M., Osborne, C. A., and Lulich, J. P. (2009). Changing paradigms of feline idiopathic cystitis. *Vet. Clin. North Am. Small Anim. Pract.* 39 (1), 15–40. doi:10.1016/j.cvsm.2008.09.008

Kullmann, F. A., McDonnell, B. M., Wolf-Johnston, A. S., Lynn, A. M., Giglio, D., Getchell, S. E., et al. (2018). Inflammation and tissue remodeling in the bladder and urethra in feline interstitial cystitis. *Front. Syst. Neurosci.* 12, 13. doi:10.3389/fnsys.2018.00013

Lai, H., Gereau, R. W., Luo, Y., O'Donnell, M., Rudick, C. N., Pontari, M., et al. (2015). Animal models of urologic chronic pelvic pain syndromes: Findings from the multidisciplinary approach to the study of chronic pelvic pain research network. *Urology* 85 (6), 1454–1465. doi:10.1016/j.urology.2015.03.007

Lai, H. H., Gardner, V., Ness, T. J., and Gereau, R. W., 4th (2014). Segmental hyperalgesia to mechanical stimulus in interstitial cystitis/bladder pain syndrome: Evidence of central sensitization. *J. Urology* 191 (5), 1294–1299. doi:10.1016/j.juro.2013.11.099

Lai, H. H., Vetter, J., Song, J., Andriole, G. L., Colditz, G. A., and Sutcliffe, S. (2019). Management of symptom flares and patient-reported flare triggers in interstitial cystitis/bladder pain syndrome (IC/BPS)-Findings from one site of the MAPP research network. *Urology* 126, 24–33. doi:10.1016/j.urology.2019.01.012

Lamb, K., Zhong, F., Gebhart, G. F., and Bielefeldt, K. (2006). Experimental colitis in mice and sensitization of converging visceral and somatic afferent pathways. *Am. J. Physiol. Gastrointest. Liver Physiol.* 290 (3), G451–G457. doi:10.1152/ajpgi.00353.2005

Landén, N. X., Li, D., and Ståhle, M. (2016). Transition from inflammation to proliferation: A critical step during wound healing. *Cell. Mol. life Sci. CMLS* 73 (20), 3861–3885. doi:10.1007/s00018-016-2268-0

Lasič, E., Višnjar, T., and Kreft, M. E. (2015). "Properties of the urothelium that establish the blood–urine barrier and their implications for drug delivery," in *Reviews of physiology, biochemistry and pharmacology*. Editor B. Nilius, et al. (Cham: Springer International Publishing), 1–29.

Lavelle, J., Meyers, S., Ramage, R., Bastacky, S., Doty, D., Apodaca, G., et al. (2002). Bladder permeability barrier: Recovery from selective injury of surface epithelial cells. *Am. J. Physiology-Renal Physiology* 283 (2), F242–F253. doi:10.1152/ajprenal.00307.2001

Lavelle, J. P., Meyers, S. A., Ruiz, W. G., Buffington, C. A., Zeidel, M. L., and Apodaca, G. (2000). Urothelial pathophysiological changes in feline interstitial cystitis: A human

model. *Am. J. Physiol. Ren. Physiol.* 278 (4), F540–F553. doi:10.1152/ajprenal.2000.278.4.F540

Lee, G., Romih, R., and Zupancic, D. (2014). Cystitis: From urothelial cell biology to clinical applications. *Biomed. Res. Int.* 2014, 473536. doi:10.1155/2014/473536

Lee, U. J., Ackerman, A. L., Wu, A., Zhang, R., Leung, J., Bradesi, S., et al. (2015). Chronic psychological stress in high-anxiety rats induces sustained bladder hyperalgesia. *Physiol. Behav.* 139, 541–548. doi:10.1016/j.physbeh.2014.11.045

Lei, Q., and Malykhina, A. P. (2012). Colonic inflammation up-regulates voltage-gated sodium channels in bladder sensory neurons via activation of peripheral transient potential vanilloid 1 receptors. *Neurogastroenterol. Motil.* 24 (6), 575–585. doi:10.1111/j.1365-2982.2012.01910.x

Leiby, B. E., Landis, J. R., Propert, K. J., and Tomaszewski, J. E.Interstitial Cystitis Data Base Study Group (2007). Discovery of morphological subgroups that correlate with severity of symptoms in interstitial cystitis: A proposed biopsy classification system. *J. Urol.* 177 (1), 142–148. doi:10.1016/j.juro.2006.08.096

Leoni, G., Neumann, P. A., Sumagin, R., Denning, T. L., and Nusrat, A. (2015). Wound repair: Role of immune–epithelial interactions. *Mucosal Immunol.* 8 (5), 959–968. doi:10.1038/mi.2015.63

Li, J., Luo, H., Dong, X., Liu, Q., Wu, C., Zhang, T., et al. (2017). Therapeutic effect of urine-derived stem cells for protamine/lipopolysaccharide-induced interstitial cystitis in a rat model. *Stem Cell. Res. Ther.* 8 (1), 107. doi:10.1186/s13287-017-0547-9

Liang, R., Ustinova, E. E., Patnam, R., Fraser, M. O., Gutkin, D. W., and Pezzone, M. A. (2007). Enhanced expression of mast cell growth factor and mast cell activation in the bladder following the resolution of trinitrobenzenesulfonic acid (TNBS) colitis in female rats. *Neurourol. Urodyn.* 26 (6), 887–893. doi:10.1002/nau.20410

Lin, Y. H., Liu, G., Kavran, M., Altuntas, C. Z., Gasbarro, G., Tuohy, V. K., et al. (2008). Lower urinary tract phenotype of experimental autoimmune cystitis in mouse: A potential animal model for interstitial cystitis. *BJU Int.* 102 (11), 1724–1730. doi:10.1111/j.1464-410X.2008.07891.x

Liu, B. K., Jin, X. W., Lu, H. Z., Zhang, X., Zhao, Z. H., and Shao, Y. (2019). The effects of neurokinin-1 receptor antagonist in an experimental autoimmune cystitis model resembling bladder pain syndrome/interstitial cystitis. *Inflammation* 42 (1), 246–254. doi:10.1007/s10753-018-0888-2

Liu, H.-T., and Kuo, H.-C. (2012). Increased urine and serum nerve growth factor levels in interstitial cystitis suggest chronic inflammation is involved in the pathogenesis of disease. *PloS one* 7 (9), e44687. doi:10.1371/journal.pone.0044687

Liu, H. T., Shie, J. H., Chen, S. H., Wang, Y. S., and Kuo, H. C. (2012a). Differences in mast cell infiltration, E-cadherin, and zonula occludens-1 expression between patients with overactive bladder and interstitial cystitis/bladder pain syndrome. *Urology* 80 (1), 225 e13–e18. doi:10.1016/j.urology.2012.01.047

Liu, W., Evanoff, D. P., Chen, X., and Luo, Y. (2007). Urinary bladder epithelium antigen induces CD8+ T cell tolerance, activation, and autoimmune response. *J. Immunol.* 178 (1), 539–546. doi:10.4049/jimmunol.178.1.539

Liu, Y.-C., Lee, W. T., Liang, C. C., Lo, T. S., Hsieh, W. C., and Lin, Y. H. (2021). Beneficial effect of Bletilla striata extract solution on zymosan-induced interstitial cystitis in rat. *Neurourol. Urodynamics* 40 (3), 763–770. doi:10.1002/nau.24630

Logadottir, Y., Delbro, D., Lindholm, C., Fall, M., and Peeker, R. (2014). Inflammation characteristics in bladder pain syndrome ESSIC type 3C/classic interstitial cystitis. *Int. J. Urol.* 21 (Suppl. 1), 75–78. doi:10.1111/iju.12370

Lulich, J., Osborne, C., and Kruger, J. (2010). What constitutes a diagnosis of feline idiopathic cystitis. *Proc. Am. Coll. Veterinary Intern. Med. Forum, Anaheim*, 630–631.

Lutgendorf, S. K., Kreder, K. J., Rothrock, N. E., Ratliff, T. L., and Zimmerman, B. (2000). Stress and symptomatology in patients with interstitial cystitis: A laboratory stress model. *J. Urol.* 164 (4), 1265–1269. doi:10.1097/00005392-200010000-00027

Lv, J., Huang, Y., Zhu, S., Yang, G., Zhang, Y., Leng, J., et al. (2012). MCP-1-induced histamine release from mast cells is associated with development of interstitial cystitis/bladder pain syndrome in rat models. *Mediat. Inflamm.* 2012, 358184. doi:10.1155/2012/358184

Maeda, D., Akiyama, Y., Morikawa, T., Kunita, A., Ota, Y., Katoh, H., et al. (2015). Hunner-type (classic) interstitial cystitis: A distinct inflammatory disorder characterized by pancystitis, with frequent expansion of clonal B-cells and epithelial denudation. *PLoS One* 10 (11), e0143316. doi:10.1371/journal.pone.0143316

Malley, S. E., and Vizzard, M. A. (2002). Changes in urinary bladder cytokine mRNA and protein after cyclophosphamide-induced cystitis. *Physiol. Genomics* 9 (1), 5–13. doi:10.1152/physiolgenomics.00117.2001

Matos, R., Serrão, P., Rodriguez, L., Birder, L. A., Cruz, F., and Charrua, A. (2017). The water avoidance stress induces bladder pain due to a prolonged alpha1A adrenoceptor stimulation. *Naunyn Schmiedeb. Arch. Pharmacol.* 390 (8), 839–844. doi:10.1007/s00210-017-1384-1

Meerveld, B. G.-V., Mohammadi, E., Tyler, K., Van Gordon, S., Parker, A., Towner, R., et al. (2015). Mechanisms of visceral organ crosstalk: Importance of alterations in permeability in rodent models. *J. Urology* 194 (3), 804–811. doi:10.1016/j.juro.2015.02.2944

Mills, K. A., West, E. J., Grundy, L., McDermott, C., Sellers, D. J., Rose'Myer, R. B., et al. (2020). Hypersensitivity of bladder low threshold, wide dynamic range, afferent fibres following treatment with the chemotherapeutic drugs cyclophosphamide and ifosfamide. *Archives Toxicol.* 94 (8), 2785–2797. doi:10.1007/s00204-020-02773-8

Mohamaden, W. I., Hamad, R., and Bahr, H. I. (2019). Alterations of pro-inflammatory cytokines and tissue protein expressions in cats with interstitial cystitis. *Pak. Veterinary J.* 39, 151–156. doi:10.29261/pakvetj/2019.026

Moloney, R. D., Johnson, A. C., O'Mahony, S. M., Dinan, T. G., Greenwood-Van Meerveld, B., and Cryan, J. F. (2016). Stress and the microbiota–gut–brain Axis in visceral pain: Relevance to irritable bowel syndrome. *CNS Neurosci. Ther.* 22 (2), 102–117. doi:10.1111/cns.12490

Ness, T. J., DeWitte, C., DeBerry, J. J., Hart, M. P., Clodfelder-Miller, B., Gu, J. G., et al. (2021). A model in female rats with phenotypic features similar to interstitial cystitis/bladder pain syndrome. *Front. Pain Res. (Lausanne)* 2, 791045. doi:10.3389/fpain.2021.791045

Nickel, J. C., Moldwin, R., Lee, S., Davis, E. L., Henry, R. A., and Wyllie, M. G. (2009). Intravesical alkalinized lidocaine (PSD597) offers sustained relief from symptoms of interstitial cystitis and painful bladder syndrome. *BJU Int.* 103 (7), 910–918. doi:10.1111/j.1464-410X.2008.08162.x

Nickel, J. C., Tripp, D. A., Pontari, M., Moldwin, R., Mayer, R., Carr, L. K., et al. (2010). Psychosocial phenotyping in women with interstitial cystitis/painful bladder syndrome: A case control study. *J. Urol.* 183 (1), 167–172. doi:10.1016/j.juro.2009.08.133

Nishi, M., Horii-Hayashi, N., and Sasagawa, T. (2014). Effects of early life adverse experiences on the brain: Implications from maternal separation models in rodents. *Front. Neurosci.* 8, 166. doi:10.3389/fnins.2014.00166

NorthShore University (2022). *IC PaIN trial: Interstitial cystitis pain improvement with Naltrexone*. Available at: https://clinicaltrials.gov/study/NCT04313972.

Nunez-Badinez, P., De Leo, B., Laux-Biehlmann, A., Hoffmann, A., Zollner, T. M., Saunders, P. T. K., et al. (2021). Preclinical models of endometriosis and interstitial cystitis/bladder pain syndrome: An innovative medicines initiative-PainCare initiative to improve their value for translational research in pelvic pain. *Pain* 162 (9), 2349–2365. doi:10.1097/j.pain.0000000000002248

Offiah, I., Didangelos, A., O'Reilly, B. A., and McMahon, S. B. (2017). Manipulating the extracellular matrix: An animal model of the bladder pain syndrome. *Pain* 158 (1), 161–170. doi:10.1097/j.pain.0000000000000749

Ogawa, T., Ishizuka, O., Ueda, T., Tyagi, P., Chancellor, M. B., and Yoshimura, N. (2015). Current and emerging drugs for interstitial cystitis/bladder pain syndrome (IC/BPS). *Expert Opin. Emerg. Drugs* 20 (4), 555–570. doi:10.1517/14728214.2015.1105216

Okinami, T., Imamura, M., Nishikawa, N., Negoro, H., Sugino, Y., Yoshimura, K., et al. (2014). Altered detrusor gap junction communications induce storage symptoms in bladder inflammation: A mouse cyclophosphamide-induced model of cystitis. *PLoS One* 9 (8), e104216. doi:10.1371/journal.pone.0104216

Padilla-Fernandez, B., Hernandez-Hernandez, D., and Castro-Diaz, D. M. (2022). Current role of neuromodulation in bladder pain syndrome/interstitial cystitis. *Ther. Adv. Urol.* 14, 17562872221135941. doi:10.1177/17562872221135941

Parsons, C. L., Bautista, S. L., Stein, P. C., and Zupkas, P. (2000). Cyto-injury factors in urine: A possible mechanism for the development of interstitial cystitis. *J. Urol.* 164 (4), 1381–1384. doi:10.1016/s0022-5347(05)67203-5

Parsons, C. L., Housley, T., Schmidt, J. D., and Lebow, D. (1994). Treatment of interstitial cystitis with intravesical heparin. *Br. J. Urol.* 73 (5), 504–507. doi:10.1111/j.1464-410x.1994.tb07634.x

Parsons, C. L., Koziol, J. A., Proctor, J. G., Zupkas, P., and Argade, S. (2015). Heparin and alkalinized lidocaine versus alkalinized lidocaine for treatment of interstitial cystitis symptoms. *Can. J. Urol.* 22 (2), 7739–7744.

Parsons, C. L., Shaw, T., Berecz, Z., Su, Y., Zupkas, P., and Argade, S. (2014). Role of urinary cations in the aetiology of bladder symptoms and interstitial cystitis. *BJU Int.* 114 (2), 286–293. doi:10.1111/bju.12603

Parsons, C. L. (2005). Successful downregulation of bladder sensory nerves with combination of heparin and alkalinized lidocaine in patients with interstitial cystitis. *Urology* 65 (1), 45–48. doi:10.1016/j.urology.2004.08.056

Parsons, C. L. (2007). The role of the urinary epithelium in the pathogenesis of interstitial cystitis/prostatitis/urethritis. *Urology* 69 (4 Suppl. l), 9–16. doi:10.1016/j.urology.2006.03.084

Parsons, C. L., Zupkas, P., Proctor, J., Koziol, J., Franklin, A., Giesing, D., et al. (2012). Alkalinized lidocaine and heparin provide immediate relief of pain and urgency in patients with interstitial cystitis. *J. Sex. Med.* 9 (1), 207–212. doi:10.1111/j.1743-6109.2011.02542.x

Peeker, R., and Fall, M. (2002). Toward a precise definition of interstitial cystitis: Further evidence of differences in classic and nonulcer disease. *J. Urol.* 167 (6), 2470–2472. doi:10.1016/s0022-5347(05)65006-9

Peters, K. M., Diokno, A. C., and Steinert, B. W. (1999). Preliminary study on urinary cytokine levels in interstitial cystitis: Does intravesical bacille calmette-guerin treat interstitial cystitis by altering the immune profile in the bladder? *Urology* 54 (3), 450–453. doi:10.1016/s0090-4295(99)00162-4

Peters, K. M., Feber, K. M., and Bennett, R. C. (2007). A prospective, single-blind, randomized crossover trial of sacral vs pudendal nerve stimulation for interstitial cystitis. *BJU Int.* 100 (4), 835–839. doi:10.1111/j.1464-410X.2007.07082.x

Peters, K. M., Killinger, K. A., Mounayer, M. H., and Boura, J. A. (2011). Are ulcerative and nonulcerative interstitial cystitis/painful bladder syndrome 2 distinct diseases? A study of coexisting conditions. *Urology* 78 (2), 301–308. doi:10.1016/j.urology.2011.04.030

Pierce, A. N., and Christianson, J. A. (2015). Stress and chronic pelvic pain. *Prog. Mol. Biol. Transl. Sci.* 131, 509–535. doi:10.1016/bs.pmbts.2014.11.009

Pierce, A. N., Di Silvestro, E. R., Eller, O. C., Wang, R., Ryals, J. M., and Christianson, J. A. (2016). Urinary bladder hypersensitivity and dysfunction in female mice following early life and adult stress. *Brain Res.* 1639, 58–73. doi:10.1016/j.brainres.2016.02.039

Pierce, A. N., Eller-Smith, O. C., and Christianson, J. A. (2018). Voluntary wheel running attenuates urinary bladder hypersensitivity and dysfunction following neonatal maternal separation in female mice. *Neurourol. Urodyn.* 37 (5), 1623–1632. doi:10.1002/nau.23530

Ramsay, S., Keightley, L., Brookes, S., and Zagorodnyuk, V. (2023). TRPV1 and TRPM8 antagonists reduce cystitis-induced bladder hypersensitivity via inhibition of different sensitised classes of bladder afferents in Guinea pigs. *Br. J. Pharmacol.* 180, 1482–1499. **n/a**(n/a). doi:10.1111/bph.16017

Randich, A., Mebane, H., and Ness, T. J. (2009). Ice water testing reveals hypersensitivity in adult rats that experienced neonatal bladder inflammation: Implications for painful bladder syndrome/interstitial cystitis. *J. Urology* 182 (1), 337–342. doi:10.1016/j.juro.2009.02.107

Randich, A., Uzzell, T., Cannon, R., and Ness, T. J. (2006b). Inflammation and enhanced nociceptive responses to bladder distension produced by intravesical zymosan in the rat. *BMC Urol.* 6, 2. doi:10.1186/1471-2490-6-2

Randich, A., Uzzell, T., DeBerry, J. J., and Ness, T. J. (2006a). Neonatal urinary bladder inflammation produces adult bladder hypersensitivity. *J. Pain* 7 (7), 469–479. doi:10.1016/j.jpain.2006.01.450

Raziyeva, K., Kim, Y., Zharkinbekov, Z., Kassymbek, K., Jimi, S., and Saparov, A. (2021). Immunology of acute and chronic wound healing. *Biomolecules* 11 (5), 700. doi:10.3390/biom11050700

Robbins, M., DeBerry, J., and Ness, T. (2007). Chronic psychological stress enhances nociceptive processing in the urinary bladder in high-anxiety rats. *Physiol. Behav.* 91 (5), 544–550. doi:10.1016/j.physbeh.2007.04.009

Roppolo, J. R., Tai, C., Booth, A. M., Buffington, C. A. T., de Groat, W. C., and Birder, L. A. (2005). Bladder Adelta afferent nerve activity in normal cats and cats with feline interstitial cystitis. *J. Urol.* 173 (3), 1011–1015. doi:10.1097/01.ju.0000145591.35569.9e

Rothrock, N. E., Lutgendorf, S. K., Kreder, K. J., Ratliff, T. L., and Zimmerman, B. (2001). Daily stress and symptom exacerbation in interstitial cystitis patients. *Urology* 57 (6), 122. doi:10.1016/s0090-4295(01)01075-5

Ryu, C.-M., Shin, J. H., Yu, H. Y., Ju, H., Kim, S., Lim, J., et al. (2019). N-acetylcysteine prevents bladder tissue fibrosis in a lipopolysaccharide-induced cystitis rat model. *Sci. Rep.* 9 (1), 8134. doi:10.1038/s41598-019-44631-3

Saban, M. R., Saban, R., Hammond, T. G., Haak-Frendscho, M., Steinberg, H., Tengowski, M. W., et al. (2002). LPS-sensory peptide communication in experimental cystitis. *Am. J. Physiol. Ren. Physiol.* 282 (2), F202–F210. doi:10.1152/ajprenal.0163.2001

Saban, M. R., Simpson, C., Davis, C., Wallis, G., Knowlton, N., Frank, M. B., et al. (2007). Discriminators of mouse bladder response to intravesical Bacillus Calmette-Guerin (BCG). *BMC Immunol.* 8, 6. doi:10.1186/1471-2172-8-6

Sahiner, I. F., Soylu, H., Ates, E., Acar, N., Ustunel, I., and Danisman, A. (2018). Impact of intravesical hyaluronic acid treatment on bladder inflammation in interstitial cystitis rat model. *Int. Braz J. Urol.* 44 (5), 1014–1022. doi:10.1590/S1677-5538.IBJU.2017.0713

Sairanen, J., Forsell, T., and Ruutu, M., LONG-TERM outcome of patients with interstitial cystitis treated with low dose cyclosporine a. *J. Urology*, 2004. 171(6 Part 1): p. 2138–2141. doi:10.1097/01.ju.0000125139.91203.7a

Sant, G. R., Kempuraj, D., Marchand, J. E., and Theoharides, T. C. The mast cell in interstitial cystitis: Role in pathophysiology and pathogenesis. *Urology*, 2007. 69(4, Suppl. ment): p. S34–S40. doi:10.1016/j.urology.2006.08.1109

Sato, K., Yang, X. l., Yudate, T., Chung, J. S., Wu, J., Luby-Phelps, K., et al. (2006). Dectin-2 is a pattern recognition receptor for fungi that couples with the fc receptor γ chain to induce innate immune responses*. *J. Biol. Chem.* 281 (50), 38854–38866. doi:10.1074/jbc.M606542200

Sharma, H., Bourlotous, G., and Grundy, L. (2023). "Post-infectious bladder hypersensitivity in the development of interstitial cystitis/bladder pain syndrome (IC/BPS)," in *Visceral pain*. Editors S. M. Brierley and N. J. Spencer (Cham: Springer International Publishing), 235–251.

Shin, K., Lee, J., Guo, N., Kim, J., Lim, A., Qu, L., et al. (2011). Hedgehog/Wnt feedback supports regenerative proliferation of epithelial stem cells in bladder. *Nature* 472 (7341), 110–114. doi:10.1038/nature09851

Sinanoglu, O., Dogan Ekici, I., and Ekici, S. (2014). Comparison of intravesical application of chondroitin sulphate and colchicine in rat protamine/lipopolysaccharide induced cystitis model. *Urol. J.* 11 (1), 1296–1300. doi:10.22037/uj.v11i1.1782

Singh, U. P., Singh, N. P., Guan, H., Hegde, V. L., Price, R. L., Taub, D. D., et al. (2013). The severity of experimental autoimmune cystitis can be ameliorated by anti-CXCL10 Ab treatment. *PLoS One* 8 (11), e79751. doi:10.1371/journal.pone.0079751

Smaldone, M. C., Vodovotz, Y., Tyagi, V., Barclay, D., Philips, B. J., Yoshimura, N., et al. (2009). Multiplex analysis of urinary cytokine levels in rat model of cyclophosphamide-induced cystitis. *Urology* 73 (2), 421–426. doi:10.1016/j.urology.2008.07.031

Soler, R., Bruschini, H., Freire, M. P., Alves, M. T., Srougi, M., and Ortiz, V. (2008). Urine is necessary to provoke bladder inflammation in protamine sulfate induced urothelial injury. *J. Urology* 180 (4), 1527–1531. doi:10.1016/j.juro.2008.06.006

Song, M., Lim, J., Yu, H. Y., Park, J., Chun, J. Y., Jeong, J., et al. (2015). Mesenchymal stem cell therapy alleviates interstitial cystitis by activating wnt signaling pathway. *Stem Cells Dev.* 24 (14), 1648–1657. doi:10.1089/scd.2014.0459

Song, P. H., Chun, S. Y., Chung, J. W., Kim, Y. Y., Lee, H. J., Lee, J. N., et al. (2017). Comparison of 5 different rat models to establish a standard animal model for research into interstitial cystitis. *Int. Neurourol. J.* 21 (3), 163–170. doi:10.5213/inj.1734898.449

Stanford, U. (2023). *Low-dose Naltrexone for bladder pain syndrome*.

Stemler, K. M., Crock, L. W., Lai, H. H., Mills, J. C., Gereau, R. W., and Mysorekar, I. U. (2013). Protamine sulfate induced bladder injury protects from distention induced bladder pain. *J. Urol.* 189 (1), 343–351. doi:10.1016/j.juro.2012.08.189

Sugino, Y., O'Malley, K. J., Wang, Z., Tyagi, P., Birder, L. A., Ogawa, O., et al. (2015). Laser-capture microdissection for analysis of cell type-specific gene expression of muscarinic receptor subtypes in the rat bladder with cyclophosphamide-induced cystitis. *Int. Urol. Nephrol.* 47 (4), 637–642. doi:10.1007/s11255-015-0926-z

Tambaro, S., Casu, M. A., Mastinu, A., and Lazzari, P. (2014). Evaluation of selective cannabinoid CB(1) and CB(2) receptor agonists in a mouse model of lipopolysaccharide-induced interstitial cystitis. *Eur. J. Pharmacol.* 729, 67–74. doi:10.1016/j.ejphar.2014.02.013

Taneja, R. (2021). Current status of oral pentosan polysulphate in bladder pain syndrome/interstitial cystitis. *Int. Urogynecol J.* 32 (5), 1107–1115. doi:10.1007/s00192-020-04517-9

Tomaszewski, J. E., Landis, J. R., Russack, V., Williams, T. M., Wang, L. P., Hardy, C., et al. (2001). Biopsy features are associated with primary symptoms in interstitial cystitis: Results from the interstitial cystitis database study. *Urology* 57 (6 Suppl. 1), 67–81. doi:10.1016/s0090-4295(01)01166-9

Tomoe, H., What type of interstitial cystitis/bladder pain syndrome is DMSO intravesical instillation therapy effective? *Transl. Androl. Urol.*, 2015. 4(6): p. 600–604. doi:10.3978/j.issn.2223-4683.2015.09.01

Towner, R. A., Smith, N., Saunders, D., Van Gordon, S. B., Tyler, K. R., Wisniewski, A. B., et al. (2015). Assessment of colon and bladder crosstalk in an experimental colitis model using contrast-enhanced magnetic resonance imaging. *Neurogastroenterol. Motil.* 27 (11), 1571–1579. doi:10.1111/nmo.12654

Tubaro, A. (2004). Defining overactive bladder: Epidemiology and burden of disease. *Urology* 64 (6 Suppl. 1), 2–6. doi:10.1016/j.urology.2004.10.047

Ueda, T., Hanno, P. M., Saito, R., Meijlink, J. M., and Yoshimura, N. (2021). Current understanding and future perspectives of interstitial cystitis/bladder pain syndrome. *Int. Neurourol. J.* 25 (2), 99–110. doi:10.5213/inj.2142084.042

Ueda, T., Yoshida, T., Tanoue, H., Ito, M., Tamaki, M., Ito, Y., et al. (2014). Urine alkalization improves the problems of pain and sleep in hypersensitive bladder syndrome. *Int. J. Urol.* 21 (5), 512–517. doi:10.1111/iju.12324

Ulrich-Lai, Y. M., and Herman, J. P. (2009). Neural regulation of endocrine and autonomic stress responses. *Nat. Rev. Neurosci.* 10 (6), 397–409. doi:10.1038/nrn2647

Underhill, D. M., Ozinsky, A., Hajjar, A. M., Stevens, A., Wilson, C. B., Bassetti, M., et al. (1999). The Toll-like receptor 2 is recruited to macrophage phagosomes and discriminates between pathogens. *Nature* 402 (6763), 811–815. doi:10.1038/44605

Ustinova, E. E., Fraser, M. O., and Pezzone, M. A. (2006). Colonic irritation in the rat sensitizes urinary bladder afferents to mechanical and chemical stimuli: An afferent origin of pelvic organ cross-sensitization. *Am. J. Physiol. Ren. Physiol.* 290 (6), F1478–F1487. doi:10.1152/ajprenal.00395.2005

Ustinova, E. E., Gutkin, D. W., and Pezzone, M. A. (2007). Sensitization of pelvic nerve afferents and mast cell infiltration in the urinary bladder following chronic colonic irritation is mediated by neuropeptides. *Am. J. Physiol. Ren. Physiol.* 292 (1), F123–F130. doi:10.1152/ajprenal.00162.2006

van Ophoven, A., Vonde, K., Koch, W., Auerbach, G., and Maag, K. P. (2019). Efficacy of pentosan polysulfate for the treatment of interstitial cystitis/bladder pain syndrome: Results of a systematic review of randomized controlled trials. *Curr. Med. Res. Opin.* 35 (9), 1495–1503. doi:10.1080/03007995.2019.1586401

Vannucchi, M. G., and Evangelista, S. (2018). Experimental models of irritable bowel syndrome and the role of the enteric neurotransmission. *J. Clin. Med.* 7 (1), 4. doi:10.3390/jcm7010004

Vasudevan, V., and Moldwin, R. (2017). Addressing quality of life in the patient with interstitial cystitis/bladder pain syndrome. *Asian J. Urol.* 4 (1), 50–54. doi:10.1016/j.ajur.2016.08.014

Wang, X., Liu, W., O'Donnell, M., Lutgendorf, S., Bradley, C., Schrepf, A., et al. (2016). Evidence for the role of mast cells in cystitis-associated lower urinary tract dysfunction: A multidisciplinary approach to the study of chronic pelvic pain research network animal model study. *PLoS One* 11 (12), e0168772. doi:10.1371/journal.pone.0168772

Wang, Z., Chang, H. H., Gao, Y., Zhang, R., Guo, Y., Holschneider, D. P., et al. (2017). Effects of water avoidance stress on peripheral and central responses during bladder filling in the rat: A multidisciplinary approach to the study of urologic chronic pelvic pain syndrome (mapp) research network study. *PLoS One* 12 (9), e0182976. doi:10.1371/journal.pone.0182976

Warren, J. W. (2014). Bladder pain syndrome/interstitial cystitis as a functional somatic syndrome. *J. Psychosom. Res.* 77 (6), 510–515. doi:10.1016/j.jpsychores.2014.10.003

Webster, D. C., and Brennan, T. (1998). Self-care effectiveness and health outcomes in women with interstitial cystitis: Implications for mental health clinicians. *Issues Ment. Health Nurs.* 19 (5), 495–519. doi:10.1080/016128498248926

Welk, B. K., and Teichman, J. M. (2008). Dyspareunia response in patients with interstitial cystitis treated with intravesical lidocaine, bicarbonate, and heparin. *Urology* 71 (1), 67–70. doi:10.1016/j.urology.2007.09.067

West, E. G., Sellers, D. J., Chess-Williams, R., and McDermott, C. (2021). Bladder overactivity induced by psychological stress in female mice is associated with enhanced bladder contractility. *Life Sci.* 265, 118735. doi:10.1016/j.lfs.2020.118735

Whitmore, K. E., Fall, M., Sengiku, A., Tomoe, H., Logadottir, Y., and Kim, Y. H. (2019). Hunner lesion versus non-Hunner lesion interstitial cystitis/bladder pain syndrome. *Int. J. Urol.* 26 (Suppl. 1), 26–34. doi:10.1111/iju.13971

Wyndaele, J. J. J., Riedl, C., Taneja, R., Lovász, S., Ueda, T., and Cervigni, M. (2019). GAG replenishment therapy for bladder pain syndrome/interstitial cystitis. *Neurourol. Urodyn.* 38 (2), 535–544. doi:10.1002/nau.23900

Xia, C. M., Gulick, M. A., Yu, S. J., Grider, J. R., Murthy, K. S., Kuemmerle, J. F., et al. (2012). Up-regulation of brain-derived neurotrophic factor in primary afferent pathway regulates colon-to-bladder cross-sensitization in rat. *J. Neuroinflammation* 9, 30. doi:10.1186/1742-2094-9-30

Yang, Y., Zhang, H., Lu, Q., Liu, X., Fan, Y., Zhu, J., et al. (2021). Suppression of adenosine A2a receptors alleviates bladder overactivity and hyperalgesia in cyclophosphamide-induced cystitis by inhibiting TRPV1. *Biochem. Pharmacol.* 183, 114340. doi:10.1016/j.bcp.2020.114340

Yoshimura, N., and de Groat, W. C. (1999). Increased excitability of afferent neurons innervating rat urinary bladder after chronic bladder inflammation. *J. Neurosci.* 19 (11), 4644–4653. doi:10.1523/JNEUROSCI.19-11-04644.1999

Yoshimura, N., Homma, Y., Tomoe, H., Otsuka, A., Kitta, T., Masumori, N., et al. (2021). Efficacy and safety of intravesical instillation of KRP-116d (50% dimethyl sulfoxide solution) for interstitial cystitis/bladder pain syndrome in Japanese patients: A multicenter, randomized, double-blind, placebo-controlled, clinical study. *Int. J. Urol.* 28 (5), 545–553. doi:10.1111/iju.14505

Yoshizumi, M., Watanabe, C., and Mizoguchi, H. (2021). Gabapentin reduces painful bladder hypersensitivity in rats with lipopolysaccharide-induced chronic cystitis. *Pharmacol. Res. Perspect.* 9 (1), e00697. doi:10.1002/prp2.697

frontiers | Frontiers in Physiology

TYPE Original Research
PUBLISHED 13 September 2023
DOI 10.3389/fphys.2023.1224505

OPEN ACCESS

EDITED BY
Ovidiu Constantin Baltatu,
Anhembi Morumbi University, Brazil

REVIEWED BY
Francisco O. Silva,
University of Texas Southwestern Medical Center, United States
Carlos Henrique Xavier,
Federal University of Goiás, Brazil
Ewa Krystyna Szczepanska-Sadowska,
Medical University of Warsaw, Poland

*CORRESPONDENCE
Monica A. Sato,
monica.akemi.sato@gmail.com

RECEIVED 17 May 2023
ACCEPTED 24 August 2023
PUBLISHED 13 September 2023

CITATION
Daiuto SA, de Carvalho RP, Vale Bd, Dsouki NA, Giannocco G, Cafarchio EM, Aronsson P and Sato MA (2023), Angiotensinergic and GABAergic transmission in the medial preoptic area: role in urinary bladder and cardiovascular control in female rats.
Front. Physiol. 14:1224505.
doi: 10.3389/fphys.2023.1224505

Angiotensinergic and GABAergic transmission in the medial preoptic area: role in urinary bladder and cardiovascular control in female rats

Sergio A. Daiuto[1], Rodrigo P. de Carvalho[1], Bárbara do Vale[1], Nuha A. Dsouki[1], Gisele Giannocco[2], Eduardo M. Cafarchio[1], Patrik Aronsson[3] and Monica A. Sato[1]*

[1]Department Morphology and Physiology, Faculdade de Medicina do ABC, Centro Universitario FMABC, Santo Andre, Brazil, [2]Department Medicine, Federal University of Sao Paulo, Sao Paulo, Brazil, [3]Department Pharmacology, Institute of Neuroscience and Physiology, Sahlgrenska Academy, University of Gothenburg, Gothenburg, Sweden

Introduction: The medial preoptic area (mPOA) participates in thermoregulatory control and blood pressure modulation as shown by studies with electrical stimulation of this area or cobalt chloride injection, a non-selective synapse inhibitor. This study aimed to investigate whether angiotensin II (Ang II) and GABA could act or not in the mPOA to mediate the cardiovascular and micturition control pathways.

Methods: Female Wistar rats were submitted to stereotaxic surgery for implantation of a guide cannula into the mPOA 7 days prior to the experiments. Afterwards, the animals were isoflurane- anesthetized and submitted to the catheterization of the femoral artery and vein and urinary bladder cannulation for mean arterial pressure (MAP), heart rate (HR), and intravesical pressure (IP) recordings, respectively. After the baseline MAP, HR, and IP recordings for 15 min, Ang II (0.1 nM, 1 µL), losartan (AT-1 receptor antagonist, 100 nM, 1 µL), GABA (50 mM, 1 µL) or saline (1 µL) were injected into the mPOA, and the variables were measured for additional 30 min. In a different group of rats, the AT-1 receptor, angiotensin II converting enzyme (ACE), and GABAa receptor gene expression was evaluated in mPOA samples by qPCR. The data are as mean ± SEM and submitted to One-way ANOVA (Tukey posttest) or paired Student t-test ($P < 0.05$).

Results: The injection of Ang II into the mPOA evoked a significant hypotension (−37±10 mmHg, n = 6, $p = 0.024$) and bradycardia (−47 ± 20 bpm, $p = 0.030$) compared to saline (+1 ± 1 mmHg and +6 ± 2 bpm, n = 6). A significant increase in IP was observed after Ang II injection into the mPOA (+72.25 ± 17.91%, $p = 0.015$ vs. −1.80 ± 2.98%, n = 6, saline). No significant changes were observed in MAP, HR and IP after the losartan injection in the mPOA compared to saline injection. Injection of GABA into the mPOA evoked a significant fall in MAP and HR (−68 ± 2 mmHg, n = 6, $p < 0.0001$ and −115 ± 14 bpm, n = 6, $p = 0.0002$ vs. −1 ± 1 mmHg and +4 ± 2 bpm, n = 6, saline), but no significant changes were observed in IP. The AT-1 receptor, ACE and GABAa receptor mRNA expression was observed in all mPOA samples.

Discussion: Therefore, in female rats, Ang II mediated transmission in the mPOA is involved in the cardiovascular regulation and in the control of central micturition pathways. A phasic control dependent on AT-1 receptors in the mPOA seems to be involved in the regulation of those cardiovascular and intravesical 3 parameters. In contrast, GABAergic transmission in the mPOA participates in the pathways of cardiovascular control in anesthetized female rats, nevertheless, this neurotransmission is not involved in the micturition control.

KEYWORDS

medial preoptic area, angiotensin II, GABA, AT-1 receptors, ACE, arterial pressure, heart rate, micturition

1 Introduction

The preoptic area is long known for its involvement in the modulation of the autonomic nervous system, demonstrated for instance by changes in blood pressure after electrical stimulation of this area in anesthetized cats (Kabat et al., 1935). The bradycardia evoked by electrical stimulation of the medial preoptic area (mPOA) is significantly attenuated by vagotomy, suggesting that this region exerts vagal activation and sympathetic inhibition (Wang and Ranson, 1941). Nevertheless, Folkow et al. (1959) have demonstrated a bradycardia and pronounced drop in blood pressure after electrical stimulation of the preoptic area in vagotomized cats with bilateral carotid occlusion, evidencing a possible sympathoinhibitory function. Despite these earlier findings, the effects on blood pressure and heart rate induced by electrical stimulation of the mPOA could not be explicitly attributed to this area. Electrical stimulation activates both neurons in the preoptic area as well as other passing fibers, which can lead to activation of neurons located outside the preoptic area.

The mPOA participates in thermoregulatory control and promotes blood pressure modulation, evidenced by studies using injection of cobalt chloride, a non-selective inhibitor of synapses (Fassini et al., 2017). It also presents neuron cell bodies with immunohistochemical labeling for angiotensin II (Ang II) (Lind et al., 1985). The mPOA contains mRNA for angiotensinogen and low density of fibers with immunoreactivity for Ang II, modest immunoreactivity for AT-1 receptors and moderate amounts of angiotensin-converting enzyme (ACE) (Bunnemann et al., 1993). However, immunoreactivity for angiotensinogen has not been reported.

Impairment of urinary bladder functions, such as difficulties in urine storage and bladder emptying affects men and women, as well as children worldwide. Among the urinary bladder dysfunctions, urinary incontinence has been reported with higher prevalence in women (Aoki et al., 2017). The central control of micturition involves a complex mechanism, which is still not fully understood. Nevertheless, maintenance of urinary excretion and storage depends on reflex mechanisms, with the initiation of voiding influenced by the Pontine Micturition Center (PMC). In contrast, urine storage is modulated by the Pontine Urine Storage Center (PUSC), located ventrolaterally to the PMC (De Groat, 1998). In rats, the PMC corresponds to Barrington's nucleus and acts as a modulator of the micturition reflex. The mechanism affects bladder pressure and volumetric control, as well as interferes with the coordination of the actions of the detrusor muscle and the urethral sphincter (Sugaya et al., 2005).

Sugaya et al. (1997) demonstrated that, in spite of the micturition in neonatal rats does not depend on neural mechanisms in the brain, many neurons in various brain regions are labeled by the pseudorabies virus (PRV) injected into the urinary bladder of rat pups at 2 and 10 days of age. This indicates that the bladder and brain are connected at very early age. However, the distribution of PRV-infected neurons is somewhat broader than in adult mice. In the first 72 h after PRV administration, the labeling is more prominent in PMC. Other neuronal populations are labeled at slightly longer times (78–84 h), including the raphe magnus nucleus, A5 and A7 clusters, parapyramidal reticular formation, periaqueductal gray (PAG), locus coeruleus, hypothalamus lateral, mPOA and frontal cortex. These areas are also labeled in adult animals. In addition, many of those areas are correspondent to sites where electrical stimulation facilitates or inhibits bladder activity in adult animals (De Groat et al., 2015).

Muscimol, a GABAa receptor agonist, injections in the mPOA increases body temperature, blood pressure and heart rate in conscious freely moving rats by affecting different circuitries in this area, i.e., one involving orexin neurons, and a separate orexin-independent circuit activated by prostaglandin E2 (Rusyniak et al., 2011). Nevertheless, it is unknown whether the GABAergic pathway could be also involved in the micturition control pathways.

Although the mPOA is one of the areas in the brain which is retrogradely labeled by PRV injected in the urinary bladder, the neurotransmission and the role of mPOA in the urinary bladder control is still largely unknown. Bastos et al. (1994) have shown that Ang II elicits dipsogenic effect and pressor response in conscious rats when injected in the mPOA. However, it is not clear if Ang II in the mPOA participates in the micturition control pathways. Therefore, in this study we focused to investigate whether Ang II and GABA could act in the pathways of mPOA to mediate intravesical pressure and/or cardiovascular control in female anesthetized rats. We also evaluated the gene expression of 1) ACE and AT-1 receptors in the mPOA in order to understand if Ang II is locally synthetized; 2) GABAa receptors to demonstrate the existence of these receptors in the mPOA neurons, where the neurotransmitter GABA could bind to exert its effects.

2 Materials and methods

2.1 Animals

Adult female Wistar rats (~260 g), provided by the Animals Care of Centro Universitario FMABC, were used. The animals had access to standard chow pellets (Nuvilab®) and tap water *ad libitum*. Before the stereotaxic surgery, rats were maintained in plastic cages in groups of 4 animals, and after the surgical procedure, each rat was

placed in an individual plastic cage. The light-dark cycle of the Animal Care in the Physiology laboratory at Centro Universitario FMABC was set as 12 h each. The humidity was also controlled at ~70%, and the room temperature was maintained at approximately 23°C. All procedures were performed in accordance with the National Institutes of Health (NIH) Guide for the Care and Use of Laboratory Animals, and were approved by the Animal Ethics Committee of the Faculdade de Medicina do ABC/Centro Universitario ABC (protocol number 02/2021).

2.2 Implantation of guide cannulas in the medial preoptic area

Rats were initially sedated with 2% isoflurane in 100% O_2 and then anesthetized with ketamine (50 mg/kg, i.p.) and xylazine (10 mg/kg, i.m.). Afterwards, the animals were placed in a stereotaxic apparatus (David Kopf®). Antisepsis in the surgical field was performed using polyvinyl-pyrrolidone (PVPI). The cranial surface was exposed to visualize the sutures (bregma and lambda). The animal's head was horizontally aligned based on the dorsoventral parameters measured at the level of the bregma and lambda, which should be coincidental. Two jeweler screws were placed in the animal's skull in order to allow the guide cannula to be anchored to the screws with acrylic cement. A hole was made in the skullcap with the aid of a dental bur and a stainless-steel guide cannula with 12 mm length (23 gauge, 0.642-mm OD, 0.337-mm ID, BD, Juiz de Fora, Brazil) was inserted and positioned towards the mPOA. The parameters to achieve the mPOA were measured as follows: 0.0 mm from bregma, ±0.7 mm lateral from midline, and −7.7 mm ventral from the cranial surface at the anteroposterior level on the spot for insertion of the guide cannula. The screws, the skullcap's hole, and the skull's surface were covered with self-curing dental acrylic cement (Jet Líquido Clássico®). At the end of the surgery, Veterinary Pentabiotic for Small Animals (2,000 U/mL, 0.1 mL/rat, i.m., Fort Dodge Saude Animal, Campinas, Brazil) was administered in a single dose as a prophylactic measure, as well as meloxicam (1.0 mg/kg/day, S.C., per day, Maxicam, Ourofino Saude Animal, Campinas, Brazil) for 3 days.

2.3 Catheterization of the femoral artery and vein

Rats anesthetized with 2% isoflurane in 100% O_2 were submitted to the cannulation of the femoral artery and vein through the insertion of a polyethylene tube (PE-50 connected to PE-10, Clay Adams, NJ, United States) for pulsatile arterial pressure (PAP), mean arterial pressure (MAP) and heart rate (HR) recordings in the data acquisition system (PowerLab 16 SP, ADInstruments, Castle Hill, AU), as well as drug administration, respectively.

2.4 Bladder cannulation and intravesical pressure measurement

Rats anesthetized with 2% isoflurane in 100% O_2 were submitted to urinary bladder cannulation by inserting a polyethylene tube (PE-50 connected to PE-10, Clay Adams, NJ), which was connected to a pressure transducer for intravesical pressure (IP) recording in the data acquisition system (PowerLab 16 SP, ADInstruments, Castle Hill, AU).

2.5 Drug microinjection in the mPOA

Drug microinjections in the mPOA were performed using a needle (27 gauge, 0.413-mm O.D., 0.210-mm I.D., 13-mm length, Injex, São Paulo, Brazil) connected to a 10-μL Hamilton syringe (Reno, NV, United States) by polyethylene tubing (PE-10, Clay Adams, NJ, United States). The volume of all the drugs injected into the mPOA was 1 μL, as previously reported in the studies by Bastos et al. (1994).

2.6 Histological analysis

At the end of the experiments, the animals were deeply anesthetized with i.v. injection of sodium thiopental 100 mg/kg (Cristália, Itapira, SP, Brazil) and 4% Chicago Sky Blue dye (Sigma Aldrich, St. Louis, MO, United States) was administered in a volume of 1 μL in the mPOA in order to determine the site of drug injections. Then, the rib cage was opened to expose the heart, and roughly 40 mL of formalin solution (10%) (Synth, Diadema, Brazil) was perfused intracardially. Afterwards, the brain was harvested and kept in the same formalin solution for at least 48 h. Subsequently, the brain was sectioned in a freezing microtome (Leica Biosystems, Buffalo Grove, IL, United States). The histological sections (40 μm) were stained with hematoxylin-eosin and analyzed in a light field microscopy (Nikon, Eclipse E-200, Tokyo, Japan). Only animals with histological confirmation of microinjection sites in the mPOA were considered in this study (Figure 1).

2.7 Gene expression of AT-1 receptors, ACE and GABAa receptor in the mPOA by quantitative real-time polymerase chain reaction (qPCR)

Total RNA was isolated from frozen mPOA samples with TRIzol Reagent® (Thermo Fisher Scientific) according to the manufacturer's protocol. RNA integrity was checked by agarose gel electrophoresis, and the RNA purity reached the following criteria: A260/280 ≥ 1.8. The extracted total RNA concentration was measured using a NanoDropTM (One-One c) spectrophotometer (Thermo Fisher Scientific), and 1 μg of total RNA was subjected to reverse transcription reaction. Complementary DNA (cDNA) synthesis was generated using ImPromIITM Reverse Transcription System (Promega, Madison, WC, United States) according to the manufacturer's protocol. Quantitative real-time PCR (qPCR) was carried out using 2 μL of cDNA and the Eva GreenTM qPCR Mix Plus (Solis BioDyne, Tartu, Estonia) in the ABI Prism 7,500 Sequence Detection System (Applied Biosystems, Foster City, CA) to amplify specific primers sequences for AT-1 receptor, ACE, GABAa receptor, Cyclophilin A (housekeeping gene), GAPDH (housekeeping gene), 18S rRNA (housekeeping gene). The procedure consisted of an initial step

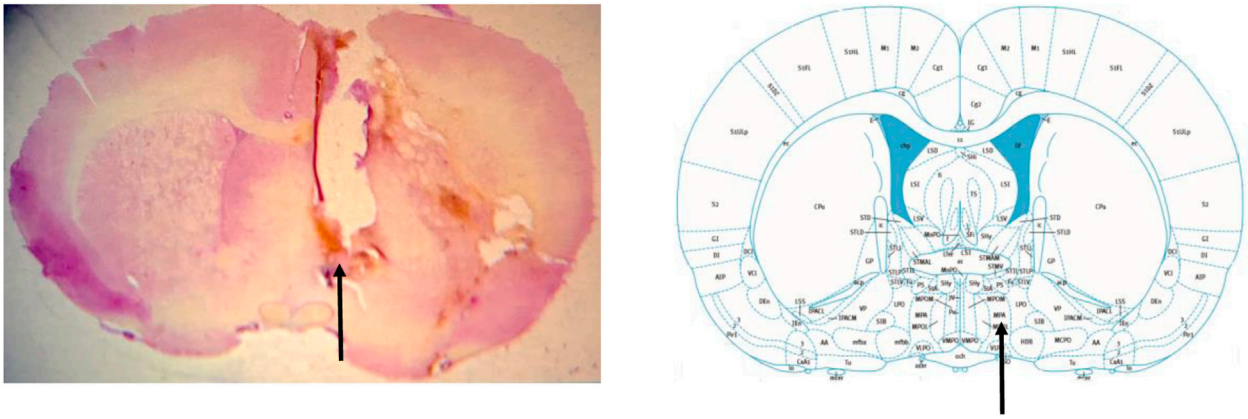

FIGURE 1
Photomicrograph of a rat from the experimental group demonstrating the drug injection site in the medial preoptic area (arrow) (left image). Schematic representation of the location of the medial preoptic area (arrow) in a section of the brain, according to the atlas of Paxinos and Watson. (2009).

of 10 min at 95°C, followed by 45 cycles of 20 s each at 95°C, 20 s at 58°C, and 20 s at 72°C. Gene expression was determined by cycle threshold (CT), and all values were expressed, using cyclophilin A or GAPDH or 18S rRNA as an internal control.

The forward and reverse primers sequences (Thermo Fisher Scientific) for rats used in this study follow below:

AT-1 receptor:
(forward)—5-AGTCCTGTTCCACCCGATCA-3′
(reverse)—5′-TCCAGACAAAATGCCAGCCA—3′
ACE:
(forward)—5′-CGGTTTTCATGAGGCTATTGG-3′
(reverse)—5′-TCGTAGCCACTGCCCTCACT-3′
GABAa receptor:
(forward)—5'-GAGCACGCAGAGTCCATGA-3'
(reverse)—5'-GAGAGGATCGCGGTGAGC-3'
Cyclophilin A (housekeeping gene):
(forward)—5′-CCCACCGTGTTCTTCGACAT-3′
(reverse)—5′-CTGTCTTTGGAACTTTGTCTGCAA-3′
GADH (housekeeping gene):
(forward)—5′-ACCACAGTCCATGCCATCAC -3′
(reverse)—5′-TCCACCACCCTGTTGCTGTA -3′
18S rRNA
(forward)—5′-CATTCGAACGTCTGCCCTAT -3′
(reverse)—5′-GTTTCTCAGGCTCCCTCTCC -3′

3 Experimental protocol

3.1 Effect of angiotensin II injection in the mPOA on intravesical pressure and cardiovascular parameters (N = 6)

This experimental protocol was aimed to assess whether or not the injection of Angiotensin II in the mPOA could change the intravesical pressure and if these changes would be related to changes in arterial pressure.

The animals were initially submitted to the stereotaxic surgery to implant a guide cannula in the mPOA. After 7 days, the animals were anesthetized with 2% isoflurane in 100% O_2 for catheterization of the femoral artery and vein and urinary bladder cannulation. The animals were maintained under the same anesthesia over the whole experimental procedure. After baseline recording of PAP, MAP, HR, and IP for 15 min, Angiotensin II (0.1 nM/μL, 1 μL) or saline (1 μL) was injected into the mPOA, and the variables were measured for additional 30 min (Figure 2).

3.2 Effect of losartan (AT-1 receptor antagonist) injection in the mPOA on intravesical pressure and cardiovascular parameters (N = 6)

This experimental protocol was intended to assess whether or not the blockade of AT-1 receptors with losartan injection in the mPOA could change the intravesical pressure and if these changes would be related to changes in arterial pressure.

In a different group of rats from section 8.1., the same surgical procedures were performed as described above (section 8.1). After measuring the baseline PAP, MAP, HR, and IP for 15 min, losartan (100 nM/μL, 1 μL) or saline (1 μL) was injected into the mPOA, and the variables were recorded for additional 30 min (Figure 2).

3.3 Effect of GABA injection in the mPOA on intravesical pressure and cardiovascular parameters (N = 6)

This experimental protocol was aimed to evaluated whether or not the GABAergic inhibition of mPOA could change the intravesical pressure and if these changes would be related to changes in arterial pressure. In addition, this protocol intended to investigate if the possible changes in intravesical pressure and

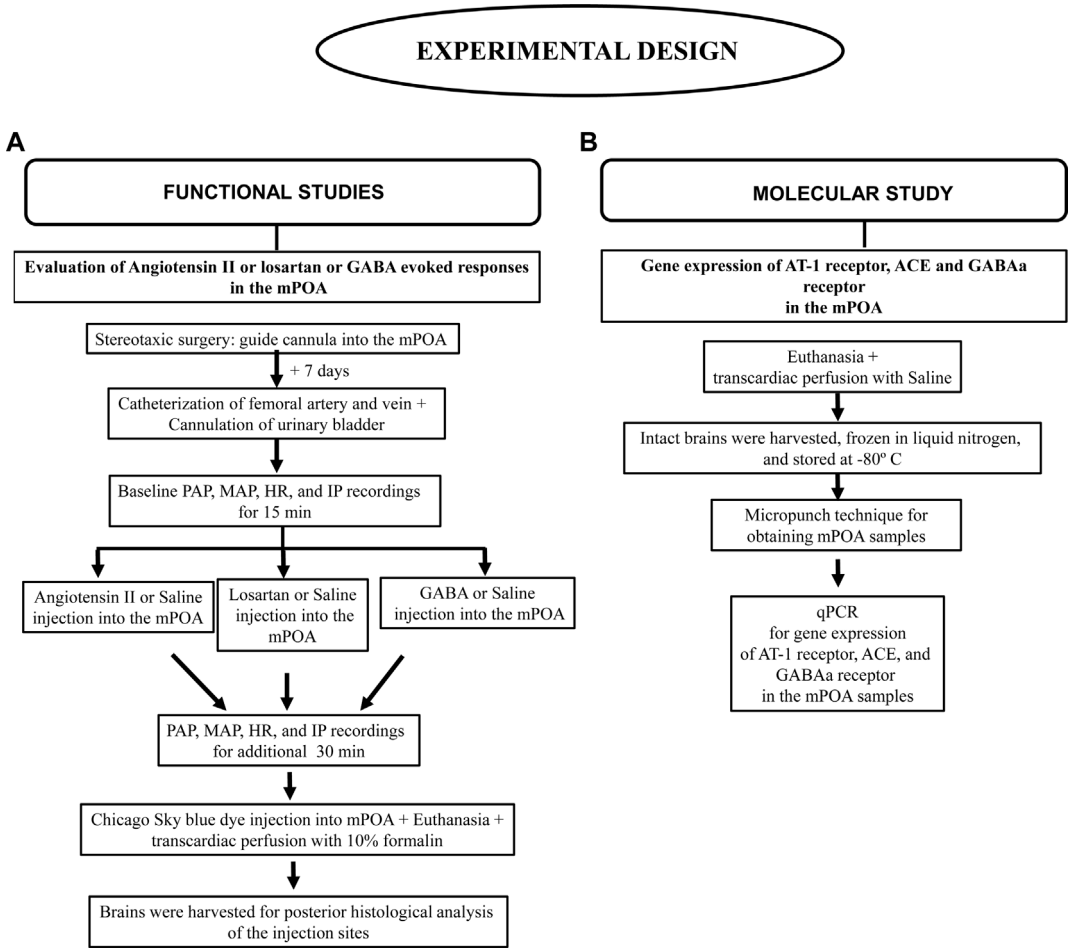

FIGURE 2
Flowchart depicting the experimental design details. **(A)** Functional studies, **(B)** Molecular study.

cardiovascular parameters showed any similarity to the responses elicited by activation or blockade of AT-1 receptors.

In a different group of rats from that used in sections 8.1 and 8.2, the same surgical procedures reported above (section 8.1) were carried out. After baseline measurement of PAP, MAP, HR and IP for 15 min, GABA (50 mM/μL, 1 μL) or saline (1 μL) was injected into the mPOA, and the variables were recorded for additionally 30 min (Figure 2).

3.4 Gene expression of AT-1 receptor, ACE, and GABAa receptor in the mPOA by quantitative real-time polymerase chain reaction (qPCR)

This experimental protocol was intended to evaluate if the genes for AT-1 receptor, ACE, and GABAa receptor were expressed in the mPOA of rats.

A different group of rats from that used in sections 8.1, 8.2 and 8.3 was used. Animals were deeply anesthetized with isoflurane 4% in 100% O_2 and submitted to a thoracotomy for transcardiac perfusion of 40 mL of phosphate buffered saline. After that, a craniotomy was performed and the brain was harvested, immediately frozen in liquid nitrogen, and stored at −80°C in an ultrafreezer (Thermo Fisher Scientific®) until the day of total RNA extraction with the TRizol® reagent. To obtain mPOA samples, the brain was sliced and a micropunch was performed on frozen sections of the rat brain. The further procedures for gene expression of AT-1 receptor, ACE, GABAa receptor by qPCR were performed as described in section 7 (Figure 2).

4 Statistical analysis

A Shapiro-Wilk test for normality was used for verifying the data distribution. Once the results fit to a normal distribution, they were expressed as mean ± S.E.M., and subjected to the One-way ANOVA followed by Tukey posttest to compare the MAP, HR and IP responses evoked by angiotensin II, losartan and saline injections in the mPOA. Paired Student´s t-tests were used to compare the MAP, HR, and IP responses induced by GABA injection in the mPOA. Statistical analysis was performed using Graph Pad Prism 9.5.0. The significance level was set at $p < 0.05$.

10.3389/fphys.2023.1224505

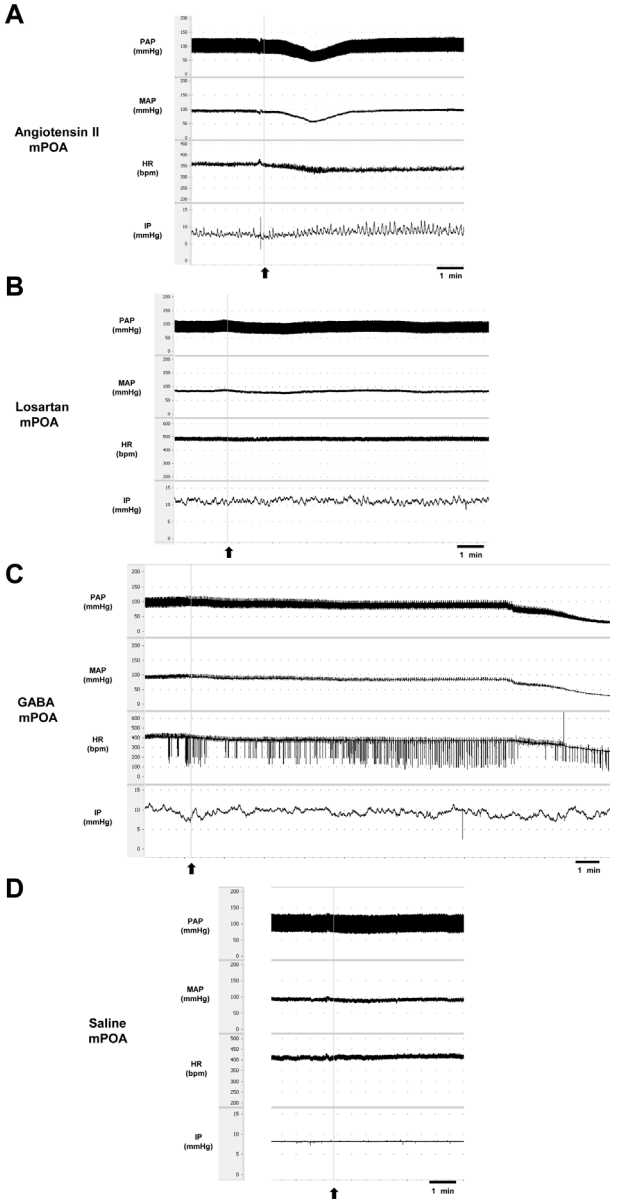

FIGURE 3
Tracings showing the baseline pulsatile arterial pressure (PAP, mmHg), mean arterial pressure (MAP, mmHg), heart rate (HR, bpm), intravesical pressure (IP, mmHg), and the responses induced by **(A)** angiotensin II (0.1 nM/μL, 1 μL) or **(B)** losartan (100 nM/μL, 1 μL) or **(C)** GABA (50 mM, 1 μL) or **(D)** saline (1 μL) into the medial preoptic area. Arrows indicate the moment of injections in the medial preoptic area.

5 Results

5.1 Responses on intravesical pressure and cardiovascular parameters in anesthetized rats evoked by angiotensin II or losartan injection in the mPOA

At baseline (before the injections in the mPOA), the SAP, DAP, MAP, and HR was 131 ± 4 mmHg, 99 ± 4 mmHg, 110 ± 3 mmHg and 433 ± 23 bpm, respectively (Ang II group, n = 6), 124 ± 3 mmHg, 106 ± 2 mmHg, 112 ± 2 mmHg and 448 ± 17 bpm, respectively (losartan group, n = 6), and 120 ± 2 mmHg, 105 ± 3 mmHg, 110 ± 3 mmHg and 424 ± 11 bpm, respectively (saline group, n = 6). The baseline IP (before the injections in the mPOA) was 7.08 ± 0.80 mmHg (Ang II group), 8.17 ± 0.65 mmHg (losartan group) and 6.99 ± 0.98 mmHg (saline group).

Injection of Ang II (n = 6) into the mPOA promoted a significant reduction in SAP (−43 ± 11 mmHg, p = 0.003), DAP (−34 ± 9 mmHg, n = 0.004), MAP (−37 ± 10 mmHg, p = 0.003) and HR (−47 ± 20 bpm, p = 0.030) compared to saline injection (−1 ± 1 mmHg, 1 ± 1 mmHg, +1 ± 1 mmHg and +6 ± 2 bpm, respectively, n = 6). In contrast, we observed a significant increase in IP (+72.25 ± 17.91%, p = 0.015) after Ang II injection into the mPOA compared to saline injection (−1.80% ± 2.98%) (Figures 3A,D; Figure 4). The latency for the peak response in MAP and HR evoked by Ang II in the mPOA was roughly 4 min, whereas the peak response in IP was achieved at ~6 min after Ang II injection in the mPOA. The duration of the Ang II evoked-response was different on the cardiovascular parameters compared to IP, as the reduction in MAP and HR lasted between 7–10 min, whereas the increase in IP persisted between 10–14 min.

Blockade of AT-1 receptors with losartan injection (n = 6) in the mPOA elicited no significant changes in SAP (−15 ± 5 mmHg, p = 0.306), DAP (−12 ± 4 mmHg, p = 0.350), MAP (−13 ± 3 mmHg, p = 0.399) and HR (+6 ± 5 bpm, p = 0.999) compared to saline injection (−1 ± 1 mmHg, 1 ± 1 mmHg, +1 ± 1 mmHg, and +6 ± 2 bpm, respectively, n = 6). Similarly, no significant changes in IP were observed after losartan injection (+2.92 ± 4.93%, n = 6, p = 0.957) compared to saline (−1.80% ± 2.98%) (Figures 3B,D; Figure 4). The latency for the peak in the weak changes in MAP and HR was observed at 9 min after losartan injection into the mPOA, whereas the small peak change for IP was achieved at 12 min after losartan injection into the mPOA. The weak change in MAP, HR and IP elicited by losartan injection in the mPOA lasted between 14–17 min.

5.2 Responses on intravesical pressure and cardiovascular parameters elicited by GABA injection in the mPOA

At baseline (before the injections in the mPOA), the SAP, DAP, MAP, and HR was 119 ± 5 mmHg, 97 ± 3 mmHg, 104 ± 3 mmHg and 415 ± 12 bpm (GABA group, n = 6) and 117 ± 5 mmHg, 94 ± 2 mmHg, 102 ± 3 mmHg and 407 ± 12 bpm, respectively (saline group, n = 6). The baseline IP was 9.00 ± 0.82 mmHg (GABA group), and 8.41 ± 0.74 mmHg (saline group).

Injection of GABA (n = 6) into the mPOA evoked a significant fall in SAP (−76 ± 2 mmHg, p <0.0001), DAP (−64 ± 2 mmHg, p <0.0001), MAP (−68 ± 2 mmHg, p <0.0001) and HR (−115 ± 14 bpm, p = 0.0003) compared to saline injection (0 ± 3 mmHg, −1 ± 1 mmHg, −1 ± 1 mmHg and +4 ± 2 bpm, respectively, n = 6). However, no significant changes were observed in IP (−12.07% ± 6.92%) after GABA injection into the mPOA compared to saline injection (0.40% ± 015%) (Figures 3C; Figure 5). The latency for the peak responses in MAP and HR evoked by GABA injected in the mPOA was ~8 min and the effect lasted for roughly 19 min.

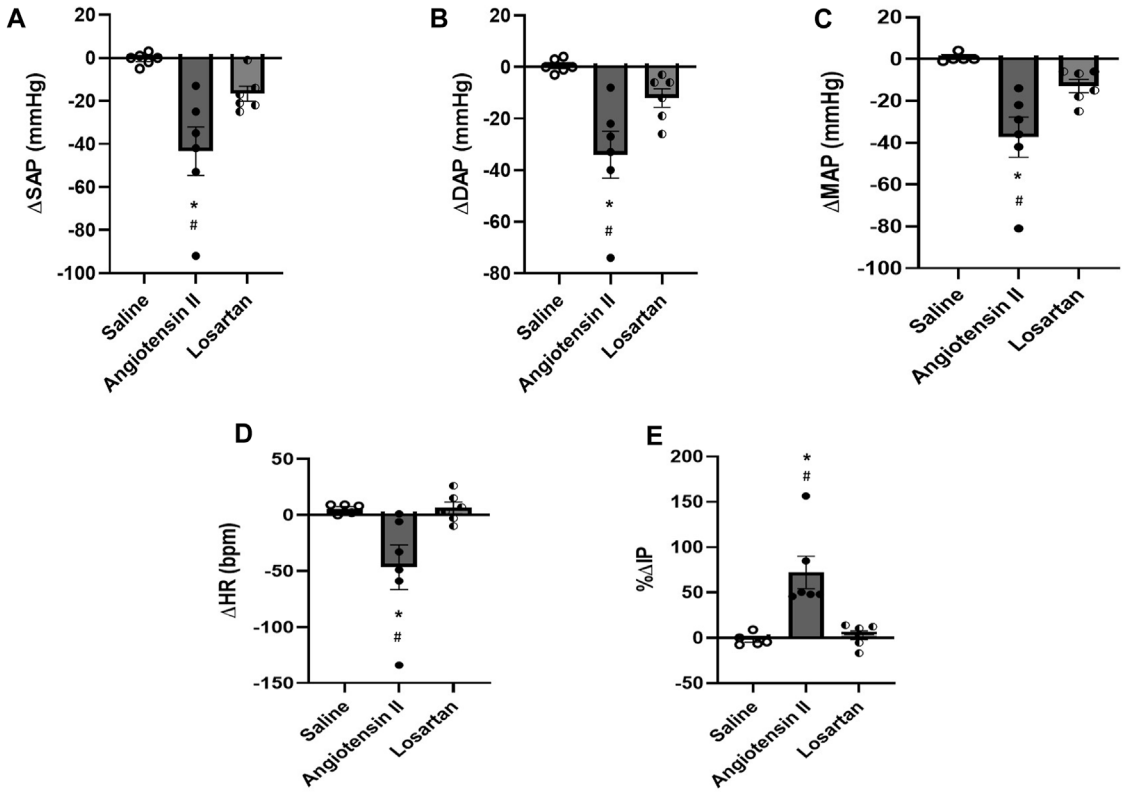

FIGURE 4
(A) Change in systolic arterial pressure (ΔSAP, mmHg), **(B)** diastolic arterial pressure (ΔDAP, mmHg), **(C)** mean arterial pressure (ΔMAP, mmHg), **(D)** change in heart rate (ΔHR, bpm), and **(E)** percent change in intravesical pressure (%ΔIP) evoked by injection of saline (1 μL), angiotensin II (0.1 nM/μL, 1 μL) or losartan (100 nM/μL, 1 μL) into the medial preoptic area (n = 6). *p < 0.05 vs. saline (One-way ANOVA, followed by Tukey posttest), #p <0.05 vs. losartan (One-way ANOVA, followed by Tukey posttest).

5.3 Determination of gene expression of AT-1 receptor, ACE and GABAa receptor in the mPOA of rats (N = 6)

The mRNA expression by RT-qPCR demonstrated that the AT-1 receptor (relative to cyclophilin A = 0.67 ± 0.22, relative to GAPDH = 1.05 ± 0.14, relative to 18S rRNA = 1.15 ± 0.27), ACE (relative to cyclophilin A = 1.11 ± 0.10, relative to GAPDH = 1.03 ± 0.11, relative to 18S rRNA = 1.15 ± 0.28), and GABAa receptor (relative to cyclophilin A = 1.08 ± 0.13, relative to GAPDH = 1.10 ± 0.24, relative to 18S rRNA = 1.02 ± 0.09) are found in the mPOA samples (n = 6) (Figure 6).

6 Discussion

The findings of this study in female rats demonstrate that Ang II injection into the mPOA yielded hypotension, bradycardia and increase in intravesical pressure. The blockade of AT-1 receptors in the mPOA by losartan elicited no significant changes in any variable studied, even though the dose administered was high in comparison to Ang II. Despite the GABAergic inhibition of mPOA evoked a marked hypotension and bradycardia similarly to Ang II, no change was observed in intravesical pressure. The present data also showed that the genes for AT-1 receptors, ACE and GABAa receptor were found in the mPOA. The mPOA samples for gene expression were obtained from intact brains, without guide cannula implantation in the mPOA, in order to exclude any influence of previous surgery on the integrity of mPOA neurons.

Although the volume of injection (1 μL) in the medial preoptic area could be considered large, the responses evoked by Ang II or GABA injections were only observed when the injection spot was centered in the medial preoptic area. Injections of Ang II or GABA located out of the medial preoptic area either more dorsal or more lateral from the midline, which was confirmed by the histological analysis, caused no change in the cardiovascular parameters and intravesical pressure. These findings suggest that the responses elicited by Ang II or GABA injections observed in the current study were specific and targeted to medial preoptic area.

The fact that the preoptic area is involved in the autonomic modulation has been known since 1935, when Kabat et al. (1935) demonstrated blood pressure changes to electrical stimulation of the POA in anesthetized cats. Nevertheless, Wang and Ranson. (1941) suggested that the preoptic area could play a dual effect on the autonomic nervous system, leading to vagal activation and causing sympathetic inhibition as the electrical stimulation elicited bradycardic response that was significantly attenuated by vagotomy. Folkow et al. (1959) have also shown that a pronounced hypotension and bradycardia can be evoked by electrical stimulation of the preoptic area in vagotomized cats

10.3389/fphys.2023.1224505

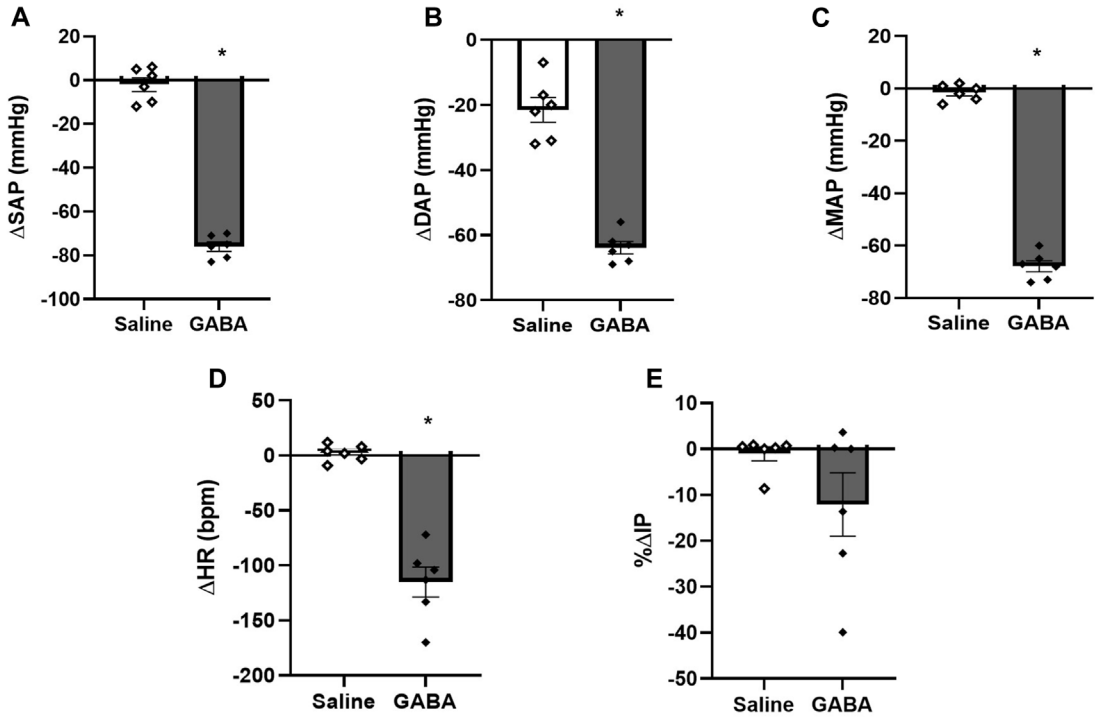

FIGURE 5
(A) Change in systolic arterial pressure (ΔSAP, mmHg), **(B)** diastolic arterial pressure (ΔDAP, mmHg), **(C)** mean arterial pressure (ΔMAP, mmHg), **(D)** change in heart rate (ΔHR, bpm), and **(E)** percent change in intravesical pressure (%ΔIP) induced by injection of saline (1 μL) or GABA (50 mM/μL, 1 μL) into the medial preoptic area (n = 6). *$p < 0.05$ vs. saline (paired Student's t-test).

with bilateral carotid occlusion, suggesting its sympathoinhibitory role. The electrical stimulation would be able to activate either cell bodies of neurons and axons, thereby those earlier studies causing nonspecific effects could also activate neurons lying outside the preoptic area. In 2017, Fassini et al. (2017) have inhibited the mPOA neurotransmission using cobalt chloride, a non-selective inhibitor of synapses. They demonstrated that this brain area exerts a tonic inhibitory function on cardiac sympathetic tone under resting and stress conditions, negatively modulating the sympathetic component of the baroreflex. However, the studies of could not demonstrate which neurotransmitter or neuromodulator would be released in the mPOA synapses to produce those effects.

In our study, either Ang II or GABA injections in the mPOA caused hypotensive and bradycardic responses, nevertheless, the latency to achieve the peak responses, intensity and duration of the responses were not equivalent. Further, the effects on intravesical pressure were different after Ang II and GABA injections in the mPOA. We observed an increase in intravesical pressure elicited by Ang II, whilst no change in intravesical pressure was caused after GABAergic inhibition. Hence, our data are suggestive that Ang II and GABA could be involved in the sympathoinibitory pathways to reduce blood pressure and heart rate, however are likely acting in different central pathways involved in micturition control.

Even though it is classically known that GABA injections induces responses with short latency and duration in areas involved in cardiovascular control, we observed a long latency for the appearance of the hypotensive response and bradycardia elicited by GABA injection in the mPOA. In addition, these responses showed a long duration. Despite we do not know the explanation for this fact, which is a limitation of this study, recent studies have also shown that injections of GABA into the shell Nucleus Accumbens evokes a huge hypotension and bradycardia, which are also long-lasting responses (~14 min) (de Carvalho et al., 2023), that is quite unusual considering the classically known shorter responses evoked by GABA.

In the present study, the blockade of AT-1 receptors with losartan injection in the mPOA elicited no significant change on resting arterial pressure, heart rate and intravesical pressure. The absence of any noticeable responses evoked by losartan suggests that neurons with AT-1 receptors in the mPOA, where Ang II binds, exert a phasic control on the pathways which regulate these physiological parameters.

In the current study, we have not tested the Ang II after losartan injection in the mPOA, which is a limitation of this study. Nonetheless, qPCR demonstrated that AT-1 receptors, ACE and GABAa receptors mRNA are present in the mPOA. The mPOA contains the mRNA for angiotensinogen, low density of fibers with immunoreactivity for Ang II, modest immunoreactivity for AT-1 receptors and moderate amounts of ACE. In contrast, immunoreactivity for angiotensinogen has not been reported (Bunnemann et al., 1983). Thus, our data showing the existence of AT-1 receptors and ACE mRNA in the mPOA is consistent with the protein expression showed by Bunnemann et al. (1983). Taken together with the fact that Ang II and GABA gave similar responses to cardiovascular parameters, but distinctly on urological, it is evident that the agonists acted selectively on the different neural pathways.

10.3389/fphys.2023.1224505

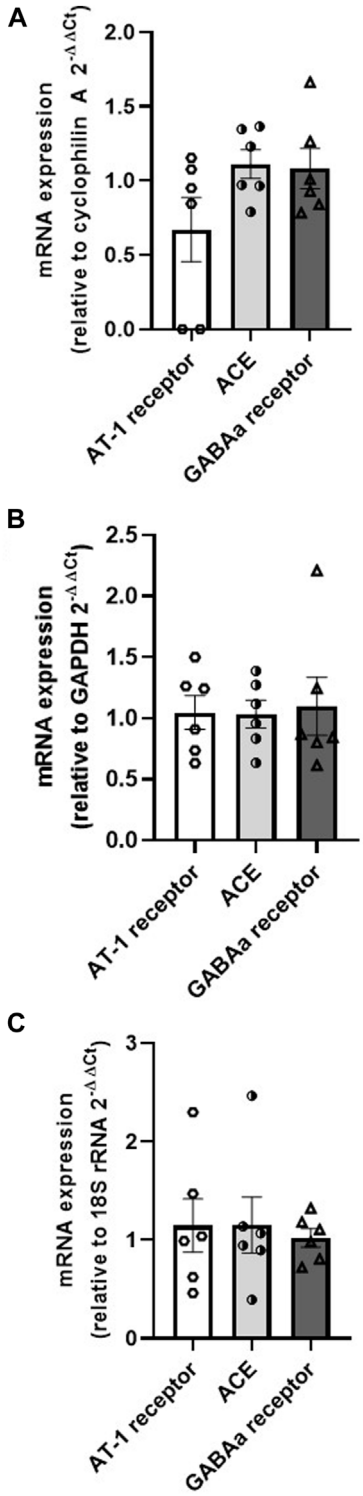

FIGURE 6
mRNA expression of AT-1 receptor, ACE and GABA in the medial preoptic area samples relative to the housekeeping genes **(A)** cyclophilin **(A,B)** GAPDH, and **(C)** 18S rRNA (N = 6).

Formation of Ang II is dependent on cleavage of Angiotensin I, which undergoes the action of ACE (Chappell et al., 2000; Rice et al., 2004). Since ACE mRNA was expressed in the mPOA, it is likely that neurons in the mPOA synthetizes Ang II, which is released in the synapses of this brain area to bind AT-1 receptors, in order to exert a phasic control of the sympathetic pathways involved in cardiovascular regulation. Despite we have not performed the gene expression of AT-2 receptors, ACE-2 or Mas receptors in the mPOA, we cannot exclude the possibility that Ang II can bind to AT-2 receptors or can be transformed to Angiotensin-(1–7) and bind to Mas receptors.

Studies by Bastos et al. (1994) have shown that Ang II injected in the mPOA in conscious male Holtzman rats induces thirst (dipsogenic effect), natriuresis, kaliuresis and diuresis. In addition, Ang II at the dose of 25 ng injected into the mPOA in conscious rats evoked a pressor response, which was attenuated by previous blockade of α1-adrenoceptors with prazosin, but not by antagonism of β1/β2 adrenoceptors with propranolol. In our study, we observed a depressor response (hypotension) after Ang II injection at the concentration of 0.1 nM (in a volume of 1 μL) in the mPOA in isoflurane anesthetized rats. Two different hypotheses could underpin the difference in the blood pressure responses. One of them could be the dose of Ang II, which was very low in our study (0.1046 pg), whilst in the study of Bastos et al. (1994), the dose injected in the mPOA was 25 ng (25,000 pg). Tentatively, a part of the differences in response could further be attributed to the anesthetic used in our study that could facilitate a depressor response.

Rusyniak et al. (2011) have shown that injection of muscimol, a GABAa receptor agonist, into the mPOA yielded a pressor response and tachycardia in conscious male Sprague-Dawley rats. Unlike the reports of Rusyniak et al. (2011), the present study showed that GABA injection in the mPOA in isoflurane-anesthetized rats caused a marked hypotensive response. The existence of GABAa receptor mRNA in the mPOA samples currently demonstrated suggests that GABA binds to these receptors in this brain area. However, it is noteworthy that the center of drug injection in the mPOA in the study of Rusyniak et al. (2011) was in a more rostral level compared to the present study. Hence, it is unknown if different populations of neurons and/or pathways in the mPOA could be affected by muscimol or GABA injections leading to opposite responses. Another source of difference to the findings of Rusyniak et al. (2011) could once again be the anesthesia used in the current study.

Micturition in neonatal rats is mediated by a spinal reflex pathway activated when the mother licks the perineum to produce an intense bladder contraction and urination. However, bladder distention, unlike what occurs in adult animals, does not induce reflex urination in neonates. As the central nervous system matures during the postnatal period, the spinal reflex is gradually replaced by a spinobulbospinal reflex pathway that is the primary mechanism for reflex urination in adult animals. This pathway has an integration center in the rostral pons and peripheral afferent and efferent pathways (Sugaya et al., 1997). Pseudorabies virus labels many neurons in various brain regions (PRV) after injected into the urinary bladder of rat pups. The distribution of PRV-infected neurons is somewhat broader than in adult mice. In adult rats, the mPOA shows labeled neuronal populations, although with less expression compared to other brain areas. The results of the current study indicate that Ang II injected into the mPOA in adult rats increased intravesical pressure in anesthetized rats, whereas the inhibition of mPOA neurons by GABA did not affect the intravesical pressure. Thereby, Ang II in the mPOA is involved in the control of the central micturition pathways, and conversely the GABAergic transmission in the mPOA does not participate in the regulation of these pathways.

The mPOA has dense bi-directional connections with the periaqueductal gray matter (PAG), which sends descending projections to the rostral ventrolateral medulla (RVML) (Rizvi et al., 1996; Murphy et al., 1999). The RVLM contains the presympathetic neurons involved in cardiovascular regulation (Colombari et al., 2001). The PAG has neurons involved in central micturition control (Fowler et al., 2008). Hence, these projections from the mPOA to RVLM and PAG could underpin the neural substrate for the responses evoked by Ang II and GABA in the current study.

Although we have used female rats, the estrous cycle was not evaluated in each animal, which is a limitation of this study. Nevertheless, the rats were maintained in groups of 4 animals per cage and their estrous cycles were likely synchronized (McClintock, 1978; McClintock, 1981). Our data was obtained in different days and over several months, with rats likely in different phases of the estrous cycle. Despite that, the changes in the cardiovascular parameters and intravesical pressure evoked by Ang II or GABA injections in the mPOA did not show huge variability, which suggests that the estrous cycle does not seem to influence the responses observed in the current study. We have not carried out the same studies in male rats. It is unknown whether the responses evaluated will be different or not depending on the gender, and this will require further investigation.

In conclusion, the Ang II mediated transmission in the mPOA has the capacity to affect the cardiovascular regulation causing hypotension and bradycardia, and further eliciting increase in intravesical pressure in anesthetized female rats, which also suggests an involvement in the control of central micturition pathways. In addition, a phasic control dependent on AT-1 receptors in the mPOA seems to be involved in the regulation of those cardiovascular and intravesical parameters. In contrast, GABAergic transmission in the mPOA participates in the pathways of cardiovascular control eliciting hypotension and bradycardia in anesthetized female rats, nevertheless, this neurotransmission is not involved in the micturition control.

Data availability statement

The original contributions presented in the study are included in the article/Supplementary Material, further inquiries can be directed to the corresponding author.

Ethics statement

The animal study was approved by the CEUA-Centro Universitario FMABC. The study was conducted in accordance with the local legislation and institutional requirements.

Author contributions

All authors listed have made a substantial, direct, and intellectual contribution to the work and approved it for publication.

Funding

This research was supported by Sao Paulo State Research Foundation (FAPESP, grant# 2018/00191-4).

Acknowledgments

We would also like to thank Mateus S. Souza for the technical assistance and care of the animals in the Physiology lab at Faculdade de Medicina do ABC, and Centro Universitario FMABC for providing all the conditions for the development of this study.

Conflict of interest

The authors declare that the research was conducted in the absence of any commercial or financial relationships that could be construed as a potential conflict of interest.

Publisher's note

References

Aoki, Y., Brown, H. W., Brubaker, L., Cornu, J. N., Daly, J. O., and Cartwright, R. (2017). Urinary incontinence in women. *Nat. Rev. Dis. Prim.* 3, 17097. doi:10.1038/nrdp.2017.97

Bastos, R., Saad, W. A., Menani, J. V., Renzi, A., Silveira, J. E. N., and Camargo, L. A. A. (1994). Role of adrenergic pathways of the medial preoptic area in ANGII-induced water intake and renal excretion in rats. *Brain. Res.* 636, 81–86. doi:10.1016/0006-8993(94)90178-3

Bunnemann, B., Fuxe, K., and Ganten, D. (1993). "Extrarenal renin systems: the brain," in *The renin-angiotensin system*. Editors J. I. S. Robertson and M. G. Nicholls (London: Mosby), 1–41.

Chappell, M. C., Gomez, M. N., Pirro, N. T., and Ferrario, C. M. (2000). Release of angiotensin-(1–7) from the rat hindlimb: influence of angiotensin converting enzyme inhibition. *Hypertension* 35, 348–352. doi:10.1161/01.hyp.35.1.348

Colombari, E., Sato, M. A., Cravo, S. L., Bergamaschi, C. T., Campos, R. R., Jr., and Lopes, O. U. (2001). Role of the medulla oblongata in hypertension. *Hypertension* 38 (32), 549–554. doi:10.1161/01.hyp.38.3.549

de Carvalho, R. P., do Vale, B., Dsouki, N. A., Cafarchio, E. M., De Luca, L. A., Aronsson, P., et al. (2023). GABAergic and glutamatergic transmission reveals novel cardiovascular and urinary bladder control features in the shell nucleus accumbens. *Brain. Res.* 1818, 148520. doi:10.1016/j.brainres.2023.148520

De Groat, W. C. (1998). Anatomy of the central neural pathways controlling the lower urinary tract. *Eur. Urol.* 34 (1), 2–5. doi:10.1159/000052265

De Groat, W. C., Griffiths, D., and Yoshimura, N. (2015). Neural control of the lower urinary tract. *Compr. Physiol.* 5 (1), 327–396. doi:10.1002/cphy.c130056

Fassini, A., Scopinho, A. A., Alves, F. H. F., Fortaleza, E. A. T., and Corrêa, F. M. A. (2017). The medial preoptic area modulates autonomic function under resting and stress conditions. *Neuroscience* 364, 164–174. doi:10.1016/j.neuroscience.2017.09.026

Folkow, B., Johansson, B., and Oberg, B. (1959). A hypothalamic structure with a marked inhibitory effect on tonic sympathetic activity. *Acta Physiol. Scand.* 47, 262–270. doi:10.1111/j.1748-1716.1960.tb00077.x

Fowler, C. J., Griffiths, D., and de Groat, W. C. (2008). The neural control of micturition. *Nat. Rev. Neurosci.* 9 (6), 453–466. doi:10.1038/nrn2401

Kabat, H., Magoun, H. W., and Ranson, S. W. (1935). Electrical stimulation of points in the forebrain and midbrain. *Arch. Neur. Psychiat.* 34, 931–955. doi:10.1001/archneurpsyc.1935.02250230003001

Lind, R. W., Swanson, L. W., and Ganten, D. (1985). Organization of angiotensin II immunoreactive cells and fibers in the rat central nervous system. An immunohistochemical study. *Neuroendocrinology* 40, 2–24. doi:10.1159/000124046

McClintock, M. K. (1978). Estrous synchrony and its mediation by airborne chemical communication (*Rattus norvegicus*). *Horm. Behav.* 10, 264–275. doi:10.1016/0018-506x(78)90071-5

McClintock, M. K. (1981). Social control of the ovarian cycle and the function of estrous synchrony. *Amer. Zool.* 21, 243–256. doi:10.1093/icb/21.1.243

Murphy, A. Z., Rizvi, T. A., Ennis, M., and Shipley, M. T. (1999). The organization of preoptic-medullary circuits in the male rat: evidence for interconnectivity of neural structures involved in reproductive behavior, antinociception and cardiovascular regulation. *Neuroscience* 91, 1103–1116. doi:10.1016/s0306-4522(98)00677-0

Paxinos, G., and Watson, C. (2009). *The rat brain in stereotaxic coordinates*. Sixth Edition. Oxford, United Kingdom: Academic Press.

Rice, G. I., Thomas, D. A., Grant, P. J., Turner, A. J., and Hooper, N. M. (2004). Evaluation of angiotensin-converting enzyme (ACE), its homologue ACE2 and neprilysin in angiotensin peptide metabolism. *Biochem. J.* 383, 45–51. doi:10.1042/BJ20040634

Rizvi, T. A., Murphy, A. Z., Ennis, M., Behbehani, M. M., and Shipley, M. T. (1996). Medial preoptic area afferents to periaqueductal gray medullo-output neurons: A combined fos and tract tracing study. *J. Neurosci.* 16, 333–344. doi:10.1523/JNEUROSCI.16-01-00333.1996

Rusyniak, D. E., Zaretisky, D. V., Zaretiskaia, M. V., and DiMicco, J. A. (2011). The role of orexin-1 receptors in physiologic responses evoked by microinjection of PgE2 or muscimol into the medial preoptic area. *Neurosci. Lett.* 498 (2), 162–166. doi:10.1016/j.neulet.2011.05.006

Sugaya, K., Nishijima, S., Miyazato, M., and Ogawa, Y. (2005). Central nervous control of micturition and urine storage. *J. Smooth Muscle Res.* 41 (3), 117–132. doi:10.1540/jsmr.41.117

Sugaya, K., Roppolo, J. R., Yoshimura, N., Card, J. P., and de Groat, W. C. (1997). The central neural pathways involved in micturition in the neonatal rat as revealed by the injection of pseudorabies virus into the urinary bladder. *Neurosci. Lett.* 223, 197–200. doi:10.1016/s0304-3940(97)13433-4

Wang, C. S., and Ranson, S. N. (1941). The rôle of the hypothalamus and preoptic region in the regulation of heart rate. *Am. J. Physiol.* 132, 5–8. doi:10.1152/ajplegacy.1941.132.1.5

frontiers | Frontiers in Physiology

TYPE Original Research
PUBLISHED 30 November 2023
DOI 10.3389/fphys.2023.1306500

OPEN ACCESS

EDITED BY
Russ Chess-Williams,
Bond University, Australia

REVIEWED BY
Lu Liu,
University of New South Wales, Australia
Masumi Eto,
Okayama University of Science, Japan

*CORRESPONDENCE
Violeta N. Mutafova-Yambolieva,
vmutafova@med.unr.edu

RECEIVED 03 October 2023
ACCEPTED 16 November 2023
PUBLISHED 30 November 2023

CITATION
Aresta Branco MSL, Perrino BA and Mutafova-Yambolieva VN (2023), Spatial mapping of ectonucleotidase gene expression in the murine urinary bladder. *Front. Physiol.* 14:1306500. doi: 10.3389/fphys.2023.1306500

Spatial mapping of ectonucleotidase gene expression in the murine urinary bladder

Mafalda S. L. Aresta Branco, Brian A. Perrino and Violeta N. Mutafova-Yambolieva*

Department of Physiology and Cell Biology, University of Nevada Reno School of Medicine, Reno, NV, United States

Purinergic signaling is important for normal bladder function, as it is thought to initiate the voiding reflex and modulate smooth muscle tone. The availability of adenine nucleotides and nucleosides (aka purines) at receptor sites of various cell types in the bladder wall is regulated by ectonucleotidases (ENTDs). ENTDs hydrolyze purines such as adenosine 5′-triphosphate (ATP) and adenosine 5′-diphosphate (ADP) with varying preference for the individual substrate. Therefore, the end effect of extracellular purines may depend significantly on the type of ENTD that is expressed in close proximity to the target cells. ENTDs likely have distinct cellular associations, but the specific locations of individual enzymes in the bladder wall are poorly understood. We used RNAscope™, an RNA *in situ* hybridization (ISH) technology, to visualize the distribution and measure the levels of gene expression of the main recognized ectonucleotidases in large high-resolution images of murine bladder sections. The relative gene expression of ENTDs was *Entpd3* > *Alpl* >> *Enpp1* = *Entpd2* >> *Enpp3* > *Entpd1* (very low to no signal) in the urothelium, *Entpd1* ≥ *Entpd2* >> *Enpp3* > *Enpp1* = *Alpl* ≥ *Nt5e* (very low to no signal) in the lamina propria, and *Entpd1* >> *Nt5e* = *Entpd2* >> *Enpp1* > *Alpl* = *Enpp3* in the detrusor. These layer-specific differences might be important in compartmentalized regulation of purine availability and subsequent functions in the bladder wall and may explain reported asymmetries in purine availability in the bladder lumen and suburothelium/lamina propria spaces.

KEYWORDS

ATP, bladder, nucleotidases, purinergic signaling, RNAscope

1 Introduction

Adenosine 5′-triphosphate (ATP) is released as a co-transmitter of acetylcholine by parasympathetic nerves and possibly as a co-transmitter of norepinephrine/noradrenaline by sympathetic nerves in the bladder (Burnstock, 2014) as well as by the urothelium into both luminal and suburothelial sides in response to bladder distension (Yu, 2015; Durnin et al., 2019). ATP released by efferent neurons can modulate smooth muscle tone via $P2X_1$ receptors (Vial and Evans, 2000), whereas urothelial ATP can act in autocrine and paracrine ways via different P2X and P2Y receptor subtypes to stimulate urothelial cells (Ferguson et al., 2015; Chess-Williams et al., 2019), suburothelial interstitial cells/myofibroblasts (Wu et al., 2004; Cheng et al., 2011), and sensory nerves (Cockayne et al., 2000; Kaan et al., 2010). Of particular relevance, $P2X_{2/3}$ and $P2X_3$ receptor activation on sensory nerves is thought to convey the sensation of bladder fullness and initiate the micturition reflex in the bladder (Cockayne et al., 2000; Kaan et al., 2010).

10.3389/fphys.2023.1306500

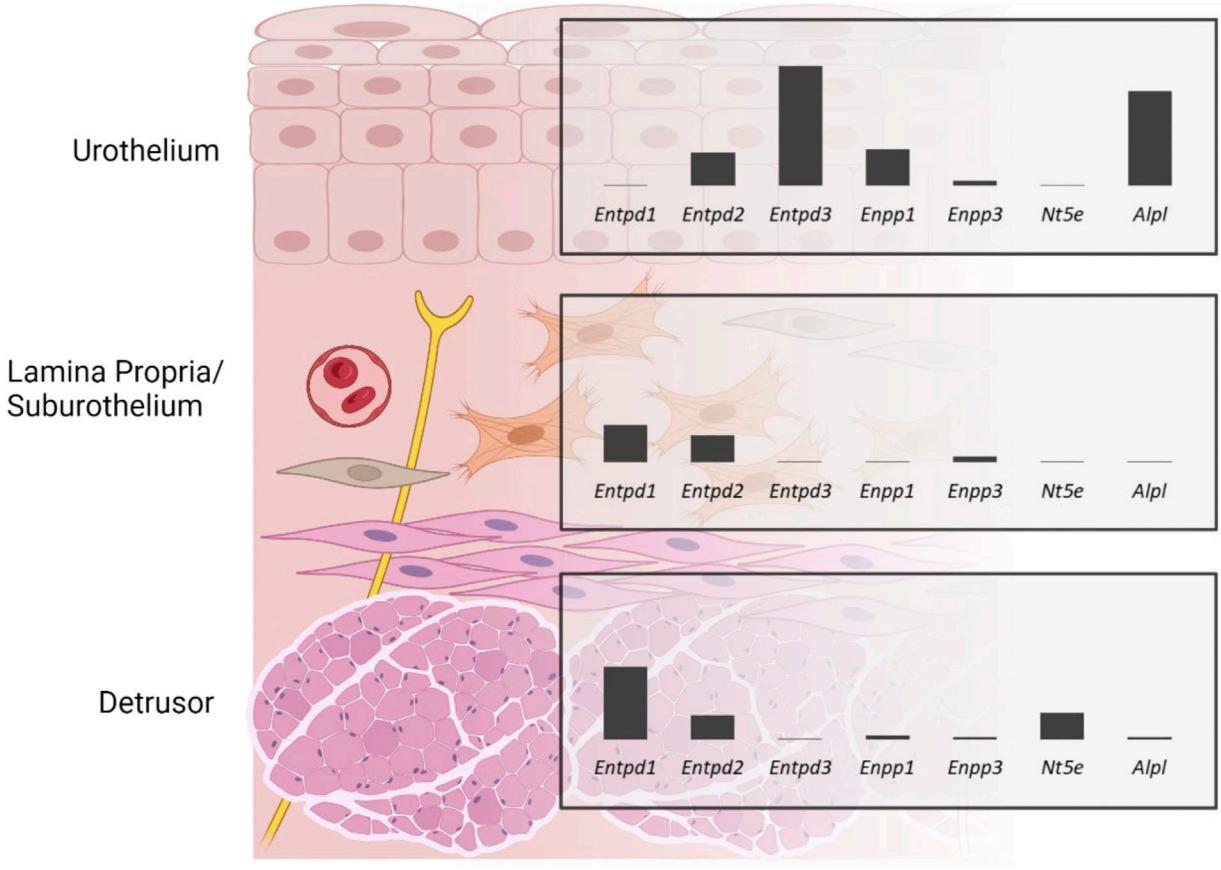

GRAPHICAL ABSTRACT
Gene expression of ectonucleotidases in the murine bladder wall demonstrates that ectonucleotidases are differentially expressed in detrusor, lamina propria, and urothelium of the murine bladder. Created with https://BioRender.com.

Released ATP is rapidly hydrolyzed by membrane-bound and soluble forms of ectonucleotidases to ADP, AMP, and adenosine (ADO) (Yu, 2015; Aresta Branco et al., 2022; Gutierrez Cruz et al., 2022). It should be noted that ADP and ADO are biologically active metabolites that can modulate detrusor excitability via G-protein-coupled P2Y purinergic and A1, A2a, A2b, and A3 adenosine receptors, respectively. While ADP actions result in detrusor muscle contraction (Yu et al., 2014), ADO acts in an opposing way, evoking smooth muscle relaxation (Hao et al., 2019). Hence, extracellular metabolism of purines is a key determinant of the availability of these mediators at receptor sites and ensuing functions in the bladder.

Remarkably, the available concentration and relative proportion of purines are asymmetrical in the luminal and suburothelial sides of the urothelium at the end of bladder filling (Durnin et al., 2019), suggesting cell-specific differences in the release and/or metabolism of purines. Immunohistochemical studies report differences in the expression and distribution of ectonucleotidases in the bladder that may explain these observations (Yu et al., 2011; Yu, 2015; Babou Kammoe et al., 2021). Furthermore, in recent studies we observed distinct profiles of purine degradation in the lamina propria/suburothelium and intraluminal space, which, interestingly, was accompanied by the differential release of soluble ectonucleotidases into these compartments (Aresta Branco et al., 2022; Gutierrez Cruz et al., 2022). Previous immunohistochemical studies provided valuable information regarding the expression and distribution of some ectonucleotidase families in the bladder (Yu et al., 2011; Yu, 2015; Babou Kammoe et al., 2021). Nevertheless, a more comprehensive study was warranted. Therefore, we used RNAscope™—a more specific, sensitive, and reliable method—to assess the distribution and to measure the expression levels of several ectonucleotidase genes *(Entpd1, Entpd2, Entpd3, Enpp1, Enpp3, Nt5e and Alpl)* in the layers of the bladder (urothelium, lamina propria, and detrusor) and subset populations of the urothelium (basal plus intermediate cells and umbrella cells) across large high-resolution images of sagittal bladder sections. The results of this study provide strong support to the idea that ectonucleotidases are differentially expressed in the layers of the bladder wall likely providing specialized regulation of amount/type of excitatory and inhibitory purine mediators at effector cells.

2 Materials and methods

2.1 Animals

Male C57BL6J (3 months old, n = 3) were purchased from Jackson Laboratory (JAX stock #000664, Bar Harbor, MN). The

mice were housed with free access to food and water and maintained in a 12 h light-dark cycle. The mice were sedated with isoflurane (AErrane; Baxter, Deerfield, IL, United States) and euthanized by cervical dislocation and exsanguination. All experimental procedures were carried out with the approval of the Institutional Animal Use and Care Committee at the University of Nevada, Reno and in accordance with the standards of the National Institutes of Health's *Guide for the Care and Use of Laboratory Animals*.

2.2 Tissue preparation

Urinary bladders together with the proximal urethras and distal ureters were excised immediately after cervical dislocation and placed in oxygenated ice-cold Krebs-bicarbonate solution (KBS; mM: 118.5 NaCl, 4.2 KCl, 1.2 $MgCl_2$, 23.8 $NaHCO_3$, 1.2 KH_2PO_4, 11.0 dextrose, and 1.8 $CaCl_2$; pH 7.4). After excess fat was removed, the whole bladders with connected proximal urethras and ureters were fixed in paraformaldehyde (PFA) 4% in phosphate-buffered saline (PBS) at 4°C for 24 h. The PFA solution was also added to the lumen of the bladder through the urethra to ensure adequate fixation. After several washes with PBS, the bladders and urethras were cut in half through the median plane with sharp blade and washed again in PBS three times at 30 min per wash. The preparations were cryopreserved by immersing the tissue for 15 min in increasing concentrations of sucrose in PBS [5%–20% (w/v)] and left overnight in 30% (w/v) sucrose in PBS at 4°C. The tissue preparations were embedded in a 1:1 mixture of 30% sucrose in PBS and O.C.T (Fisher, TX, United States), positioned in a cryomold with the cut side facing down, and frozen at −80°C. The blocks were cut into 14 µm sagittal cross sections using a Leica CM3050 S cryostat and placed onto VWR® Premium Superfrost® Plus Microscope Slides. Sections were left to air dry for 60 min at −20°C and then stored with desiccants at −20°C. Tissue preparation was carried out according to protocol provided by Advanced Cell Diagnostics (ACD, Bio-Techne, Newark, CA, United States) for fixed frozen tissue.

2.3 RNA *in situ* hybridization

Tissue preparations, pre-treatments, and RNAscope™ assays were performed according to ACD user manual (Document UM 323100) instructions for fixed frozen tissue, using RNAscope™ Multiplex Fluorescent Reagent Kit V2 (ACDBio Cat. No. 323100). Briefly, this involves sequential permeabilization of the tissue, hybridization of probes with target RNA, and amplification of signal. RNAscope™ probes were used to target *Krt20* (Cat. No. 402301-C3), *Krt5* (Cat. No. 415041 or 415041-C2), *Entpd1* (Cat. No. 475761), *Entpd2* (Cat. No. 579591-C2), *Entpd3* (Cat. No. 1236741-C1), *Enpp1* (Cat. No. 441191), *Enpp3* (Cat. No. 1236751-C1), *Nt5e* (Cat. No. 437951) and *Alpl* (Cat. No. 441161). As recommended by the manufacturer, the 3-plex Positive Control Probes [POLR2A (Channel C1), PPIB (Channel C2), UBC (Channel C3), Cat.No.320881] were used to help qualify samples and interpret assay results and the 3-plex Negative Control Probe (Cat. No. 320871) that targets the bacterial *dapB* gene was used to control for background noise and to help interpret assay results. The following Opal fluorophore reagents (Akoya Biosciences, MA, United States) were used to detect up to three targets in a single image: Opal™ 520 (Cat. No. FP1487001KT), Opal™ 570 (Cat. No. FP1488001KT), and Opal™ 690 (Cat. No. FP1497001KT). Nuclear counterstain was achieved with DAPI (included in the RNAscope™ Multiplex Fluorescent Reagent Kit V2). Slides were mounted with VECTASHIELD Vibrance® Antifade Mounting Medium (Vector laboratories, CA, United States).

2.4 Image acquisition

Tissue sections were imaged with a Leica Stellaris 5 HyD S Confocal Microscope with a HC PL APO 40x/1,30 OIL CS2 lens (Leica, Wetzlar, Germany), using the laser lines 405 nm, 488 nm, 561 nm, and 638 nm and the following parameters: format 1024 × 1024, speed 600 Hz, zoom factor of 1, pinhole size 1.00 AU. Multi-tile images of the whole area of the sections combined with z-stacks (size 0.50 µm, 6-9 steps) were obtained.

2.5 Image analysis

Images were processed and analyzed using Fiji (Fiji is just ImageJ) software (Schindelin et al., 2012). Brightness and contrast were adjusted uniformly across all images. False colors were applied to each channel to optimize visual contrast and ensure the figures were color-blind safe. Nuclei are shown in blue and each nucleotidases is shown in the grey scale. *Krt5* expression (shown in green) was used to identify basal and intermediate urothelial cells and *Krt20* expression (shown in magenta) was used to identify umbrella cells, as these are well-established markers for these cell types (Colopy et al., 2014; Papafotiou et al., 2016), and were not subjected to further analysis. A grid that segmented the sagittal sections of proximal urethra and bladder in five columns was used to support analysis (Figure 1). The leftmost column (column one) refers to the proximal urethra/bladder neck region, column two contains the trigone region, whereas columns three to five include the body of the bladder (with the apex/dome situated in column five). This approach was chosen in order to identify possible regional differences/gradients from bladder neck to dome as demonstrated previously for bladder innervations (Pirker et al., 2005; Smith-Anttila et al., 2021). Two regions of interest of the detrusor (50 000 μm^2), lamina propria (25 000 μm^2), and urothelium (along a 250 µm straight line) per upper and bottom part of each column were selected for analysis (making for a total of 20 ROI per layer, per section). Each region of interest was only analyzed in one XY-plane. ACD guidelines for analysis of RNAscope data using Fiji/ImageJ were followed. Briefly, for each region of interest, the number of nuclei were counted by duplicating the original image, selecting the individual channel for DAPI, applying an appropriate threshold, and making the image binary, followed by analysis of the particles (size 4-infinite μm^2, circularity 0-infinite). The detected particles were compared to the original image and the number of nuclei was corrected based on visual inspection, if necessary. In cases where segregation of nuclei was not successfully achieved, to allow for the use of "Analyze particles", the multi-point tool was used to manually count each nucleus. Each dot referring to an ecto-nucleotidase RNA transcript was counted in a similar way, by applying the default 7–255 threshold with dark background, which we

10.3389/fphys.2023.1306500

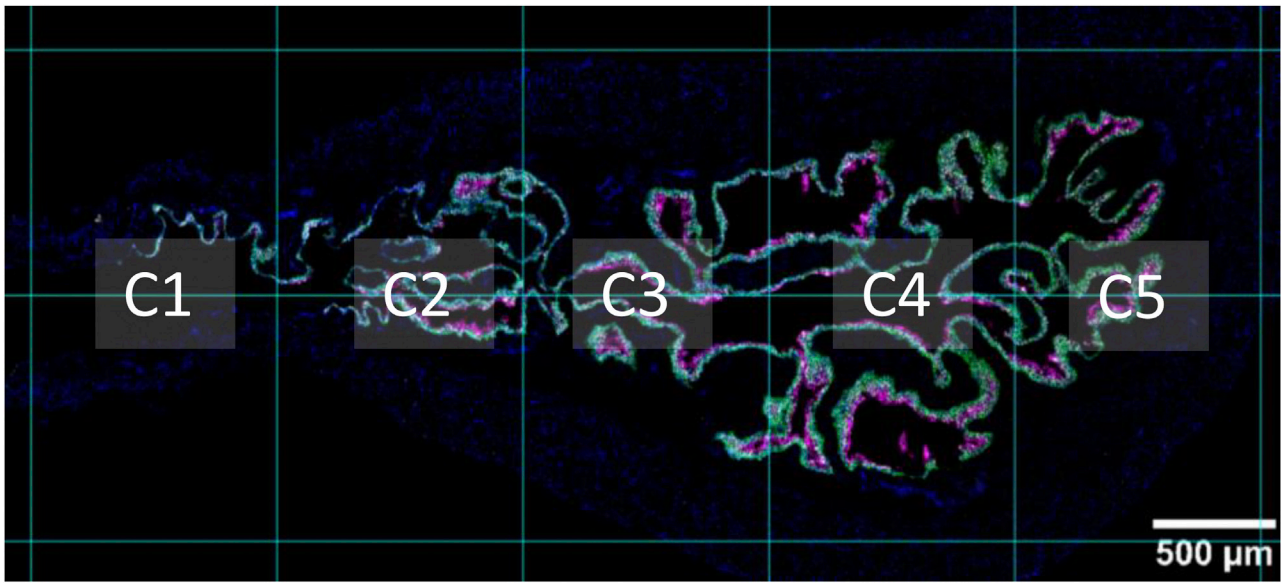

FIGURE 1
Sagittal view of proximal urethra and bladder. A supporting grid was used throughout analysis, which segmented the proximal urethra and bladder into five columns. Column one (C1) refers to the proximal urethra/neck region. Column two (C2) is the region that contains the trigone. Columns three to five include the bladder body. The apex of the bladder (bladder dome) can be seen in column five. Nuclei are shown in blue, *Krt5* expression is shown in green, and *Krt20* expression is shown in magenta.

selected based on acquisition parameters and negative and positive controls, and making the image binary, followed by analysis of the particles (size 0.4-infinite µm^2, circularity 0-infinite) in the region of interest. RNAscope signal is detected as punctate dots but clusters can result from overlapping signals from multiple mRNA molecules that are in close proximity to each other. The total probe count within each cluster was estimated by dividing the area of the cluster by a single probe area. Average number of dots/cell per layer was determined for each column. Results for columns 2–5 (excluding urethra) were averaged for each bladder section imaged (n = 3). Mean ± SD of dots/cell for each layer was plotted in graph bars. Additionally, results are reported as a score in accordance with the semi-quantitative scoring guideline provided by Advanced Cell Diagnostics (accessed at https://acdbio.com/dataanalysisguide) as follows: score 0: no staining or <1 dot/10 cells; score 1: 1-3 dots/cell; score 2: 4-9 dots/cell, no or very few dot clusters; score 3: 10–15 dots/cell and/or <10% of dots are in clusters; score 4: >15 dots/cell and/or >10% of dots are in clusters. Additionally, a score of 0.5 was used when the average number of dots was above 1 dot/10 cells but less than 0.5 dot/cell. The terms very low, low, medium, high, and very high expression used throughout the text refer to the scores of 0.5, 1, 2, 3, and 4, respectively.

3 Results

3.1 RNAscope™ sample validation

The RNAscope 3-plex negative control (Figures 2a, I, II), which targets the bacterial *dabB* gene (dihydrodipicolinate *B. subtilis* reductase) generated a score of 0, thus confirming the absence of background noise in the study conditions. The RNAscope 3-plex positive control (Figures 2b, III, IV), which targets the mouse house-keeping genes *Polr2A* (RNA polymerase II subunit A), *PPIB* (peptidylprolyl isomerase B), and *UBC* (Ubiquitin C) generated scores of 1-2 (low to medium expression), 2–3 (medium to high expression), and 4 (very high expression), respectively. These results confirmed the integrity of the tissue.

3.2 Entpd1

High to very high *Entpd1* mRNA expression (Figure 3) was detected in the detrusor of the bladder. *Entpd1* expression was medium to high in the lamina propria of the bladder. However, the expression was low in the neck and proximal urethra region for both detrusor and lamina propria. *Entpd1* was mostly absent in the urothelium, although it was observed in a very small population of basal cells, often in clusters.

3.3 Entpd2

Entpd2 mRNA transcripts (Figure 4) were found in all layers of the bladder, with similar levels of expression (~4 dots/cell on average). As an exception, umbrella cells exhibited a very high expression of *Entpd2* (21.60 ± 5.29 dots/cell). The density of distribution of *Entpd2* was not remarkably different from the neck to dome of the bladder.

3.4 Entpd3

Entpd3 mRNA (Figure 5) was very highly expressed in the urothelium of the bladder body and medium to highly expressed

10.3389/fphys.2023.1306500

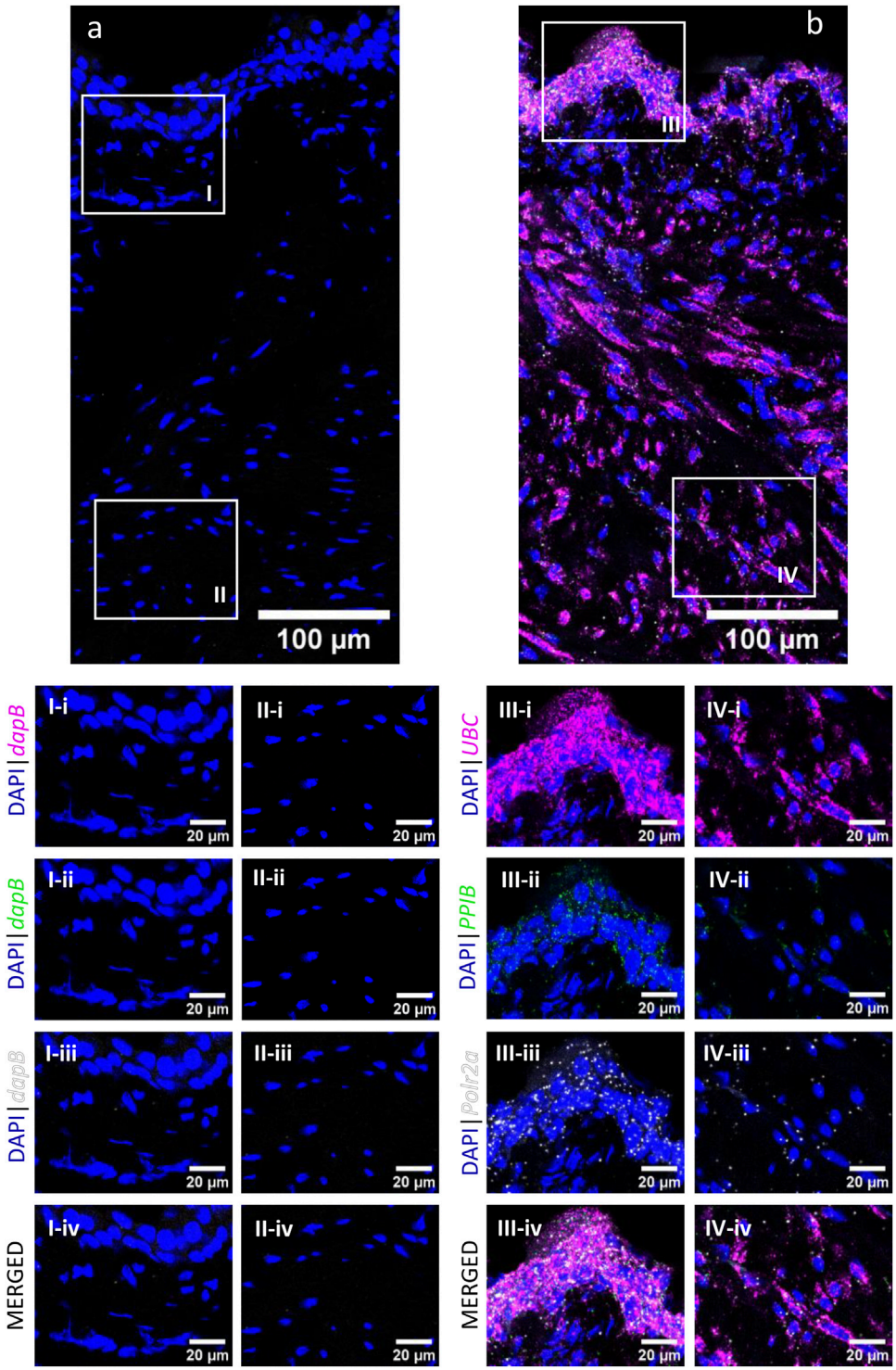

FIGURE 2
RNAscope 3-plex negative and positive controls in the murine urinary bladder. RNAscope 3-plex negative control, which targets the bacterial *dapB*, is shown in a representative cross-section of the bladder **(A)** and enlarged images of the mucosa **(I)** and detrusor **(II)**. RNAscope 3-plex positive control probes, which target murine *UBC* (magenta), *PPIB* (green) and *Polr2a* (grey) are depicted in a representative cross-section of the bladder **(B)** and enlarged images of the mucosa **(III)** and detrusor **(IV)**. Nuclear counterstaining with DAPI (blue) was applied.

in the urothelium of neck/proximal urethra region. The expression in umbrella cells was on average 48.15 ± 7.90 dots/cell. As the cell boundaries between basal and intermediate cells are not well defined, we did not differentiate between the two populations of cells in our measurements. However, we observed a clear trend of higher distributions of *Entpd3* dots in intermediate cells than basal cells. *Entpd3* was not found to be expressed in the detrusor nor in the lamina propria.

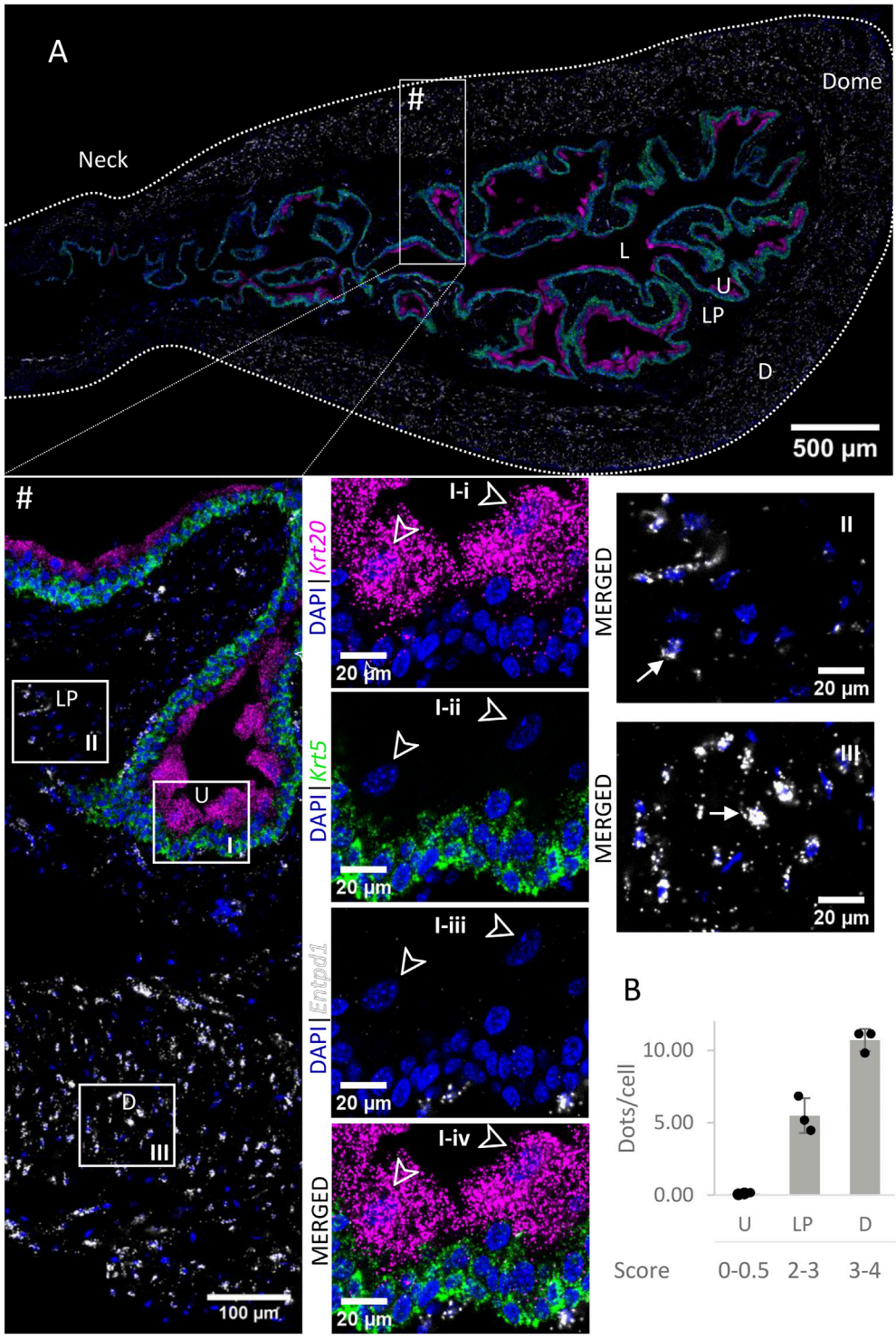

FIGURE 3
Spatial detection of *Entpd1* (grey scale), *Krt5* (green) and *Krt20* (magenta) mRNA transcripts in a cross-section of murine urinary bladder. Nuclear counterstaining with DAPI (blue) was applied. A high resolution large tiled image of the bladder cross-section **(A)** was obtained with a 4000× total magnification. L, bladder lumen; U, urothelium; LP, lamina propria; D, bladder detrusor. Enlarged images of all layers (#, flipped vertically), urothelium (U, **I**), lamina propria (LP, **II**) and detrusor muscle (D, **III**). *Krt5* mRNA detection was used to identify basal and intermediate urothelial cells, whereas very high detection of *Krt20* was used to identify umbrella cells (arrow heads, **I-i-iv**). *Entpd1* was predominantly detected in the lamina propria and detrusor (white arrows denote examples of *Entpd1* transcripts). Average dots/cell and score per layer **(B)** are shown for *Entpd1*.

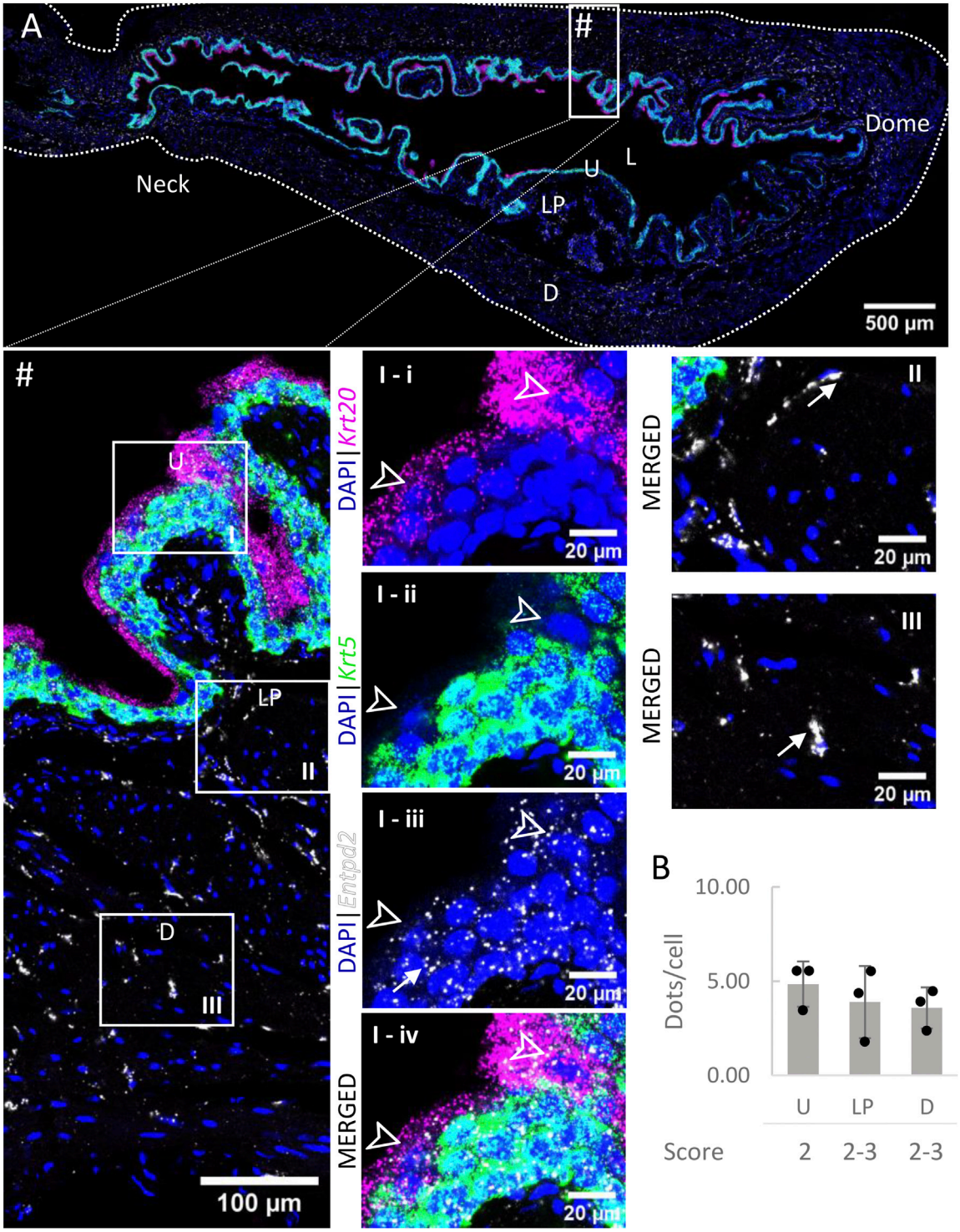

FIGURE 4
Spatial detection of *Entpd2* (grey scale), *Krt5* (green) and *Krt20* (magenta) mRNA transcripts in a cross-section of murine urinary bladder. Nuclear counterstaining with DAPI (blue) was applied. A high resolution large tiled image of the bladder cross-section **(A)** was obtained with a 4000× total magnification. L, bladder lumen; U, urothelium; LP, lamina propria; D, bladder detrusor. Enlarged images of all layers (#, flipped vertically), urothelium (U, **I**), lamina propria (LP, **II**) and detrusor muscle (D, **III**). *Krt5* mRNA detection was used to identify basal and intermediate urothelial cells, whereas very high detection of *Krt20* was used to identify umbrella cells (arrow heads, **I-i-iv**). *Entpd2* was detected in all layers, with medium expression. Average dots/cell and score per layer **(B)** are shown for *Entpd2*.

10.3389/fphys.2023.1306500

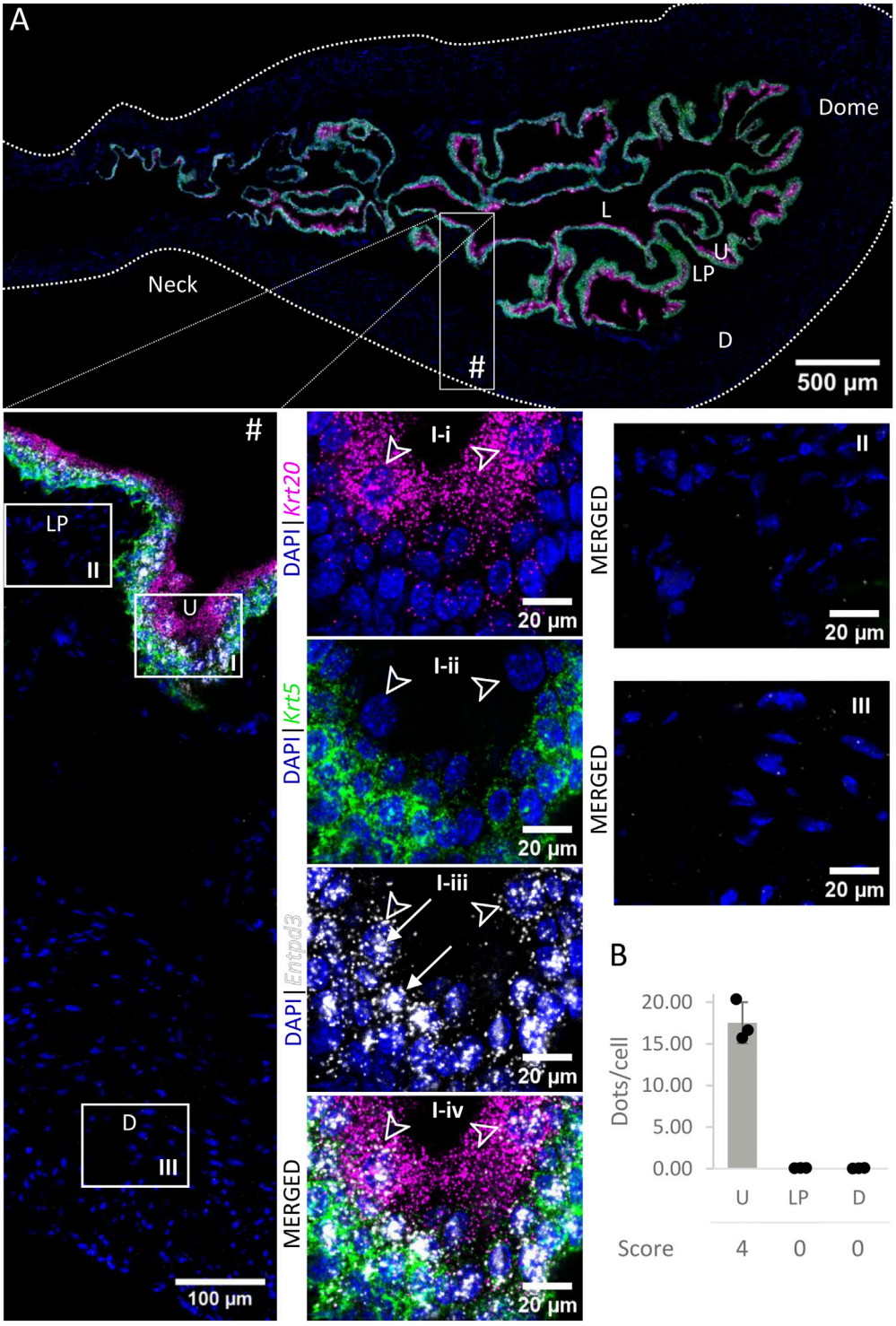

FIGURE 5
Spatial detection of *Entpd3* (grey scale), *Krt5* (green) and *Krt20* (magenta) mRNA transcripts in a cross-section of murine urinary bladder. Nuclear counterstaining with DAPI (blue) was applied. A high resolution large tiled image of the bladder cross-section **(A)** was obtained with a 4000× total magnification. L, bladder lumen; U, urothelium; LP, lamina propria; D, bladder detrusor. Enlarged images of all layers (#), urothelium (U, **I**), lamina propria (LP, **II**) and detrusor muscle (D, **III**). *Krt5* mRNA detection was used to identify basal and intermediate urothelial cells, whereas high detection of *Krt20* was used to identify umbrella cells (arrow heads, **I-i–iv**). *Entpd3* mRNA was found to be very highly expressed in urothelial cells (white arrows denote examples of *Entpd3* transcripts) but was absent in the detrusor and lamina propria. Average dots/cell and score per layer **(B)** are shown for *Entpd3*.

10.3389/fphys.2023.1306500

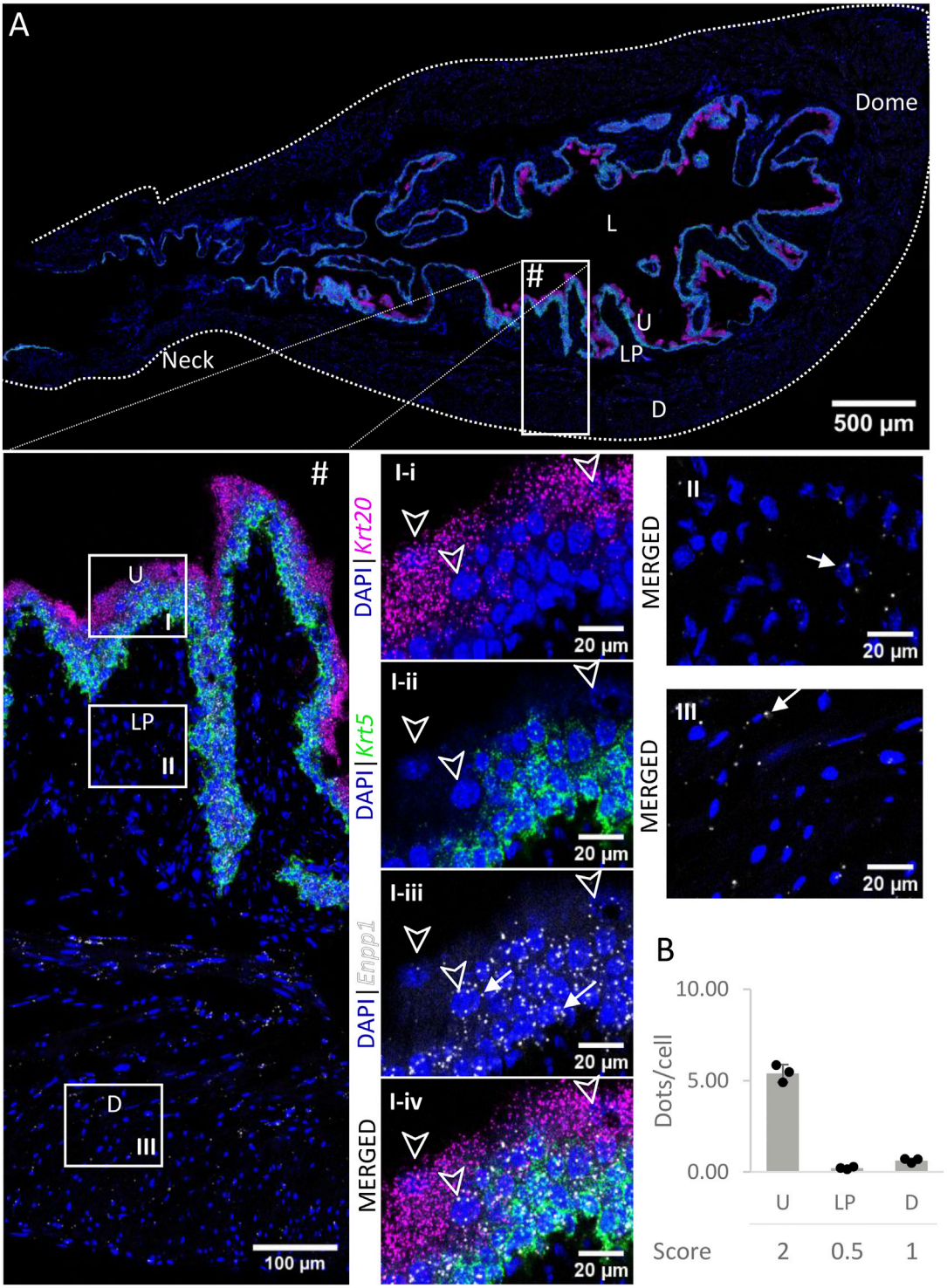

FIGURE 6
Spatial detection of *Enpp1* (grey scale), *Krt5* (green) and *Krt20* (magenta) mRNA transcripts in a cross-section of murine urinary bladder. Nuclear counterstaining with DAPI (blue) was applied. A high resolution large tiled image of the bladder cross-section **(A)** was obtained with a 4000× total magnification. L, bladder lumen; U, urothelium; LP, lamina propria; D, bladder detrusor. Enlarged images of all layers (#), urothelium (U, **I**), lamina propria (LP, **II**) and detrusor muscle (D, **III**). *Krt5* mRNA detection was used to identify basal and intermediate urothelial cells, whereas very high detection of *Krt20* was used to identify umbrella cells (arrow heads, **I-i-iv**). Urothelial cells exhibited a medium expression of *Enpp1* mRNA, whereas the lamina propria and detrusor showed a very low and low expression, respectively (white arrows denote examples of *Enpp1* transcripts). Average dots/cell and score per layer **(B)** are shown for *Enpp1*.

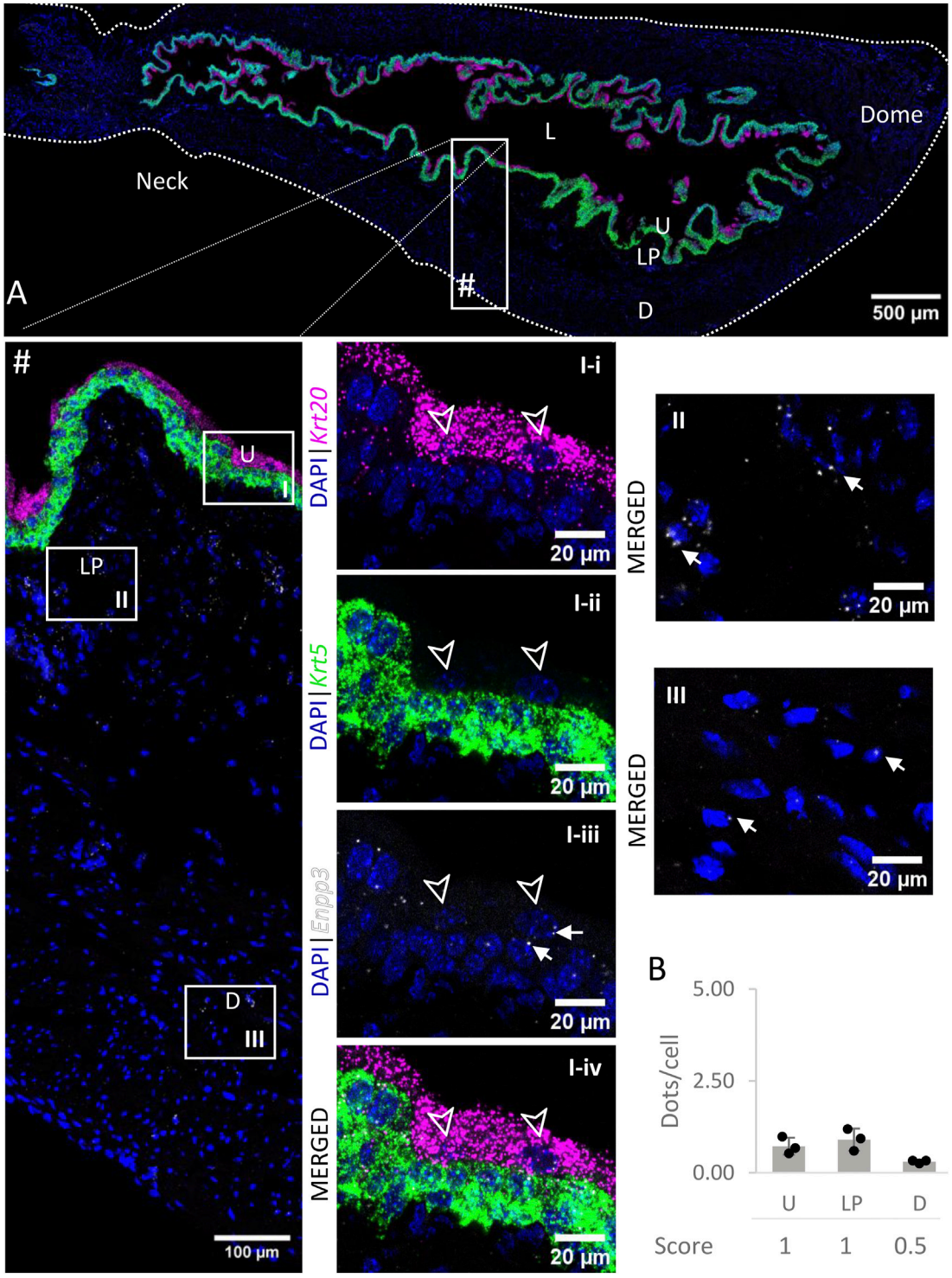

FIGURE 7
Spatial detection of *Enpp3* (grey scale), *Krt5* (green) and *Krt20* (magenta) mRNA transcripts in a cross-section of murine urinary bladder. Nuclear counterstaining with DAPI (blue) was applied. A high resolution large tiled image of the bladder cross-section **(A)** was obtained with a 4000× total magnification. L, bladder lumen; U, urothelium; LP, lamina propria; D, bladder detrusor. Enlarged images of all layers (#), urothelium (U, **I**), lamina propria (LP, **II**) and detrusor muscle (D, **III**). *Krt5* mRNA detection was used to identify basal and intermediate urothelial cells, whereas very high detection of *Krt20* was used to identify umbrella cells (arrow heads, **I-i-iv**). The urothelium and lamina propria exhibited a low expression of *Enpp3* mRNA, whereas the detection in the detrusor was very low (white arrows depict examples of *Enpp3* transcripts). Average dots/cell and score per layer **(B)** are shown for *Enpp3*.

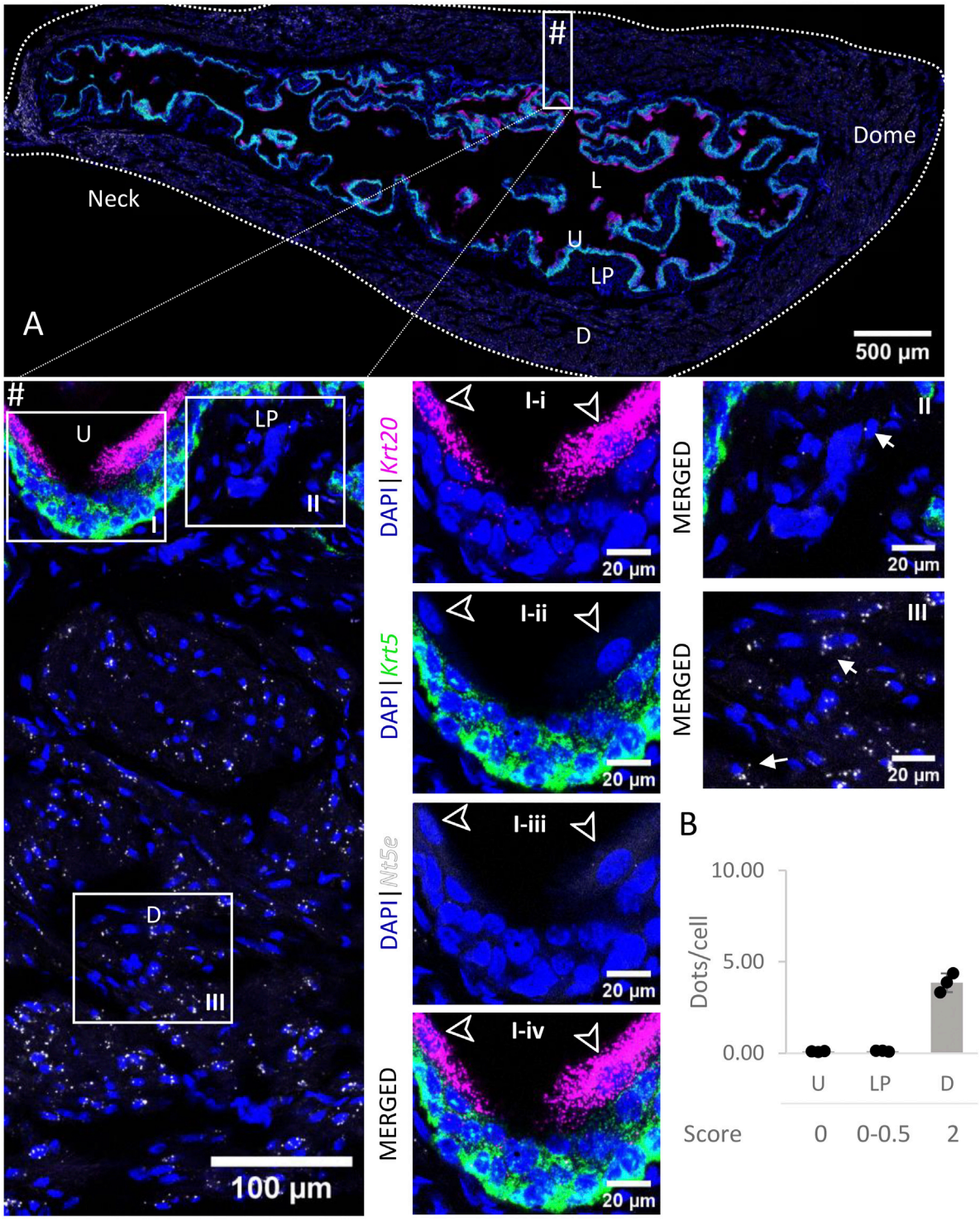

FIGURE 8
Spatial detection of *Nt5e* (grey scale), *Krt5* (green) and *Krt20* (magenta) mRNA transcripts in a cross-section of murine urinary bladder. Nuclear counterstaining with DAPI (blue) was applied. A high resolution large tiled image of the bladder cross-section **(A)** was obtained with a 4000× total magnification. L, bladder lumen; U, urothelium; LP, lamina propria; D, bladder detrusor. Enlarged images of all layers (#, flipped vertically), urothelium (U, **I**), lamina propria (LP, **II**) and detrusor muscle (D, **III**). *Krt5* mRNA detection was used to identify basal and intermediate urothelial cells, whereas very high detection of *Krt20* was used to identify umbrella cells (arrow heads, **I-i-iv**). *Nt5e* transcripts were mostly detected in the detrusor, with a medium level of expression. Average dots/cell and score per layer **(B)** are shown for *Nt5e*.

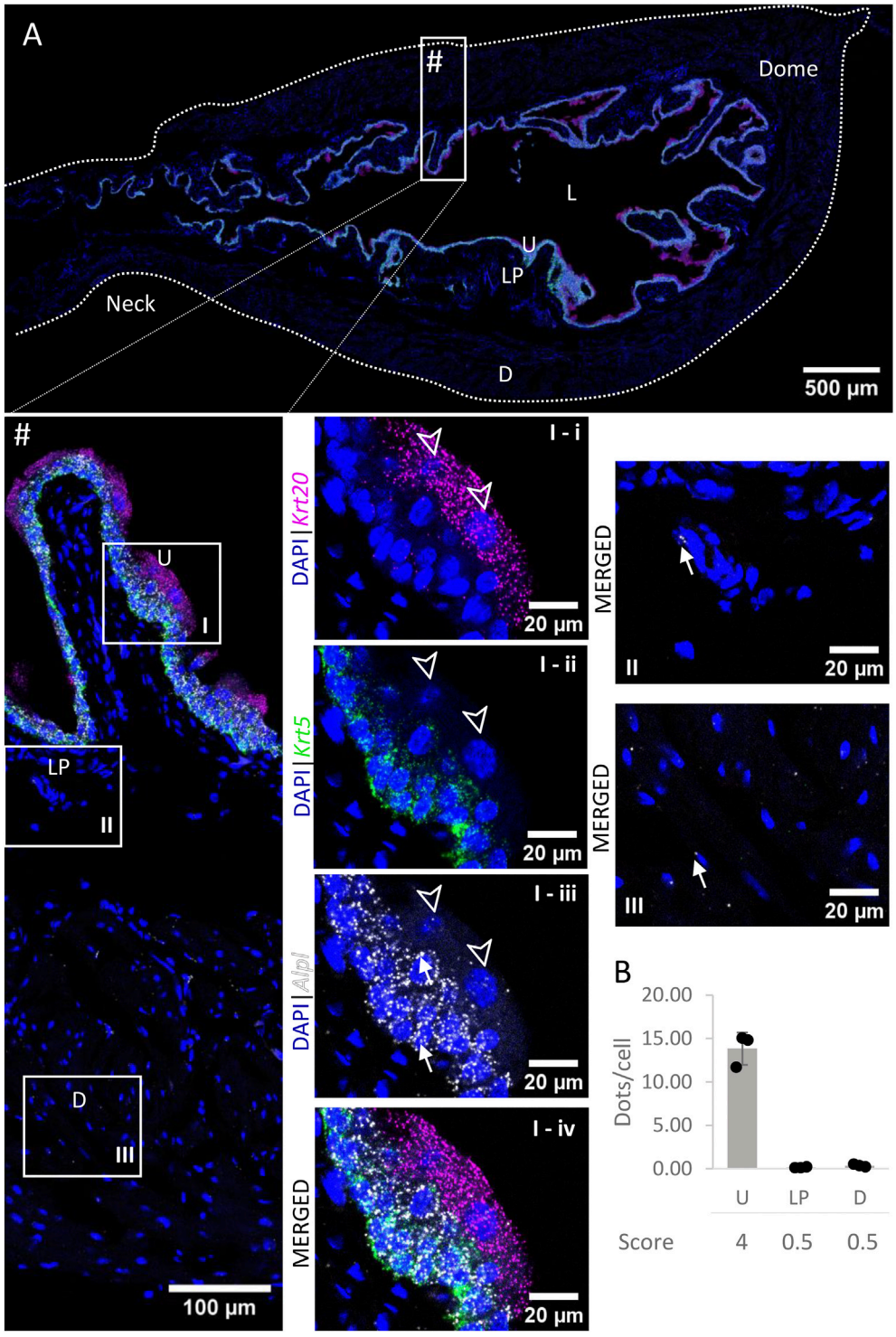

FIGURE 9
Spatial detection of *Alpl* (grey scale), *Krt5* (green) and *Krt20* (magenta) mRNA transcripts in a cross-section of murine urinary bladder. Nuclear counterstaining with DAPI (blue) was applied. A high resolution large tiled image of the bladder cross-section **(A)** was obtained with a 4000× total magnification. L, bladder lumen; U, urothelium; LP, lamina propria; D, bladder detrusor. Enlarged images of all layers (#, flipped vertically), urothelium (U, **I**), lamina propria (LP, **II**) and detrusor muscle (D, **III**). *Krt5* mRNA detection was used to identify basal and intermediate urothelial cells, whereas very high detection of *Krt20* was used to identify umbrella cells (arrow heads, I-i-iv). *Alpl* was predominantly detected in the urothelium (white arrows depict examples of *Alpl* transcripts). Average dots/cell and score per layer **(B)** are shown for *Alpl*.

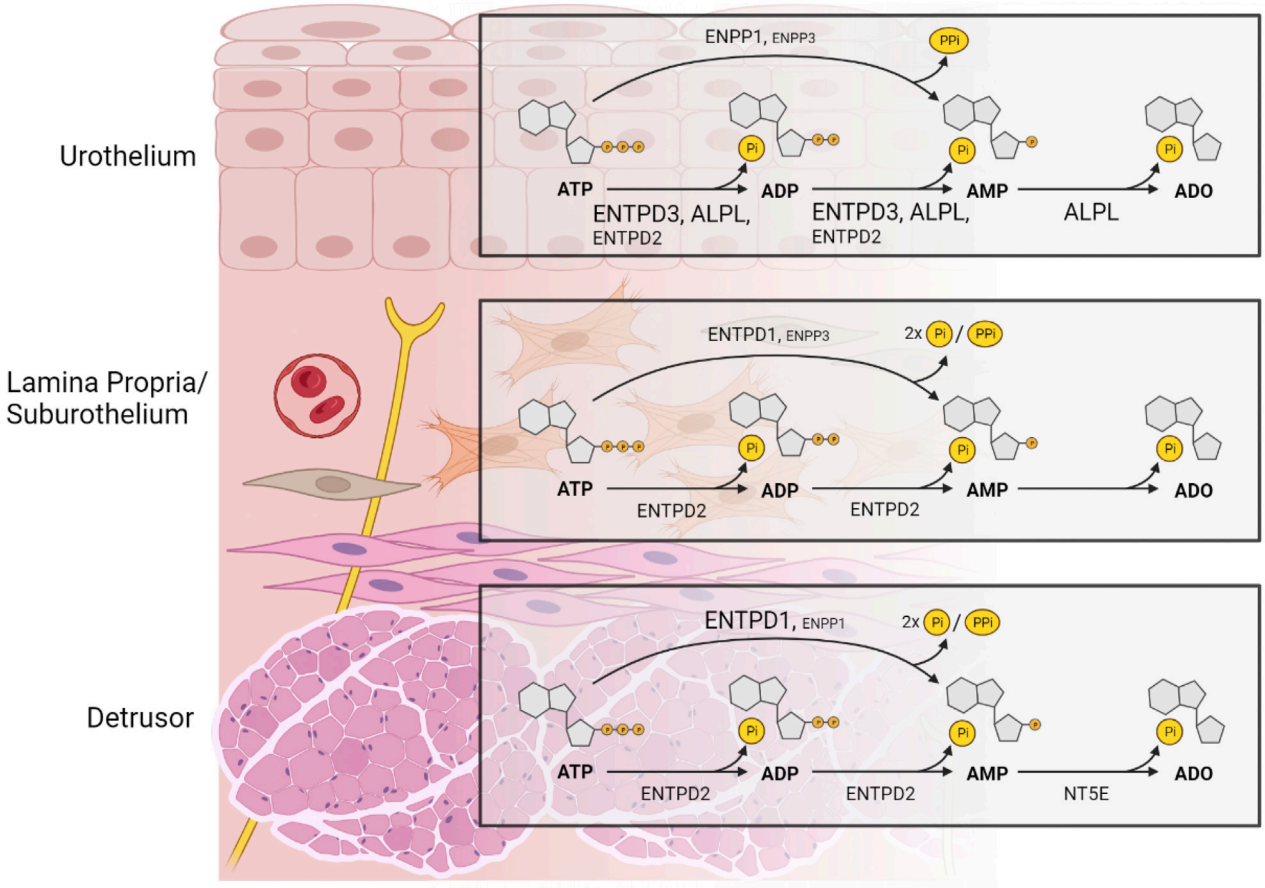

FIGURE 10
A model depicting the distribution of ectonucleotidases responsible for product formation with substrate ATP in key layers of the murine bladder wall that is based on the distribution of mRNA of selected ectonucleotidases. The size of the label indicates the relative expression of an ectonucleotidase. In the urothelium, ENTPD3 and ALPL and to a lesser degree ENTPD2 dephosphorylate sequentially ATP to ADP and AMP. ATP is also directly hydrolyzed to AMP and inorganic pyrophosphate (PPi) by ENPP1, and to a lesser degree by ENPP3 whereas production of ADO from AMP is exclusively mediated by ALPL. ENTPD1 and NT5E do not have a substantial role in adenine nucleotide and nucleoside formation in the urothelium. In the lamina propria/suburothelium, ENTPD1 catalyzes ATP to AMP and two phosphate groups (2xPi), with minimal accumulation of ADP, whereas ENTPD2 hydrolyzes sequentially ATP to ADP and AMP with sustained accumulation of ADP. AMP in the lamina propria can also, to a lesser extent, be formed directly from ATP by ENPP3. Lamina propria/suburothelium lacks enzymatic machinery to produce adenosine from extracellular adenine nucleotides. Therefore, presence of ADO in the suburothelium/lamina propria is likely a result of ADO release through nucleoside transporters. In addition, ADO might result from activity of soluble ectonucleotidases released into this space from adjacent layers. In the detrusor layer, ADP and AMP are produced by ENTPD2-mediated hydrolysis of ATP, whereas AMP is the main product of ENTPD1 catalysis and to a lesser degree of ENPP1. NT5E is the primary enzyme responsible for the formation of ADO from AMP in the detrusor muscle layer. The activation of specific purinergic receptors at precise loci within the bladder wall depends on the hydrolysis of extracellular purines mediated by multiple ectonucleotidases with various substrate specificity and product formation. The regulation of adenine nucleotides (purine) signaling in the bladder wall is remarkably complex. Created with https://BioRender.com.

3.5 *Enpp1*

Enpp1 mRNA (Figure 6) was detected in the urothelium with medium expression. Levels of expression were similar across the layers of the urothelium. Expression was very low in the lamina propria and low in the detrusor. There was no significant difference between the distribution in the urothelium of the neck, body or dome of the bladder.

3.6 *Enpp3*

The levels of expression of *Enpp3 mRNA* (Figure 7) were low in the urothelium and lamina propria, and very low in the detrusor across all regions.

3.7 *Nt5e*

Nt5e mRNA transcripts (Figure 8) were detected in the detrusor, with medium levels of expression whereas the urothelium and lamina propria exhibited very low to no expression of *Nt5e*. In each layer, the levels of expression were similar across all regions of the bladder.

3.8 *Alpl*

Very high levels of *Alpl* mRNA (Figure 9) were detected in the basal and intermediate urothelial cells, whereas umbrella cells exhibited a medium expression (5.53 ± 2.09 dots/cell) of this

gene. In contrast, expression levels were very low in the lamina propria and detrusor. There were no remarkable differences in levels of expression across the bladder regions.

4 Discussion

There are four main families of ectonucleotidases with different substrate affinity and specificity, namely ecto-nucleoside triphosphate diphosphohydrolases (ENTPDases; EC 3.6.1.5), ecto-nucleotide pyrophosphatase/phosphodiesterases (ENPPs; EC 3.6.1.9; EC 3.1.4.1), alkaline phosphatase/tissue-nonspecific isozyme (ALPL/TNAP; EC 3.1.3.1), and 5′-nucleotidase (NT5E/CD73; EC 3.1.3.5) (Zimmermann et al., 2012). ENTPDs differ significantly in product formation. This is of significant consequence for the regulation of nucleotide signaling. Thus, ENTPDs generally hydrolyze nucleoside triphosphate (e.g., ATP, UTP) and diphosphate (e.g., ADP, UDP), to generate nucleoside monophosphates as the final product (e.g., AMP, UMP). Among ENTPD1, ENTPD2, and ENTPD3, ENTPD1 has the highest affinity for ATP. ATP is hydrolyzed by ENTPD1 directly to AMP without significant amounts of ADP appearing as an intermediate (Heine et al., 1999; Kukulski et al., 2005). ENTPD2 and ENTPD3, on the other hand, hydrolyze ATP to ADP, which is released from the enzyme and further hydrolyzed to AMP. In the case of ENTPD2, considerable amounts of ADP accumulate before it is further hydrolyzed to AMP. ENPPs display broader substrate specificities, being able to hydrolyze nucleoside triphosphates and diphosphates as well as dinucleoside polyphosphates, ADP ribose, and nicotinamide adenine dinucleotide (NAD^+), and a variety of artificial substrates, but not AMP. Of ENPP1 and ENPP2, ENPP1 hydrolyzes ATP to a higher degree than ENPP3 (Zimmermann et al., 2012). NT5E is nucleotide-specific and is regarded as the major enzyme that dephosphorylates AMP to generate extracellular ADO (Zimmermann, 2020). ALPL metabolizes a broad spectrum of substrates including 5′-nucleotides (ATP, ADP, and AMP), monophosphates, and pyrophosphate (Zimmermann et al., 2012). Therefore, ALPL is capable of catabolizing completely ATP to ADO providing an alternative pathway to NT5E for production of ADO. In general, all ENTPDs are highly active at physiological pH; they also differ in the breadth of optimal pH (Zimmermann et al., 2012). Since substrate preferences and product formation differ for many ENTDs, tissue distribution and cellular localization of individual ENTDs may determine the response of target cells to extracellular purines.

Functions of ENTDs can result in achieving effective agonist concentrations at receptor sites, prevention of receptor desensitization, termination of receptor activation or receptor activation by biologically active metabolites (Zimmermann et al., 2012). Numerous purinergic receptors are expressed throughout the bladder wall and regulate bladder excitability (Burnstock, 2014). However, tissue distribution and cellular localization of ENTDs in the bladder wall is not well understood. We focused our study on the distribution and gene expression of *Entpd1, Entpd2, Entpd3, Enpp1, Enpp3, Nt5e*, and *Alpl*, as these are thought to be the most prevalent ectonucleotidases in the bladder, with recognized protein cell-surface expression and functions in this organ (Yu et al., 2011; Babou Kammoe et al., 2021; Aresta Branco et al., 2022; Gutierrez Cruz et al., 2022). We used RNAscope, a commercially available RNA *in situ* hybridization (ISH) technology that is highly specific, sensitive, fast, reproducible, and a solid alternative or complement to immunohistochemistry techniques (Erben and Buonanno, 2019). This assay allows for multiplex detection for up to four target genes at a single cell level, within the spatial and morphological tissue context. Briefly, RNAscope uses oligonucleotide RNA probes with a Z design, consisting of bases complementary to the target-RNA which are linked to a preamplifier binding region. The probes are hybridized in pairs to form a landing platform for the preamplifier which then binds to an array of identical amplifiers, providing multiple binding sites for label probes, thus greatly enhancing the signal-to-noise ratio (Wang et al., 2012). The number of dots quantitatively represent mRNA levels and these dots can be compared between different probes (Erben and Buonanno, 2019; Jolly et al., 2019; Caldwell et al., 2021).

We found that 1) the genes of all seven ectonucleotidases tested are expressed in the murine bladder wall; 2) the relative expression of individual ectonucleotidases differs between the principal layers of the bladder wall (i.e., detrusor, lamina propria, and urothelium); 3) there were no clear regional differences in the mRNA expression of ectonucleotidases with the exception of the neck region in which *Entpd1* and *Entpd3* showed lower expression in the detrusor and urothelium, respectively.

In this study, we show that *Entpd1* is the most expressed ectonucleotidase gene in the detrusor and lamina propria, with high to very high and medium to high mRNA expressions in the bladder body, respectively. These results together with an absence of signal in the urothelium are consistent with the distribution of ENTPD1 protein reported in two immunohistochemical studies in murine bladders (Yu et al., 2011; Babou Kammoe et al., 2021). ENTPD1 was also found to be the most expressed ectonucleotidase in the detrusor using RT-qPCR (Babou Kammoe et al., 2021) and in mucosa homogenates using automated capillary based immunodetection Wes technology (Aresta Branco et al., 2022). Furthermore, ENTPD1 was found in releasable/soluble form in concentrated extraluminal (i.e., from the lamina propria side) solutions (cELS) collected from distended detrusor-free bladder preparations (Aresta Branco et al., 2022), but not in intraluminal solutions (ILS) using the same model (Gutierrez Cruz et al., 2022). In the presence of membrane-bound ENTPD1, ATP is hydrolyzed almost directly to AMP (Robson et al., 2006). Therefore, ENTPD1 should terminate the activation of ADP-specific (e.g., P2Y1,12,13) receptors far more efficiently than the other ENTPDs. Functional studies have shown more potent muscle contractions evoked by nucleotides in detrusor strips from *Entpd1*$^{-/-}$ mice than wild-type mice (Babou Kammoe et al., 2021). Together, these findings suggest a critical role of ENTPD1 in terminating the actions of ATP (and ADP) in the lamina propria and detrusor layers. Interestingly, we observed that *Entpd1* expression was lower towards the bladder neck and proximal urethra, which might be an important regional difference in the regulation of smooth muscle tone. Regional differences have been described for the innervation of the bladder (Fowler et al., 2008). For example, a prominent suburothelial plexus of sensory nerves is described in the bladder base and neck, whereas such nerves are relatively sparse at the bladder dome (Gabella and Davis, 1998). Parasympathetic nerves that mediate contraction during micturition are dominant in the detrusor of the bladder body but sympathetic nerves that contribute to continence are widespread in the bladder

neck, but sparsely distributed in the muscle (Beckel and Holstege, 2011).Very little is known about regional differences in purinergic signaling in the bladder. Experiments in pigs and mini-pigs have suggested that purinergic innervation may play a role at the start of micturition by activation of P2X receptors and inducing the initial detrusor muscle contraction and at the same time relaxing the bladder neck via P2Y receptor stimulation to facilitate micturition (Hernández et al., 2009; Burnstock, 2014). It is possible that lower *Entpd1* expression is associated with higher preservation of ATP concentrations at P2Y purinergic receptors that mediate relaxation of the bladder neck and proximal urethra during micturition.

Here, we report that *Entpd2* mRNA transcripts are present in all layers, including urothelium, with identical levels of expression. In immunohistochemical studies it was suggested that ENTPD2 proteins are localized between smooth muscle bundles and in the lamina propria, but not in the urothelium (Yu et al., 2011; Babou Kammoe et al., 2021). However, ENTPD2 was found in low concentration in ILS of detrusor-free bladder preparations, which supports protein expression in the urothelium and regulated release into the lumen (Gutierrez Cruz et al., 2022). ENTPD2 was also found expressed in mucosa homogenates and cELS of detrusor-free bladder preparations using Wes (Aresta Branco et al., 2022). RT-qPCR performed in smooth muscle cells of the detrusor also confirmed *Entpd2* expression in this layer (Babou Kammoe et al., 2021). Additionally, pharmacological studies showed a stronger inhibition of ATP degradation in cELS and cILS by POM-1 (a polyoxometalate that inhibits ENTPD1, 2 and 3 (Müller et al., 2006)) more than ARL67156 (a competitive inhibitor of ENTPD1, ENTPD3, and ENPP1 (Lévesque et al., 2007)), which can in part be explained by differences in specificity towards ENTPD2 (Aresta Branco et al., 2022). ENTPD2 is expected to promote the activation of ADP specific receptors, because in the presence of ATP it produces a sustained accumulation of ADP (Kukulski et al., 2005; Zimmermann et al., 2012).

Entpd3 mRNA expression was restricted to the urothelium and was the most prevalent in this layer. Signal appeared to be greater in intermediate and umbrella cells than in basal urothelial cells. *Entpd3* expression in the urothelium was slightly lower in the bladder neck and proximal urethra than in the bladder body, which might be relevant in specialized regional regulation of purines. ENTPD3 immunolocalization has also been reported to be limited to the urothelium (Yu et al., 2011; Yu, 2015; Babou Kammoe et al., 2021), although signal distribution across the urothelial layers seems to differ slightly depending on the antibody used. In agreement with our results, ENTPD3 was the major soluble ectonucleotidase released into the bladder lumen of detrusor-free preparations at the end of bladder filling (Gutierrez Cruz et al., 2022). ENTPD3 was also detected using Wes in bladder mucosa preparations and was the second largest soluble ectonucleotidase released into the lamina propria space (Aresta Branco et al., 2022), which might have originated from regulated release by the basal urothelial layer. ENTPD3 shows substrate preference of ATP over ADP, and causes moderate accumulation of ADP in the presence of ATP. Therefore it is likely to lead to transient ADP accumulation and activation of ADP-specific receptors (Kukulski et al., 2005). Overall, these findings suggest that ENTPD3 is the major ATPase and ADPase produced in the urothelium, which not only contributes to urothelial hydrolysis of ATP to AMP but is also likely aiding the regulation of purines availability and subsequent activity in the lamina propria as a result of urothelial enzyme release.

ENPPs exhibit nucleotide pyrophosphatase and phosphodiesterase enzymatic activity to generate nucleoside 5′-monophosphates (Borza et al., 2022). To our knowledge the distribution of ENPP1 and ENPP3 in the bladder has not been described previously. In this study we report that *Enpp1* transcripts are mostly expressed in the urothelium, with similar levels of expression as *Entpd2*. In agreement with this result, we have previously shown that ENPP1 is the second most prevalent enzyme in the pool of soluble ectonucleotidases released into the bladder lumen (Gutierrez Cruz et al., 2022). ENPP1 has also been detected by PCR in porcine bladder (Petersen et al., 2007) and by Wes in the mucosa of murine bladder (Aresta Branco et al., 2022). ENPP1 displays a high catalytic efficiency in hydrolyzing ATP to AMP with formation of inorganic pyrophosphate (Borza et al., 2022). Therefore, ENPP1 is likely to play a role in hydrolysis of ATP to AMP in the urothelium and bladder lumen, without accumulation of ADP.

In situ hybridization also revealed low to very low levels of expression of *Enpp3* in the bladder. We previously reported low levels of ENPP3 protein expression in the murine bladder mucosa (Aresta Branco et al., 2022), as well as a low release of this enzyme into the lamina propria and luminal spaces. ENPP3 shows low specificity for the different nucleotides, presenting only a two-fold preference for ATP (Borza et al., 2022). It is possible that ENPP3 has only a minor role in bladder purinergic signaling.

Nt5e transcripts were found in the detrusor layer primarily. This is in agreement with immunohistochemical findings (Yu et al., 2011; Babou Kammoe et al., 2021) and RT-qPCR results showing that *Nt5e* was the second most expressed ectonucleotidase in the detrusor (Babou Kammoe et al., 2021). Therefore, NT5E is likely the major AMPase in the detrusor. *Nt5e* mRNA expression was difficult to resolve in the urothelium or LP in the present study. However, low levels of NT5E in the mucosa of the bladder, cELS and cILS of detrusor-free bladder preparations were detected previously using Wes methodology (Aresta Branco et al., 2022; Gutierrez Cruz et al., 2022). Remarkably, degradation of 1,N^6-etheno-AMP (eAMP, a highly fluorescent analog of AMP) to eADO was significantly hampered in ILS of *Nt5e*$^{-/-}$ preparations, when compared to wild-type (Aresta Branco et al., 2022). This suggests that even at low levels of expression, the catalytic activity of NT5E may be a determining factor of the AMP/ADO ratio in the bladder mucosa.

Expression of *Alpl* mRNA was higher in basal and intermediate urothelial cell than in umbrella cells, which was in agreement with immunohistochemical observations (Yu, 2015). However, this is in discrepancy with our Wes data that showed low expression of this enzyme in the bladder mucosa (Aresta Branco et al., 2022). It is possible that the antibody for ALPL/TNAP was not of sufficient quality to detect the enzyme accurately. ALPL/TNAP shows wide substrate specificity, thus it is able to sequentially hydrolyze ATP all the way to ADO (Zimmermann et al., 2012). Differential distribution of ALPL in the urothelium can help explain asymmetries in purine metabolism in the basal and apical layers of the urothelium.

In conclusion, this study highlights the differences in gene expression of the main ectonucleotidases in the murine bladder

and provides a rationale for regional and layer-specific asymmetries in the metabolism of purines and resultant function. Based on our results, a compartmentalized regulation of extracellular purine concentrations in the layers of the bladder wall should be expected (Figure 10). This provides a solid foundational work for future studies aimed at understanding a possible role of ectonucleotidases in bladder dysfunction.

Data availability statement

The raw data supporting the conclusion of this article will be made available by the authors, without undue reservation.

Ethics statement

The animal study was approved by the Institutional Animal Care and Use Committee, IACUC, University of Nevada Reno, Protocol #20-09-1077. The study was conducted in accordance with the local legislation and institutional requirements.

Author contributions

MA: Conceptualization, Data curation, Formal Analysis, Investigation, Methodology, Visualization, Writing–original draft. BP: Methodology, Supervision, Writing–review and editing. VM-Y: Conceptualization, Funding acquisition, Project administration, Resources, Supervision, Writing–review and editing.

Funding

The author(s) declare financial support was received for the research, authorship, and/or publication of this article. This research is funded by a R01 grant DK119482 from the National Institute of Diabetes and Digestive and Kidney Diseases awarded to the Principal Investigator VM-Y (corresponding author). The project described was also supported by a grant from the National Institute of General Medical Sciences (P20GM130459).

Acknowledgments

We would like to thank Nathan Grainger, Ph.D. for his assistance in using the Leica Stellaris 5 HyD S Confocal Microscope.

Conflict of interest

The authors declare that the research was conducted in the absence of any commercial or financial relationships that could be construed as a potential conflict of interest.

Publisher's note

References

Aresta Branco, M. S. L., Gutierrez Cruz, A., Dayton, J., Perrino, B. A., and Mutafova-Yambolieva, V. N. (2022). Mechanosensitive hydrolysis of ATP and ADP in lamina propria of the murine bladder by membrane-bound and soluble nucleotidases. *Front. Physiol.* 13, 918100. doi:10.3389/fphys.2022.918100

Babou Kammoe, R. B., Kauffenstein, G., Pelletier, J., Robaye, B., and Sévigny, J. (2021). NTPDase1 modulates smooth muscle contraction in mice bladder by regulating nucleotide receptor activation distinctly in male and female. *Biomolecules* 11, 147. doi:10.3390/biom11020147

Beckel, J. M., and Holstege, G. (2011). Neuroanatomy of the lower urinary tract. *Handb. Exp. Pharmacol.* 202, 99–116. doi:10.1007/978-3-642-16499-6_6

Borza, R., Salgado-Polo, F., Moolenaar, W. H., and Perrakis, A. (2022). Structure and function of the ecto-nucleotide pyrophosphatase/phosphodiesterase (ENPP) family: tidying up diversity. *J. Biol. Chem.* 298, 101526. doi:10.1016/j.jbc.2021.101526

Burnstock, G. (2014). Purinergic signalling in the urinary tract in health and disease. *Purinergic Signal* 10, 103–155. doi:10.1007/s11302-013-9395-y

Caldwell, C., Rottman, J. B., Paces, W., Bueche, E., Reitsma, S., Gibb, J., et al. (2021). Validation of a DKK1 RNAscope chromogenic *in situ* hybridization assay for gastric and gastroesophageal junction adenocarcinoma tumors. *Sci. Rep.* 11, 9920–10012. doi:10.1038/s41598-021-89060-3

Cheng, S., Scigalla, F. P., Speroni di Fenizio, P., Zhang, Z. G., Stolzenburg, J.-U., and Neuhaus, J. (2011). ATP enhances spontaneous calcium activity in cultured suburothelial myofibroblasts of the human bladder. *PLoS One* 6, e25769. doi:10.1371/journal.pone.0025769

Chess-Williams, R., Sellers, D. J., Brierley, S. M., Grundy, D., and Grundy, L. (2019). Purinergic receptor mediated calcium signalling in urothelial cells. *Sci. Rep.* 9, 16101. doi:10.1038/S41598-019-52531-9

Cockayne, D. A., Hamilton, S. G., Zhu, Q. M., Dunn, P. M., Zhong, Y., Novakovic, S., et al. (2000). Urinary bladder hyporeflexia and reduced pain-related behaviour in P2X3-deficient mice. *Nat* 407, 1011–1015. doi:10.1038/35039519

Colopy, S. A., Bjorling, D. E., Mulligan, W. A., and Bushman, W. (2014). A population of progenitor cells in the basal and intermediate layers of the murine bladder urothelium contributes to urothelial development and regeneration. *Dev. Dyn.* 243, 988–998. doi:10.1002/dvdy.24143

Durnin, L., Kwok, B., Kukadia, P., McAvera, R., Corrigan, R. D., Ward, S. M., et al. (2019). An *ex vivo* bladder model with detrusor smooth muscle removed to analyse biologically active mediators released from the suburothelium. *J. Physiol.* 597, 1467–1485. doi:10.1113/JP276924

Erben, L., and Buonanno, A. (2019). Detection and quantification of multiple RNA sequences using emerging ultrasensitive fluorescent *in situ* hybridization techniques. *Curr. Protoc. Neurosci.* 87, e63. doi:10.1002/CPNS.63

Ferguson, A. C., Sutton, B. W., Boone, T. B., Ford, A. P., and Munoz, A. (2015). Inhibition of urothelial P2X3 receptors prevents desensitization of purinergic detrusor contractions in the rat bladder. *BJU Int.* 116, 293–301. doi:10.1111/BJU.13003

Fowler, C. J., Griffiths, D., and de Groat, W. C. (2008). The neural control of micturition. *Nat. Rev. Neurosci.* 9, 453–466. doi:10.1038/nrn2401

Gabella, G., and Davis, C. (1998). Distribution of afferent axons in the bladder of rats. *J. Neurocytol.* 27, 141–155. doi:10.1023/A:1006903507321

Gutierrez Cruz, A., Aresta Branco, M. S. L., Perrino, B. A., Sanders, K. M., and Mutafova-Yambolieva, V. N. (2022). Urinary ATP levels are controlled by nucleotidases released from the urothelium in a regulated manner. *Metabolites* 13, 30. doi:10.3390/metabo13010030

Hao, Y., Wang, L., Chen, H., Hill, W. G., Robson, S. C., Zeidel, M. L., et al. (2019). Targetable purinergic receptors P2Y12 and A2b antagonistically regulate bladder function. *JCI Insight* 4, e122112. doi:10.1172/jci.insight.122112

Heine, P., Braun, N., Heilbronn, A., and Zimmermann, H. (1999). Functional characterization of rat ecto-ATPase and ecto-ATP diphosphohydrolase after heterologous expression in CHO cells. *Eur. J. Biochem.* 262, 102–107. doi:10.1046/j.1432-1327.1999.00347.x

Hernández, M., Knight, G. E., Wildman, S. S., and Burnstock, G. (2009). Role of ATP and related purines in inhibitory neurotransmission to the pig urinary bladder neck. *Br. J. Pharmacol.* 157, 1463–1473. doi:10.1111/j.1476-5381.2009.00314.x

Jolly, S., Lang, V., Koelzer, V. H., Sala Frigerio, C., Magno, L., Salinas, P. C., et al. (2019). Single-cell quantification of mRNA expression in the human brain. *Sci. Rep.* 9, 12353–12359. doi:10.1038/s41598-019-48787-w

Kaan, T. K. Y., Yip, P. K., Grist, J., Cefalu, J. S., Nunn, P. A., Ford, A. P. D. W., et al. (2010). Endogenous purinergic control of bladder activity via presynaptic P2X 3 and P2X 2/3 receptors in the spinal cord. *J. Neurosci.* 30, 4503–4507. doi:10.1523/JNEUROSCI.6132-09.2010

Kukulski, F., Lévesque, S. A., Lavoie, É. G., Lecka, J., Bigonnesse, F., Knowles, A. F., et al. (2005). Comparative hydrolysis of P2 receptor agonists by NTPDases 1, 2, 3 and 8. *Purinergic Signal* 1, 193–204. doi:10.1007/S11302-005-6217-X

Lévesque, S. A., Lavoie, É. G., Lecka, J., Bigonnesse, F., and Sévigny, J. (2007). Specificity of the ecto-ATPase inhibitor ARL 67156 on human and mouse ectonucleotidases. *Br. J. Pharmacol.* 152, 141–150. doi:10.1038/sj.bjp.0707361

Müller, C. E., Iqbal, J., Baqi, Y., Zimmermann, H., Röllich, A., and Stephan, H. (2006). Polyoxometalates—a new class of potent ecto-nucleoside triphosphate diphosphohydrolase (NTPDase) inhibitors. *Bioorg. Med. Chem. Lett.* 16, 5943–5947. doi:10.1016/j.bmcl.2006.09.003

Papafotiou, G., Paraskevopoulou, V., Vasilaki, E., Kanaki, Z., Paschalidis, N., and Klinakis, A. (2016). KRT14 marks a subpopulation of bladder basal cells with pivotal role in regeneration and tumorigenesis. *Nat. Commun.* 7, 11914–12011. doi:10.1038/ncomms11914

Petersen, C. B., Nygård, A.-B., Viuff, B., Fredholm, M., Aasted, B., and Salomonsen, J. (2007). Porcine ecto-nucleotide pyrophosphatase/phosphodiesterase 1 (NPP1/CD203a): cloning, transcription, expression, mapping, and identification of an NPP1/CD203a epitope for swine workshop cluster 9 (SWC9) monoclonal antibodies. *Dev. Comp. Immunol.* 31, 618–631. doi:10.1016/j.dci.2006.08.012

Pirker, M. E., Montedonico, S., Rolle, U., Austvoll, H., and Puri, P. (2005). Regional differences in nitrergic neuronal density in the developing porcine urinary bladder. *Pediatr. Surg. Int.* 21, 161–168. doi:10.1007/s00383-004-1313-5

Robson, S. C., Sévigny, J., and Zimmermann, H. (2006). The E-NTPDase family of ectonucleotidases: structure function relationships and pathophysiological significance. *Purinergic Signal* 2, 409–430. doi:10.1007/S11302-006-9003-5

Schindelin, J., Arganda-Carreras, I., Frise, E., Kaynig, V., Longair, M., Pietzsch, T., et al. (2012). Fiji: an open-source platform for biological-image analysis. *Nat. Methods* 97 (9), 676–682. doi:10.1038/nmeth.2019

Smith-Anttila, C. J. A., Morrison, V., and Keast, J. R. (2021). Spatiotemporal mapping of sensory and motor innervation of the embryonic and postnatal mouse urinary bladder. *Dev. Biol.* 476, 18–32. doi:10.1016/j.ydbio.2021.03.008

Vial, C., and Evans, R. J. (2000). P2X receptor expression in mouse urinary bladder and the requirement of P2X 1 receptors for functional P2X receptor responses in the mouse urinary bladder smooth muscle. *Br. J. Pharmacol.* 131, 1489–1495. doi:10.1038/sj.bjp.0703720

Wang, F., Flanagan, J., Su, N., Wang, L.-C., Bui, S., Nielson, A., et al. (2012). RNAscope: A novel in situ RNA analysis platform for formalin-fixed, paraffin-embedded tissues. *J. Mol. Diagnostics* 14, 22–29. doi:10.1016/j.jmoldx.2011.08.002

Wu, C., Sui, G. P., and Fry, C. H. (2004). Purinergic regulation of Guinea pig suburothelial myofibroblasts. *J. Physiol.* 559, 231–243. doi:10.1113/jphysiol.2004.067934

Yu, W. (2015). Polarized ATP distribution in urothelial mucosal and serosal space is differentially regulated by stretch and ectonucleotidases. *Am. J. Physiol. Physiol.* 309, F864–F872. doi:10.1152/ajprenal.00175.2015

Yu, W., Robson, S. C., and Hill, W. G. (2011). Expression and distribution of ectonucleotidases in mouse urinary bladder. *PLoS One* 6, e18704. doi:10.1371/journal.pone.0018704

Yu, W., Sun, X., Robson, S. C., and Hill, W. G. (2014). ADP-induced bladder contractility is mediated by P2Y 12 receptor and temporally regulated by ectonucleotidases and adenosine signaling. *FASEB J.* 28, 5288–5298. doi:10.1096/fj.14-255885

Zimmermann, H. (2020). Ectonucleoside triphosphate diphosphohydrolases and ecto-5′-nucleotidase in purinergic signaling: how the field developed and where we are now. *Purinergic Signal* 171 (17), 117–125. doi:10.1007/S11302-020-09755-6

Zimmermann, H., Zebisch, M., and Sträter, N. (2012). Cellular function and molecular structure of ecto-nucleotidases. *Purinergic Signal* 8, 437–502. doi:10.1007/s11302-012-9309-4

frontiers | Frontiers in Physiology

TYPE Original Research
PUBLISHED 08 December 2023
DOI 10.3389/fphys.2023.1308077

OPEN ACCESS

EDITED BY
Russ Chess-Williams,
Bond University, Australia

REVIEWED BY
Donna Jayne Sellers,
Bond University, Australia
Warren G. Hill,
Beth Israel Deaconess Medical Center and Harvard Medical School,
United States

*CORRESPONDENCE
Edson Antunes,
eantunes@unicamp.br,
edson.antunes@uol.com.br

RECEIVED 05 October 2023
ACCEPTED 27 November 2023
PUBLISHED 08 December 2023

CITATION
Oliveira AL, Medeiros ML, Gomes EdT, Mello GC, Costa SKP, Mónica FZ and Antunes E (2023), TRPA1 channel mediates methylglyoxal-induced mouse bladder dysfunction.
Front. Physiol. 14:1308077.
doi: 10.3389/fphys.2023.1308077

TRPA1 channel mediates methylglyoxal-induced mouse bladder dysfunction

Akila L. Oliveira[1], Matheus L. Medeiros[1], Erick de Toledo Gomes[1], Glaucia Coelho Mello[1], Soraia Katia Pereira Costa[2], Fabíola Z. Mónica[1] and Edson Antunes[1]*

[1]Department of Pharmacology, University of Campinas (UNICAMP), São Paulo, Brazil, [2]Department of Pharmacology, Institute of Biomedical Sciences, University of São Paulo (USP), São Paulo, Brazil

Introduction: The transient receptor potential ankyrin 1 channel (TRPA1) is expressed in urothelial cells and bladder nerve endings. Hyperglycemia in diabetic individuals induces accumulation of the highly reactive dicarbonyl compound methylglyoxal (MGO), which modulates TRPA1 activity. Long-term oral intake of MGO causes mouse bladder dysfunction. We hypothesized that TRPA1 takes part in the machinery that leads to MGO-induced bladder dysfunction. Therefore, we evaluated TRPA1 expression in the bladder and the effects of 1 h-intravesical infusion of the selective TRPA1 blocker HC-030031 (1 nmol/min) on MGO-induced cystometric alterations.

Methods: Five-week-old female C57BL/6 mice received 0.5% MGO in their drinking water for 12 weeks, whereas control mice received tap water alone.

Results: Compared to the control group, the protein levels and immunostaining for the MGO-derived hydroimidazolone isomer MG-H1 was increased in bladders of the MGO group, as observed in urothelium and detrusor smooth muscle. TRPA1 protein expression was significantly higher in bladder tissues of MGO compared to control group with TRPA1 immunostaining both lamina propria and urothelium, but not the detrusor smooth muscle. Void spot assays in conscious mice revealed an overactive bladder phenotype in MGO-treated mice characterized by increased number of voids and reduced volume per void. Filling cystometry in anaesthetized animals revealed an increased voiding frequency, reduced bladder capacity, and reduced voided volume in MGO compared to vehicle group, which were all reversed by HC-030031 infusion.

Conclusion: TRPA1 activation is implicated in MGO-induced mouse overactive bladder. TRPA1 blockers may be useful to treat diabetic bladder dysfunction in individuals with high MGO levels.

KEYWORDS

urothelium, lamina propria, cystometry, void spot assay, MG-H1, glyoxalase

Introduction

Diabetes Mellitus (DM) is a metabolic disease associated with high blood glucose levels and affects an increasing number of individuals worldwide (American Diabetes Association ADA, 2018). Life-threatening multi-organ complications associated with DM include cardiovascular diseases such as hypertension, stroke, and myocardial infarction, as well as conditions like retinopathy, peripheral neuropathy, and nephropathy (Wittig et al., 2019).

Besides, diabetic bladder dysfunction (DBD) or diabetic cystopathy is a prevalent urological complication that refers to a group of bladder symptoms mainly found in long-standing and poorly controlled diabetic patients (Golbidi and Laher, 2010). Clinical symptoms of DBD can range from bladder overactivity, which includes urinary urgency, urge urinary incontinence, frequency, and nocturia during the early stages of the disease, to impaired bladder contractility during the late stages (Daneshgari et al., 2017; Song et al., 2022).

Elevated glycemic levels in diabetic patients lead to the accumulation of highly reactive dicarbonyl compounds in both plasma and urine, such as methylglyoxal (MGO) (Harkin et al., 2023). MGO is formed endogenously from 3-carbon glycolytic intermediates of glycolysis, despite it can be also generated as a byproduct of protein, lipid, and ketones (Kalapos, 1999; Thornalley et al., 1999; Lai et al., 2022). Once generated, MGO initiates post-translational modification of peptides and proteins, ultimately resulting in the generation of advanced glycation end products (AGEs), such as the arginine-derived hydroimidazolone (MG-H1). These AGEs interact with the cell membrane-anchored ligand receptor RAGE, triggering multiple signaling pathways that lead to production of inflammatory and pro-oxidant mediators (Schalkwijk and Stehouwer, 2020; Zhang et al., 2023). The enzymatic detoxification systems glyoxalase 1 (Glo1) and glyoxalase 2 (Glo2) play a pivotal role in converting MGO into its end-product, D-lactate (Rabbani and Thronalley, 2019). Recent studies revealed that supplementing the drinking water of both non-diabetic male and non-diabetic female mice with MGO for 4–12 weeks results in an overactive bladder phenotype, as assessed by voiding behavior and cystometric assays in awake and anesthetized animals, as well as by *in vitro* bladder contractility to electrical-field stimulation (EFS) and muscarinic receptor activation with carbachol (de Oliveira et al., 2020; Oliveira et al., 2021; Oliveira et al., 2022). Furthermore, diabetic obese ob/ob mice displaying high levels of MG-H1 and RAGE in bladder tissues also exhibit voiding dysfunction, suggesting that activation of the MGO-AGEs-RAGE pathway in the bladder wall contributes to the pathogenesis of diabetes-associated bladder dysfunction (Oliveira et al., 2023).

TRPA1 is embedded in the cell membrane and presents itself as a tetrameric form of a Ca^{2+} influx channel (Brauchi and Rothberg, 2020). Consequently, upon TRPA1 activation, the influx of Ca^{2+}, along with other extracellular cations such as Na^{+} and H^{+}, plays a pivotal role in triggering noxious responses, mostly associated with pain, cold, and itch (Gao et al., 2020). A large array of endogenously released chemical mediators, including nitric oxide, hydrogen sulfide, hydrogen peroxide, prostaglandin J, among others, as well as exogenous stimuli like cinnamaldehyde, allicin, allyl isothiocyanate, ligustilide, and acrolein can modulate the activity of TRPA1 channels (Gao et al., 2020). Additionally, MGO has been shown to activate the TRPA1 channel, particularly in diabetic neuropathic pain conditions (Ohkawara et al., 2012; Andersson et al., 2013; Huang et al., 2016; Griggs et al., 2017; Becker et al., 2023). The TRPA1 channel is expressed in the lower urinary tract, including nerve endings of the bladder wall (Andrade et al., 2011; Steiner et al., 2018; Andersson, 2019; de Oliveira et al., 2020; Kudsi et al., 2022; Zhao et al., 2022; Hayashi et al., 2023), and is believed to mediate bladder sensory transduction and contractility in diabetes (Philyppov et al., 2016; Blaha et al., 2019; Vanneste et al., 2021). TRPA1 mRNA expression has been detected in the bladder mucosa and bladder muscular layer, with upregulation seen in tissues obtained from patients with bladder outlet obstruction (Du et al., 2008). Given the implication of the TRPA1 channel in diabetes-related complications, we hypothesized that the TRPA1 channel plays an important role in the pathophysiology of urinary bladder dysfunction induced by chronic MGO intake. Therefore, the main objectives of this study were to identify alterations in TRPA1 expression in the bladder wall (mucosa and detrusor smooth muscle), and to evaluate the effects of the TRPA1 antagonist HC-030031 (Eid et al., 2008) on the *in vivo* and *in vitro* bladder dysfunction resulting from a 12-week treatment with MGO in female mice.

Materials and methods

Animals

Five-week-old female C57BL/6 mice weighing 19 ± 0.30 g at the beginning of the study were provided by Multidisciplinary Center for Biological Research on Laboratory Animal Science (CEMIB) of the State University of Campinas (UNICAMP, Sao Paulo, Brazil). Mice were housed in cages made of polypropylene with dimensions 30 × 20 × 13 cm placed in ventilated cage shelters with a constant humidity of 55% ± 5% and temperature of 24°C ± 1°C under a 12 h light-dark cycle. The animals (three mice per cage) were acclimated for 10 days before starting the treatments. Animals received standard food and filtered water *ad libitum*. Animal procedures and experimental protocols were approved by Ethics Committee in Animal Use of UNICAMP (CEUA-UNICAMP; protocol numbers 5443-1/2019 and 5842-1/2021). Animal studies follow the ARRIVE guidelines.

Experimental design

We initially employed a randomization calculator, which is available at https://www.graphpad.com to allocate the mice into two groups, namely, Control group (n = 51) and MGO group (n = 51). In the MGO group, the animals received 0.5% MGO (Sigma Aldrich, Missouri, United States) in their drinking water for a duration of 12 weeks, as outlined in our previous study (Medeiros et al. 2021). The control group received only tap water. In the first part of this study, animals in the MGO group exhibiting voiding dysfunction through the void spot assay in filter paper were anesthetized using isoflurane and subsequently euthanized by cervical dislocation. Their bladders were then exposed and removed for the subsequent immunohistochemical and Western blotting assays, as described below. The same procedure was carried out in the control group. In the second phase of this study, filling cytometry in anesthetized animals and *in vitro* bladder contractility were selected to test the TRPA1 blocker HC-030031 in both control and MGO groups. The HC-030031 dose was set at 1 nmol/min for the 1-h intravesical infusion during cystometry or 10 μM for the *in vitro* assays.

Void spot assay in filter paper

The objective of this test was to analyze the voiding behavior of animals that had been chronically administered MGO for 12 weeks.

The analyzed parameters included the total void volume (the overall volume voided in 3 h), volume per void (average volume per void), and the total number of voids. Additionally, the number of voids was categorized based on volumes lower than 25 µL, volumes between 25 and 100 µL, and volumes higher than 100 µL. We also registered the distribution of voids in the center and corner of the filter paper to observe changes in spot distribution and normal micturition behavior, which involves animals seeking the corners of the cage, a phenomenon known as thigmotaxis (Hill et al., 2018). As such, the animals were individually housed in clean cages, each covered with a filter paper measuring 25 × 15 cm (qualitative filter paper 250 g Unifil®, Cod. 502.1250). Animals had no access to water but were provided with unrestricted access to food. The experiment was consistently conducted during a specific time window (9–10 a.m. to 12–13 p.m.), lasting for a duration of 3 h within the cages. The temperature of the room was maintained at 24 ± 1°C with a humidity level of 53% ± 1%. The animals were acclimated to the filter paper for 2 days, and void measurements were performed on the third day. At the conclusion of the assay, the animals were returned to their regular housing condition. Following the test, the voiding points were encircled with a pencil, and overlapping points were marked for subsequent quantification. The filter papers were dried and imaged using UV light (Photo-documenter Chemi-Doc, Bio-Rad, California, United States). The filter papers were then analyzed using the Fiji version of ImageJ Software (version 1.46r) (http://fiji.sc/wiki/index.php/Fiji), as previously described (Oliveira et al., 2021). Particles smaller than 0.20 cm^2 (equivalent to 2 µL) were disregarded from consideration to minimize potential interference related to the paws or tail marks of the animals.

Filling cystometry in anesthetized mice and TRPA1 antagonism with HC-030031

Filling cystometry was conducted following the method outlined as previously described (Oliveira et al., 2021). The animals were anesthetized using a rodent inhalation anesthesia system (Harvard Apparatus) and were maintained under anesthesia with a mixture of 2% isoflurane and 98% oxygen at a rate of 2 L/min. An abdominal incision was made to expose the urinary bladder. A PE10 catheter was carefully inserted into the apex of the bladder and fixed in place using a 6-0 nylon suture. Subsequently, the bladder was repositioned, and the surrounding musculature and skin were sutured closed. Following the completion of this surgical procedure, isoflurane anesthesia was discontinued, and an intraperitoneal injection of urethane (1.2 g/kg) was administered. The cannula was then connected to a 3-way tap, with one port linked to an infusion pump via a PE-10 catheter. Before initiating cystometry, a 10-min stabilization period was observed, after which continuous intravesical saline infusion was maintained at a rate of 0.6 mL/h for 1 h. Subsequently, the animals underwent continuous intravesical infusion for 1 h with either saline (0.01 mL/min), vehicle (0.001% DMSO) or the selective TRPA1 channel blocker HC-030031 (1 nmol/min; Catalogue No. H4415, Sigma-Aldrich, United States). Data acquisition was carried out using PowerLab system, and subsequent analyzes were performed using LabChart® Software (ADInstruments Inc., Sydney, AU, https://www.adinstruments.com/products/labchart). The following parameters were assessed during the first hour of data acquisition: voiding frequency (number of voids/minute), bladder capacity (functional bladder capacity, which represents the volume infused during the intermicturition interval), voided volume (volume released during a voiding event), compliance (the ratio between capacity and threshold pressure, expressed in µl/mmHg), basal pressure (the minimum pressure observed between two voiding events), threshold pressure (the intravesical pressure immediately before voiding events), and maximum pressure (the highest bladder pressure recorded during a void). All the parameters were evaluated across all micturition cycles during the first hour of data acquisition. At the conclusion of the experimental protocols, the animals were euthanized and disposed of accordingly.

Exploring the effects of HC-030031 on the bladder contractions induced by electrical-field stimulation (EFS) and carbachol

At the conclusion of the 12-week MGO treatment, the animals were anesthetized with isoflurane, administered at a concentration exceeding 5%. Subsequently, cervical dislocation was performed to confirm euthanasia. The bladder was then removed and carefully divided into two strips, each representing an intact portion of the bladder. Strips were mounted in 10-mL organ baths containing Krebs-Henseleit solution, composed of the following constituents: 117 mM NaCl, 4.7 mM KCl, 2.5 mM $CaCl_2$, 1.2 mM $MgSO_4$, 1.2 mMKH_2PO_4, 25 mM $NaHCO_3$ and 11 mM Glucose, pH 7.4. The solution was continuously oxygenated with a mixture of 95% O_2 and 5% CO_2. The tissues were allowed to equilibrate for 45 min under resting tension and were subsequently adjusted to a force of 5 mN. Changes in isometric force were recorded using a PowerLab system (ADInstruments Inc., Sydney, AU). After the stabilization period, one strip was incubated with the vehicle (0.001% DMSO) while the other was exposed to the selective TRPA1 antagonist HC-030031 (10 µM) for a duration of 30 min. Following the incubation period, EFS was applied using platinum ring electrodes placed between two strips, and connected to a stimulator (Grass Technologies, RI, United States). EFS was conducted at 80 V, with a pulse width of 1 ms pulse width, and trains of stimuli lasting 10 s were administered at varying frequencies ranging from 1 to 32 Hz, with 2-min intervals between each stimulation. Subsequently, cumulative concentration-response curves were generated for the muscarinic receptor agonist carbachol ranging from 1 nM to 100 µM (Sigma Aldrich, MI, United States). Non-linear regression analysis to determine the potency (pEC_{50}) of carbachol was carried out using GraphPad Prism (GraphPad Software, Inc., CA, United States) with the constraint that F = 0. The concentration-response data were fitted to a logarithmic dose-response function with a variable slope in the form: E = Emax/([1 + (10c/10x) n] + F), where E is the effect of above basal, E_{max} is the maximum response produced by agonists; c is the logarithm of the pEC_{50}, the concentration of drug that produces a half maximal response; x is the logarithm of the concentration of the drug; the exponential term, n, is a curve-fitting parameter that defines the slope of the concentration–response line, and F is the response observed in the absence of added drug. The contractile responses to EFS or carbachol were expressed as mN/mg.

Immunohistochemistry for MG-H1 in bladder tissues

Bladder immunoperoxidase reactions were processed based on a previous study (Oliveira et al., 2022). Briefly, whole bladders were removed, immersed in 10% formalin fixative solution for 48 h, and embedded in paraffin. Five-micron sections were mounted onto aminopropyltriethoxysilane-coated glass slides. Sections were deparaffinized, rehydrated, and washed with 0.05 M Tris buffer solution (TBS) at pH 7.4. Subsequently, for antigen retrieval, sections were treated with 0.01 M citrate buffer containing 0.05% Tween-20 (pH 6.0) for 40 min at 98°C. Endogenous peroxidase activity was inhibited with 0.3% hydrogen peroxide (H_2O_2) solution. For blocking the non-specific sites, a 5% bovine serum albumin (BSA) solution containing 0.1% Tween-20 for 60 min was used. Sections were incubated with mouse monoclonal anti-MG-H1 primary antibody (1:90; Cell Biolabs, INC., Catalogue No. STA-011, San Diego, United States) diluted in TBS containing 3% BSA overnight at 4°C. Subsequently, sections were washed, and incubated with biotinylated goat anti-mouse IgG, avidin and biotinylated HRP (1:20; Catalogue No. EXTRA2, Sigma Aldrich, St Louis, MO, United States) following the manufacturer's instructions. For detection of the immunostained area with MG-H1, a 3.3′diaminobenzidine solution (DAB; Catalogue No. D4293, Sigma Aldrich) was employed. As a negative control, a section was used in parallel to primary antibody omission. All slides were counterstained with hematoxylin and mounted for observation by microscopy. Representative images were acquired using a light microscope (OPTIKA ITALY B-1000 Series, OPTIKA S.r.l., Ponteranica, BG, Italy) equipped with a digital camera under a 4 × and 10 × objective.

Immunohistochemistry for TRPA1 in bladder tissues

For immunohistochemistry of TRPA1, we followed the manufacturer's instructions. The sections were deparaffinized, rehydrated, and washed with 1× phosphate buffered saline containing 0.1% Tween-20 (PBS-T). For antigen retrieval, the slides were boiled in 0.01 M sodium citrate buffer (pH 6.0) for 10 min, then cooled on bench top for 30 min. The sections were washed in distilled H_2O (dH_2O) three times for 5 min each, followed by a washing section 1 × PBS-T for 5 min. Endogenous peroxidase activity was inhibited with a 0.3% H_2O_2 solution. Each section with blocking solution (5% BSA) was blocked in 1× PBS-T solution for 1 h at room temperature. The blocking solution was then removed, and the primary antibody was diluted in 1× PBS-T with 5% BSA and added to each section and incubated overnight at 4°C with TRPA1 antibody (1:60; Catalogue No. 40763, Novus Biologicals, LLC, United States). The antibody solution was removed by washing 1 × PBS-T; and biotinylated secondary antibody diluted in 1 × PBS-T with 5% BSA was incubated for 30 min at room temperature (1:20; Catalogue No. EXTRA2, Sigma Aldrich, St Louis, MO, United States). The secondary antibody was removed by washing 1 × PBS-T and 100 µL streptavidin HRP reagent (1:20) was incubated for 30 min at room temperature in each section. For detection of the immunostained area with TRPA1, a 3.3′diaminobenzidine solution (DAB; Catalogue No. D4293, Sigma Aldrich) was employed, and sections were immersed in dH_20. The sections were counterstained in hematoxylin and mounted for observation by microscopy. Representative images were acquired using a light microscope (OPTIKA ITALY B-1000 Series, OPTIKA S.r.l., Ponteranica, BG, Italy) equipped with a digital camera under a 40 × objective.

Western blot analysis of MG-H1, Glo1 and TRPA1 in bladder tissues

Total protein extracts were obtained from homogenized bladders using RIPA buffer (Catalogue No. R0278, Sigma-Aldrich, Darmstadt, Germany) containing protease inhibition cocktail (10 µL/mL; Catalogue No. P8340, Sigma-Aldrich, Darmstadt, Germany). The samples were incubated for 1 h at 4°C and then centrifuged at 12.000 g for 15 min at 4°C. Protein concentrations in the supernatants were determined using the DC Protein Assay Kit I (Catalogue No. 5000111EDU, BioRad, Hercules, CA, United States). An equal amount of protein (30 µg) from each sample was treated with 4× Laemmli buffer containing 355 mM of 2-mercaptoethanol (Catalogue No. 161-0747, BioRad, Hercules, CA, United States). The samples were heated in boiling water bath for 5 min and resolved by sodium dodecyl sulfate-polyacrylamide gel electrophoresis (SDS-PAGE). The proteins were then electrotransferred to a nitrocellulose membrane at 20 V for 20 min using a semi-dry device (Bio-Rad, Hercules, CA, United States). To reduce nonspecific protein binding, the membrane was pre-incubated overnight at 4°C in blocking buffer (0.5% non-fat dried milk, 10 mM Tris, 100 mM NaCl, and 0.02% Tween 20). Primary antibodies for mouse monoclonal MG-H1 (1:1000; Cell Biolabs, INC., Cat. No STA-011, San Diego, United States), Glo1 (Cat. No. ab96032, Abcam), TRPA1 (cat. No. 40763, Novus Biologicals, LLC, United States) and monoclonal β-actin peroxidase (1:50000, Catalogue No. A3854, Sigma-Aldrich, Darmstadt, Germany) were diluted in basal solution containing 3% BSA. These primary antibodies were validated and tested according to previous studies (Lee et al., 2016; Jandova and Wondrak, 2021; Smith et al., 2022; Chandrakumar et al., 2023; Luostarinen et al., 2023). The antibody was incubated overnight at 4°C, while the β-actin antibody was incubated for 1 h at room temperature. Subsequently, the membranes were incubated with the secondary antibody HRP-linked anti-rabbit IgG (1:5000; Catalogue No. 7074S, Cell Signaling Technology, Massachusetts, United States) diluted in basal solution for 1 h. Immunoreactive bands were detected using the Clarity Western ECL Substrate (Catalogue No. 1705061, BioRad, Hercules, CA, United States), an enhanced BioRad chemiluminescence system. Densitometry analysis was performed using the Image Lab Software Version 6.1 (BioRad, Hercules, CA, United States). The results were represented as the ratio of protein expression relative to β-actin.

Assessment of Glo 1 activity in bladder tissues

The bladders were isolated, homogenized in 350 µL of PBS (pH 7.0), and then centrifuged at 2000 × g for 30 min at 4°C.

10.3389/fphys.2023.1308077

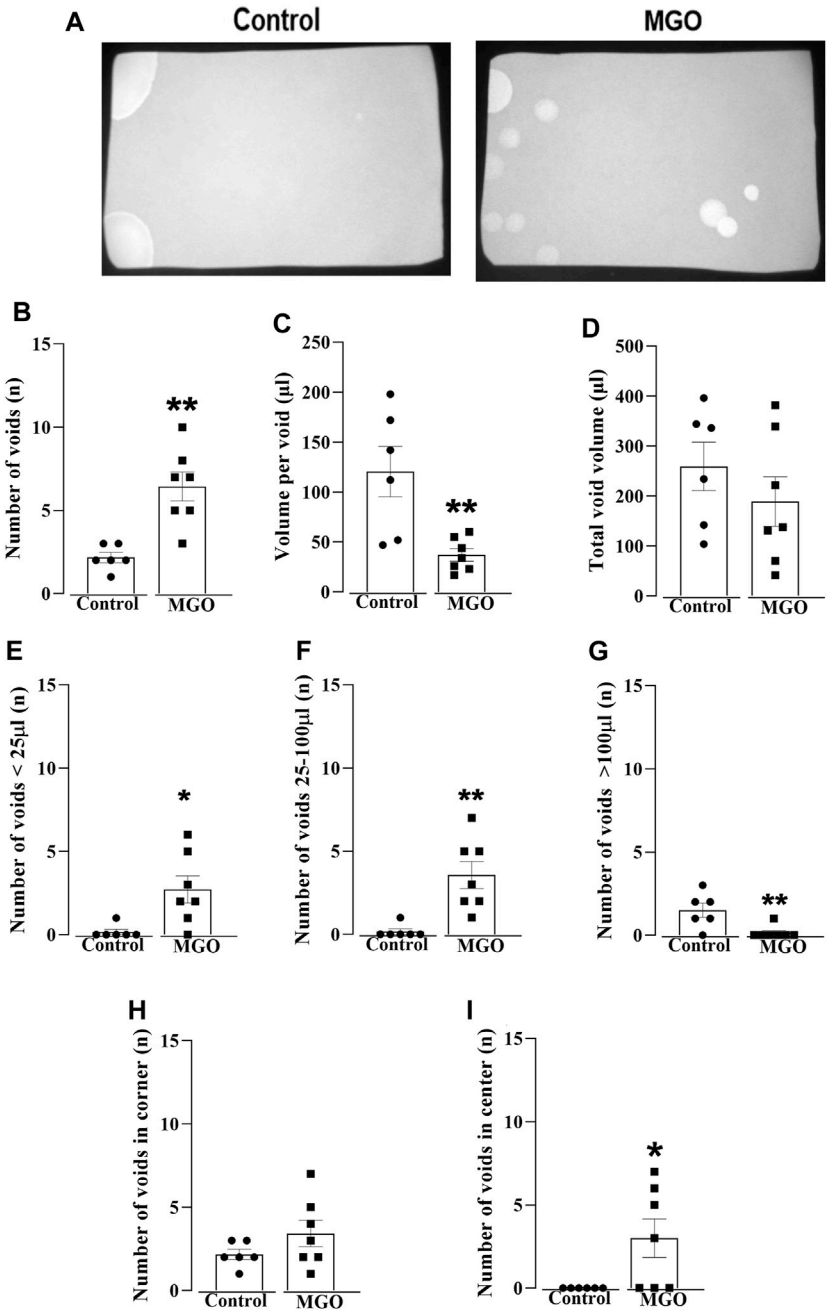

FIGURE 1
Void spot analysis in female mice exposed to 0.5% methylglyoxal (MGO) for 12 weeks. **(A)** displays representative images of the void spot assay in both the control group (receiving tap water alone) and the MGO-exposed groups. **(B–D)** show data on the number of voids, volume per void, and total void volume, respectively. The distribution of void spots across different volume ranges is shown in **(E)** (<25 µL), **(F)** (between 25 and 100 µL), and **(G)** (>100 µL). The number of voids in the corner and the center on the filter paper is illustrated in **(H,I)**, respectively. The data are expressed as the mean ± SEM (n = 6–7 animals per group). *p < 0.05, **p < 0.01 compared to control group (unpaired t-test).

Following centrifugation, the supernatant was removed and placed on ice. Glyoxalase I activity was assessed in duplicate using the Glyoxalase activity assay kit (Catalogue No. MAK114, Sigma-Aldrich, United States), following the manufacturer's instructions. To normalize the results, the total protein content of the samples was determined in triplicated using the DC™ Protein Assay Kit II (Catalogue No. 5000112, Bio-Rad Laboratories, Inc. California, United States).

Statistical analysis

The GraphPad Prism Version 6 Software (GraphPad Software, Inc., San Diego, CA, United States) was used for all statistical analysis. The parametric distribution of the data was assessed using the Shapiro test. Statistical difference between two groups was determined using Student's unpaired t-test. One-way ANOVA followed by Dunnett's multiple comparison test was used when

10.3389/fphys.2023.1308077

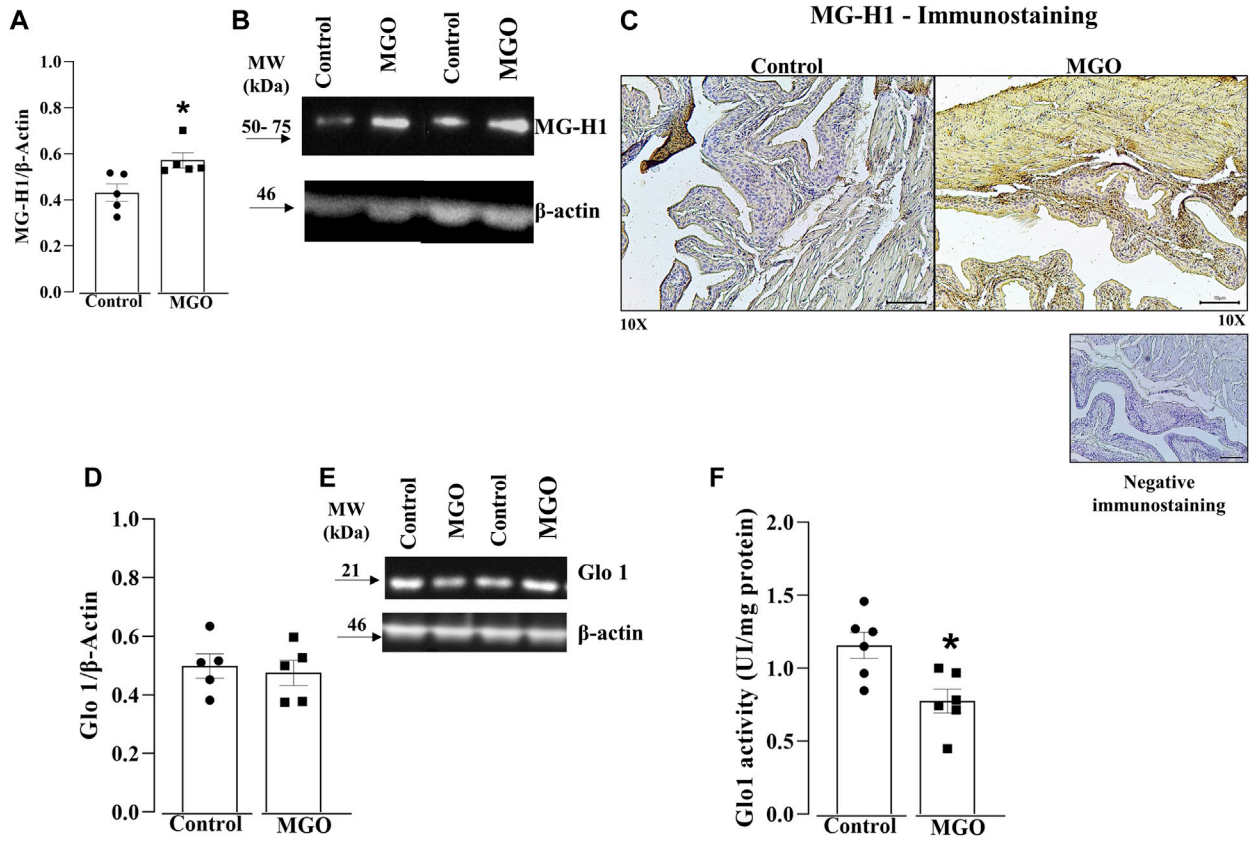

FIGURE 2
Quantification of methylglyoxal (MGO)-derived hydroimidazolone MG-H1 and glyoxalase 1 (Glo1) in the bladders of MGO-treated mice. **(A,B)** display densitometry analyses and representative Western blots of MG-H1, respectively. **(C)** depicts immunohistochemistry for MG-H1, demonstrating negative staining (absence of primary antibody binding) and positive immunostainings in control and MGO groups. In the control group, there is a weak positive staining observed in the urothelium, while in the MGO group, a strong positive staining is observed in both the urothelium and detrusor smooth muscle. In **(C)**, black bars represent a scale of 10 μm (×10 objectives). **(D,E)** display the protein expression, whereas **(F)** shows the Glo1 activity. The data are expressed as mean ± SEM (n = 5–6 animals per group). *p < 0.05 compared to control group (unpaired t-test).

comparing more than two groups with control group and one-way ANOVA followed by Tukey or Bonferroni's test were used when comparing all groups together. All results are presented as the means ± standard error of the mean (SEM). Results with p-values lower than 0.05 were considered significant.

Results

Alterations in void spot patterns on the filter paper assay

The voiding dysfunction induced by a 12-week oral intake of MGO was initially screened in conscious mice using the void spot assay on filter paper (Figure 1). Figure 1A shows representative images of the void spot assays, revealing a significant increase in the number of spots in the MGO compared to the control group (p < 0.01; n = 6–7; Figure 1B). Furthermore, the volume per void (Figure 1C) was significantly reduced in the MGO group compared to the control group (p < 0.01), while no significant differences in total void volume were observed (Figure 1D). The number of voids based on their volume sizes revealed that mice treated with MGO exhibited a higher number of spots with volumes lower than 25 μL (p < 0.05; Figure 1E) and between 25 and 100 μL (p < 0.05; Figure 1F), along with a decreased number of spots with volumes greater than 100 μL (p < 0.01; Figure 1G) compared to control group. Notably, in the control group, void spots were essentially concentrated in the corner of the filter paper with no voids in the center, as expected under normal conditions. In contrast, the MGO-treated group exhibited a different distribution pattern of void spots, with voids now detected both in the center and the corner of the filter (Figures 1H, I).

Protein levels and immunohistochemistry for MG-H1 in the bladder

Higher protein levels of MG-H1 were found in MGO compared to control group (p < 0.05; Figures 2A, B; Supplementary Figure S1A). Immunohistochemical assays showed a marked MG-H1 immunostaining in both the urothelium and detrusor smooth muscle layers of MGO-treated mice, whereas only minimal MG-H1 immunostaining intensity was detected in the urothelium of the control group (Figure 2C).

10.3389/fphys.2023.1308077

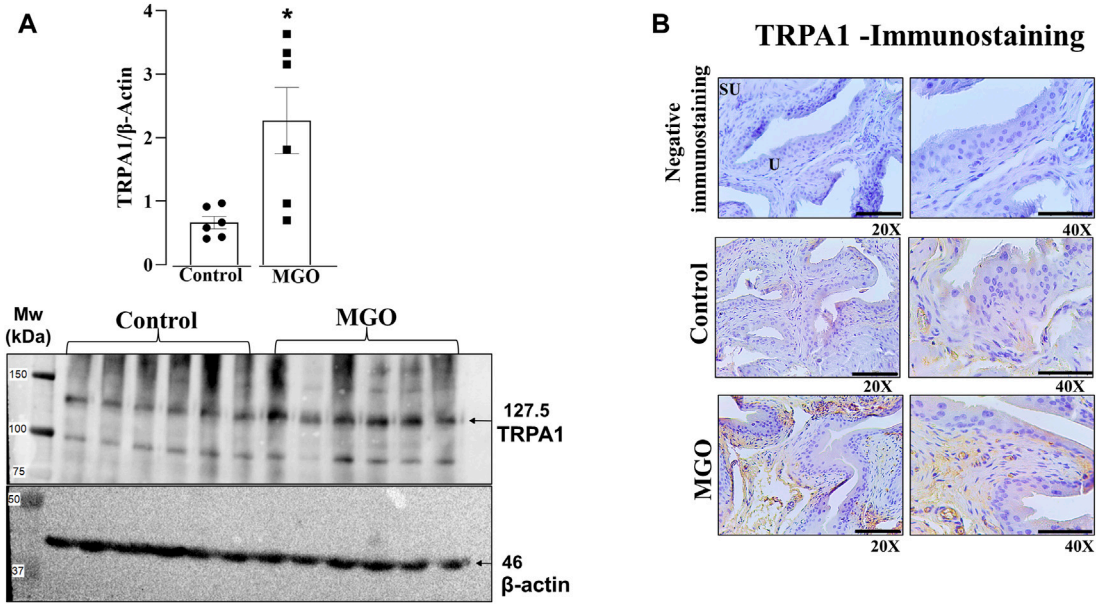

FIGURE 3
Protein expression of TRPA1 in the bladders of mice was assessed following a 12-week treatment with 0.5% methylglyoxal (MGO) or in control animals receiving tap water alone. **(A)** illustrates the results of protein expression analysis using Western Blotting analysis. **(B)** displays the immunohistochemistry for TRPA1 in bladder, showing negative immunostaining (absence of the antibody signal), and positive immunostainings in control and MGO groups. Positive immunostaining is observed in lamina propria and urothelial cells. The black bars in **(B)** represent a scale of 10 μm, as viewed under ×20 and ×40 objectives. In **(A)**, data are expressed as mean ± SEM (n = 7–8 animals per group). *p < 0.05 compared to control group (unpaired t-test).

Protein levels and enzyme activity of Glo1 in the bladder

Protein levels of Glo1 in bladder tissues did not significantly differ between the control and MGO groups (Figures 2D, E; Supplementary Figure S1B). However, MGO treatment led to a significant decrease in Glo1 activity in bladder tissues compared to control group (Figure 2F).

Levels of TRPA1 are enhanced in the bladder of MGO-Treated mice

Western blotting and immunohistochemistry assays were carried out in bladder tissues obtained from control and MGO-treated mice to investigate the expression of TRPA1. The results revealed a marked increase in TRPA1 protein levels in the bladder of MGO-treated mice compared to control groups (p < 0.05; Figure 3A; Supplementary Figure S2). In both control and MGO-treated groups, TRPA1 immunostaining was detected in the bladder mucosa, including the lamina propria and urothelial cells. Notably, the MGO-treated group exhibited a substantially higher intensity of TRPA1 immunostaining (Figure 3B). It is worthing mentioning that no TRPA1 immunostaining was detected in the detrusor smooth muscle layer of either group.

Intravesical infusion of HC-030031 reverses cystometric alterations in MGO-Treated mice

In order to evaluate the role of TRPA1 on voiding dysfunction induced by chronic MGO intake, we moved to the model of filling cystometry assays in anesthetized mice, which allowed us testing the TRPA1 antagonist HC-030031 by intravesical infusion on the resulting voiding dysfunction. Control and MGO-treated mice were intravesically infused with HC-030031 (1 nmol/min), saline or vehicle (0.001% DMSO; n = 5–7 animals per group). Compared to control group, a different pattern of voiding was found in MGO groups infused with either saline or vehicle, as characterized by a significantly higher voiding frequency (Figures 4A, B), paralleling significant reductions of bladder capacity (Figure 4C), voided volume (Figure 4D) and compliance (Figure 4E). The basal pressure (Figure 4F), threshold pressure (Figure 4G), and maximum pressure (Figure 4H) did not significantly differ between control and MGO groups. In MGO-treated mice, the infusion of HC-030031 almost completely reversed the changes in voiding frequency, bladder capacity, voided volume, and compliance. The basal pressure, threshold pressure, and maximum pressure remained unaltered. Infusion of HC-030031 at the same dose into the control group did not have a significant effect in any of the cystometric parameters. There were no statistical differences in any parameter between the saline and vehicle infusions in both the control and MGO groups.

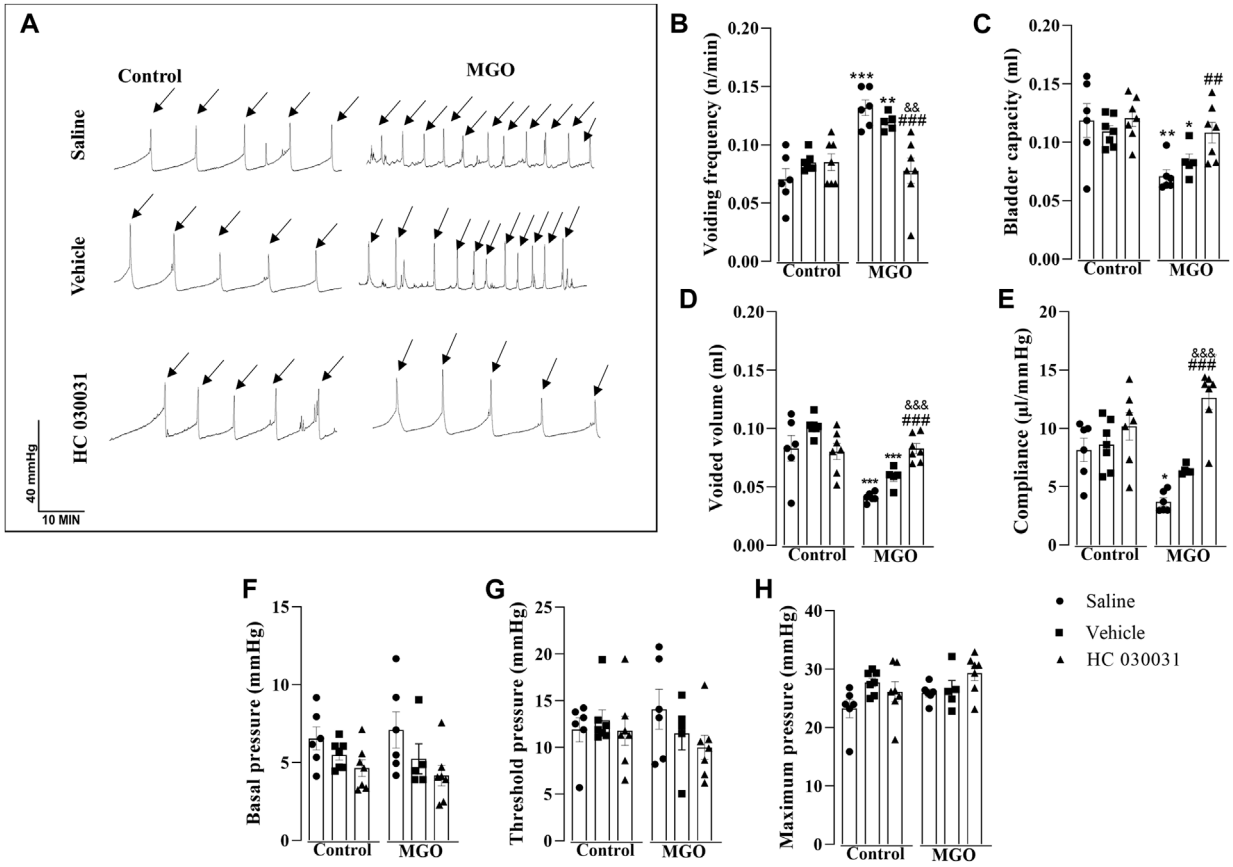

FIGURE 4
Effect of continuous infusion of the selective TRPA1 antagonist HC-030031 on cystometric changes in mice following 12-week treatment with 0.5% methylglyoxal (MGO) or control animals receiving tap water alone. In control and MGO groups, animals were infused continuously with saline (0.01 mL/min), vehicle (0.001% DMSO) or HC-030031 (1 nmol/min) for 1 h. **(A)** shows representative cystometric tracings from each sub-group, with arrows indicating micturition peaks. **(B–H)** show data on voiding frequency, bladder capacity, voided volume, compliance, basal pressure, threshold pressure and maximum pressure, respectively. All data are expressed as mean ± SEM (n = 5–7 animals per group). $^{*}p < 0.05$, $^{**}p < 0.01$, $^{***}p < 0.001$ compared to respective control group; $^{\#\#}p < 0.01$, $^{\#\#\#}p < 0.001$ compared to saline infusion in MGO group; $^{\&\&}p < 0.01$, $^{\&\&\&}p < 0.001$ compared vehicle infusion in MGO group (one-way ANOVA followed by Dunnett's multiple comparisons test for comparison to the control group and Bonferroni's multiple comparisons test to compare all groups).

HC-030031 reduces the *in vitro* bladder contractility of MGO-Treated mice

The contractile responses elicited by EFS and carbachol were examined in intact bladder strips (Figure 5). Electrical-field stimulation at a frequency of 1–32 Hz produced frequency-dependent bladder contractions in both the control and MGO groups. However, the contractions in the MGO were significantly higher than those in the control group, as evidenced at frequencies of 1–16 Hz (Figure 5A). In the control group, the prior incubation of bladder strips with HC-030031 (10 µM, 30 min) had no significant effect on EFS-induced contractions. Conversely, in the MGO group, HC-030031 completely restored the contractile responses to the levels observed in the control group (Figure 5A).

Addition of carbachol (10^{-10} to 3×10^{-5} M) produced concentration-dependent bladder contractions with no differences between MGO and control groups (Figure 5B). However, in the MGO group, HC-030031 (10 µM, 30 min) significantly reduced the carbachol-induced contractions, whereas in the control group HC-030031 had no significant effect (Figures 5B, C). The pEC_{50} values for carbachol did not significantly differ between groups, with values of 6.06 ± 0.11 for control + vehicle, 5.98 ± 0.06 for control + HC-030031, 6.09 ± 0.10 for MGO + vehicle, and 5.85 ± 0.08 for MGO + HC-030031.

Discussion

Chronic exposure to MGO induces an overactive bladder phenotype in mice, as observed in previous studies (de Oliveira et al., 2020; Oliveira et al., 2021; Oliveira et al., 2022). TRPA1 is expressed in human (Du et al., 2008), rat (Streng et al., 2008; Andrade et al., 2011) and mouse bladders (de Oliveira et al., 2020) and is upregulated in pathological conditions such as bladder outlet obstruction and spinal cord injury. We tested here the hypothesis that TRPA1 activation in bladder tissues contributes, at least in part, to MGO-induced bladder dysfunction in female mice.

Initially, we assessed voiding dysfunction in MGO-treated mice using the void spot on the filter paper assay (Hill et al., 2018). The

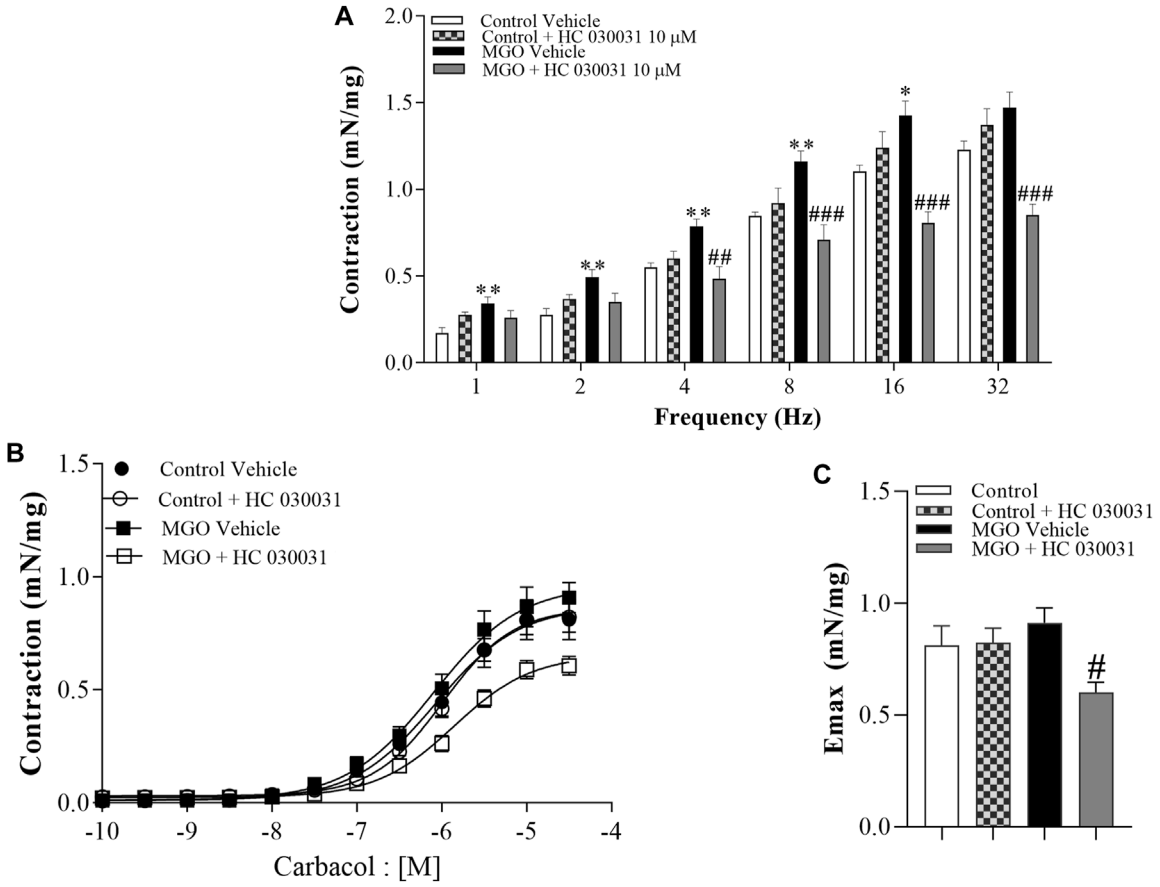

FIGURE 5
Effects of the selective TRPA1 antagonist HC-030031 on the contractile responses induced by electrical-field stimulation (EFS) and the muscarinic agonist carbachol in intact bladder strips obtained from mice treated with 0.5% methylglyoxal (MGO, 12 weeks) or tap water (control group). **(A)** illustrates the contractions induced by EFS at frequencies ranging from 1 to 32 Hz in both the control and MGO-treated groups in the presence of vehicle (0.001% DMSO) or HC-030031 (10 µM, 30 min). **(B)** displays the contractions induced by carbachol at concentrations ranging from 10^{-10} to 3×10^{-5} M in both the control and MGO-treated groups, in the presence of vehicle or HC-030031. **(C)** shows the maximal responses (E_{max}) to carbachol in all experimental groups. The data are expressed as mean ± SEM (n = 7 animals per group). $^{*}p < 0.05$, $^{**}p < 0.01$ compared to corresponding control vehicle group. $^{\#}p < 0.05$ $^{\#\#}p < 0.01$ $^{\#\#\#}p < 0.001$ compared to respective MGO vehicle group (One-way ANOVA followed by the Tukey).

data confirmed the presence of an overactive phenotype in MGO-treated male mice (de Oliveira et al., 2020), as evidenced by an increased number of urine spots together with a reduction in voided volume per void. Furthermore, the MGO-treated group exhibited a higher number of voids with small volumes (less than 25 µL and between 25 and 100 µL), primarily concentrated in the center of the filter paper. Despite the bladder weight increases by about of 20% in female mice treated with MGO, the water consumption does not significantly differ between MGO and vehicle groups (Oliveira et al., 2022), suggesting that alterations of voiding behavior in MGO-treated mice does not reflect mechanisms dependent on fluid intake, as observed in streptozotocin-injected animals, leptin-deficient ob/ob mice, and leptin receptor-deficient db/db mice (Suriano et al., 2021; Yesilyurt et al., 2022). Subsequently, we evaluated the protein levels and immunostaining of the MGO adduct MG-H1 in bladder tissues of both controls and MGO-treated mice. Compared to control group, the MGO-treated mice displayed higher protein levels and increased immunostaining of the MG-H1 in both the urothelium and detrusor smooth muscle. Dicarbonyl stress is characterized by an abnormal glycolytic overload and elevated cellular MGO concentration, which is critically regulated by Glo1 activity, one of the primary enzymes involved in MGO detoxification (Rabbani and Thornalley, 2019; He et al., 2020). In the present study, the protein expression of Glo1 in bladder tissues remained unchanged following MGO treatment. However, Glo1 activity was significantly reduced in the MGO compared to control group. This reduction in Glo1 activity in MGO-treated mice is likely attributed to the accumulation of MGO in the bladders, as evidenced by the higher levels of the MGO adduct MG-H1, consistent with the presence of a true dicarbonyl stress in bladder tissues of these animals.

We then explored the role of TRPA1 in MGO-induced voiding dysfunction. Higher levels of TRPA1 protein were found in the bladder tissues of MGO-treated mice as compared to control group. Additionally, intense TRPA1 immunostaining was detected in the lamina propria of the MGO group, despite urothelial cells expressing TRPA1 being also observed. Nevertheless, no TRPA1 immunostaining was detected in the detrusor smooth muscle layer. In a separate set of experiments, cystometric assays were conducted in anaesthetized control and

MGO-treated mice, with and without intravesical infusion of the TRPA1 blocker HC-030031, vehicle (0.001% DMSO) or saline. Methylglyoxal-treated mice displayed increased voiding frequency along with reductions of voided volume, bladder capacity, and compliance, consistent with the voiding alterations observed in conscious animals using the void spot assay. Importantly, these MGO-induced cystometric alterations were all reversed by intravesical infusion of HC-030031, indicating that TRPA1 activation in the urothelium plays a role in the machinery leading to overactive bladder.

Next, we assessed *in vitro* bladder contractions in response to EFS and carbachol in both control and MGO-treated mice. EFS-induced bladder contractions are chiefly mediated by acetylcholine release from parasympathetic fiber terminals, acting through the activation of post-synaptic muscarinic M_3 receptor in detrusor smooth muscle (Fry et al., 2010; Sellers and Chess-Williams, 2012). Muscarinic M3 receptors coupled to phospholipase C-dependent signals mediate bladder contractions via generation of the second messenger inositol triphosphate (IP_3), which activates the IP receptor to release Ca^{2+} from internal stores, in addition to extracellular Ca^{2+} influx secondary to L-type Ca^{2+} channel opening (Abrams et al., 2006; Frazier et al., 2008; Leiria et al., 2011). Nerve-mediated ATP release is also observed in mouse detrusor smooth muscle, which is said to mediate the atropine-resistant bladder contraction through P2X1 receptor activation (Tsai et al., 2012; Hao et al., 2019; McCarthy et al., 2019; Chakrabarty et al., 2022). A crosstalk between the purinergic and cholinergic transmitter systems, where ATP appears to induce the release of acetylcholine has also been reported (Stenqvist et al., 2020). We then assessed *in vitro* bladder contractions in response to EFS and carbachol in both control and MGO-treated mice. A previous study of our group showed that the contractile responses to the selective muscarinic agonist carbachol in MGO-treated mice remain unchanged intact bladder strips, but mucosal removal significantly increases in carbachol-induced bladder contractions (Oliveira et al., 2022). Interestingly, however, in the present study using intact bladder strip preparations, HC-030031 significantly reduced the carbachol-induced contractions in MGO-treated mice. On the other hand, MGO exposure was described to significantly enhance the contractile responses to both EFS and α,β-methylene ATP (a P2X1 purinergic receptor agonist) independently of the presence or not of urothelium (Oliveira et al., 2022). In the present study, the higher contractile response to EFS in bladders of MGO-treated mice was normalized by prior incubation with HC-030031. These data are indicative that MGO exposure via TRPA1 activation leads to enhancement of purinergic over cholinergic neurotransmission in the bladder. Of interest, interaction of TRPA1 and purinergic P2X receptors has been proposed to explain the pain pathophysiology in models of formalin-induced behavioral nociceptive responses in the rat (Krimon et al., 2013) and intracolonic administration of a low dose mustard oil in mice (Gonzalez-Cano et al., 2021). However, future experiments exploring the P2X1 purinergic component of the EFS-induced excitatory transmission might help to shed some light on the potential interactions of P2X and TRPA1 receptors in bladder of MGO-treated mice.

Collectively, our data from molecular and functional (*in vivo* and *in vitro*) studies support an important role of urothelial TRPA1 in modulating the bladder contractile responses after exposure to MGO. A previous study carried out in diabetic rats showed an increased mRNA expression of TRPA1 in dorsal root ganglia (DRG) that innervate the bladder and TRPA1 activation enhances the amplitude of EFS-induced detrusor smooth muscle contractions through mechanisms related to the activation of the tachykininergic and prostanoid systems (Philyppov et al., 2016). Increased TRPA1 expression was also seen in the bladders of insulin-resistant obese Zucker rats, but EFS-induced bladder contractions were instead reduced being this reduction attributed to excessive oxidative stress and downregulation of the cysthathionine-γ-lyase (CSE)/hydrogen sulfide (H_2S) pathway (Blaha et al., 2019). TRPA1 has been proposed to serve as an oxidative stress sensor (Yamamoto and Shimizu, 2016; Anraku, 2022), and exposure to MGO increases the production of reactive-oxygen species (ROS) that in turn leads to activation of Rho kinase system in detrusor smooth muscle, ultimately promoting detrusor overactivity (Oliveira et al., 2022). Therefore, further investigation is needed to identify the intracellular signal mediated by MGO that upregulates TRPA1 in bladder urothelium and lamina propria, thereby enhancing detrusor smooth muscle contractility.

Conclusion

In conclusion, this study shows that prolonged exposure to MGO in mice results in elevated levels of the advanced glycation end product MG-H1 in bladder tissues, inducing an upregulation of TRPA1 expression in the mucosal layer (lamina propria and urothelium). The effective blockade of TRPA1 with HC-030031 efficiently mitigated MGO-induced overactive bladder and detrusor hyperactivity. TRPA1 antagonists could potentially serve as a valuable therapeutic approach for managing diabetic bladder dysfunction in individuals with high MGO levels.

Data availability statement

The raw data supporting the conclusion of this article will be made available by the authors, without undue reservation.

Ethics statement

The animal study was approved by the Multidisciplinary Center for Biological Research on Laboratory Animal Science (CEMIB) of the State University of Campinas (UNICAMP, Sao Paulo, Brazil). The study was conducted in accordance with the local legislation and institutional requirements.

Author contributions

AO: Conceptualization, Investigation, Methodology, Writing–original draft. MM: Investigation, Methodology, Writing–original draft. EG: Investigation, Methodology, Writing–original draft. GM: Investigation, Project administration, Writing–original draft. SC: Writing–original draft, Writing–review and editing. FM: Formal Analysis, Funding acquisition, Writing–original draft, Writing–review and editing. EA: Formal Analysis, Funding acquisition, Project administration, Resources, Supervision, Writing–original draft, Writing–review and editing.

Funding

The author(s) declare financial support was received for the research, authorship, and/or publication of this article. We gratefully acknowledge São Paulo Research Foundation (FAPESP; Grant No. 2017/15175-1).

Conflict of interest

The authors declare that the research was conducted in the absence of any commercial or financial relationships that could be construed as a potential conflict of interest.

Publisher's note

Supplementary material

The Supplementary Material for this article can be found online at: https://www.frontiersin.org/articles/10.3389/fphys.2023.1308077/full#supplementary-material

References

Abrams, P., Andersson, K. E., Buccafusco, J. J., Chapple, C., de Groat, W. C., Fryer, A. D., et al. (2006). Muscarinic receptors: their distribution and function in body systems, and the implications for treating overactive bladder. *Br. J. Pharmacol.* 148 (5), 565–578. doi:10.1038/sj.bjp.0706780

American Diabetes Association (ADA) (2018). 2. Classification and diagnosis of diabetes: *Standards of medical Care in diabetes-2018. Diabetes Care* 41, S13–S27. doi:10.2337/dc18-S002

Andersson, D. A., Gentry, C., Light, E., Vastani, N., Vallortigara, J., Bierhaus, A., et al. (2013). Methylglyoxal evokes pain by stimulating TRPA1. *PLoS One* 8 (10), e77986. Erratum in: PLoS One. 2013;8(12). 10.1371/annotation/e707d50a-13b3. doi:10.1371/journal.pone.0077986

Andersson, K. E. (2019). TRP channels as lower urinary tract Sensory targets. *Med. Sci. (Basel)* 7 (5), 67. doi:10.3390/medsci7050067

Andrade, E. L., Forner, S., Bento, A. F., Leite, D. F., Dias, M. A., Leal, P. C., et al. (2011). TRPA1 receptor modulation attenuates bladder overactivity induced by spinal cord injury. *Am. J. Physiol Ren. Physiol.* 300 (5), F1223–F1234. doi:10.1152/ajprenal.00535.2010

Anraku, T. (2022). Anoxia/reoxygenation enhances spontaneous contractile activity via TRPA1 channel and COX2 activation in isolated rat whole bladder. *Neurourol. Urodyn.* 41 (8), 1692–1702. doi:10.1002/nau.25045

Becker, A. K., Babes, A., Düll, M. M., Khalil, M., Kender, Z., Gröner, J., et al. (2023). Spontaneous activity of specific C-nociceptor subtypes from diabetic patients and mice: involvement of reactive dicarbonyl compounds and (sensitized) transient receptor potential channel A1. *J. Peripher. Nerv. Syst.* 28 (2), 202–225. doi:10.1111/jns.12546

Blaha, I., López-Oliva, M. E., Martínez, M. P., Recio, P., Agis-Torres, Á., Martínez, A. C., et al. (2019). Bladder dysfunction in an obese Zucker rat: the role of TRPA1 channels, oxidative stress, and hydrogen sulfide. *Oxidative Med. Cell. Longev.* 2019, 5641645. doi:10.1155/2019/5641645

Brauchi, S. E., and Rothberg, B. S. (2020). Gating and calcium-sensing mechanisms of TRPA1 channels revealed. *Cell Calcium* 91, 102278. doi:10.1016/j.ceca.2020.102278

Chakrabarty, B., Aitchison, K., White, P., McCarthy, C. J., Kanai, A. J., and Fry, C. H. (2022). Frequency-dependent characteristics of nerve-mediated ATP and acetylcholine release from detrusor smooth muscle. *Exp. Physiol.* 107, 350–358. doi:10.1113/EP090238

Chandrakumar, S., Santiago Tierno, I., Agarwal, M., Matisioudis, N., Kern, T. S., and Ghosh, K. (2023). Subendothelial matrix stiffening by lysyl oxidase enhances RAGE-mediated retinal endothelial activation in diabetes. *Diabetes* 72 (7), 973–985. PMID: 37058096; PMCID: PMC10281239. doi:10.2337/db22-0761

Daneshgari, F., Liu, G., and Hanna-Mitchell, A. T. (2017). Path of translational discovery of urological complications of obesity and diabetes. *Am. J. Physiol Ren. Physiol.* 312 (5), F887–F896. doi:10.1152/ajprenal.00489.2016

de Oliveira, M. G., de Medeiros, M. L., Tavares, E. B. G., Mónica, F. Z., and Antunes, E. (2020). Methylglyoxal, a reactive glucose metabolite, induces bladder overactivity in addition to inflammation in mice. *Front. Physiol.* 11, 290. doi:10.3389/fphys.2020.00290

Du, S., Araki, I., Kobayashi, H., Zakoji, H., Sawada, N., and Takeda, M. (2008). Differential expression profile of cold (TRPA1) and cool (TRPM8) receptors in human urogenital organs. *Urology* 72 (2), 450–455. doi:10.1016/j.urology.2007.11.127

Eid, S. R., Crown, E. D., Moore, E. L., Liang, H. A., Choong, K. C., Dima, S., et al. (2008). HC-030031, a TRPA1 selective antagonist, attenuates inflammatory- and neuropathy-induced mechanical hypersensitivity. *Mol. Pain* 4, 48. doi:10.1186/1744-8069-4-48

Frazier, E. P., Peters, S. L., Braverman, A. S., Ruggieri, M. R., Sr, and Michel, M. C. (2008). Signal transduction underlying the control of urinary bladder smooth muscle tone by muscarinic receptors and beta-adrenoceptors. *Naunyn Schmiedeb. Arch. Pharmacol.* 377 (4-6), 449–462. doi:10.1007/s00210-007-0208-0

Fry, C. H., Meng, E., and Young, J. S. (2010). The physiological function of lower urinary tract smooth muscle. *Aut. Neurosci.* 154 (1-2), 3–13. doi:10.1016/j.autneu.2009.10.006

Gao, S., Kaudimba, K. K., Guo, S., Zhang, S., Liu, T., Chen, P., et al. (2020). Transient Receptor potential ankyrin type-1 channels as a potential target for the treatment of cardiovascular diseases. *Front. Physiol.* 11, 836. doi:10.3389/fphys.2020.00836

Golbidi, S., and Laher, I. (2010). Bladder dysfunction in diabetes mellitus. *Front. Pharmacol.* 1, 136. doi:10.3389/fphar.2010.00136

Gonzalez-Cano, R., Montilla-García, Á., Perazzoli, G., Torres, J. M., Cañizares, F. J., Fernández-Segura, E., et al. (2021). Intracolonic mustard oil induces visceral pain in mice by TRPA1-dependent and -independent mechanisms: role of tissue injury and P2X receptors. *Front. Pharmacol.* 11, 613068. PMID: 33551815; PMCID: PMC7859884. doi:10.3389/fphar.2020.613068

Griggs, R. B., Laird, D. E., Donahue, R. R., Fu, W., and Taylor, B. K. (2017). Methylglyoxal Requires AC1 and TRPA1 to produce pain and spinal neuron activation. *Front. Neurosci.* 11, 679. doi:10.3389/fnins.2017.00679

Hao, Y., Wang, L., Chen, H., Hill, W. G., Robson, S. C., Zeidel, M. L., et al. (2019). Targetable purinergic receptors P2Y12 and A2b antagonistically regulate bladder function. *J. Clin. Investigation Insight* 4 (16), e122112. PMID: 31434806; PMCID: PMC6777812. doi:10.1172/jci.insight.122112

Harkin, C., Cobice, D., Watt, J., Kurth, M. J., Brockbank, S., Bolton, S., et al. (2023). Analysis of reactive aldehydes in urine and plasma of type-2 diabetes mellitus patients through liquid chromatography-mass spectrometry: reactive aldehydes as potential markers of diabetic nephropathy. *Front. Nutr.* 9, 997015. doi:10.3389/fnut.2022.997015

Hayashi, N., Kawamorita, N., Ishizuka, Y., Kimura, S., Satake, Y., and Ito, A. (2023). Ectopic endometriosis in the pelvic cavity evokes bladder hypersensitivity via transient receptor potential ankyrin 1 hyperexpression in rats. *Int. Urogynecol. J.* 34 (6), 1211–1218. doi:10.1007/s00192-022-05335-x

He, Y., Zhou, C., Huang, M., Tang, C., Liu, X., Yue, Y., et al. (2020). Glyoxalase system: a systematic review of its biological activity, related diseases, screening methods, and small molecule regulators. *Biomed. Pharmacother.* 131, 110663. doi:10.1016/j.biopha.2020.110663

Hill, W. G., Zeidel, M. L., Bjorling, D. E., and Vezina, C. M. (2018). Void spot assay: recommendations on the use of a simple micturition assay for mice. *Am. J. Physiol Ren. Physiol.* 315 (5), F1422–F1429. doi:10.1152/ajprenal.00350.2018

Huang, Q., Chen, Y., Gong, N., and Wang, Y. X. (2016). Methylglyoxal mediates streptozotocin-induced diabetic neuropathic pain via activation of the peripheral TRPA1 and Nav1.8 channels. *Metabolism* 65 (4), 463–474. doi:10.1016/j.metabol.2015.12.002

Jandova, J., and Wondrak, G. T. (2021). Genomic GLO1 deletion modulates TXNIP expression, glucose metabolism, and redox homeostasis while accelerating human A375 malignant melanoma tumor growth. *Redox Biol.* 9, 101838. Epub 2020 Dec 17. PMID: 33360689; PMCID: PMC7772567. doi:10.1016/j.redox.2020.101838

Kalapos, M. P. (1999). Methylglyoxal in living organisms: chemistry, biochemistry, toxicology and biological implications. *Toxicol. Lett.* 110 (3), 145–175. doi:10.1016/s0378-4274(99)00160-5

Krimon, S., Araldi, D., do Prado, F. C., Tambeli, C. H., Oliveira-Fusaro, M. C., and Parada, C. A. (2013). P2X3 receptors induced inflammatory nociception modulated by

TRPA1, 5-HT3 and 5-HT1A receptors. *Pharmacol. Biochem. Behav.* 112, 49–55. Epub 2013 Oct 9. PMID: 24120766. doi:10.1016/j.pbb.2013.09.017

Kudsi, S. Q., Piccoli, B. C., Ardisson-Araújo, D., and Trevisan, G. (2022). Transcriptional landscape of TRPV1, TRPA1, TRPV4, and TRPM8 channels throughout human tissues. *Life Sci.* 308, 120977. doi:10.1016/j.lfs.2022.120977

Lai, S. W. T., Lopez Gonzalez, E. D. J., Zoukari, T., Ki, P., and Shuck, S. C. (2022). Methylglyoxal and its adducts: induction, repair, and association with disease. *Chem. Res. Toxicol.* 35 (10), 1720–1746. doi:10.1021/acs.chemrestox.2c00160

Lee, K. I., Lee, H. T., Lin, H. C., Tsay, H. J., Tsai, F. C., Shyue, S. K., et al. (2016). Role of transient receptor potential ankyrin 1 channels in Alzheimer's disease. *J. Neuroinflammation* 13 (1), 92. PMID: 27121378; PMCID: PMC4847235. doi:10.1186/s12974-016-0557-z

Leiria, L. O., Mónica, F. Z., Carvalho, F. D., Claudino, M. A., Franco-Penteado, C. F., Schenka, A., et al. (2011). Functional, morphological, and molecular characterization of bladder dysfunction in streptozotocin-induced diabetic mice: evidence of a role for L-type voltage-operated Ca^{2+} channels. *Br. J. Pharmacol.* 163 (6), 1276–1288. doi:10.1111/j.1476-5381.2011.01311.x

Luostarinen, S., Hämäläinen, M., Pemmari, A., and Moilanen, E. (2023). The regulation of TRPA1 expression and function by Th1 and Th2-type inflammation in human A549 lung epithelial cells. *Inflamm. Res.* 72 (7), 1327–1339. Epub 2023 Jun 29. PMID: 37386145; PMCID: PMC10352175. doi:10.1007/s00011-023-01750-y

McCarthy, C. J., Ikeda, Y., Skennerton, D., Chakrabarty, B., Kanai, A. J., Jabr, R. I., et al. (2019). Characterisation of nerve-mediated ATP release from bladder detrusor muscle and its pathological implications. *Br. J. Pharmacol.* 176 (24), 4720–4730. doi:10.1111/bph.14840

Medeiros, M. L., Oliveira, A. L., de Oliveira, M. G., Mónica, F. Z., and Antunes, E. (2021). Methylglyoxal exacerbates lipopolysaccharide-induced acute lung injury via RAGE-induced ROS generation: protective effects of metformin. *J. Inflamm. Res.* 14, 6477–6489. doi:10.2147/JIR.S337115

Ohkawara, S., Tanaka-Kagawa, T., Furukawa, Y., and Jinno, H. (2012). Methylglyoxal activates the human transient receptor potential ankyrin 1 channel. *J. Toxicol. Sci.* 37 (4), 831–835. doi:10.2131/jts.37.831

Oliveira, A. L., de Oliveira, M. G., Medeiros, M. L., Mónica, F. Z., and Antunes, E. (2021). Metformin abrogates the voiding dysfunction induced by prolonged methylglyoxal intake. *Eur. J. Pharmacol.* 910, 174502. doi:10.1016/j.ejphar.2021.174502

Oliveira, A. L., Medeiros, M. L., de Oliveira, M. G., Teixeira, C. J., Mónica, F. Z., and Antunes, E. (2022). Enhanced RAGE expression and excess reactive-oxygen species production mediates Rho kinase-dependent detrusor overactivity after methylglyoxal exposure. *Front. Physiol.* 13, 860342. doi:10.3389/fphys.2022.860342

Oliveira, A. L., Medeiros, M. L., Ghezzi, A. C., Dos Santos, G. A., Mello, G. C., Mónica, F. Z., et al. (2023). Evidence that methylglyoxal and receptor for advanced glycation end products are implicated in bladder dysfunction of obese diabetic ob/ob mice. *Am. J. Physiol. Ren. Physiol.* 325 (4), F436–F447. doi:10.1152/ajprenal.00089.2023

Philyppov, I. B., Paduraru, O. N., Gulak, K. L., Skryma, R., Prevarskaya, N., and Shuba, Y. M. (2016). TRPA1-dependent regulation of bladder detrusor smooth muscle contractility in normal and type I diabetic rats. *J. Smooth Muscle Res.* 52, 1–17. doi:10.1540/jsmr.52.1

Rabbani, N., and Thornalley, P. J. (2019). Glyoxalase 1 modulation in obesity and diabetes. *Antioxid. Redox Signal* 30, 354–374. doi:10.1089/ars.2017.7424

Schalkwijk, C. G., and Stehouwer, C. D. A. (2020). Methylglyoxal, a highly reactive dicarbonyl compound, in diabetes, its vascular complications, and other age-related diseases. *Physiol. Rev.* 100 (1), 407–461. doi:10.1152/physrev.00001.2019

Sellers, D. J., and Chess-Williams, R. (2012). Muscarinic agonists and antagonists: effects on the urinary bladder. *Handb. Exp. Pharmacol.* 208, 375–400. doi:10.1007/978-3-642-23274-9_16

Smith, A. J., Advani, J., Brock, D. C., Nellissery, J., Gumerson, J., Dong, L., et al. (2022). GATD3A, a mitochondrial deglycase with evolutionary origins from gammaproteobacteria, restricts the formation of advanced glycation end products. *BMC Biol.* 20 (1), 68. PMID: 35307029; PMCID: PMC8935817. doi:10.1186/s12915-022-01267-6

Song, Q. X., Sun, Y., Deng, K., Mei, J. Y., Chermansky, C. J., and Damaser, M. S. (2022). Potential role of oxidative stress in the pathogenesis of diabetic bladder dysfunction. *Nat. Rev. Urol.* 19 (10), 581–596. doi:10.1038/s41585-022-00621-1

Steiner, C., Gevaert, T., Ganzer, R., De Ridder, D., and Neuhaus, J. (2018). Comparative immunohistochemical characterization of interstitial cells in the urinary bladder of human, Guinea pig, and pig. *Histochem. Cell Biol.* 149 (5), 491–501. doi:10.1007/s00418-018-1655-z

Stenqvist, J., Carlsson, T., Winder, M., and Aronsson, P. (2020). Functional atropine sensitive purinergic responses in the healthy rat bladder. *Aut. Neurosci.* 227, 102693. Epub 2020 Jun 9. PMID: 32563054. doi:10.1016/j.autneu.2020.102693

Streng, T., Axelsson, H. E., Hedlund, P., Andersson, D. A., Jordt, S. E., Bevan, S., et al. (2008). Distribution and function of the hydrogen sulfide-sensitive TRPA1 ion channel in rat urinary bladder. *Eur. Urol.* 53 (2), 391–399. doi:10.1016/j.eururo.2007.10.024

Suriano, F., Vieira-Silva, S., Falony, G., Roumain, M., Paquot, A., Pelicaen, R., et al. (2021). Novel insights into the genetically obese (ob/ob) and diabetic (db/db) mice: two sides of the same coin. *Microbiome* 9 (1), 147. doi:10.1186/s40168-021-01097-8

Thornalley, P. J., Langborg, A., and Minhas, H. S. (1999). Formation of glyoxal, methylglyoxal and 3-deoxyglucosone in the glycation of proteins by glucose. *Biochem. J.* 344 (Pt 1), 109–116. doi:10.1042/bj3440109

Tsai, M. H., Kamm, K. E., and Stull, J. T. (2012). Signalling to contractile proteins by muscarinic and purinergic pathways in neurally stimulated bladder smooth muscle. *J. Physiol.* 590 (20), 5107–5121. Epub 2012 Aug 13. PMID: 22890701; PMCID: PMC3497566. doi:10.1113/jphysiol.2012.235424

Vanneste, M., Segal, A., Voets, T., and Everaerts, W. (2021). Transient receptor potential channels in sensory mechanisms of the lower urinary tract. *Nat. Rev. Urol.* 18 (3), 139–159. doi:10.1038/s41585-021-00428-6

Wittig, L., Carlson, K. V., Andrews, J. M., Crump, R. T., and Baverstock, R. J. (2019). Diabetic bladder dysfunction: a review. *Urology* 123, 1–6. doi:10.1016/j.urology.2018.10.010

Yamamoto, S., and Shimizu, S. (2016). Significance of TRP channels in oxidative stress. *Eur. J. Pharmacol.* 793, 109–111. doi:10.1016/j.ejphar.2016.11.007

Yesilyurt, Z. E., Matthes, J., Hintermann, E., Castañeda, T. R., Elvert, R., Beltran-Ornelas, J. H., et al. (2022). Analysis of 16 studies in nine rodent models does not support the hypothesis that diabetic polyuria is a main reason of urinary bladder enlargement. *Front. Physiol.* 13, 923555. doi:10.3389/fphys.2022.923555

Zhang, X., Scheijen, J. L. J. M., Stehouwer, C. D. A., Wouters, K., and Schalkwijk, C. G. (2023). Increased methylglyoxal formation in plasma and tissues during a glucose tolerance test is derived from exogenous glucose. *Clin. Sci. Lond.* 137 (8), 697–706. doi:10.1042/CS20220753

Zhao, M., Chen, Z., Liu, L., Ding, N., Wen, J., Liu, J., et al. (2022). Functional expression of transient receptor potential and Piezo1 channels in cultured interstitial cells of human-bladder lamina propria. *Front. Physiol.* 12, 762847. doi:10.3389/fphys.2021.762847

frontiers | Frontiers in Physiology

TYPE Original Research
PUBLISHED 19 July 2024
DOI 10.3389/fphys.2024.1369120

OPEN ACCESS

EDITED BY
Russ Chess-Williams,
Bond University, Australia

REVIEWED BY
M. Dennis Leo,
University of Tennessee Health Science Center (UTHSC), United States
Alberto Fernando Oliveira Justo,
University of São Paulo, Brazil

*CORRESPONDENCE
Fábio Henrique Silva,
fabio.hsilva@usf.edu.br,
fabiohsilva87@gmail.com

RECEIVED 11 January 2024
ACCEPTED 20 May 2024
PUBLISHED 19 July 2024

CITATION
Silveira THRe, Pereira DA, Pereira DA, Calmasini FB, Burnett AL, Costa FF and Silva FH (2024), Impact of intravascular hemolysis on functional and molecular alterations in the urinary bladder: implications for an overactive bladder in sickle cell disease.
Front. Physiol. 15:1369120.
doi: 10.3389/fphys.2024.1369120

Impact of intravascular hemolysis on functional and molecular alterations in the urinary bladder: implications for an overactive bladder in sickle cell disease

Tammyris Helena Rebecchi e Silveira[1], Dalila Andrade Pereira[1], Danillo Andrade Pereira[1], Fabiano Beraldi Calmasini[2], Arthur L. Burnett[3], Fernando Ferreira Costa[4] and Fábio Henrique Silva[1]*

[1]Laboratory of Pharmacology, São Francisco University Medical School, Bragança Paulista, Brazil, [2]Department of Pharmacology, Escola Paulista de Medicina, Universidade Federal de São Paulo, São Paulo, Brazil, [3]The James Buchanan Brady Urological Institute and Department of Urology, The Johns Hopkins School of Medicine, Baltimore, MD, United States, [4]Hematology and Hemotherapy Center, University of Campinas, Campinas, Brazil

Patients with sickle cell disease (SCD) display an overactive bladder (OAB). Intravascular hemolysis in SCD is associated with various severe SCD complications. However, no experimental studies have evaluated the effect of intravascular hemolysis on bladder function. This study aimed to assess the effects of intravascular hemolysis on the micturition process and the contractile mechanisms of the detrusor smooth muscle (DSM) in a mouse model with phenylhydrazine (PHZ)-induced hemolysis; furthermore, it aimed to investigate the role of intravascular hemolysis in the dysfunction of nitric oxide (NO) signaling and in increasing oxidative stress in the bladder. Mice underwent a void spot assay, and DSM contractions were evaluated in organ baths. The PHZ group exhibited increased urinary frequency and increased void volumes. DSM contractile responses to carbachol, KCl, α-β-methylene-ATP, and EFS were increased in the PHZ group. Protein expression of phosphorylated endothelial NO synthase (eNOS) (Ser-1177), phosphorylated neuronal NO synthase (nNOS) (Ser-1417), and phosphorylated vasodilator-stimulated phosphoprotein (VASP) (Ser-239) decreased in the bladder of the PHZ group. Protein expression of oxidative stress markers, NOX-2, 3-NT, and 4-HNE, increased in the bladder of the PHZ group. Our study shows that intravascular hemolysis promotes voiding dysfunction correlated with alterations in the NO signaling pathway in the bladder, as evidenced by reduced levels of p-eNOS (Ser-1177), nNOS (Ser-1417), and p-VASP (Ser-239). The study also showed that intravascular hemolysis increases oxidative stress in the bladder. Our study indicates that intravascular hemolysis promotes an OAB phenotype similar to those observed in patients and mice with SCD.

KEYWORDS

cyclic guanosine monophosphate, nitric oxide, oxidative stress, NADPH oxidase, urinary dysfunction

1 Introduction

Sickle cell disease (SCD), an autosomal recessive genetic disorder, is characterized by abnormal hemoglobin S (HbS) production due to a single amino acid substitution in the β-globin chain (Kato et al., 2018). This genetic mutation triggers the polymerization of HbS under hypoxic or dehydrated conditions, forming sickle-shaped erythrocytes. These altered cells exhibit increased stiffness and a reduced lifespan, leading to intravascular and extravascular hemolysis, which are critical features of SCD and contribute to its diverse clinical manifestations (Kato et al., 2018). A significant molecular consequence of intravascular hemolysis is the reduction of nitric oxide (NO) bioavailability due to direct NO-hemoglobin interaction and increased reactive oxygen species (ROS) production, which act as NO scavengers (Reiter et al., 2002; Vona et al., 2021). This reduction in NO is associated with various severe SCD complications, including leg ulceration, pulmonary hypertension, priapism, and overactive bladder (OAB) (Nolan et al., 2005; Kato et al., 2006; Cita et al., 2016).

The functions of the urinary bladder, encompassing urine storage and voiding, are regulated by a complex interplay of neurotransmitters (Andersson and Arner, 2004). OAB, a clinical condition marked by persistent urgency to urinate, may occur with or without urge incontinence and is commonly accompanied by increased urination frequency and nocturia (Eapen and Radomski, 2016). Notably, in SCD patients, the prevalence of OAB is significant, with clinical studies suggesting that up to 40% of these patients may exhibit symptoms of OAB (Portocarrero et al., 2012; Anele et al., 2015). A common contributor to OAB is the heightened contraction of the detrusor smooth muscle during the urine storage phase, leading to detrusor overactivity (Michel and Chapple, 2009).

The NO-cyclic guanosine monophosphate (cGMP) signaling pathway plays an essential role in the normal functioning of the urinary tract. NO, synthesized by endothelial NO synthase (eNOS) and neuronal NO synthase (nNOS), is crucial for maintaining the tone and functionality of detrusor smooth muscle (Burnett et al., 1997; Mónica et al., 2008; Karakus et al., 2019). NO deficiency has been linked with the OAB phenotype and increased detrusor smooth muscle contraction in SCD mice and various experimental models (Khan et al., 1999; Mónica et al., 2011; Leiria et al., 2013; Leiria et al., 2014; Karakus et al., 2019; Musicki et al., 2019; Karakus et al., 2020; Lee et al., 2021). Furthermore, increased superoxide production by the NOX-2 isoform of NADPH oxidase, which acts by activating NO, also contributes to the pathophysiology of OAB in animal models (Alexandre et al., 2016; 2018; Akakpo et al., 2017; de Oliveira et al., 2022) but has not yet been evaluated in the lower urinary tract in SCD.

To date, previous studies have used SCD transgenic mice to investigate bladder alterations (Claudino et al., 2015; Karakus et al., 2019; 2020; Musicki et al., 2019). These studies reported voiding dysfunction and detrusor hypercontractility associated with reduced NO bioavailability in the bladder. However, the exclusive effects of intravascular hemolysis on the bladder have not been independently analyzed. Given the critical role of intravascular hemolysis in SCD and its potential impact on the NO signaling pathway in the bladder, we hypothesize that intravascular hemolysis contributes significantly to micturition dysfunction.

The phenylhydrazine (PHZ)-induced hemolysis model permits precise control over the onset and intensity of hemolysis (Lim et al., 1998; Dutra et al., 2014; Gotardo et al., 2023), enabling a direct correlation between hemolysis and the observed functional and molecular changes in the bladder. This model is precious when the aim is to study the exclusive effect of intravascular hemolysis, as SCD mice exhibit additional alterations beyond intravascular hemolysis. This study endeavors to fill this critical gap in knowledge, providing an in-depth understanding of the mechanisms underlying intravascular hemolysis-induced micturition dysfunction.

This study is designed to delineate the consequences of intravascular hemolysis on the micturition process and the contractile mechanisms of the detrusor smooth muscle in a mouse model of PHZ-induced hemolysis. Furthermore, we investigate the role of intravascular hemolysis in elevating ROS production in the bladder, as well as to assess changes in phosphorylated eNOS (Ser-1177), phosphorylated nNOS (Ser-1417), and phosphorylated vasodilator-stimulated phosphoprotein (p-VASP Ser-239).

2 Materials and methods

2.1 Ethical approval

All animal study protocols in this study were approved by the Ethics Committee on Animal Use of the University of San Francisco (CEUA/USF, Permit number V3:008.06.2021).

2.2 Animals and treatment

Animal procedures and experimental protocols were performed in accordance with the ethical principles in animal research adopted by the Brazilian College for Animal Experimentation and followed the Guide for the Care and Use of Laboratory Animals. All mouse strains were originally purchased from Jackson Laboratories (Bar Harbor, ME). Characterization and breeding were performed at the Multidisciplinary Center for the Investigation of Biological Science in Laboratory Animals of the University of Campinas. We used C57BL/6 male mice (control), aged 3–4 months old, housed five per cage on a 12 h light–dark cycle.

We injected PHZ at 50 mg/kg in C57BL/6 mice intraperitoneally to induce intravascular hemolysis. The mice were reinjected with 50 mg/kg 8 h later and were sacrificed 4 days after starting PHZ treatment. Control mice were treated with the saline vehicle simultaneously with the PHZ group (Henrique Silva et al., 2018).

2.3 Void spot assay

Mice were moved individually to empty mouse cages with precut qualitative filter paper (250 g) on the bottom. They were provided with food but no water. After 4 hours, the filter papers were removed and allowed to dry before being imaged using UV light transillumination and captured using the ChemiDoc MP imaging system with Image Laboratory software (Bio-Rad Laboratories, Hercules, CA). Captured images were saved in grayscale-tagged image file format (TIFF) (Figure 2A) and analyzed using ImageJ Software (National Institute of Health, Bethesda-MD, United States

of America). ImageJ particle analysis was performed on >0.02 cm^2 spots to reduce areas of non-specific fluorescence and artifacts that may have been created by debris and feces (Keil et al., 2016). A linear standard measurement curve was used to convert void spot areas to volumes, and total volumes were normalized to body weight. Assays were performed for each animal between 9 a.m. and 2 p.m.

2.4 Functional studies of bladder strips and concentration–response curves

Two longitudinal detrusor smooth muscle strips with intact urothelium were obtained from each bladder. The strips were mounted in 5 mL myograph organ baths (Danish Myo Technology, Aarhus, Denmark) containing Krebs–Henseleit solution composed of 117 mM NaCl, 4.7 mM KCl, 2.5 mM $CaCl_2$, 1.2 mM $MgSO_4$, 1.2 mM KH_2PO_4, 25 mM $NaHCO_3$, and 11 mM glucose, continuously bubbled with a mixture of 95% O_2 and 5% CO_2 (pH 7.4) at 37°C. Changes in isometric force were recorded using a PowerLab Data Acquisition System (Software LabChart, version 7.0, ADInstruments, MA, United States of America).The resting tension was adjusted to 5 mN at the beginning of the experiments. The equilibration period was 60 min, and the bathing medium was changed every 15 min.

Cumulative concentration-response curves for the full muscarinic agonist carbachol (1 nM–30 μM) and potassium chloride (KCl; 1–300 mM) were obtained in detrusor strips. In separate experiments, electrical field stimulation (EFS)-induced contraction (20 V, 10 s of stimulation at varying frequencies, a 2-min interval between each pulse) was carried out. Non-cumulative concentration–response curves were also made for the purinergic agonist (P2X), α-β-methylene-ATP (1 μM, 3 μM, and 10 μM).

Non-linear regression analysis used GraphPad Prism (GraphPad Software, San Diego, CA, United States of America). Maximal response (E_{max}) data were normalized to the wet weight of the respective urinary bladder strips. Using GraphPad Prism software, EC_{50} values, represented as the negative logarithm (pEC50), were calculated by fitting the concentration–response relationship to a sigmoidal model (log-concentrations vs. response).

2.5 Western blot analysis

The separation of proteins from biological samples of tissue homogenates (detrusor) was performed through electrophoresis in 4%–20% polyacrylamide with 0.1% sodium sulfate (SDS-Page). Then, the protein bands were transferred electrophoretically into a submerged nitrocellulose membrane system. Non-specific protein binding to nitrocellulose was reduced by "overnight" pre-incubation of the membrane with a blocking solution (5% milk powder, 10 mm Tris, 100 mm NaCl, and 0.02% Tween 20). The bladder from each mouse was homogenized in lysis buffer and centrifuged at 12,000 g for 20 min at 4°C. Homogenates containing 70 μg of total proteins were run on 4%–20% Tris-HCl gels (Bio-Rad Laboratories, Hercules, CA, United States of America) and transferred to a nitrocellulose membrane. Non-fat dry milk (5%) (Bio-Rad) in Tris-buffered saline/Tween was used for 60 min at 24°C to block non-specific binding sites. Membranes were incubated for 15–18 h at 4°C with the following antibodies: monoclonal anti-3-nitrotyrosine (3-NT; 1:3000, Abcam), polyclonal anti-4-HNE antibody (1:3000, Abcam), anti-NOX-2 antibody (1:1000, Sigma-Aldrich), monoclonal anti-phospho(p)-eNOS (Ser-1177) antibody (1:1000, Cell Signaling), polyclonal anti-eNOS antibody (1:1000, Cell Signaling), polyclonal anti-phospho(p)-VASP (Ser-239) (1:1000, Cell Signaling), monoclonal anti-VASP antibody (1:1000, Cell Signaling), polyclonal phospho(p)-nNOS antibody (Ser-1417) (1:1000, Abcam), nNOS (1:1000, Millipore), and β-actin (1:5000, Santa Cruz Biotechnology). Densitometry was analyzed using ImageJ software (National Institute of Health, Bethesda-MD, United States of America). Quantified densitometry results were normalized to β-actin.

2.6 Drugs

Carbachol, α-β-methylene-ATP, PHZ, and KCl were purchased from Sigma-Aldrich (St Louis, MO, United States of America. All reagents were required to be of analytical grade. Deionized water was used as a solvent, and working solutions were diluted prior to use.

2.7 Statistical analysis

The GraphPad Prism Program (GraphPad Software Inc.) was used for statistical analysis. Data are expressed as the mean ± SEM of N experiments. Statistical comparisons were made using the Student's unpaired *t*-test. A value of $p < 0.05$ was considered statistically significant.

3 Results

3.1 Hematological parameters

Mice treated with PHZ exhibited significantly reduced levels of red blood cells (Figure 1A) and total hemoglobin (Figure 1B) compared to the control group ($p < 0.05$). Furthermore, there was a marked increase in plasma hemoglobin concentrations in the PHZ group ($p < 0.05$) compared to the control (Figure 1C), confirming the occurrence of intravascular hemolysis.

3.2 Intravascular hemolysis leads to increased urinary frequency and increased void volumes

Figure 2A presents filter paper examples from the control and PHZ-treated mice. The PHZ group showed a significant increase in urinary spots compared to the control group ($p < 0.05$), indicating a hyperactive voiding behavior (Figure 2B). Additionally, the total void volumes produced by the PHZ-treated mice were significantly greater than those of the control mice ($p < 0.05$) (Figure 2C).

3.3 Intravascular hemolysis leads to detrusor hypercontractility

EFS of 4–32 Hz induced frequency-dependent contractions in the detrusor smooth muscle in both control and PHZ-treated mice.

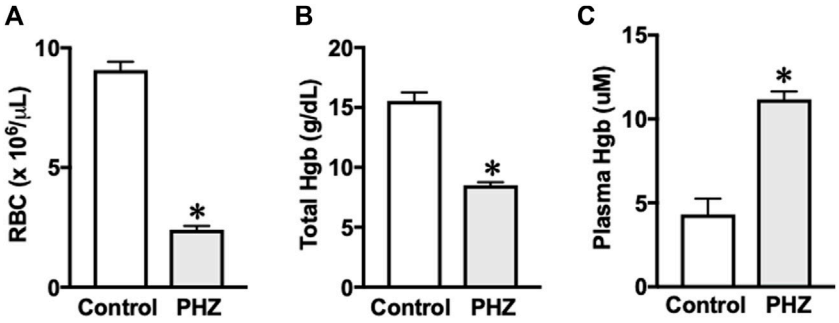

FIGURE 1
(A) Red blood cell, **(B)** hemoglobin, and **(C)** plasma hemoglobin. Data are shown as the mean ± SEM of 5–7 mice per group. *$p < 0.05$ vs. control group.

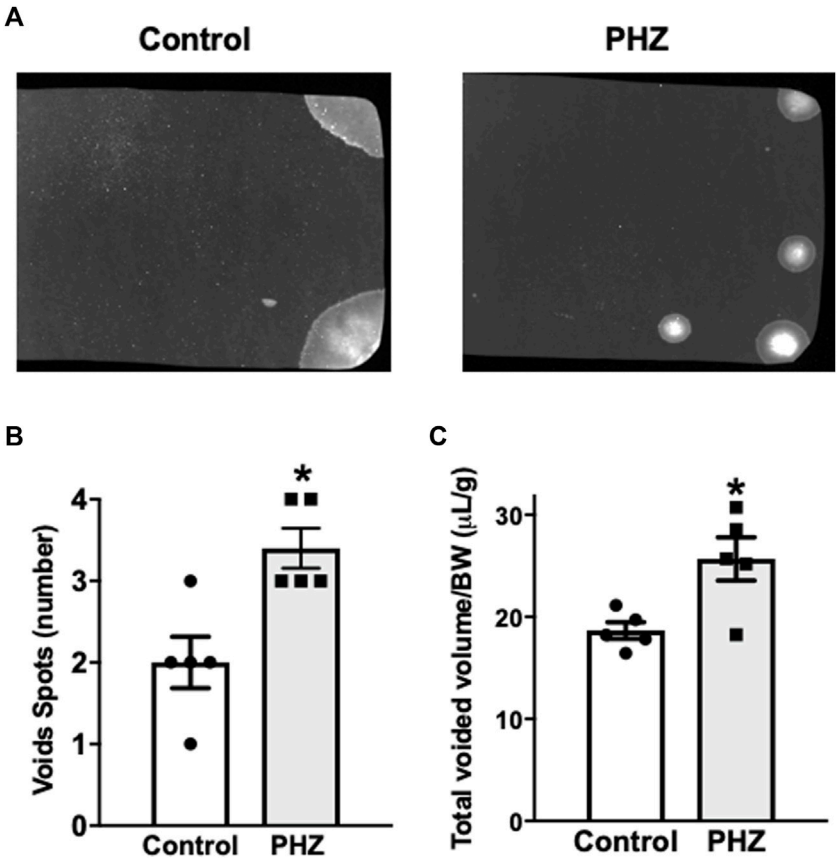

FIGURE 2
(A) Representative void spot assays, **(B)** number of spots, and **(C)** normalized voided volume in control and PHZ mice. Data are shown as the mean ± SEM of five mice per group. *$p < 0.05$ vs. control group.

Notably, the PHZ group exhibited significantly higher contractions at all frequencies compared to the control group ($p < 0.05$) (Figure 3A).

Contractile response to α-β-methylene-ATP in the detrusor smooth muscle was assessed through non-cumulative concentration-effect curves (1 μM, 3 μM, and 10 μM) for both groups (Figure 3B). Detrusor smooth muscle from PHZ-treated mice displayed a significantly enhanced contractile response to α-β-methylene-ATP at all tested concentrations compared to the control ($p < 0.05$) (Figure 3B).

Contraction responses to carbachol were evaluated in detrusor smooth muscle from both PHZ and control mice through concentration-effect curves for the agonist (1 nM–30 μM) (Figure 3C). The maximal contractile response (E_{max}) elicited by carbachol was significantly greater in the detrusor smooth muscle of the PHZ group ($p < 0.05$) than that of the control group (Figure 3D),

10.3389/fphys.2024.1369120

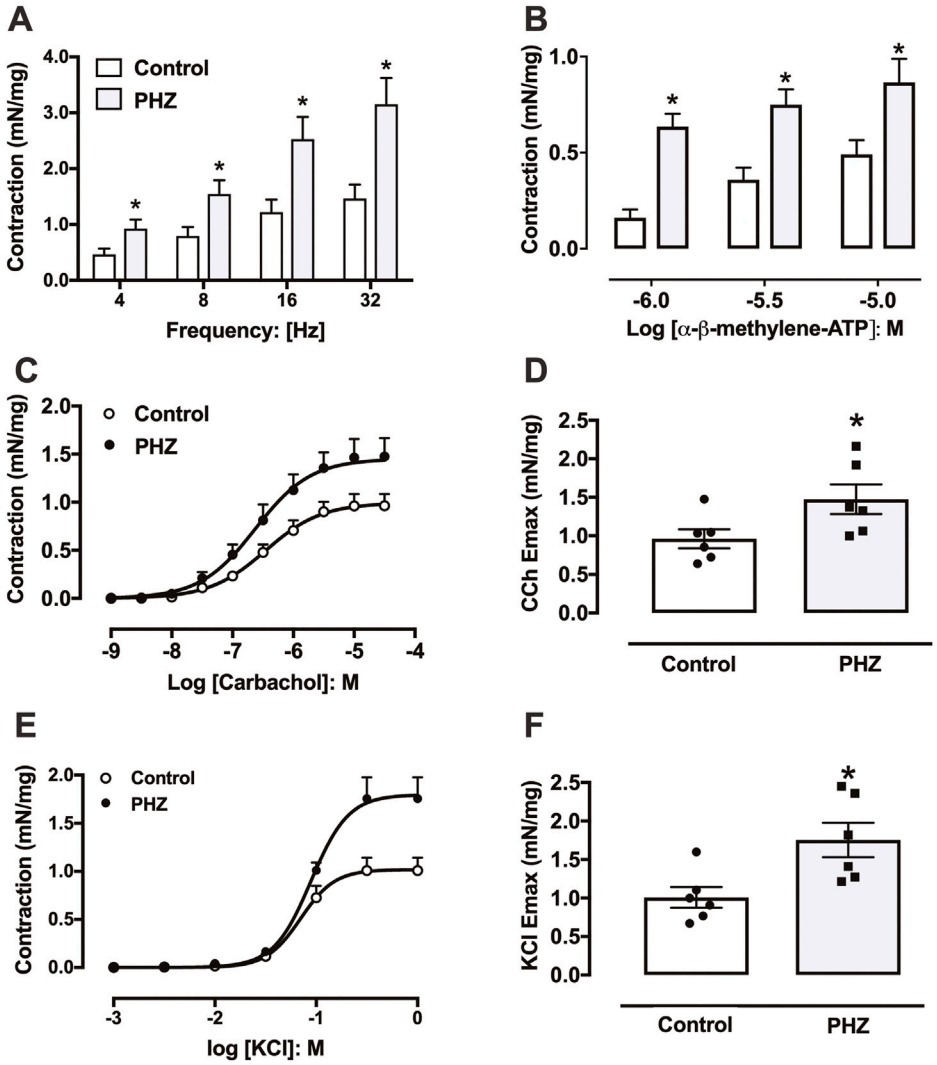

FIGURE 3
Contractile responses to **(A)** electrical field stimulation, **(B)** α-β-methylene-ATP, **(C)** carbachol, and **(E)** KCl in the bladder from control and PHZ mice. **(D)** E_{max} values for **(D)** carbachol and **(F)** KCl. Data are shown as the mean ± SEM of six mice per group. *$p < 0.05$ vs. control group.

with no notable differences in potency (pEC50) between the control (6.45 ± 0.12) and PHZ-treated mice (6.62 ± 0.09). Similarly, KCl induced concentration-dependent contractions in both groups (Figure 3E). Notably, E_{max} to KCl was significantly greater in the PHZ group than in the control group (Figure 3F). No significant differences in potency (pEC50) for KCl were observed between the control group (1.01 ± 0.06) and the PHZ-treated group (6.62 ± 0.09).

Representative traces of responses to EFS, α-β-methylene-ATP, carbachol, and KCl are shown in Figure 4.

3.4 Intravascular hemolysis decreased protein expressions of p-eNOS (Ser-1177), p-nNOS (Ser-1417), and p-VASP (Ser-239) in the mouse bladder

Protein expression of activated (phosphorylated) forms of eNOS (p-eNOS Ser-1177), nNOS (p-nNOS Ser-1417), and VASP (p-VASP Ser-239) was investigated to understand the impact of intravascular hemolysis on signaling of nitric oxide (NO) in the bladder. These enzymes play fundamental roles in the regulation of smooth muscle tone: eNOS and nNOS are responsible for the production of NO, an important mediator of smooth muscle relaxation, while VASP is a substrate of the cGMP-protein kinase G (PKG) pathway, reflecting the activity of NO-cGMP-PKG signaling. PKG, activated by cGMP, is essential for mediating the effects of NO on smooth muscle, promoting relaxation, and directly influencing bladder function (Oelze et al., 2000; Francis et al., 2010). In the PHZ-treated mice, the activated (phosphorylated) forms of p-eNOS (Ser-1177), p-nNOS (Ser-1417), and p-VASP (Ser-239) were significantly reduced in the bladder compared to the control group ($p < 0.05$), as shown in Figure 5. These results suggest that intravascular hemolysis compromises NO signaling in the bladder, potentially contributing to voiding dysfunction.

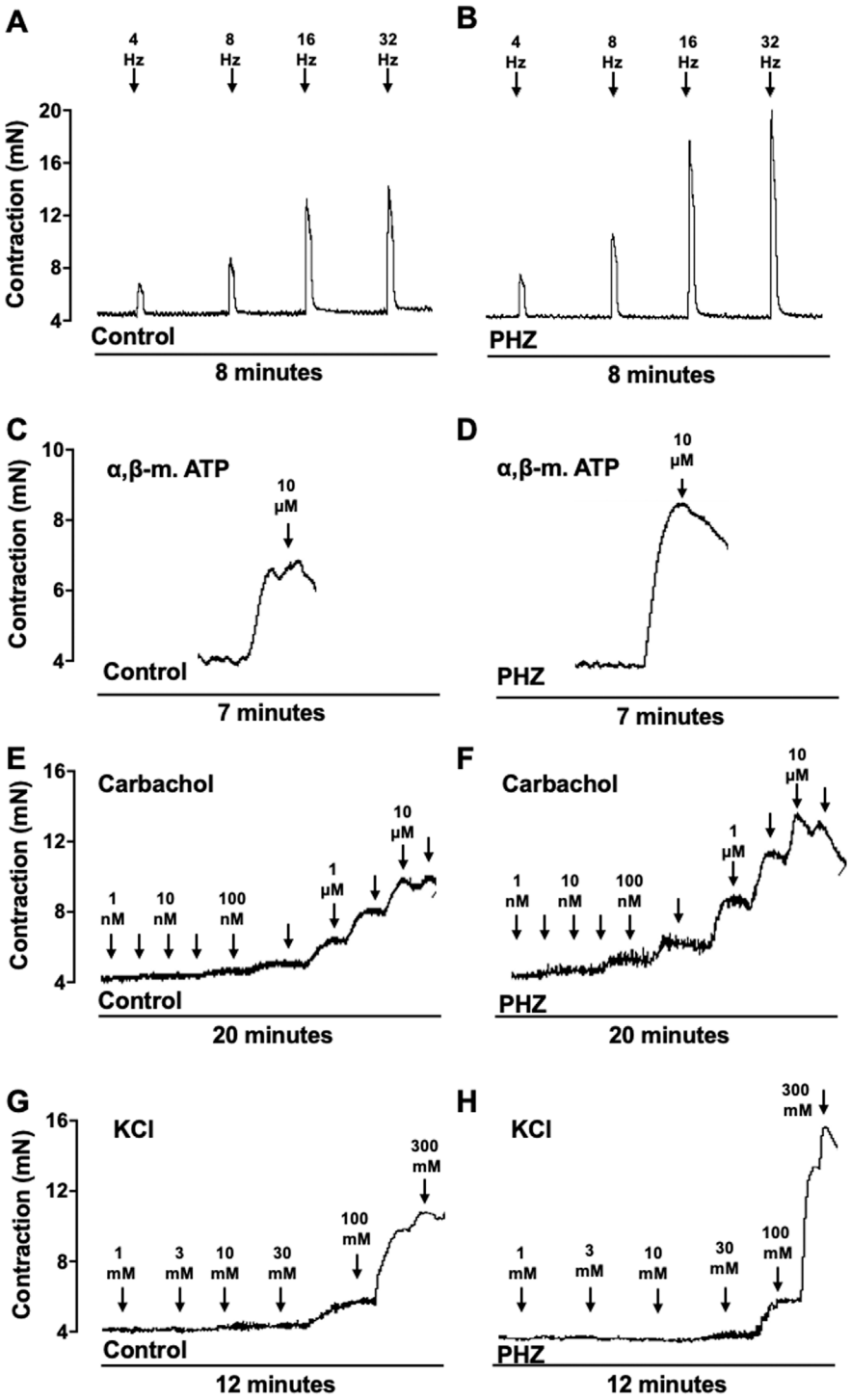

FIGURE 4
Representative tracings of contraction response to EFS, α-β-methylene-ATP, carbachol, and KCl from control and PHZ mice.

3.5 Intravascular hemolysis leads to increased oxidative stress markers in the mouse bladder

To assess the impact of intravascular hemolysis on oxidative stress in the bladder, the protein expression of oxidative stress markers, including NOX-2, 3-NT, and 4-HNE, was examined. NOX-2 is an important enzyme in ROS production, while 3-NT and 4-HNE are products of oxidative damage to proteins, serving as markers of nitrosative and oxidative stress, respectively (Pacher et al., 2007; Vermot et al., 2021). In the PHZ-treated mice, there was a significant increase in the protein expression of oxidative stress markers NOX-2, 3-NT, and 4-HNE in the

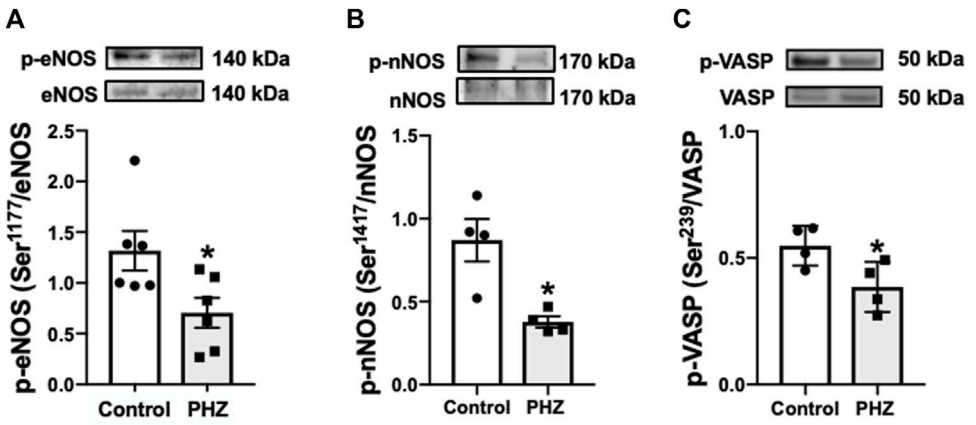

FIGURE 5
Representative images of Western blotting (top panels) and protein values (bottom panels) for **(A)** p-eNOS (ser-1177) (n = 6), **(B)** p-nNOS (ser-1417) (n = 4), and **(C)** p-VASP (Ser-239) (n = 4) in homogenates of bladder from control and PHZ mice. Data are shown as the mean ± SEM. *$p < 0.05$ vs. control group.

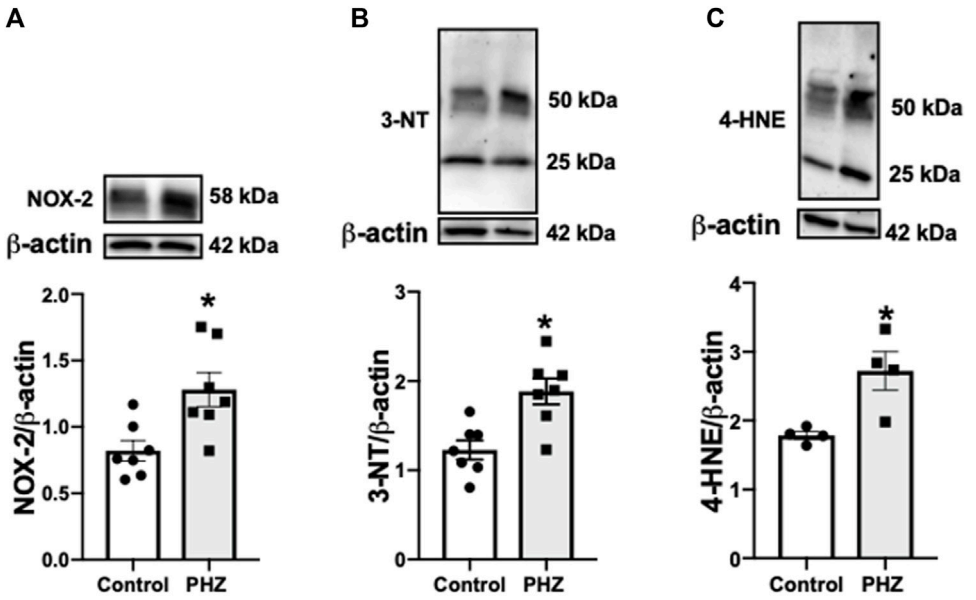

FIGURE 6
Representative images of Western blotting (top panels) and protein values (bottom panels) of **(A)** NOX-2 (n = 7), **(B)** 3-NT (n = 7), and **(C)** 4-HNE (n = 4) in homogenates of the bladder from control and PHZ mice. Data are shown as the mean ± SEM. *$p < 0.05$ vs. control group.

bladder compared to the control group ($p < 0.05$), as shown in Figure 6. This increase in oxidative stress markers indicates that intravascular hemolysis promotes a pro-oxidative environment in the bladder, which may impair organ function and contribute to the development of OAB phenotypes such as those observed in SCD models.

4 Discussion

In this study, PHZ-induced hemolysis in mice led to significant hematological changes, mirroring aspects of SCD. The increased urinary frequency and volume increase in PHZ-treated mice aligns with OAB symptoms, suggesting a link between intravascular hemolysis and bladder dysfunction. Notably, the enhanced contractility of the detrusor muscle in these mice indicates a direct impact of hemolysis on bladder smooth muscle activity. The decreased expression of p-eNOS (Ser-1177), nNOS (Ser-1417), and p-VASP (Ser-239) in the bladder tissue indicates a dysregulated NO signaling pathway in the impaired bladder function. Additionally, elevated oxidative stress markers in the bladders of PHZ-treated mice reinforce the role of oxidative stress in OAB phenotypes.

A central aspect of SCD is intravascular hemolysis, where red blood cell contents like hemoglobin, arginase, and other cellular components are released into the plasma (Kato et al., 2017). The PHZ-induced intravascular hemolysis model in mice is widely utilized for assessing the specific effects of intravascular hemolysis (Vannucchi et al., 2001; Henrique Silva et al., 2018; Iacopucci et al., 2022; Gotardo et al., 2023). Our study corroborates previous findings and confirms that PHZ-induced intravascular hemolysis in mice led to significant hematological changes, closely replicating the hemolytic environment seen in SCD. Free hemoglobin ($HbFe^{2+}$) in the plasma or interstitial space quickly reacts with NO, leading to nitrate production and the formation of methemoglobin ($HbFe^{3+}$), the oxidized form of hemoglobin (Reiter et al., 2002). This process significantly reduces NO bioavailability, contributing to tissue damage (Gladwin et al., 2012; Kato et al., 2017; Kato et al., 2018). An efficient pharmacological strategy that has been studied to limit the effects of hemoglobin involves treatment with haptoglobin. This plasma protein binds to free hemoglobin, forming a complex that is then cleared from circulation by the macrophages of the reticuloendothelial system (Buehler et al., 2020).

NO plays a crucial role in the physiology of the lower urinary tract, with its diminished bioavailability linked to micturition dysfunction. The OAB in SCD mice is associated with decreased expression of phosphorylated eNOS at its positive regulatory site Ser-1177 and phosphorylated nNOS at its positive regulatory site Ser-1412 in the bladder. Similarly, in our study, PHZ mice displayed decreased expression of p-eNOS (Ser-1177) and p-nNOS (Ser-1417), indicating lower NO production in the bladder. NO activates soluble guanylate cyclase (sGC) in smooth muscle, enhancing cGMP production. cGMP activates protein kinase G, which phosphorylates VASP at Ser-239, a reliable biomarker for monitoring the NO-stimulated cGMP-protein kinase G pathway (Oelze et al., 2000; Francis et al., 2010). In our study, protein expression for p-VASP (Ser-239) was lower in the bladder in the PHZ group, indicating decreased cGMP levels. Mice lacking nNOS exhibit bladder hypertrophy, dysfunctional urinary outlets, and increased urinary frequency (Burnett et al., 1997). Additionally, rats treated chronically with a NOS inhibitor develop an OAB phenotype (Mónica et al., 2008; Mónica et al., 2011). Altered micturition patterns have been previously reported in cGMP-dependent protein kinase I gene-deficient mice (Persson et al., 2000). PHZ-treated mice exhibited increased urinary spots and higher total void volumes. These results align with findings from animal models lacking both eNOS and nNOS, as well as SCD mice (Karakus et al., 2019; Musicki et al., 2019; Karakus et al., 2020), reinforcing the importance of NO pathways in urinary function. A prior study speculated that the augmented urine volumes observed in double-NOS (eNOS and nNOS) or triple-NOS (eNOS, nNOS, and iNOS) knockout mice could be attributed to impairments in renal function, specifically in the ability to concentrate urine, leading to polyuria (Morishita et al., 2005).

Acetylcholine, primarily through muscarinic M3 receptors, is the primary excitatory neurotransmitter in the parasympathetic nerve endings of detrusor smooth muscle (Andersson and Arner, 2004). Co-stored and co-released ATP with acetylcholine also play a significant role in nerve-mediated bladder contraction, contributing to efficient urine elimination (Burnstock, 2011). In our study, detrusor contractions induced by EFS were significantly higher in the PHZ-treated group. In parallel, the responses of detrusor smooth muscle to both muscarinic and purinergic receptor agonists (carbachol and α, β-methylene-ATP, respectively), as well as to the receptor-independent agent KCl, were also increased in PHZ-treated mice. These findings indicate that intravascular hemolysis leads to detrusor hypercontractility. The increase in detrusor muscle contraction is likely secondary to the low accumulation of cGMP in bladder tissue, a well-known secondary messenger that counteracts the contractile mechanisms of smooth muscle (Mónica and Antunes, 2018). Rats treated chronically with a non-selective inhibitor of NOS (L-NAME) show increased detrusor contraction induced by muscarinic receptor agonists (Mónica et al., 2008), as well as animal models deficient in both eNOS and nNOS (Karakus et al., 2019), highlighting the importance of the integrity of the NO pathway in bladder function.

Increased oxidative stress, characterized by elevated ROS production or reduced antioxidant capacity, is associated with the development of OAB in experimental models and participates in the pathophysiology of SCD (Alexandre et al., 2016; Silva et al., 2016; Akakpo et al., 2017; Alexandre et al., 2018; Vona et al., 2021; de Oliveira et al., 2022). NOX-2, an important NADPH oxidase isoform, catalyzes electron transfer to oxygen, generating a superoxide anion (Vermot et al., 2021). Excess superoxide reacts with NO, producing peroxynitrite, a highly toxic reactive nitrogen species (Pacher et al., 2007). Increased expression of NOX-2 has been reported in animal models with OAB (Alexandre et al., 2016; Akakpo et al., 2017; Alexandre et al., 2018; de Oliveira et al., 2022). Our study found increased NOX-2 expression in the bladder of PHZ-treated mice and elevated markers of oxidative and nitrosative stress, 4-HNE, and 3-NT. These results fit with our previous findings that demonstrate that PHZ-treated mice exhibit increased oxidative markers like 3-NT, 4-HNE, and NOX-2 in the penis (Iacopucci et al., 2022). Prior research has shown NOX-2 downregulation through NO-cGMP-dependent mechanisms (Teixeira et al., 2007). In contrast, NO inhibits NADPH oxidase-dependent superoxide anion production by a cGMP-independent mechanism without altering the protein expression of NOX-2 (Selemidis et al., 2007). In this context, this suggests that increased plasma hemoglobin may trigger oxidative stress elevation, reducing NO and cGMP bioavailability, as evidenced by reduced p-VASP (Ser-239).

In the present study, we used a PHZ-induced hemolysis model instead of transgenic mice with SCD for a few fundamental reasons. First, the PHZ-induced hemolysis model allows precise control over the onset and intensity of hemolysis, facilitating the direct correlation between hemolysis and the functional and molecular changes observed in the bladder. This precise control is important, as it allowed us to establish a direct relationship between intravascular hemolysis and the observed dysfunctions. Furthermore, this model is widely recognized for its ability to simulate key aspects of intravascular hemolysis observed in sickle cell disease, allowing specific investigation of the mechanisms underlying urinary complications. However, we recognize the value of transgenic models of SCD to study the disease in a broader context.

5 Conclusion

Our study is the first to show that intravascular hemolysis promotes voiding dysfunction correlated with alterations in the NO signaling pathway in the bladder, as evidenced by reduced levels of p-eNOS (Ser-

1177), nNOS (Ser-1417), and p-VASP (Ser-239). The study also showed that intravascular hemolysis increases oxidative stress in the bladder. Our study indicates that intravascular hemolysis promotes OAB phenotypes similar to those observed in patients and mice with SCD, suggesting a potential mechanistic link. These findings suggest that pharmacologic interventions targeting intravascular hemolysis may ameliorate voiding dysfunction in SCD.

Data availability statement

The raw data supporting the conclusion of this article will be made available by the authors, without undue reservation.

Ethics statement

The animal study was approved by the Ethics Committee on Animal Use of the University of San Francisco. The study was conducted in accordance with the local legislation and institutional requirements.

Author contributions

TS: data curation, formal analysis, investigation, methodology, writing–original draft, and writing–review and editing. DlP: formal analysis, investigation, and writing–original draft. DnP: formal analysis, investigation, and writing–original draft. FBC: conceptualization and writing–review and editing. AB: conceptualization, writing–original draft, and writing–review and editing. FFC: conceptualization, writing–original draft, and writing–review and editing. FS: conceptualization, formal analysis, funding acquisition, methodology, writing–original draft, and writing–review and editing.

Funding

The author(s) declare that financial support was received for the research, authorship, and/or publication of this article. This work was supported by São Paulo Research Foundation (grant numbers: 2017/08122-9 and 2019/18886-1).

Conflict of interest

The authors declare that the research was conducted in the absence of any commercial or financial relationships that could be construed as a potential conflict of interest.

Publisher's note

All claims expressed in this article are solely those of the authors and do not necessarily represent those of their affiliated organizations, or those of the publisher, the editors, and the reviewers. Any product that may be evaluated in this article, or claim that may be made by its manufacturer, is not guaranteed or endorsed by the publisher.

References

Akakpo, W., Musicki, B., and Burnett, A. L. (2017). cAMP-dependent regulation of RhoA/Rho-kinase attenuates detrusor overactivity in a novel mouse experimental model. *BJU Int.* 120, 143–151. doi:10.1111/bju.13847

Alexandre, E. C., Calmasini, F. B., de Oliveira, M. G., Silva, F. H., da Silva, C. P. V., André, D. M., et al. (2016). Chronic treatment with resveratrol improves overactive bladder in obese mice via antioxidant activity. *Eur. J. Pharmacol.* 788, 29–36. doi:10.1016/j.ejphar.2016.06.017

Alexandre, E. C., Calmasini, F. B., Sponton, A. C. da S., de Oliveira, M. G., André, D. M., Silva, F. H., et al. (2018). Influence of the periprostatic adipose tissue in obesity-associated mouse urethral dysfunction and oxidative stress: effect of resveratrol treatment. *Eur. J. Pharmacol.* 836, 25–33. doi:10.1016/j.ejphar.2018.08.010

Andersson, K.-E., and Arner, A. (2004). Urinary bladder contraction and relaxation: physiology and pathophysiology. *Physiol. Rev.* 84, 935–986. doi:10.1152/physrev.00038.2003

Anele, U. A., Morrison, B. F., Reid, M. E., Madden, W., Foster, S., and Burnett, A. L. (2015). Overactive bladder in adults with sickle cell disease. *Neurourol. Urodyn.* 35, 642–646. doi:10.1002/nau.22777

Buehler, P. W., Humar, R., and Schaer, D. J. (2020). Haptoglobin therapeutics and compartmentalization of cell-free hemoglobin toxicity. *Trends Mol. Med.* 26, 683–697. doi:10.1016/j.molmed.2020.02.004

Burnett, A. L., Calvin, D. C., Chamness, S. L., Liu, J. X., Nelson, R. J., Klein, S. L., et al. (1997). Urinary bladder-urethral sphincter dysfunction in mice with targeted disruption of neuronal nitric oxide synthase models idiopathic voiding disorders in humans. *Nat. Med.* 3, 571–574. doi:10.1038/nm0597-571

Burnstock, G. (2011). Therapeutic potential of purinergic signalling for diseases of the urinary tract. *BJU Int.* 107, 192–204. doi:10.1111/j.1464-410X.2010.09926.x

Cita, K.-C., Brureau, L., Lemonne, N., Billaud, M., Connes, P., Ferdinand, S., et al. (2016). Men with sickle cell anemia and priapism exhibit increased hemolytic rate, decreased red blood cell deformability and increased red blood cell aggregate strength. *PLoS ONE* 11, e0154866. doi:10.1371/journal.pone.0154866

Claudino, M. A., Leiria, L. O. S., da Silva, F. H., Alexandre, E. C., Renno, A., Mónica, F. Z., et al. (2015). Urinary bladder dysfunction in transgenic sickle cell disease mice. *PLoS ONE* 10, e0133996. doi:10.1371/journal.pone.0133996

de Oliveira, M. G., Monica, F. Z., Passos, G. R., Victorio, J. A., Davel, A. P., Oliveira, A. L. L., et al. (2022). Selective pharmacological inhibition of NOX2 by GSK2795039 improves bladder dysfunction in cyclophosphamide-induced cystitis in mice. *Antioxidants (Basel)* 12, 92. doi:10.3390/antiox12010092

Dutra, F. F., Alves, L. S., Rodrigues, D., Fernandez, P. L., de Oliveira, R. B., Golenbock, D. T., et al. (2014). Hemolysis-induced lethality involves inflammasome activation by heme. *Proc. Natl. Acad. Sci. U.S.A.* 111, E4110–E4118. doi:10.1073/pnas.1405023111

Eapen, R. S., and Radomski, S. B. (2016). Review of the epidemiology of overactive bladder. *RRU* 8, 71–76. doi:10.2147/RRU.S102441

Francis, S. H., Busch, J. L., Corbin, J. D., and Sibley, D. (2010). cGMP-dependent protein kinases and cGMP phosphodiesterases in nitric oxide and cGMP action. *Pharmacol. Rev.* 62, 525–563. doi:10.1124/pr.110.002907

Gladwin, M. T., Kanias, T., and Kim-Shapiro, D. B. (2012). Hemolysis and cell-free hemoglobin drive an intrinsic mechanism for human disease. *J. Clin. Investig.* 122, 1205–1208. doi:10.1172/JCI62972

Gotardo, É. M. F., Brito, P. L., Gushiken, L. F. S., Chweih, H., Leonardo, F. C., Costa, F. F., et al. (2023). Molecular and cellular effects of *in vivo* chronic intravascular hemolysis and anti-inflammatory therapeutic approaches. *Vasc. Pharmacol.* 150, 107176. doi:10.1016/j.vph.2023.107176

Henrique Silva, F., Yotsumoto Fertrin, K., Costa Alexandre, E., Beraldi Calmasini, F., Fernanda Franco-Penteado, C., and Ferreira Costa, F. (2018). Impairment of nitric oxide pathway by intravascular hemolysis plays a major role in mice esophageal hypercontractility: reversion by soluble guanylyl cyclase stimulator. *J. Pharmacol. Exp. Ther.* 367, 194–202. doi:10.1124/jpet.118.249581

Iacopucci, A. P. M., da Silva Pereira, P., Pereira, D. A., Calmasini, F. B., Pittalà, V., Reis, L. O., et al. (2022). Intravascular hemolysis leads to exaggerated corpus cavernosum relaxation: implication for priapism in sickle cell disease. *FASEB J.* 36, e22535. doi:10.1096/fj.202200867R

Karakus, S., Anele, U. A., Silva, F. H., Musicki, B., and Burnett, A. L. (2019). Urinary dysfunction in transgenic sickle cell mice: model of idiopathic overactive bladder syndrome. *Am. J. Physiol. Ren. Physiol.* 317, F540-F546–F546. doi:10.1152/ajprenal.00140.2019

Karakus, S., Musicki, B., Navati, M. S., Friedman, J. M., Davies, K. P., and Burnett, A. L. (2020). NO-releasing nanoparticles ameliorate detrusor overactivity in transgenic sickle cell mice via restored NO/ROCK signaling. *J. Pharmacol. Exp. Ther.* 373, 214–219. doi:10.1124/jpet.119.264697

Kato, G. J., McGowan, V., Machado, R. F., Little, J. A., Taylor, J., Morris, C. R., et al. (2006). Lactate dehydrogenase as a biomarker of hemolysis-associated nitric oxide resistance, priapism, leg ulceration, pulmonary hypertension, and death in patients with sickle cell disease. *Blood* 107, 2279–2285. doi:10.1182/blood-2005-06-2373

Kato, G. J., Piel, F. B., Reid, C. D., Gaston, M. H., Ohene-Frempong, K., Krishnamurti, L., et al. (2018). Sickle cell disease. *Nat. Rev. Dis. Prim.* 4, 18010. doi:10.1038/nrdp.2018.10

Kato, G. J., Steinberg, M. H., and Gladwin, M. T. (2017). Intravascular hemolysis and the pathophysiology of sickle cell disease. *J. Clin. Investig.* 127, 750–760. doi:10.1172/JCI89741

Keil, K. P., Abler, L. L., Altmann, H. M., Bushman, W., Marker, P. C., Li, L., et al. (2016). Influence of animal husbandry practices on void spot assay outcomes in C57BL/6J male mice. *Neurourol. Urodyn.* 35, 192–198. doi:10.1002/nau.22692

Khan, M. A., Dashwood, M. R., Thompson, C. S., Mumtaz, F. H., Mikhailidis, D. P., and Morgan, R. J. (1999). Up-regulation of endothelin (ET(A) and ET(B)) receptors and down-regulation of nitric oxide synthase in the detrusor of a rabbit model of partial bladder outlet obstruction. *Urol. Res.* 27, 445–453. doi:10.1007/s002400050134

Lee, W.-C., Leu, S., Wu, K. L. H., Tain, Y.-L., Chuang, Y.-C., and Chan, J. Y. H. (2021). Tadalafil ameliorates bladder overactivity by restoring insulin-activated detrusor relaxation via the bladder mucosal IRS/PI3K/AKT/eNOS pathway in fructose-fed rats. *Sci. Rep.* 11, 8202. doi:10.1038/s41598-021-87505-3

Leiria, L. O., Silva, F. H., Davel, A. P. C., Alexandre, E. C., Calixto, M. C., De Nucci, G., et al. (2014). The soluble guanylyl cyclase activator BAY 60-2770 ameliorates overactive bladder in obese mice. *J. Urol.* 191, 539–547. doi:10.1016/j.juro.2013.09.020

Leiria, L. O., Sollon, C., Báu, F. R., Mónica, F. Z., D'Ancona, C. L., De Nucci, G., et al. (2013). Insulin relaxes bladder via PI3K/AKT/eNOS pathway activation in mucosa: unfolded protein response-dependent insulin resistance as a cause of obesity-associated overactive bladder. *J. Physiol.* 591, 2259–2273. doi:10.1113/jphysiol.2013.251843

Lim, S. K., Kim, H., Lim, S. K., bin Ali, A., Lim, Y. K., Wang, Y., et al. (1998). Increased susceptibility in Hp knockout mice during acute hemolysis. *Blood* 92, 1870–1877. doi:10.1182/blood.v92.6.1870

Michel, M. C., and Chapple, C. R. (2009). Basic mechanisms of urgency: preclinical and clinical evidence. *Eur. Urol.* 56, 298–307. doi:10.1016/j.eururo.2009.05.028

Mónica, F. Z., and Antunes, E. (2018). Stimulators and activators of soluble guanylate cyclase for urogenital disorders. *Nat. Rev. Urol.* 15, 42–54. doi:10.1038/nrurol.2017.181

Mónica, F. Z., Reges, R., Cohen, D., Silva, F. H., De Nucci, G., D'Ancona, C. A. L., et al. (2011). Long-term administration of BAY 41-2272 prevents bladder dysfunction in nitric oxide-deficient rats. *Neurourol. Urodyn.* 30, 456–460. doi:10.1002/nau.20992

Mónica, F. Z. T., Bricola, A. a. O., Báu, F. R., Freitas, L. L. L., Teixeira, S. A., Muscará, M. N., et al. (2008). Long-term nitric oxide deficiency causes muscarinic supersensitivity and reduces beta(3)-adrenoceptor-mediated relaxation, causing rat detrusor overactivity. *Br. J. Pharmacol.* 153, 1659–1668. doi:10.1038/bjp.2008.39

Morishita, T., Tsutsui, M., Shimokawa, H., Sabanai, K., Tasaki, H., Suda, O., et al. (2005). Nephrogenic diabetes insipidus in mice lacking all nitric oxide synthase isoforms. *Proc. Natl. Acad. Sci. U. S. A.* 102, 10616–10621. doi:10.1073/pnas.0502236102

Musicki, B., Anele, U. A., Campbell, J. D., Karakus, S., Shiva, S., Silva, F. H., et al. (2019). Dysregulated NO/PDE5 signaling in the sickle cell mouse lower urinary tract: reversal by oral nitrate therapy. *Life Sci.* 238, 116922. doi:10.1016/j.lfs.2019.116922

Nolan, V. G., Wyszynski, D. F., Farrer, L. A., and Steinberg, M. H. (2005). Hemolysis-associated priapism in sickle cell disease. *Blood* 106, 3264–3267. doi:10.1182/blood-2005-04-1594

Oelze, M., Mollnau, H., Hoffmann, N., Warnholtz, A., Bodenschatz, M., Smolenski, A., et al. (2000). Vasodilator-stimulated phosphoprotein serine 239 phosphorylation as a sensitive monitor of defective nitric oxide/cGMP signaling and endothelial dysfunction. *Circ. Res.* 87, 999–1005. doi:10.1161/01.res.87.11.999

Pacher, P., Beckman, J. S., and Liaudet, L. (2007). Nitric oxide and peroxynitrite in health and disease. *Physiol. Rev.* 87, 315–424. doi:10.1152/physrev.00029.2006

Persson, K., Pandita, R. K., Aszòdi, A., Ahmad, M., Pfeifer, A., Fässler, R., et al. (2000). Functional characteristics of urinary tract smooth muscles in mice lacking cGMP protein kinase type I. *Am. J. Physiol. Regul. Integr. Comp. Physiol.* 279, R1112–R1120. doi:10.1152/ajpregu.2000.279.3.R1112

Portocarrero, M. L., Portocarrero, M. L., Sobral, M. M., Lyra, I., Lordêlo, P., and Barroso, Jr. U. (2012). Prevalence of enuresis and daytime urinary incontinence in children and adolescents with sickle cell disease. *J. Urology* 187, 1037–1040. doi:10.1016/j.juro.2011.10.171

Reiter, C. D., Wang, X., Tanus-Santos, J. E., Hogg, N., Cannon, R. O., Schechter, A. N., et al. (2002). Cell-free hemoglobin limits nitric oxide bioavailability in sickle-cell disease. *Nat. Med.* 8, 1383–1389. doi:10.1038/nm1202-799

Selemidis, S., Dusting, G. J., Peshavariya, H., Kemp-Harper, B. K., and Drummond, G. R. (2007). Nitric oxide suppresses NADPH oxidase-dependent superoxide production by S-nitrosylation in human endothelial cells. *Cardiovasc. Res.* 75, 349–358. doi:10.1016/j.cardiores.2007.03.030

Silva, F. H., Karakus, S., Musicki, B., Matsui, H., Bivalacqua, T. J., Dos Santos, J. L., et al. (2016). Beneficial effect of the nitric oxide donor compound 3-(1,3-Dioxoisoindolin-2-yl)Benzyl nitrate on dysregulated phosphodiesterase 5, NADPH oxidase, and nitrosative stress in the sickle cell mouse penis: implication for priapism treatment. *J. Pharmacol. Exp. Ther.* 359, 230–237. doi:10.1124/jpet.116.235473

Teixeira, C. E., Priviero, F. B. M., and Webb, R. C. (2007). Effects of 5-Cyclopropyl-2-[1-(2-fluoro-benzyl)-1H-pyrazolo[3,4-b]pyridine-3-yl]pyrimidin-4-ylamine (BAY 41-2272) on smooth muscle tone, soluble guanylyl cyclase activity, and NADPH oxidase activity/expression in corpus cavernosum from wild-type, neuronal, and endothelial nitric-oxide synthase null mice. *J. Pharmacol. Exp. Ther.* 322, 1093–1102. doi:10.1124/jpet.107.124594

Vannucchi, A. M., Bianchi, L., Cellai, C., Paoletti, F., Carrai, V., Calzolari, A., et al. (2001). Accentuated response to phenylhydrazine and erythropoietin in mice genetically impaired for their GATA-1 expression (GATA-1(low) mice). *Blood* 97, 3040–3050. doi:10.1182/blood.v97.10.3040

Vermot, A., Petit-Härtlein, I., Smith, S. M. E., and Fieschi, F. (2021). NADPH oxidases (NOX): an overview from discovery, molecular mechanisms to physiology and pathology. *Antioxidants (Basel)* 10, 890. doi:10.3390/antiox10060890

Vona, R., Sposi, N. M., Mattia, L., Gambardella, L., Straface, E., and Pietraforte, D. (2021). Sickle cell disease: role of oxidative stress and antioxidant therapy. *Antioxidants* 10, 296. doi:10.3390/antiox10020296

frontiers | Frontiers in Immunology

TYPE Original Research
PUBLISHED 28 November 2024
DOI 10.3389/fimmu.2024.1413078

OPEN ACCESS

EDITED BY
Monica Akemi Sato,
Faculdade de Medicina do ABC, Brazil

REVIEWED BY
Warren G. Hill,
Beth Israel Deaconess Medical Center, Harvard Medical School, United States
Cristiano Gonçalves Ponte,
Federal University of Rio de Janeiro, Brazil

*CORRESPONDENCE
Kexin Xu
cavinx@yeah.net
Qi Wang
15810797491@163.com

†These authors have contributed equally to this work and share first authorship

RECEIVED 06 April 2024
ACCEPTED 08 November 2024
PUBLISHED 28 November 2024

CITATION
Ke H, Zhu L, Zhang W, Wang H, Ding Z, Su D, Wang Q and Xu K (2024) PACAP/PAC1 regulation in cystitis rats: induction of bladder inflammation cascade leading to bladder dysfunction. *Front. Immunol.* 15:1413078. doi: 10.3389/fimmu.2024.1413078

PACAP/PAC1 regulation in cystitis rats: induction of bladder inflammation cascade leading to bladder dysfunction

Hanwei Ke[1,2†], Lin Zhu[3†], Weiyu Zhang[1,2], Huanrui Wang[1,2], Zehua Ding[1,2], Dongyu Su[1,2], Qi Wang[1,2*] and Kexin Xu[1,2*]

[1]Department of Urology, Peking University People's Hospital, Beijing, China, [2]Peking University Applied Lithotripsy Institute, Peking University People's Hospital, Beijing, China, [3]Department of Plastic Surgery, Affiliated Beijing Chaoyang Hospital of Capital Medical University, Beijing, China

Introduction: Interstitial Cystitis/Bladder Pain Syndrome (IC/BPS) is a chronic and debilitating condition marked by bladder pain, urinary urgency, and frequency. The pathophysiology of IC/BPS remains poorly understood, with limited therapeutic options available. The role of Pituitary Adenylate Cyclase-Activating Polypeptide (PACAP) and its receptor PAC1 in IC/BPS has not been thoroughly investigated, despite their potential involvement in inflammation and sensory dysfunction. This study aims to examine the expression and functional role of the PACAP/PAC1 signaling pathway in the pathogenesis of IC/BPS.

Methods: Bladder tissue samples from IC/BPS patients and a rat model of cystitis were analyzed to evaluate PACAP and PAC1 expression. Transcriptomic analysis, immunohistochemistry, and bladder function assays were employed to assess the correlation between PACAP/PAC1 activation, bladder inflammation, and sensory dysfunction. Additionally, modulation of the PACAP/PAC1 pathway was tested in rats to determine its effects on bladder inflammation and function.

Results: Our results demonstrate significant upregulation of PACAP and PAC1 in both human bladder tissues from IC/BPS patients and in the rat cystitis model. This upregulation was associated with increased bladder inflammation and sensory dysfunction. Intervention with PACAP/PAC1 pathway modulation in rats resulted in a marked reduction in bladder inflammation and improvement in bladder function, suggesting the pathway's pivotal role in disease progression.

Discussion: The findings provide compelling evidence that the PACAP/PAC1 pathway is involved in the inflammatory and sensory changes observed in IC/BPS. By targeting this signaling pathway, we may offer a novel therapeutic approach to mitigate the symptoms of IC/BPS. This study enhances our understanding of the molecular mechanisms driving IC/BPS and opens avenues for the development of targeted treatments.

KEYWORDS

interstitial cystitis, bladder pain syndrome, PACAP, PAC1 receptor, bladder inflammation

Introduction

Interstitial cystitis/bladder pain syndrome (IC/BPS) is a complex chronic inflammatory bladder disorder, marked by bladder pain, nocturia, urgency, sterile urine, and frequent urination (1, 2). Despite various hypotheses, the origin of IC/BPS remains unclear, and its pathophysiology is poorly understood (3). IC/BPS primarily affects females, with an estimated prevalence of 6.53% among women in the U.S (4). No therapeutic approach has yet consistently succeeded in providing lasting relief from IC/BPS symptoms (5). The exact origin and pathophysiology of IC/BPS remain unclear, though emerging research highlights bladder urothelial injury or dysfunction and a sustained inflammatory cycle as key factors (6, 7).

Pituitary adenylate cyclase-activating polypeptide (PACAP), a neuropeptide, plays a role in regulating lower urinary tract (LUT) functions (8–10). Part of the vasoactive intestinal polypeptide (VIP), secretin, and glucagon hormone family, PACAP shares about 68% homology with VIP. Neuropeptides such as PACAP are expressed in both neural and non-neural tissues of the LUT, including afferent neurons, neural pathways, plasma, inflammation or injury sites, bladder fibroblasts, detrusor muscle, and urothelium (11). PACAP immunoreactivity appears in the C-fiber bladder afferents of the dorsal root ganglia (DRG), bladder smooth muscle, sub-urothelial nerve plexus, and peri-vascular nerve fibers (12). Urothelial cells express the PACAP receptor PAC1, which releases ATP upon PACAP stimulation, activating receptors on sub-urothelial sensory nerve fibers (13). Braas et al. demonstrated PACAP's role in micturition, emphasizing how inflammation-induced changes in peripheral and central micturition pathways can contribute to bladder dysfunction (10).

The pathophysiology of IC/BPS involves a complex sequence of inflammatory responses, possibly initiated or aggravated by neuropeptide dysregulation, including PACAP. However, the exact role and regulatory mechanisms of these neuropeptides in bladder inflammation and post-inflammatory dysfunction remain poorly understood. Although previous research has highlighted PACAP's general involvement in inflammation and its potential relevance to IC/BPS, a substantial gap remains in understanding the specific mechanisms by which PACAP/PAC1 interactions impact the inflammatory cascade in IC/BPS. This study aims to narrow this gap by examining the regulatory role of PACAP/PAC1 in a rat model of bladder cystitis, focusing on PACAP induction, inflammation progression, and its effects on bladder function in IC/BPS.

Materials and methods

Ethical approval and informed consent

The research protocol was approved by the Ethics Committee of Peking University People's Hospital and complies with the principles outlined in the Helsinki Declaration. The ethical approval number is 2022PHB400-001. All patients have provided informed consent.

Sample collection

Bladder tissue specimens were collected from patients diagnosed with IC/BPS during cystoscopy and biopsy at Peking University People's Hospital. The diagnostic criteria for IC/BPS were based on the guidelines of the American Urological Association (14). Control bladder specimens were taken from normal tissue adjacent to cancerous areas in patients with bladder cancer. Six Hunner-type interstitial cystitis (HIC) samples and three normal samples were used for transcriptome sequencing and immunohistochemical validation.

Transcriptomic research methods of bladder biopsy

RNA extraction and sequencing

Tissue samples were collected, and RNA was extracted using the Trizol reagent kit (Invitrogen, Carlsbad, CA, USA) following the manufacturer's guidelines. RNA quality was assessed with the Agilent 2100 Bioanalyzer (Agilent Technologies, Palo Alto, CA, USA). After total RNA extraction, eukaryotic mRNA was enriched using Oligo(dT). The mRNA was then fragmented and reverse-transcribed into cDNA using the NEBNext Ultra RNA Library Prep Kit for Illumina (NEB#7530, New England Biolabs, Ipswich, MA, USA), and sequenced on an Illumina Novaseq6000 platform by Gene Denovo Biotechnology Co. (Guangzhou, China).

Partial least squares-discriminant analysis

To investigate molecular differences between Hunner-type interstitial cystitis (HIC) patients and normal controls, we performed PLS-DA. This method identifies variables with high separation capability, focusing on differences in gene expression profiles from high-throughput RNA sequencing data. Before analysis, data were log-transformed and auto-scaled to stabilize variance and ensure comparability across samples.

Immunoinfiltration analysis

The extent and patterns of immune cell infiltration in bladder tissues were analyzed through immunohistochemistry. Specific markers for immune cells, such as CD4, CD8, and FoxP3, were used to stain tissue sections. High-resolution microscope images were captured, and the percentage of positively stained cells was quantified with ImageJ software. This approach provided insights into the immune landscape of HIC and normal bladder tissues.

RNA data analysis

Ribosomal RNA alignment was followed by genome alignment using HISAT2 and quantification with StringTie. FPKM values were calculated with RSEM software. Differential expression analysis between groups was conducted using DESeq2, applying criteria of fold change ≥ 2 and FDR < 0.05. Gene Ontology (GO) and Kyoto Encyclopedia of Genes and Genomes (KEGG) enrichment analyses of differentially expressed mRNAs (DEmRNAs) were performed using hypergeometric tests.

Additionally, gene set enrichment analysis (GSEA) was used to determine the functions of differentially expressed genes between groups.

Animals

Sprague-Dawley female rats (7 weeks old) were obtained from Janvier Labs. The animals were kept at a controlled temperature (21 ± 3°C) on a 12-hour light/dark cycle with free access to food and water. Rats were acclimated to laboratory conditions for at least 3 days before the start of experiments. At the end of the procedures, rats were euthanized humanely using CO2 inhalation (100%, 3 L/min), followed by cervical dislocation. All animal experiments were approved by the Medical Ethics Committee of Peking University People's Hospital (Approval number: 2019PHE060).

Induction of cystitis and drug treatments

Chronic cystitis was induced in Sprague-Dawley rats through intraperitoneal injections of cyclophosphamide (CYP) from Sigma-Aldrich, St. Louis, MO, USA, at 25 mg/kg every third day (days 0, 3, 6). Control rats received intraperitoneal injections of 0.9% NaCl saline (5 ml/kg) under the same conditions. The study included 42 rats, randomized into six groups: Con-Con (intraperitoneal and intravesical saline), CYP-Con (intraperitoneal CYP and intravesical saline), CYP-PAC (intraperitoneal CYP and intravesical PACAP6-38), Con-PAC (intraperitoneal saline and intravesical PACAP6-38), CYP-Treated (intraperitoneal CYP and intrathecal PACAP6-38), and CYP-Untreated (intraperitoneal CYP and intrathecal saline). PACAP6-38, a potent PAC1 receptor antagonist (15), was administered at 300 nM for intravesical and 50 nM for intrathecal administration to explore its therapeutic potential in alleviating symptoms associated with interstitial cystitis, particularly those induced by cyclophosphamide (CYP). Intravesical infusion was performed under anesthesia with a clamped urethra for 30 minutes. Intrathecal injection was conducted at the S1 spinal segment, with tail flicking indicating successful puncture. These procedures were carried out two days post-modeling. Intravesical infusion was performed under anesthesia with a clamped urethra for 30 minutes. Intrathecal injection was conducted at the S1 spinal segment, with tail flicking indicating successful puncture. These procedures were carried out two days post-modeling (Figure 1).

Von Frey filaments test

Following the third CYP or saline bladder instillation and subsequent drug treatment, nociceptive responses were assessed. Mechanical stimulation of the lower abdomen near the bladder was conducted using eight von Frey filaments with progressively increasing force (North Coast, USA), following previous protocols (16). To maintain consistency in pain testing, all tests were conducted by a single experimenter under standardized conditions. Before testing, the designated abdominal area on each rat was shaved. The rats were placed in individual transparent Plexiglas boxes on an elevated wire mesh floor and acclimated for at least 30 minutes. During the von Frey test, each filament was applied through the mesh for 1–2 seconds with sufficient force to bend slightly. This process was repeated three times for each filament with a 5-second interval between applications, and care was taken to vary the stimulated areas near the bladder to prevent desensitization. Nociceptive response scoring was defined as follows: 0 = no response; 1 = abdominal retraction; 2 = retraction plus position change; 3 = retraction, position change, licking the stimulated area, and/or vocalization. The nociceptive score was calculated as a percentage of the maximum possible score from the three pooled applications (17).

Urination patterns

During the experiment, Sprague-Dawley (SD) rats were individually placed in standard cages for 1 hour, with the bedding replaced by Whatman Grade 3 filter paper. The rats had unrestricted access to food and water. Urine spots were photographed under UV light to measure the percentage of the area they covered. The area of the urine spots was analyzed and calculated using ImageJ software.

Filling cystometry

Before the experiment, air is removed from the infusion pump and tubing, and the pump is set to 6 mL/h. Anesthesia is induced in the rat using inhaled isoflurane and maintained with an animal face mask while the rat is placed in a supine position on the platform. The urethral orifice is disinfected, and a 19G pressure catheter is carefully inserted 3 cm deep into the bladder through the urethra and secured with adhesive tape. With a physiological saline infusion, urinary dynamics are monitored via computer software, and data is recorded using the pressure gauge. The experiment begins once the urinary dynamic curve stabilizes.

Immunohistochemistry

Paraffin sections were deparaffinized and rehydrated using dewaxing solution and graded ethanol. Antigen retrieval was subsequently performed through microwave treatment in citrate buffer (pH 6.0). After natural cooling, sections were rinsed with PBS and blocked for endogenous peroxidase using a 3% hydrogen peroxide solution. Serum blocking with 3% BSA was conducted, and primary antibodies were applied and incubated overnight at 4°C. After washing, appropriate secondary antibodies were applied, and the sections were incubated at room temperature. DAB staining followed, monitored under a microscope, and was stopped with tap water rinsing. Counterstaining with hematoxylin, graded dehydration, and mounting with coverslips were followed by microscopic examination for results. Aipathwell software was used

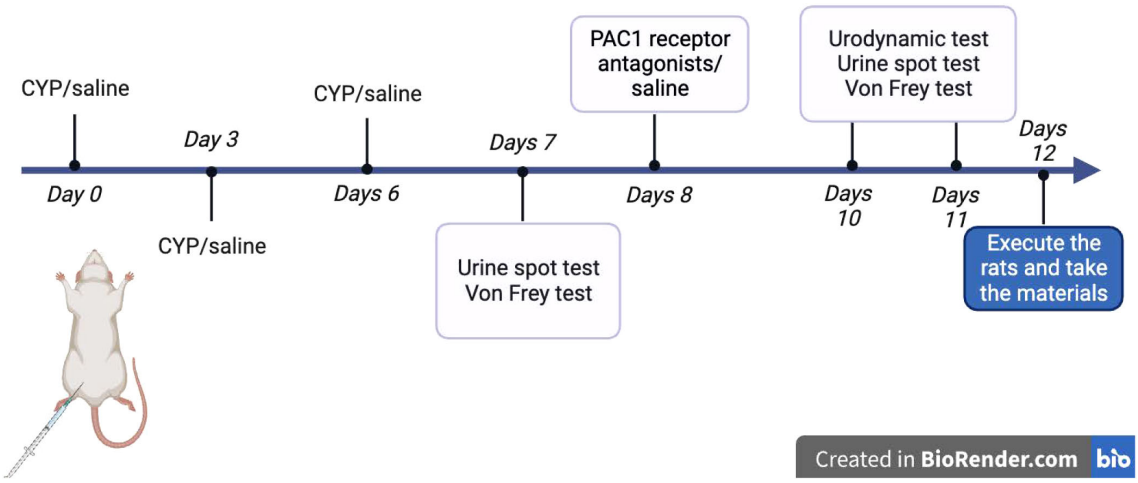

FIGURE 1
Schematic diagram of methodology for animal experiments: Schematic diagram illustrating the methodology for animal experiments conducted with Sprague-Dawley rats. This includes the steps of inducing chronic cystitis via intraperitoneal injections of cyclophosphamide (CYP), control treatments, and subsequent administrations of PACAP6-38, both intravesically and intrathecally, with specific concentrations. Tail flicking in response to intrathecal injections in the S1 spinal segment confirmed the accuracy of the procedure.

for automated positioning, positive expression determination, and H-SCORE calculation based on staining intensity percentages. (H-SCORE = Σ(pi × i) = (percentage of weak intensity × 1) + (percentage of moderate intensity × 2) + (percentage of strong intensity × 3)).

Bladder inflammation assessment and histopathology

Animals were sacrificed at the indicated times after the first injection of CYP or saline. Urinary bladders were quickly collected and assessed for bladder weight, wall thickness, and edema evaluation. Urinary bladders were quickly collected and assessed for bladder weight, wall thickness, and edema evaluation. Each bladder was examined macroscopically for edema and scored based on criteria established by Gray et al. (18) as follows: absent (0), mild (1), moderate (2), and severe (3). Edema was classified as severe when fluid was observed both externally and internally on the bladder wall. Edema confined to the internal mucosa was classified as moderate. Edema between normal and moderate was defined as mild. Bladders were fixed in 10% formalin and embedded in paraffin. Bladder sections were stained with hematoxylin and eosin (HE) and digitized using a slide scanner (Nanozoomer, Hamamatsu, objective ×20).

Statistical analysis

Statistical analysis and visualization in this study were conducted using R software (version 3.6.3). For normally distributed quantitative data, results were presented as mean ± standard deviation, while non-normally distributed data were represented as median and interquartile range. Comparisons between two groups with normally distributed data were assessed using an independent samples t-test, while a paired t-test was used for pre- and post-treatment efficacy comparisons. For data that did not pass the Shapiro-Wilk normality test, statistical analysis was performed using the Wilcoxon rank sum test. For data that did not meet the normality assumptions for multiple groups, the Kruskal-Wallis rank sum test was used, and significance was corrected with the Bonferroni method.

Result

Elucidating the immunopathogenesis of IC/BPS: insights from molecular profiling and pathway analysis

PLS-DA revealed discernible differences between the two sample cohorts, with minimal overlap, indicating statistically significant distinctions (Figure 2A).

GO analysis highlighted significant biological processes, molecular functions, and cellular components, especially those related to immune processes and cell signaling. More than 11,000 entries were associated with immune system processes. KEGG analysis demonstrated the importance of various pathways, such as Hematopoietic cell lineage and Allograft rejection, highlighting the immunological aspect of IC/BPS pathology (Figures 2B, C).

GSEA identified 326 enriched KEGG pathways, of which 126 were significant. Pathways related to infection and immunity, such as Autoimmune thyroid disease and Allograft rejection, were upregulated in IC, while pathways like Valine degradation were downregulated, suggesting links to IC/BPS pathology (Supplementary Figure S1). Overall, these analyses reveal a strong

10.3389/fimmu.2024.1413078

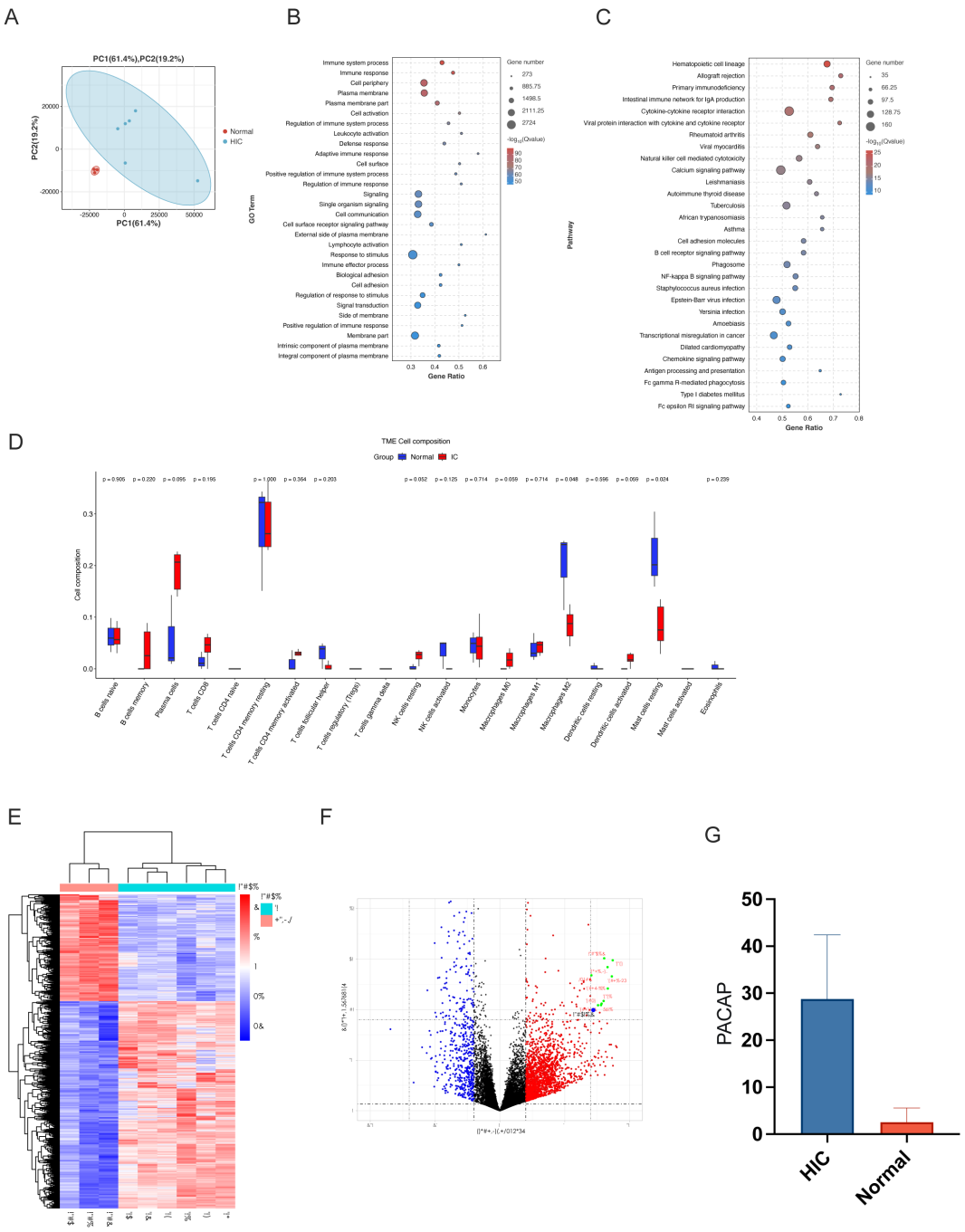

FIGURE 2
Molecular and immune analysis in IC/BPS patient samples. **(A)** PLS-DA Plot of Molecular Profiles in IC/BPS vs. Control Groups: Partial least squares-discriminant analysis (PLS-DA) plot showcasing the clear separation between normal controls and HIC patient groups, reflecting significant differences in their respective molecular profiles in human subjects. **(B)** GO Term Enrichment Analysis for IC/BPS Samples: Gene Ontology (GO) term enrichment analysis results, identifying key biological processes, molecular functions, and cellular components, predominantly associated with immune response and signaling. **(C)** KEGG Pathway Enrichment Analysis in IC/BPS Pathology: Kyoto Encyclopedia of Genes and Genomes (KEGG) pathway enrichment analysis highlighting pathways relevant to hematopoietic cell lineage and allograft rejection, suggesting an immune response involvement in interstitial cystitis/bladder pain syndrome (IC/BPS) pathology. **(D)** Immune Infiltration Analysis in IC/BPS vs. Control Groups: Immune Infiltration Analysis indicating minimal alterations in most immune cell types between IC/BPS and control groups, except for resting mast cells and monocytes, suggesting their potential role in IC/BPS pathogenesis. **(E)** Heatmap of Differential Gene Expression in IC/BPS: Heatmap representation of transcriptomic data contrasting gene expression profiles between IC specimens and normal controls, emphasizing the differential expression of ADCYAP1. **(F)** Volcano Plot of Gene Expression in IC/BPS Samples: Volcano plot illustrating the differential gene expression between control and Hunner type interstitial cystitis (HIC) patient groups. Red points represent genes that are significantly upregulated, highlighting ADCYAP1 due to its substantial upregulation in IC samples compared to controls, marking it as a prominent biomarker and potential therapeutic target for IC/BPS. Blue points indicate significantly downregulated genes, and black points denote genes without significant changes. **(G)** Bar Graph of PACAP Expression in IC/BPS vs. Control Tissues: Bar graph depicting the increased expression of PACAP in surgical specimens from IC/BPS patients compared to normal tissues, confirming its role as a diagnostic and therapeutic marker.

TABLE 1 Comparison of urodynamic parameters and body weight ratios across control and cystitis-induced rat groups post-treatment.

characteristics	Con-Con	CYP-Con	Con-PAC	CYP-PAC	CYP-Treated	CYP-Untreated
(mL)	1.28 ± 0.38	0.63 ± 0.22***	1.272± 0.39	1.13± 0.77	1.86 ± 0.82^^	0.88 ± 0.13
Pdet(cmH2O)	41.77 ± 12.02	35.58 ± 3.04	39.02± 5.70	38.82 ± 12.15	40.52 (34.45, 43.88)	37.66 (31.92, 40.92)
BC(mL/cmH2O)	0.045 ± 0.010	0.026 ± 0.010*	0.046 ± 0.015	0.047 ± 0.037	0.058 ± 0.023^	0.033± 0.008
Baseline (cmH20)	10.96 (9.58, 12.10)	10.88 (10.34, 12.33)	9.9 (9.59, 10.26)	9.56 (9.07, 12.19)	9.81 (9.72, 9.97)	10.21 (9.47, 10.82)
Pre-Body weight(g)	224.57 ± 11.63	229.57 ± 7.68	230.14 ± 4.74	227 ± 4.47	225.14 ± 9.19	234 ± 11.55
Post-Body weight(g)	249.29 ± 12.88	236.29 ± 7.63*	264.14 ± 11.13	256 ± 10.07	263 (250.5, 267.5)^^	242 (233, 246)
Bladder weight (g)	0.12 ± 0.016	0.16 ± 0.019**	0.11 ± 0.0216	0.12 ± 0.012	0.10± 0.019^	0.127± 0.019
Bladder(g)/Body Weight(g)	0.49 (0.43, 0.52)	0.65 (0.58, 0.72)**	0.4 (0.4, 0.5)	0.5 (0.45, 0.5)	0.402 ± 0.059^^^	0.582 ± 0.088

MBC, maximal bladder capacity, Bladder Compliance (BC), Maximum Bladder Pressure (Pdet), *p values < 0.05, **p values < 0.01, ***p values<0.001 when compared with controls;^ p values between CYP-Treated and CYP-Untreated.

immunological component in the pathophysiology of IC/BPS, with significant upregulation and downregulation of specific pathways, offering insights into potential pathological mechanisms.

Immune infiltration analysis

Analysis of immune infiltration patterns within the IC/BPS group shows that, except for resting mast cells and monocytes, most immune cell types show minimal changes compared to the control group. This observation highlights the potential pivotal role of resting mast cells and monocytes in IC/BPS pathogenesis, warranting further investigation (Figure 2D).

In transcriptomic data analysis, a notable bifurcation in gene expression was observed using a heat map comparing six IC specimens and a cohort of three normal specimens (Figure 2E). The gene of interest, ADCYAP1 (commonly known as PACAP), stood out with significant distinction, showing a marked increase in expression in the IC group. This was prominently indicated by its unique presence in the upper red quadrant of the volcano plot (Figure 2F). This significant upregulation suggests that ADCYAP1 plays a pivotal role in IC/BPS pathogenesis, marking it as a potential biomarker and therapeutic target. The pronounced disparity in ADCYAP1 expression between IC samples and normal specimens presents a promising avenue for elucidating the complex molecular mechanisms underlying IC/BPS.

Surgical specimen validation

Building on the insights from the transcriptomic analysis, we further validated the expression profile of PACAP (ADCYAP1) through an empirical evaluation of surgical specimens from IC/BPS patients. A collection of nine samples, consisting of three normal specimens and six IC/BPS specimens, was subjected to PACAP immunohistochemical staining assays (Supplementary Figure S2). The immunohistochemical data revealed a significant increase in PACAP expression within IC/BPS tissues compared to normal tissues (Figure 2G). This significant elevation in PACAP levels supports its potential as a diagnostic marker and therapeutic target in IC/BPS pathophysiology.

Enhancement of bladder function following intravesical instillation of PACAP6-38/Saline

Building on the foundational transcriptomic sequencing analysis and subsequent immunohistochemical validation with surgical specimens, we expanded the research to animal models. We employed the Urine Spot Assay to analyze micturition patterns in SD rats. The resulting data, shown graphically, indicated that rats in the CYP-PAC cohort exhibited a statistically significant increase in urine spot frequency post-infusion compared to the pre-infusion baseline ($P < 0.05$). In contrast, as shown in Table 1, no statistical difference was observed in urine spot area before and after PACAP6-38 administration across the cohorts under investigation. Notably, the urine spot frequency in the CYP-Control group was significantly higher compared to the other three groups (Figures 3A, B).

Further exploration involved the use of urodynamic testing to evaluate bladder function in the SD rat cohorts. The tabulated data showed that the CYP-Control group had a significant reduction in both Maximum Bladder Capacity (MBC) and Bladder Compliance (BC) compared to the other three groups ($P < 0.05$). However, when evaluating Maximum Bladder Pressure (Pdet) and baseline, no statistically significant differences were found in the intergroup comparisons (Table 1).

Mitigation of bladder inflammation with PACAP6-38/saline intravesical instillation

The immunohistochemical findings, presented in Figures 3C–J, reveal a clear upregulation in the expression of several cytokines and growth factors—specifically CCL3, IL-6, IL-8, TNF-α, and VEGF—within the CYP-Control cohort, with statistically significant differences ($P < 0.05$). Furthermore, the concentration of Nerve Growth Factor (NGF) in the CYP-Control group was higher than levels observed in both the CYP-PAC and Control-PAC groups. Similarly, PACAP expression levels were higher in the CYP-Control and CYP-PAC groups compared to the Con-PAC and Con-Con

10.3389/fimmu.2024.1413078

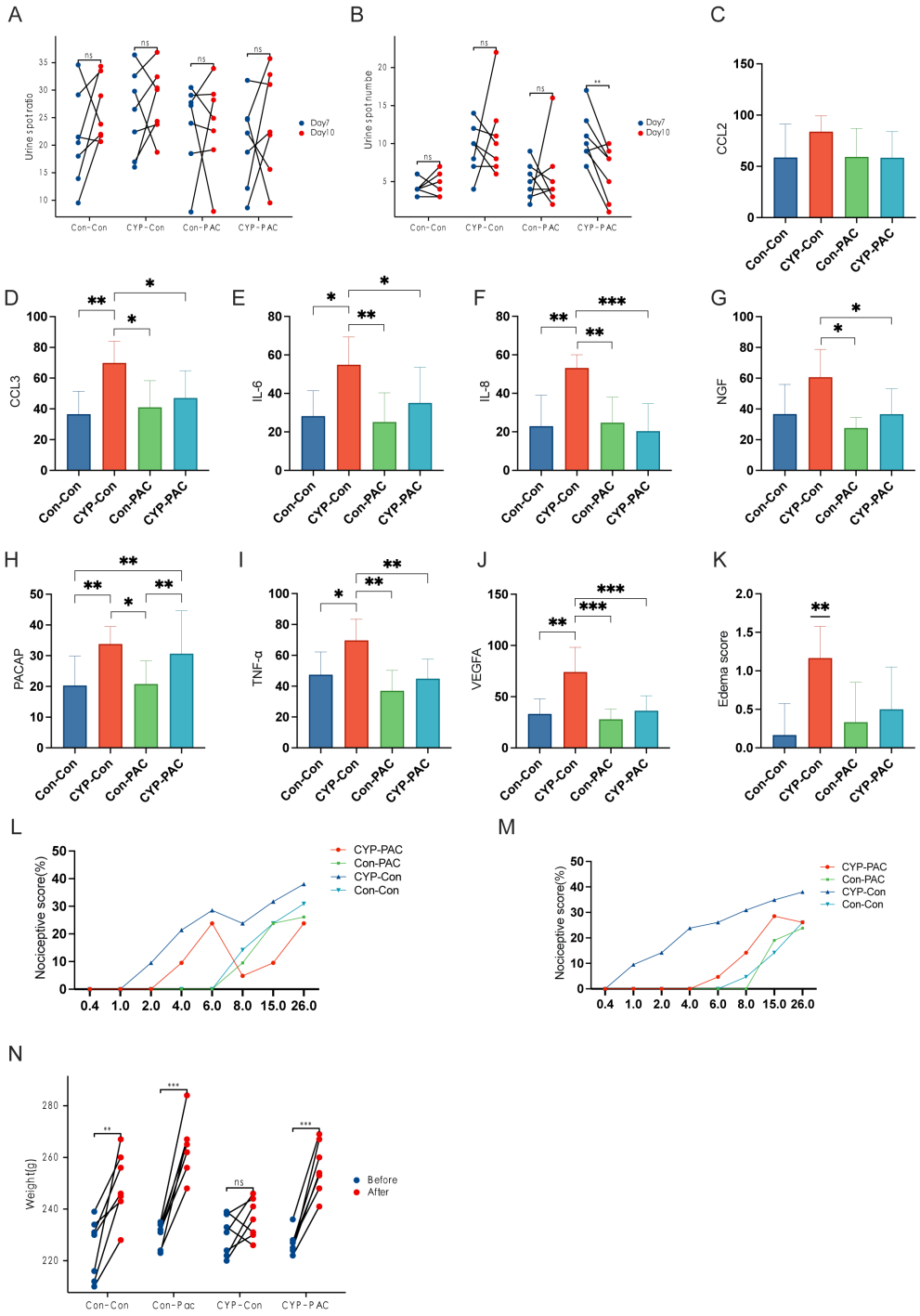

FIGURE 3
Effects of CYP and PACAP treatments on bladder inflammation and pain sensitivity in rat models. **(A, B)** Sequential Urine Spot Frequency and Area Analysis Post-Treatment: Sequential urine spot assay results indicating a significant increase in urine spot frequency in the CYP-PAC group post-treatment ($P<0.05$), without notable changes in urine spot area. **(C–J)** Immunohistochemical Analysis of Cytokines in Bladder Tissues: Immunohistochemical analysis of bladder tissues showing elevated levels of cytokines and growth factors—CCL3, IL-6, IL-8, TNF-α, and VEGF—in the CYP-Control group, with a significant increase in NGF levels compared to CYP-PAC and Control-PAC groups ($P < 0.05$). PACAP expression was similarly upregulated in the CYP-Control and CYP-PAC groups relative to the Con-PAC and Con-Con groups. **(K)** Pre-Treatment von Frey Test Response Curve: Assessment of bladder tissue edema scores, illustrating significant inflammation in the CYP-Con group compared to the Con-Con group ($p < 0.01$) and no significant difference between the CYP-PAC and Con-Con groups. **(L)** Post-Treatment von Frey Test Results: von Frey test response curves pre-treatment demonstrating increased sensitivity to stimuli in the CYP-treated groups. **(M)** Weight Progression of Rats Over the Experiment Period: Post-treatment von Frey test results showing a significant reduction in visceral pain in the CYP-PAC group compared to the CYP-Con group ($p < 0.05$). **(N)** Graph showing the weight progression of rats over the course of the experiment. Weight measurements were taken on Day 0 and Day 11 to track growth and development during the treatment period. *: $p < 0.05$; **; $p < 0.01$; ***; $p < 0.001$.

groups. Supporting the immunohistochemical results, the edema score in the CYP-Con group was significantly higher, reinforcing our histological findings with strong statistical significance ($P < 0.01$). No statistical difference was observed between the CYP-PAC group and the Con-Con group (Figure 3K).

Improvement of general condition following PACAP6-38/saline intravesical instillation

Nociceptive responses were assessed using the von Frey test. Figures 3L, M show the von Frey test performed on day 7 before treatment after the induction of chronic cystitis. At this stage, the CYP-PAC and CYP-Con groups, which received chronic CYP injections, exhibited visceral pain marked by increased responses to normally innocuous 1-8g von Frey forces (abnormal pain) and heightened reactions to noxious 10-26g von Frey forces (hyperalgesia) (Figure 3L). After treatment, the CYP-PAC group showed a significant reduction in chronic visceral pain induced by CYP compared to the control group ($P < 0.05$) and the sham group (Figure 3M).

As shown in Figure 3N, all groups except the CYP-Con group exhibited an increase in body weight at the second measurement. Additionally, the bladder weight-to-body weight ratio was significantly higher in the CYP-Con group compared to the other three groups (Table 1).

Enhancement of bladder function following intrathecal instillation of PACAP6-38/saline

Figure 4A shows no substantial differences in the dimensions of urine spots across the groups, both before and after the intrathecal infusion. After intrathecal administration of PACAP6-38, the CYP-treated cohort showed a significant reduction in urine spot frequency compared to their pre-injection state, with statistical significance ($P < 0.01$), as shown in Figure 4B. Furthermore, as shown in Table 1, the CYP-Untreated group had reduced MBC and BC compared to the CYP-Treated cohort, achieving statistical significance ($P < 0.05$). However, the comparison of Pdet and baseline between these cohorts did not reveal any statistically significant differences.

Mitigation of bladder inflammation with Pacap6-38/saline intrathecal instillation

The levels of IL-6, IL-8, NGF, TNF-α, and VEGF in the CYP-Untreated group were higher than those in the CYP-Treated group, with statistically significant differences ($P < 0.05$) (Figures 4C–J). The edema score in the CYP-Untreated group was higher than that in the CYP-Treated group ($P < 0.01$) (Figure 4K).

Improvement of general condition following PACAP6-38/saline intrathecal instillation

Following CYP infusion, both the CYP-Treated and CYP-Untreated groups showed an increase in the curves, with no statistically significant difference between the two cohorts (Figure 4L). After intrathecal administration of PACAP-38, the CYP-Treated group showed a significant reduction in chronic visceral pain induced by CYP post-treatment ($P < 0.05$) (Figure 4M). As shown in Figure 4N, the CYP-Treated group demonstrated a significant increase in weight at the second measurement ($P < 0.05$). In contrast, no significant difference in weight was observed before and after treatment in the CYP-Untreated group. Additionally, both bladder weight and the bladder weight-to-body weight ratio were higher in the CYP-Untreated group compared to the CYP-Treated group (Table 1).

Discussion

PACAP and its receptor PAC1 play essential roles in regulating urinary tract function, particularly in conditions such as bladder pain syndrome (BPS)/interstitial cystitis (IC), which are marked by chronic pelvic pain and urinary dysfunction. PACAP is expressed in neurons in the brainstem and hypothalamus and activates preganglionic sympathetic neurons in the spinal cord during inflammatory stress. This results in PACAP influencing the immune response in the thymus, lymph nodes, and spleen through PAC1 receptors on sympathetic neurons (19). Blocking PAC1 receptors could represent a novel therapeutic strategy to improve bladder function and alleviate pelvic pain (20).

Our PLS-DA and KEGG pathway analyses revealed distinct metabolic and immunological differences in IC/BPS, supported by GO analysis that identified key immune components and highlighted specific altered pathways and genes. Notably, GSEA identified upregulation in autoimmune and infectious disease pathways, suggesting immune system dysregulation as a primary pathogenic mechanism in IC/BPS. Concurrently, downregulated metabolic pathways indicate changes in energy metabolism. Additionally, varied patterns of immune cell infiltration, particularly by mast cells and monocytes, are crucial in IC/BPS pathogenesis and warrant further investigation. Furthermore, our research establishes a strong link between PACAP expression and IC/BPS. Transcriptomic analysis revealed significant differences in PACAP expression between healthy individuals and IC/BPS patients, emphasizing its role in the disease's immunological and potential neuroinflammatory aspects. This aligns with the broader metabolic and immunological irregularities observed in our comprehensive analyses, underscoring the complexity of IC/BPS pathophysiology.

In our study, the CYP-Con group exhibited significant bladder inflammation, indicated by increased levels of CCL3, IL-6, IL-8, TNF-α, and VEGF, highlighting the PACAP/PAC1 pathway's role in this

10.3389/fimmu.2024.1413078

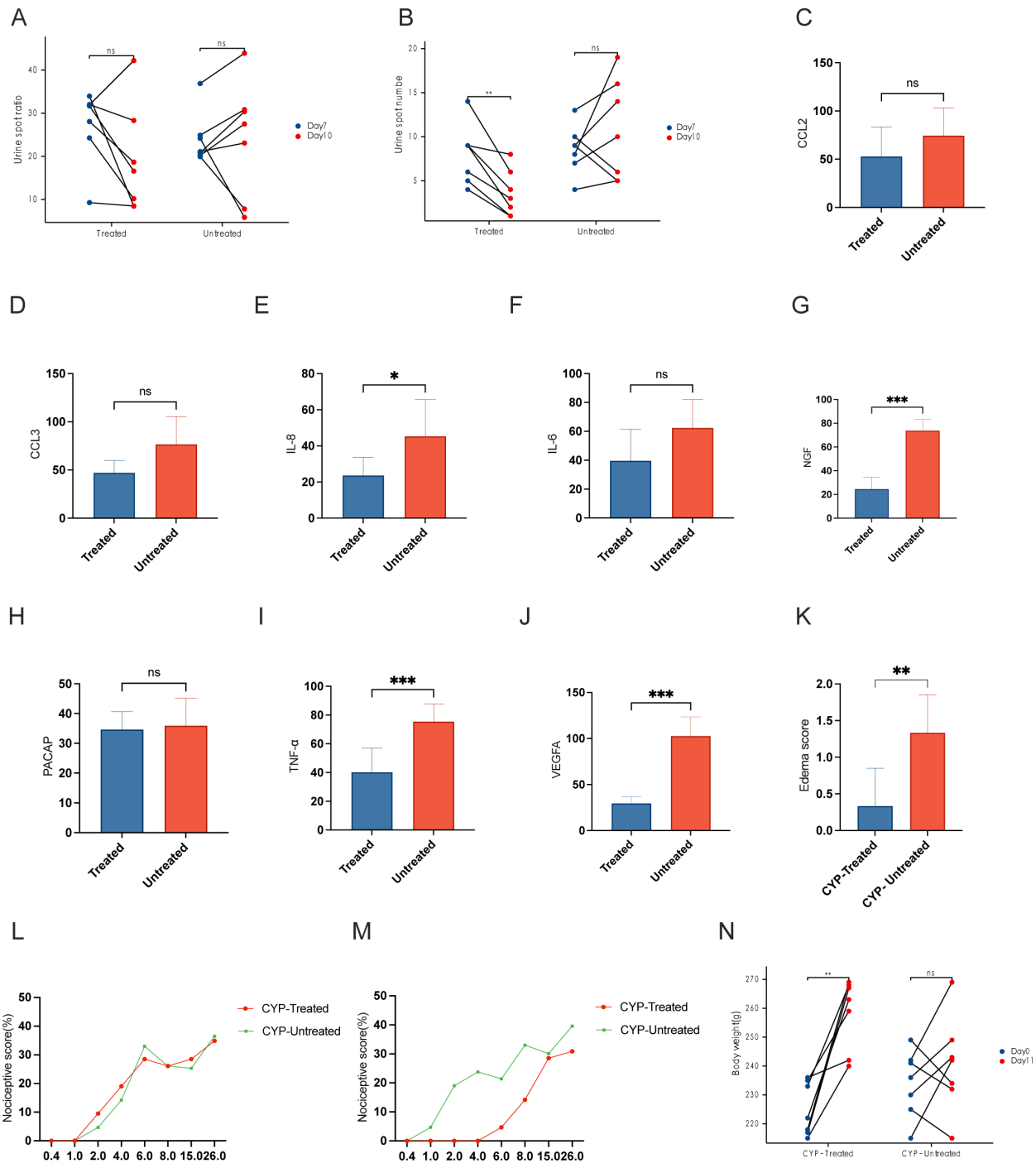

FIGURE 4
Effects of PACAP6-38 treatment on bladder function and inflammatory markers in CYP-treated rat models. **(A)** Urine Spot Size Analysis Pre- and Post-Treatment: "Comparative analysis of urine spot dimensions before and after intrathecal instillation in the CYP-treated and untreated groups. The analysis shows no significant size variation across groups, indicating that the treatment does not affect the size of urine spots. **(B)** Reduction in Urine Spot Frequency Post-PACAP6-38 Treatment: Graph depicting a reduction in urine spot frequency following intrathecal instillation of PACAP6-38 in the CYP-treated group, signifying a statistically significant improvement in bladder function ($P < 0.01$). This result highlights the therapeutic potential of PACAP6-38 in modulating bladder activity post-treatment. **(C–J)** Quantitative Immunohistochemical Analysis of Inflammatory Markers in CYP-Treated vs. Untreated Groups: Quantitative immunohistochemical analysis of inflammatory markers including IL-6, IL-8, NGF, TNF-α, and VEGF, indicating a significant reduction in the CYP-Treated group as opposed to the CYP-Untreated group ($P < 0.05$). **(K)** Bladder Tissue Edema Score: Evaluation of bladder tissue edema scores demonstrating decreased inflammation in the CYP-Treated group compared to the CYP-Untreated group ($p < 0.01$). **(L)** von Frey Test Response Curve Post-CYP Infusion: von Frey test response curves post-CYP infusion showing elevated sensitivity to mechanical force in both CYP-Treated and CYP-Untreated groups, with no significant difference observed between them. **(M)** Reduction in Chronic Visceral Pain Post-PACAP6-38 Treatment: A significant decrease in chronic visceral pain in the CYP-Treated group following treatment with PACAP6-38, as shown by the von Frey test ($p < 0.05$). **(N)** Body Weight Changes in CYP-Treated and Untreated Groups: The CYP-Treated group exhibits a significant increase in body weight after treatment ($p < 0.05$), in contrast to the CYP-Untreated group which showed no such difference. *: $p < 0.05$; **; $p < 0.01$; ***; $p < 0.001$.

inflammation. This suggests that CYP treatment alone triggers significant inflammation. In contrast, the CYP-PAC group, treated with PACAP6-38, showed reduced inflammatory markers, indicating that PACAP6-38 may counter CYP-induced inflammation by inhibiting the PACAP/PAC1 pathway, likely through reducing inflammatory cell recruitment and mediator regulation. Additionally, intrathecal administration of PACAP6-38 highlighted its significant effect in the dorsal root ganglion (DRG), which is crucial for pain and inflammation management. This suggests its ability to modify pain perception and inflammatory responses, as shown by reduced pain and inflammation. This underscores its role in managing neuroinflammation in interstitial cystitis. Intravesical administration of PACAP6-38 effectively reduced bladder inflammation, supporting the PACAP/PAC1 pathway's role in reducing inflammatory markers and improving bladder function. These findings reveal PACAP6-38's dual action in the DRG and bladder, suggesting it alleviates interstitial cystitis symptoms by reducing neuroinflammation and pain in the DRG while directly addressing bladder inflammation to improve function.

In the CYP-PAC group, PACAP6-38 treatment significantly reduced urine spot count without affecting the spot area, suggesting an impact on bladder voiding function. This reduction in urine spot count indicates decreased bladder hyperactivity, a key clinical indicator in interstitial cystitis. Moreover, the CYP-Con group showed lower maximum bladder capacity and compliance compared to other groups, highlighting bladder dysfunction caused by CYP treatment. Conversely, the improved bladder capacity and compliance in the CYP-PAC group underscore PACAP6-38's effectiveness in restoring bladder function affected by inflammation. Additionally, Von Frey test results in the CYP-PAC group showed a significant decrease in chronic visceral pain post-treatment, likely due to PACAP6-38's modulation of bladder inflammation and sensory function. This result, combined with observed physiological weight gain, reinforces PACAP6-38's role in improving overall health under chronic inflammatory conditions.

Vizzard et al. demonstrated an upregulation of PACAP expression in the DRG segments associated with the micturition reflex in cyclophosphamide-induced chronic cystitis rats (21). Braas et al. found that intrathecal injection or bladder instillation of the PAC1 antagonist PACAP (6-38) reduced voiding frequency in animals with cystitis (9). Victory May et al. noted that during detrusor muscle contraction, PACAP promotes ATP release from the urothelium. PACAP gene knockout mice showed increased bladder mass, fewer but larger urine spots in the micturition imprint test, thicker lamina propria and detrusor smooth muscle, but no significant differences in the urothelium. Additionally, PACAP gene knockout mice showed increased bladder capacity, voiding volume, significantly longer voiding intervals, prolonged detrusor muscle contraction duration, and increased residual urine volume. PACAP (+/-) heterozygous gene knockout mice also showed bladder dysfunction, albeit to a lesser extent (22). These findings suggest that PACAP mediates changes in bladder function by modulating ATP release. Recent research by Atsuko Hayata-Takano et al. showed that PACAP-deficient mice exhibited motor and cognitive abnormalities, which were improved with a 5-HT receptor antagonist. They confirmed that PACAP induces increased internalization of 5-HT (2A) in HEK293T cells, but not of 5-HT (1A), 5-HT (2C), dopamine D2 receptors, or metabotropic glutamate receptor 2, thereby attenuating 5-HT (2A)-mediated signaling. This effect was inhibited by protein kinase C inhibitors, β-arrestin2 silencing (a key protein regulating endothelial nitric oxide synthase activity), the PAC1 receptor antagonist PACAP6-38, and PAC1 silencing (23).

The urinary epithelium is a specialized epithelial tissue that lines most urinary tract structures, forming a barrier against urine components passing into underlying tissues and the bloodstream (24, 25). Damage to the urinary epithelium increases its permeability, allowing urea, potassium, and other urinary solutes to penetrate the bladder wall. This activates an inflammatory response and mast cell secretion, which subsequently increases the production of pro-inflammatory mediators such as tumor necrosis factor-alpha (TNF-α), interleukin (IL)-1β, and IL-8. These mediators sensitize nerve endings, leading to increased release of neuropeptides that promote mast cell degranulation and exacerbate the inflammatory process. Inflammation directly impacts bladder function. In acute inflammation, such as urinary tract infections (UTIs), inflammatory mediators are released, damaging the urinary epithelium and causing bladder wall irritation. These inflammatory changes result in clinical symptoms such as urgency, dysuria, frequency, nocturia, and fever. In acute inflammation, these changes are transient and resolve once the harmful stimuli are removed. If the harmful stimuli persist, they can lead to chronic inflammation, causing recurrent damage to the bladder mucosa and other functional pathological changes such as fibrosis. These pathological changes contribute to symptoms commonly seen in interstitial cystitis (IC), such as urgency, frequency, dysuria, and cystoscopic findings (26). Vascular endothelial growth factor (VEGF) is overexpressed in 58% of IC bladders (27), along with IL-6 and IL-8. The release of vasoactive and inflammatory mediators by mast cells accounts for many IC symptoms. IC is characterized by the infiltration of mononuclear cells, including macrophages, lymphocytes, eosinophils, mast cells, and plasma cells, leading to irreversible tissue damage, functional dysregulation such as fibrosis and poor compliance, detrusor muscle overactivity, and visceral hypersensitivity, resulting in chronic pain and lower urinary tract symptoms. An increase in mast cell numbers in the submucosal and detrusor layers is particularly evident in classic IC with Hunner's ulcers (28).

Typically, the half-life of inflammatory mediators is short, but in IC, prolonged exposure to harmful stimuli leads to increased secretion of inflammatory mediators, resulting in vascular edema, vasculitis, and neuroinflammation. This process promotes neurotransmitter secretion, further stimulating mast cells and creating a vicious cycle of sustained inflammation and repeated damage to the urinary epithelium. Clinically, this manifests as visceral hypersensitivity, leading to difficulty in urination, urgency, and lower urinary tract symptoms. We speculate that pathological changes, such as the loss of the urinary epithelial glycosaminoglycan

(GAG) layer, impaired immune function, and infections, lead to alterations in the PACAP/PAC1-related regulatory molecular network in the bladder, resulting in inflammatory cascades and excessive mast cell expression. This can trigger either Hunner's ulcerative IC or non-ulcerative IC. Simultaneously, direct stimulation of the urinary epithelium by urine leads to C-fiber overactivation, resulting in chronic pain symptoms. The PACAP/PAC1 pathway further increases inflammatory mediator secretion, promotes neurotransmitter release, and stimulates mast cells, leading to sustained inflammation, repeated damage to the urinary epithelium, and the development of inflammatory cascades and bladder dysfunction.

Conclusion

In conclusion, PACAP and its receptor PAC1 play a complex and multifaceted role in the pathogenesis of IC/BPS, influencing various physiological systems to maintain homeostasis. Our findings, along with previous research, highlight PACAP's significance in IC/BPS, particularly regarding immune and neuroinflammatory aspects. The differential expression of PACAP observed in normal and IC/BPS patients underscores its crucial role. Modulating the PACAP/PAC1 pathway through interventions such as PAC1 antagonists has shown promise in reducing bladder inflammation and improving function. PACAP's role in sensory nerve regulation and neurotransmitter release, along with its interaction with mast cells and inflammatory mediators, further emphasizes its importance in IC/BPS. Chronic and neurogenic inflammation associated with IC/BPS symptoms such as bladder pain and urgency are linked to dysregulated pathways influenced by factors such as immune dysfunction and infections. Our research highlights PACAP's complex role in IC/BPS and its therapeutic potential, emphasizing the need for further investigation into its specific mechanisms and interactions to develop targeted treatments.

Data availability statement

The data presented in the study are deposited in the NCBI Sequence Read Archive (SRA) under the accession numbers SRR31282777-SRR31282785, available at https://www.ncbi.nlm.nih.gov/sra/PRJNA1183631.

Ethics statement

The studies involving humans were approved by the Medical Ethics Committee of Peking University People's Hospital. The studies were conducted in accordance with the local legislation and institutional requirements. The participants provided their written informed consent to participate in this study. The animal study was approved by The Medical Ethics Committee of Peking University People's Hospital. The study was conducted in accordance with the local legislation and institutional requirements.

Author contributions

HK: Conceptualization, Data curation, Methodology, Validation, Visualization, Writing – original draft, Writing – review & editing. LZ: Data curation, Methodology, Visualization, Writing – review & editing. WZ: Methodology, Supervision, Writing – review & editing. HW: Methodology, Supervision, Writing – review & editing. ZD: Formal analysis, Validation, Writing – review & editing. DS: Methodology, Supervision, Writing – review & editing. QW: Conceptualization, Funding acquisition, Methodology, Supervision, Writing – review & editing. KX: Conceptualization, Funding acquisition, Methodology, Supervision, Writing – review & editing.

Funding

The author(s) declare that financial support was received for the research, authorship, and/or publication of this article. This study was supported by the National Natural Science Foundation of China (Grant No.81970660); Beijing Natural Science Foundation (7242153) and Research and Development Fund of Peking University People's Hospital (2147000692).

Conflict of interest

The authors declare that the research was conducted in the absence of any commercial or financial relationships that could be construed as a potential conflict of interest.

Publisher's note

Supplementary material

The Supplementary Material for this article can be found online at: https://www.frontiersin.org/articles/10.3389/fimmu.2024.1413078/full#supplementary-material

SUPPLEMENTARY FIGURE 1
Gene Set Enrichment Analysis (GSEA) of KEGG pathways associated with interstitial cystitis/bladder pain syndrome (IC/BPS).

SUPPLEMENTARY FIGURE 2
Immunohistochemical Staining of Bladder Tissue for PACAP in HIC Patients and Normal Group. **(A-F)** Display PACAP immunohistochemical staining in bladder tissues from patients with Hunner type interstitial cystitis (HIC). **(G-I)**: Show PACAP staining in bladder tissues from the normal control group, serving as a baseline comparison to highlight the differential expression observed in the HIC group.

References

1. Hanno PM, Erickson D, Moldwin R, Faraday MM. Diagnosis and treatment of interstitial cystitis/bladder pain syndrome: AUA guideline amendment. *J Urol*. (2015) 193:1545–53. doi: 10.1016/j.juro.2015.01.086

2. Leppilahti M, Sairanen J, Tammela T, Aaltomaa S, Lehtoranta K, Auvinen A, et al. Prevalence of clinically confirmed interstitial cystitis in women: A population based study in Finland. *J Urol*. (2005) 174:581–3. doi: 10.1097/01.ju.0000165452.39125.98

3. Nickel JC, Doiron RC. Dangerous fluoroquinolones: The urologist's dilemma. *CUAJ*. (2020) 14:85–6. doi: 10.5489/cuaj.6498

4. Berry SH, Elliott MN, Suttorp M, Bogart LM, Stoto MA, Eggers P, et al. Prevalence of symptoms of bladder pain syndrome/interstitial cystitis among adult females in the United States. *J Urol*. (2011) 186:540–4. doi: 10.1016/j.juro.2011.03.132

5. Anger JT, Zabihi N, Clemens JQ, Payne CK, Saigal CS, Rodriguez LV. Treatment choice, duration, and cost in patients with interstitial cystitis and painful bladder syndrome. *Int Urogynecol J*. (2011) 22:395–400. doi: 10.1007/s00192-010-1252-8

6. Grundy L, Caldwell A, Brierley SM. Mechanisms underlying overactive bladder and interstitial cystitis/painful bladder syndrome. *Front Neurosci*. (2018) 12:931. doi: 10.3389/fnins.2018.00931

7. Patnaik SS, Laganà AS, Vitale SG, Butticè S, Noventa M, Gizzo S, et al. Etiology, pathophysiology and biomarkers of interstitial cystitis/painful bladder syndrome. *Arch Gynecol Obstet*. (2017) 295:1341–59. doi: 10.1007/s00404-017-4364-2

8. Vizzard MA. Up-regulation of pituitary adenylate cyclase-activating polypeptide in urinary bladder pathways after chronic cystitis. *J Comp Neurol*. (2000) 420:335–48. doi: 10.1002/(SICI)1096-9861(20000508)420:3<335::AID-CNE5>3.0.CO;2-#

9. Herrera GM, Braas KM, May V, Vizzard MA. PACAP enhances mouse urinary bladder contractility and is upregulated in micturition reflex pathways after cystitis. *Ann New York Acad Sci*. (2006) 1070:330–6. doi: 10.1196/annals.1317.040

10. Braas KM, May V, Zvara P, Nausch B, Kliment J, Dunleavy JD, et al. Role for pituitary adenylate cyclase activating polypeptide in cystitis-induced plasticity of micturition reflexes. *Am J Physiology-Regulatory Integr Comp Physiol*. (2006) 290: R951–62. doi: 10.1152/ajpregu.00734.2005

11. Girard BM, Campbell SE, Beca KI, Perkins M, Hsiang H, May V, et al. Intrabladder PAC1 receptor antagonist, PACAP(6-38), reduces urinary bladder frequency and pelvic sensitivity in mice exposed to repeated variate stress (RVS). *J Mol Neurosci*. (2021) 71:1575–88. doi: 10.1007/s12031-020-01649-x

12. Fahrenkrug J, Hannibal J. Pituitary adenylate cyclase activating polypeptide immunoreactivity in capsaicin-sensitive nerve fibres supplying the rat urinary tract. *Neuroscience*. (1998) 83:1261–72. doi: 10.1016/S0306-4522(97)00474-0

13. Cheppudira BP, Girard BM, Malley SE, Schutz KC, May V, Vizzard MA. Upregulation of vascular endothelial growth factor isoform VEGF-164 and receptors (VEGFR-2, Npn-1, and Npn-2) in rats with cyclophosphamide-induced cystitis. *Am J Physiology-Renal Physiol*. (2008) 295:F826–36. doi: 10.1152/ajprenal.90305.2008

14. Hanno PM, Burks DA, Clemens JQ, Dmochowski RR, Erickson D, FitzGerald MP, et al. AUA guideline for the diagnosis and treatment of interstitial cystitis/bladder pain syndrome. *J Urol*. (2011) 185:2162–70. doi: 10.1016/j.juro.2011.03.064

15. Girard BM, Malley SE, Mathews MM, May V, Vizzard MA. Intravesical PAC1 receptor antagonist, PACAP(6–38), reduces urinary bladder frequency and pelvic sensitivity in NGF-OE mice. *J Mol Neurosci*. (2016) 59:290–9. doi: 10.1007/s12031-016-0764-1

16. Augé C, Chene G, Dubourdeau M, Desoubzdanne D, Corman B, Palea S, et al. Relevance of the cyclophosphamide-induced cystitis model for pharmacological studies targeting inflammation and pain of the bladder. *Eur J Pharmacol*. (2013) 707:32–40. doi: 10.1016/j.ejphar.2013.03.008

17. Augé C, Gamé X, Vergnolle N, Lluel P, Chabot S. Characterization and validation of a chronic model of cyclophosphamide-induced interstitial cystitis/bladder pain syndrome in rats. *Front Pharmacol*. (2020) 11:1305. doi: 10.3389/fphar.2020.01305

18. Gray KJ, Engelmann UH, Johnson EH, Fishman IJ. Evaluation of misoprostol cytoprotection of the bladder with cyclophosphamide (Cytoxan) therapy. *J Urol*. (1986) 136:497–500. doi: 10.1016/S0022-5347(17)44929-9

19. Van C, Condro MC, Lov K, Zhu R, Ricaflanca PT, Ko HH, et al. PACAP/PAC1 regulation of inflammation via catecholaminergic neurons in a model of multiple sclerosis. *J Mol Neurosci*. (2019) 68:439–51. doi: 10.1007/s12031-018-1137-8

20. Ojala J, Tooke K, Hsiang H, Girard BM, May V, Vizzard MA. PACAP/PAC1 expression and function in micturition pathways. *J Mol Neurosci*. (2019) 68:357–67. doi: 10.1007/s12031-018-1170-7

21. Girard BM, Malley SE, Vizzard MA. Neurotrophin/receptor expression in urinary bladder of mice with overexpression of NGF in urothelium. *Am J Physiol Renal Physiol*. (2011) 300:F345–355. doi: 10.1152/ajprenal.00515.2010

22. May V, Parsons RL. G protein-coupled receptor endosomal signaling and regulation of neuronal excitability and stress responses: signaling options and lessons from the PAC1 receptor. *J Cell Physiol*. (2017) 232:698–706. doi: 10.1002/jcp.25615

23. Hayata-Takano A, Shintani Y, Moriguchi K, Encho N, Kitagawa K, Nakazawa T, et al. PACAP-PAC1 signaling regulates serotonin 2A receptor internalization. *Front Endocrinol*. (2021) 12:732456. doi: 10.3389/fendo.2021.732456

24. Lasič E, Višnjar T, Kreft ME. Properties of the urothelium that establish the blood–urine barrier and their implications for drug delivery. *Rev Physiol Biochem Pharmacol*. (2015) 168:1–29. doi: 10.1007/112_2015_22

25. Kreft ME, Hudoklin S, Jezernik K, Romih R. Formation and maintenance of blood–urine barrier in urothelium. *Protoplasma*. (2010) 246:3–14. doi: 10.1007/s00709-010-0112-1

26. Grover S, Srivastava A, Lee R, Tewari AK, Te AE. Role of inflammation in bladder function and interstitial cystitis. *Ther Adv Urol*. (2011) 3:19–33. doi: 10.1177/1756287211398255

27. Tamaki M, Saito R, Ogawa O, Yoshimura N, Ueda T. Possible mechanisms inducing glomerulations in interstitial cystitis: relationship between endoscopic findings and expression of angiogenic growth factors. *J Urol*. (2004) 172:945–8. doi: 10.1097/01.ju.0000135009.55905.cb

28. Johansson SL, Fall M. Clinical features and spectrum of light microscopic changes in interstitial cystitis. *J Urol*. (2017) 143:1118–24. doi: 10.1016/s0022-5347(17)40201-1

Frontiers in Physiology

Understanding how an organism's components work together to maintain a healthy state

The second most-cited physiology journal, promoting a multidisciplinary approach to the physiology of living systems - from the subcellular and molecular domains to the intact organism and its interaction with the environment.

Discover the latest Research Topics

See more →

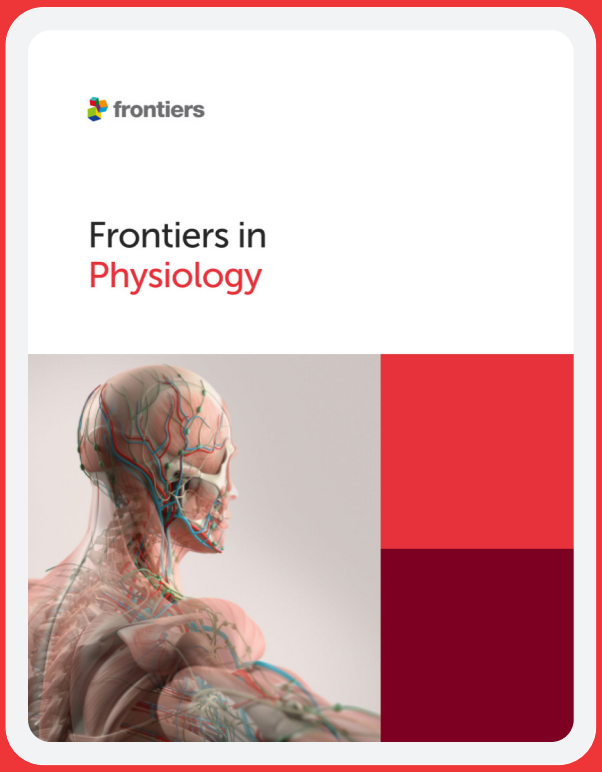

Frontiers

Avenue du Tribunal-Fédéral 34
1005 Lausanne, Switzerland
frontiersin.org

Contact us

+41 (0)21 510 17 00
frontiersin.org/about/contact